DEPARTAMENTO DE QUÍMICA ORGÁNICA

SYNTHESIS, AGGREGATION AND PHOTOPHYSICAL STUDIES OF A_2B_2 PHTHALOCYANINES: NOVEL ARCHETYPES FOR ANTICANCER AND ANTIMICROBIAL PHOTODYNAMIC THERAPY

Doctoral Thesis presented by

MIGUEL ÁNGEL REVUELTA MAZA

to opt for the grade of

DOCTOR IN ORGANIC CHEMISTRY

Madrid, December 2019

The present work has been developed at the Organic Chemistry Department of Universidad Autónoma de Madrid, under the supervision of Dra. Gema de la Torre Ponce and Prof. Tomás Torres Cebada.

The research in this work has been funded by the Universidad Autónoma de Madrid: Contratos Predoctorales para Formación de Personal Investigador 2015 (FPI-UAM).

During the development of the present work, a predoctoral internship has been conducted in the following research centre:

Institut Químic de Sarrià (IQS). Universitat Ramon Llull (URL). Barcelona.

Research group: Química Fotobiológica Aplicada.

Supervision: Prof. Santi Nonell

Date: October-December 2018

PhD thesis presented as a compendium of publications.

To date, the results reported in this thesis have led to several publications in scientific journals:

Chapter 1: Revuelta-Maza, M.A.; Nonell, S.; de la Torre, G.; Torres, T. Boosting the singlet oxygen photosensitization abilities of Zn(II) phthalocyanines through functionalization with bulky fluorinated substituents. *Org. Biomol. Chem.* **2019**, *17*, 7448–7454.

Chapter 2: Revuelta-Maza, M.A.; Hally, C.; Nonell, S.; de la Torre, G.; Torres, T. Crosswise phthalocyanines with collinear functionalization: New paradigmatic derivatives for efficient singlet oxygen photosensitization. *Chempluschem* **2019**, *84*, 673–679.

Chapter 3: Submitted to *Molecules* Revuelta-Maza, M. A.; Mascaraque, M.; González-Jiménez, P.; González-Camuñas, A.; Nonell, S.; Juarranz, A.; de la Torre, G. and Torres, T. Assessing amphiphilic ABAB Zn(II) phthalocyanines with enhanced photosensitization abilities in in vitro photodynamic therapy studies against cancer. *Molecules* **2020**, *25*, 213; https://doi.org/10.3390/molecules25010213.

Chapter 4 Miguel.Á. Revuelta-Maza, P. González-Jiménez, C. Hally, M. Agut, S. Nonell, G. de la Torre, Tomá. Torres, Fluorine-substituted tetracationic ABAB-phthalocyanines for efficient photodynamic inactivation of Gram+ and Gram-bacteria, *European Journal of Medicinal Chemistry* **2020**, *187*, 1119572. doi: https://doi.org/10.1016/j.ejmech.2019.111957.

Chapter 5: Revuelta-Maza, M.A.; Torres, T.; Torre, G. de la Synthesis and Aggregation Studies of Functional Binaphthyl-Bridged Chiral Phthalocyanines. *Org. Lett.* **2019**, *21*, 8183–8186.

Chapter 6: Revuelta-Maza, M.A.; Agut; M. Nonell, S.; de la Torre, G.; Torres, T. Binaphthyl-bridged tetracationic AABB-phthalocyanines: Self-assembled amphiphiles for efficient antimicrobial photodynamic therapy. In preparation to be submitted to *Chem. Commun.*

Other manuscript in preparation related to this thesis include the content exposed in Chapter 7.

Abbreviations

Throughout the present thesis 'Standard Organic Chemistry Abbreviations and Acronyms', following the recommendations of the "guidelines for authors" published by *J. Org. Chem.* **2016**, have been used, and can be found on the journal webpage (http://pubs.acs.org/paragonplus/submission/joceah/joceah_authguide.pdf and https://pubsapp.acs.org/paragonplus/submission/joceah/joceah_abbreviations.pdf).

Furthermore, the next abbreviations and acronyms have also been used:

$^1O_2$	Singlet oxygen
$^3O_2$	Molecular (triplet) oxygen
Φ_Δ	Singlet oxygen quantum yield
Φ_t	High triplet quantum yield
Φ_f	Fluorescence quantum yield
ALA	5-aminolevulinic acid
ADME	Absorption – distribution – metabolism - excretion
aPDT	Antibacterial PDT
aza-BODIPY	Azadipyrromethene
BODIPY	Boron-dipyrromethene
CD	Circular dichroism
CFU	Colony forming unit
CTAB	Cetyltrimethylammonium bromide
DBU	1,8-diazabicyclo[5.4.0]undec-7-ene
DLS	Dynamic light scattering
DMAE	2-Dimethylaminoethanol
DPBF	1,3-Diphenylisobenzofuran
DSSC	Dye-sensitized solar cells
EPR	Enhanced permeability and retention
FDA	Food and Drug Administration
Hb	Deoxyhemoglobin
HBC	Hexabenzocoronene
HbO_2	Oxyhemoglobin
HMDS	Hexamethyldisilazane
HOMO	Highest occupied molecular orbital
Hp	Hematoporphyrin

H_2Pc	Metal-free phthalocyanine
HpD	Hematoporphyrin derivative
HPLC	High-performance liquid chromatography
IC	Internal conversion
IC_{50}	Half maximal inhibitory concentration
ISC	Intersystem crossing
LED	Light emitting diode
LUMO	Lowest unoccupied molecular orbital
MCD	Magnetic circular dichroism
MTT	3-(4,5- Dimethylthiazol-2-yl)-2,5-diphenyltetrazolium bromide
MPc	Metallophthalocyanine
NIR	Near-infrared
NLO	Non-linear optical
OLEDs	Organic light emitting devices
o-DCB	*Ortho*-dichlorobenzece
OPV	Organic photovoltaics
OTFTs	Organic thin-film transistors
PBI	Prylene bisimide
PBS	Phosphate buffered saline
Pc	Phthalocyanine
PEG	Polyethylene glycol
Por	Porphyrin
PS	Photosensitizer or photosensitizing agent
$^1PS^*$	Singlet excited state
$^3PS^*$	Triplet excited state
PBI	Perylene bisimide
PDI	Photodynamic inactivation
PDT	Photodynamic therapy
ROS	Reactive oxygen species
S	Substrate
S_0	Singlet state
S_1	Singlet excited state
SAXS	Small-angle X-ray scattering
SEC	Size exclusion chromatography

SEM	Scanning electron microscope
SOC	Spin-orbit coupling
SubPc	Subphthalocyanine
T_1	Triplet excited state
TEM	Transition electron microscopy
TLC	Thin layer chromatography
TSB	Tryptic soy broth
UV-vis	Ultraviolet-visible
VR	Vibrational relaxation
WAXS	Wide-angle X-ray scattering

Table of contents

SYNTHESIS, AGGREGATION AND PHOTOPHYSICAL STUDIES OF A_2B_2 PHTHALOCYANINES: NOVEL ARCHETYPES FOR ANTICANCER AND ANTIMICROBIAL PHOTODYNAMIC THERAPY

SÍNTESIS, ESTUDIOS FOTOFÍSICOS Y DE AGREGACIÓN DE FTALOCIANINAS A_2B_2: NUEVOS ARQUETIPOS PARA TERAPIA FOTODINÁMICA ANTIMICROBIANA Y CONTRA EL CÁNCER

Autor: Miguel Ángel Revuelta Maza

Directores: Dra. Gema de la Torre Ponce and Prof. Tomás Torres Cebada

En esta tesis doctoral se han desarrollado nuevos fotosensibilizadores para su aplicación en terapia fotodinámica. Este tratamiento aplica luz del espectro visible, sobre una molécula fotosensible capaz de activar el oxígeno molecular presente en el entorno celular, produciendo especies activadas citotóxicas de oxígeno, como oxígeno singlete, capaces de inducir muerte celular. Concretamente se han preparado fotosensibilizadores de segunda generación de tipo porfirinoide basados en ftalocianinas de Zn(II) (Zn(II)Pcs). En concreto, en este trabajo hemos elegido como objetivo la preparación de Zn(II)Pcs formadas por dos tipos de isoindoles con diferente sustitución, denominadas comúnmente como A_2B_2, que pueden presentar dos variantes estructurales, es decir, ABAB y AABB. Estas geometrías altamente orientadas, permiten combinar sustituyentes hidrófobos e hidrófilos para dar lugar a anfífilos con la capacidad de interaccionar con medios lipófilos celulares así como facilitar el transporte en medios acuosos.

La Parte 1 de esta tesis doctoral está orientada a la preparación de Zn(II)Pcs ABAB. La síntesis en todos los casos está dirigida por el uso de un ftalonitrilo que presenta grupos voluminosos que impiden la formación de la especie AABB. Estos grupos voluminosos, además, poseen unidades fluoradas que dotan a la estructura final de unas características electrónicas peculiares. Esta particular sustitución, no solo evita fenómenos de agregación, unos de los principales factores limitantes del uso de macrociclos porfirinoides en terapia fotodinámica, sino que además potencia la capacidad de las ftalocianinas para producir especies reactivas de oxígeno, como oxígeno singlete. Hemos sido capaces de combinar este patrón de sustitución con sustituyentes hidrófilos formando anfífilos. La introducción de sustituyentes con cadenas de tipo polietilenglicol destruye eficientemente cultivos celulares *in vitro* de cáncer de piel y de cuello de útero,

y se ha demostrado cómo el patrón de sustitución ABAB es más efectivo que otros dentro de la misma familia (A_3B y A_4). Por otra parte, la incorporación de grupos funcionales cargados positivamente convierte estos compuestos en antimicrobianos frente S. aureus y E. coli.

En la Parte 2 de esta tesis doctoral se ha trabajado con Zn(II)Pcs de tipo AABB, las cuales se han preparado utilizando un conector binaftol que evita la formación de especies ABAB. En este caso el conectol binaftol presenta quiralidad por restricción conformacional, lo que ha permitido obtener Zn(II)Pcs quirales que pueden ser estudiadas y caracterizadas por dicroísmo circular. Este tipo de compuestos pueden presentar cierta capacidad de auto-ensamblaje dependiendo del medio elegido, y que está influida por el conector quiral. De nuevo la incorporación de sustituyentes hidrófilos permite la formación de especies anfifílicas, de tal forma que la organización inducida en medio acuoso ha dado lugar a la formación de nanoestructuras de tipo micelar o vesicular, mientras que en medios más apolares como puede ser el interior celular, se encuentran molecularmente disueltas. Concretamente se han preparado derivados AABB funcionalizados con cargas positivas, efectivos en la inactivación de bacterias Gram positivas y Gram negativas. Además, también se ha decorado el conector binaltol con cadenas de polietilenglicol y se ha hecho un estudio en profundidad de su capacidad de organización en medios polares como el agua.

INTRODUCTION

Index

1. Phthalocyanines

Phthalocyanines (Pcs) are aromatic macrocyclic compounds recognized as synthetic porphyrin (Por) analogues,[1–6] with similar structure to biologically crucial molecules such as chlorophyll and heme group of hemoglobin (Figure 1). The word '*phthalocyanine*' comes from their origin from phthalic anhydride (*phthalo*) and similarity in color to dark blue cyanine dyes (*cyanine*).[7]

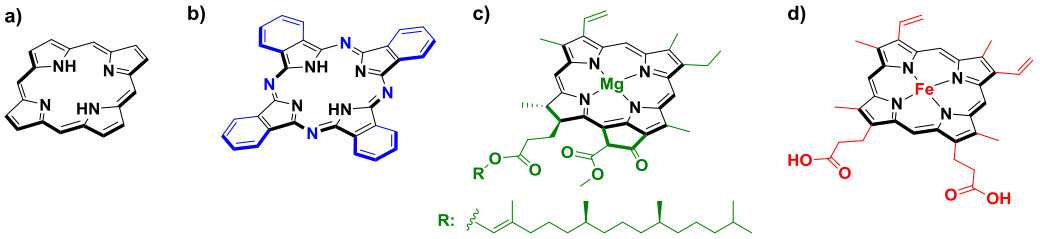

Figure 1. Structures of: a) Porphyrin; b) phthalocyanine; c) chlorophyll and d) heme group of hemoglobin.

1.1. History

Pcs were discovered accidentally more than a century ago, in 1907, when A.V. Braun and J. Tcherniac isolated a blue compound as a byproduct of the preparation of *o*-cyanobenzamide, later identified as the metal-free Pc (H_2Pc).[8] In 1927, the first Cu(II)Pc was prepared by H. de Diesbach and E. von der Weid while attempting to prepare phthalonitrile by heating *o*-dibromobenzene, cuprous cyanide and pyridine in a sealed tube.[9] In 1928, scientists at Scottish Dyes Ltd observed a greenish compound as a contaminant of phthalimide prepared from molten phthalic anhydride and ammonia, in an enameled cast-iron crucible that was chipped, the resulting greenish impurity being identified as Fe(II)Pc. Some experiments for replacing iron inside the Pc cavity by other metals were performed and, eventually, Scottish Dye Works patented the Cu(II)Pc in 1929.[10] It was only in the thirties that Linstead and Roberson determined the crystal structures of some H_2Pcs and MPcs, publishing the correct structure in 1934 at Imperial College.[11–14]

1.2. Structure

Pcs are planar heteroannulene macrocycles constituted by four isoindole units linked together through aza bridges at 1 and 3 positions, presenting an 18-π-electron aromatic internal cloud.[1,2,4] The 42 π-electrons of the Pc ring are distributed over 32 carbon and 8

nitrogen atoms, but the electronic delocalization mainly takes place at the inner ring that is constituted by 16 atoms and 18 π-electrons, with the outer benzene rings maintaining their electronic structure.[15] In Figure 2 the structures of both metal-free (H_2Pcs) and metallophthalocyanines (MPcs) are shown. The hydrogen atoms of the central cavity can be replaced by more than 70 different elements.[6] The internal and external positions of the fused benzene rings are also commonly known as α- and β-positions, respectively. Regarding the nomenclature, the systematic name of Pcs according to the IUPAC rules is tetrabenzol[b,g,l,q]-5,10,15,20-tetraazaporphyrin, where all C and N atoms of Pc are numbered, with the exception of C atoms that correspond to the fusion of pyrrole and benzene rings.[16]

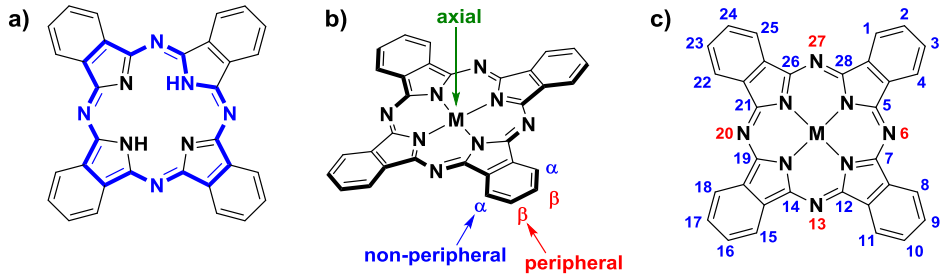

Figure 2. Structure of a) metal-free Pc with the main electron delocalization; b) MPc general structure (α: peripheral, β: non-peripheral and axial positions) and c) general numeration of MPcs.

One of the most outstanding properties of Pcs is their high thermal and chemical stability, which is an important requirement for most technological applications.[17] MPcs are usually stable at high temperatures and resist strong acids (i.e. concentrated H_2SO_4) or bases; notably, the most stable Pc derivatives are only decomposed by strong oxidizing agents, such as dichromate or ceric salts. Also, they show a great structural versatility that enables fine-tuning of the optical, electronical and aggregation properties. The functional groups attached to the peripheral positions of Pcs allow to modify their properties and have a deep impact on both electronic and chemical characteristics (e.g. solubility and aggregation). On the other hand, depending on the central metal incorporated in the Pc cavity, it is in some cases possible to further amplify the versatility of the macrocycles by incorporating different functional groups at axial positions of the central atom. This is the case for ruthenium (Ru(II)Pc), aluminium (Al(III)Pc), and silicon (Si(IV)Pc), among others (Figure 3). For silicon and aluminium Pcs, the axial substituents are covalently linked to the central atom,[18,19] while for ruthenium Pcs bearing *N*-containing ligands the bond is supramolecular in nature.[20] When the central metal allows the conjugation of two axial ligands, symmetrically and asymmetrically substituted Pcs can be obtained in a statistical manner.

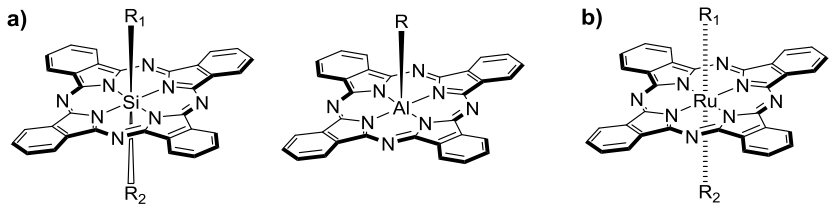

Figure 3. Axially substituted Pcs: a) Si(IV)Pc and Al(III)Pc (where R = alkoxy, phenoxy, silyloxy); b) Ru(II)Pc where R= N-containing ligands or CO.

Owing to their inherent structure and extended conjugation, Pcs exhibit a high aggregation tendency in solution, as a consequence of the π-π interactions between macrocycles and solvophobic effects, forming dimers, trimers and higher oligomers.[21] The aggregation state has a strong influence on their photochemical and photophysical properties,[22,23] but it can be reduced or avoided by using coordinating solvents and/or by introducing bulky substituents at the axial and/or peripheral positions of the macrocycle. In addition, the rich redox chemistry of Pcs can be also tuned by introduction of different metal centers in the inner cavity, or peripheral, non-peripheral, and axial substituents.

The structure of the Pc can also be modified, giving rise to several analogues (Figure 4)[24–29] via atom substitution;[30] extension or reduction of the aromatic system;[26,31] variation in the number of isoindole units;[28,32] and formation of covalent dimers or oligomers.[27,33,34] All these modifications have a strong impact on the electronic features of the macrocycles. From all these analogues, the most relevant are the subphthalocyanines (SubPcs), lower Pc homologues consisting of three isoindole units linked through aza bridges with boron in their central cavity, which is coordinated by three nitrogen atoms of the macrocycle and one axial substituent.[35,36]

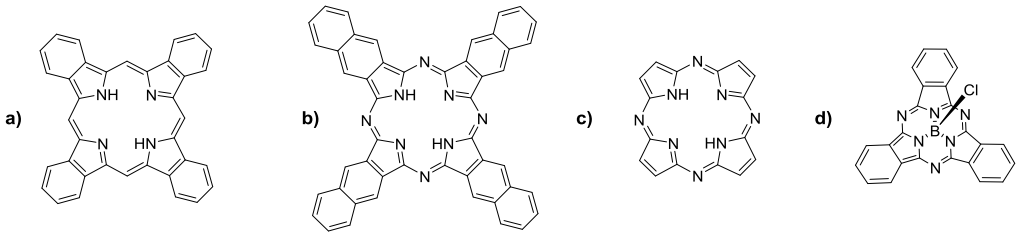

Figure 4. Phthalocyanine analogues: a) Tetrabenzoporphyrin; b) 2,3-naphthalocyanine; c) porphyrazine; d) subphthalocyanine.

1.3. Spectroscopic characteristics

The heteroaromatic delocalized π-electron system of Pcs, that is 18 π-electrons over the inner 16 atoms of the macrocycle, defines their optical characteristics, namely, high

optical stability, and absorption of radiation corresponding to visible light. The electronic absorption spectrum of Pcs (Figure 5) presents two main regions, the *Q*-band and the Soret/*B*-band, both corresponding to π→π* transitions. The *Q*-band, centered in the visible region in the range between 620-720 nm, is a quite intense absorption with molar absorption coefficients (ε) in the order of 10^5 $M^{-1}\cdot cm^{-1}$. It derives from the transition from the ground state of a_{1g} symmetry to the first excited state of e_u symmetry (HOMO-LUMO transition). The position and shape of this band is responsible for the characteristic blue/green colour of these compounds. The *B*-band is a broad and low intense band around 350 nm, with typical ε in the order of 10^4 $M^{-1}\cdot cm^{-1}$, and it is related to π→π* transitions from lower-energy molecular orbitals, namely (HOMO-1)-LUMO transitions.

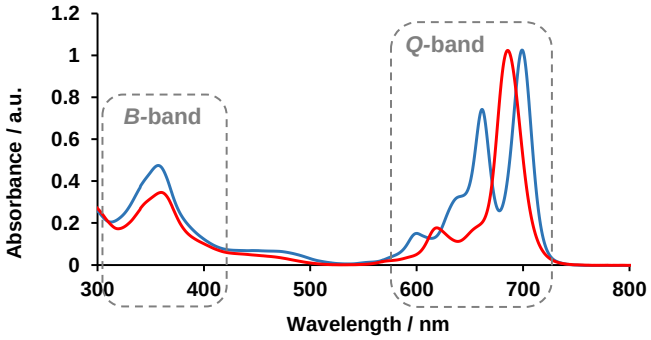

Figure 5. UV-vis spectra of a metal free Pc (blue) and a Zn(II)Pc (red).

The central metal, the presence of axial ligands, solvent, (non-)peripheral substitution, and the extension of the conjugation are the main factors that are able to change the shape and position of the absorption bands of Pcs, (particularly the *Q*-band). For example, while metal-free Pcs have a D_{2h} symmetry with a *Q*-band split into two main absorptions due to their double degenerated LUMO, metallation imposes a D_{4h} symmetry where the LUMO level is fully degenerated, and so MPcs show a unique *Q*-band in their absorption spectrum corresponding to a single HOMO-LUMO transition. The introduction of metal ions inside the Pc cavity, which reduce the electron density of the Pc, generates also a slight blue shift of the *Q*-band. In fact, the more electronegative the metal ion is, the more the *Q*-band is blue-shifted.[37] Modulating the electronic properties of porphyrinoids constitutes a voyage from the violet to the infrared regions of the electromagnetic spectrum (Figure 6).[38]

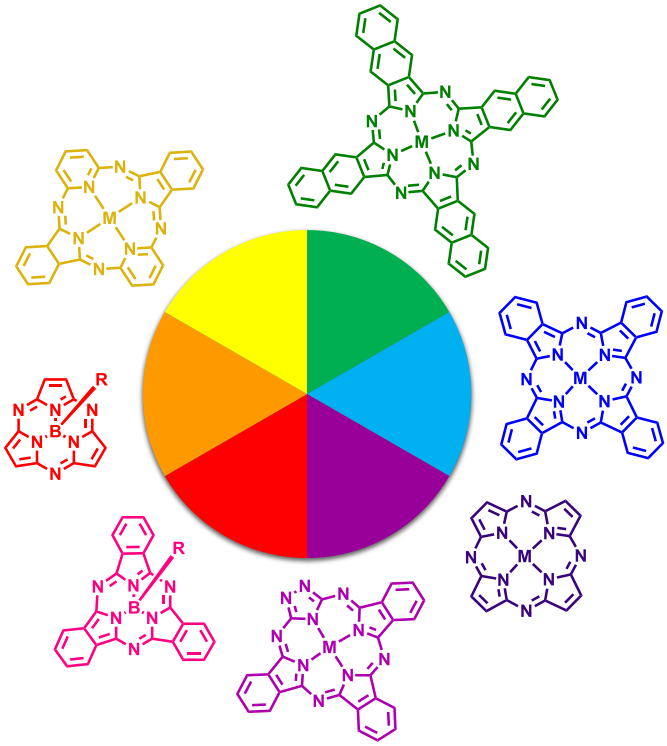

Figure 6. Variation of porphyrinoids color from red to violet, depending on their electronic structure.

Other photophysical properties like fluorescence, triplet excited state generation and phosphorescence, are also strongly influenced by the presence and nature of the central atom.[38–40] For example, the characteristic emission of fluorescence from the singlet excited state S_1, shows a strong dependence on the metal ion coordinated in the center of the macrocycle. For instance, H_2Pcs generally display higher fluorescence quantum yields when compared with the corresponding Zn(II)Pcs, due to the heavy-metal effect of Zn.[41] The heavy atom effect results from the enhanced spin-orbit coupling between the d-orbitals of the metal ion and the π-system of the macrocycle. Therefore, such MPcs exhibit a greater tendency to undergo intersystem crossing (ISC) from the singlet excited state S_1 to the triplet excited state T_1 as the central atom mass increases, which is reflected by high triplet state quantum yields.[21,40,42,43]

1.4. Synthesis

Synthesis of Pcs is traditionally based on cyclotetramerization reactions of 1,2–dicyanobenzenes,[44] but also a variety of *ortho*-phthalic acid derivatives (i.e. anhydrides, imides and amides) can be used (Scheme 1). Pc precursors can be mono, di-, tri- or

tetrafunctionalized, depending on the desired number of functional groups in the final Pc. The two most important synthetic pathways for the preparation of substituted phthalonitriles are the direct cyanation of *ortho*-dihalide benzenes catalyzed by Cu or Pd,[45] and the phthalic acid transformation (i.e. the so-called 'acidic' route involving the acid – anhydride – imide – amide – nitrile sequence). Classically, MPcs have been prepared heating a mixture of the corresponding precursors together with a metal salt in a high boiling point solvent (1-pentanol, 2-dimethylaminoethanol (DMAE), DMF, *ortho*-dichlorobenzene (*o*-DCB)). When phthalonitriles are used as starting materials, this metal-templated reaction requires also a basic catalyst that, in the presence of an alcohol such as DMAE or 1-pentanol, generates an alkoxide that triggers the macrocyclization. One of the most widely employed basic catalyst is 1,8-diazabicyclo[5.4.0]undec-7-ene (DBU).

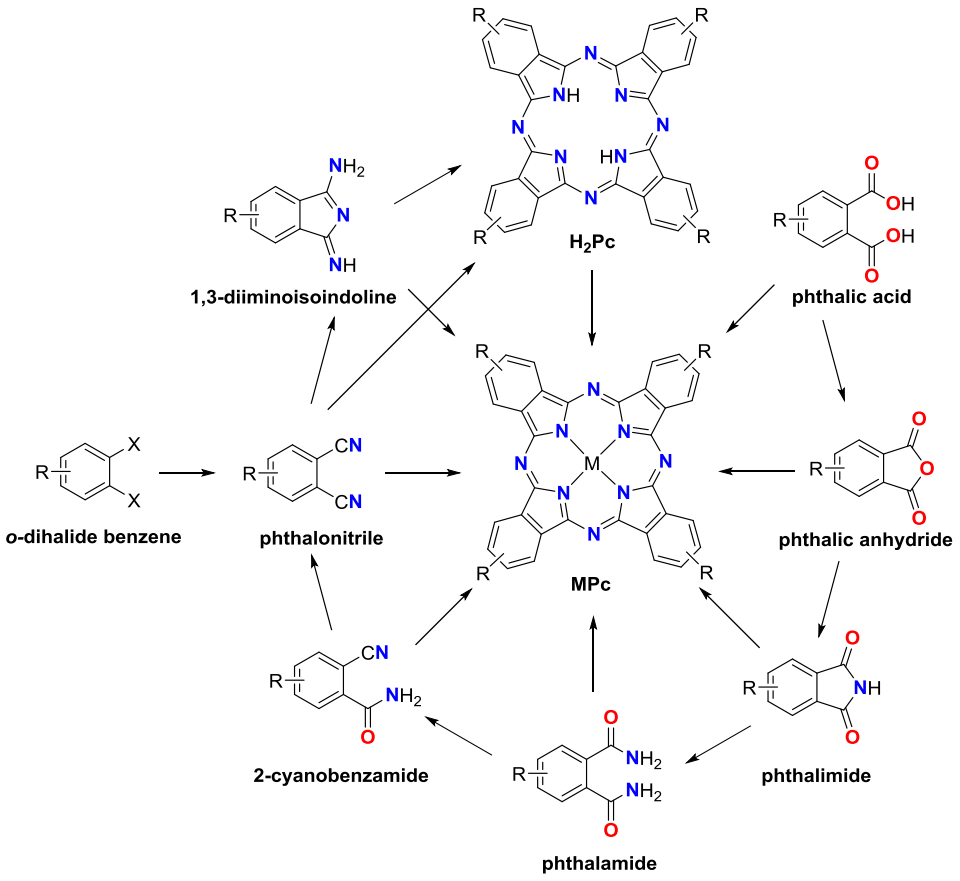

Scheme 1. Synthesis of phthalonitrile derivatives and symmetrically substituted Pcs.

To obtain metal free-Pcs, activated phthalonitrile derivatives such as 1,3-diiminoisoindolines can be used as starting materials in the absence of metal salts, but

they can be also obtained from the reaction of phthalonitriles with lithium alkoxides, which yields lithium Pcs that can be converted into the corresponding free base by treatment with a mineral acid.[46] In turn, the treatment of metal free Pcs with a metal salt produces the corresponding metallic Pc. More recently, various new methods to prepare Pcs in high yields and under rather mild conditions have been described, for instance, the treatment of phthalimides, phthalic anhydrides and phthalonitriles with metal salts and hexamethyldisilazane (HMDS) in DMF,[47,48] the double addition of oximes to phthalonitriles,[49] and microwave-assisted protocols.[50]

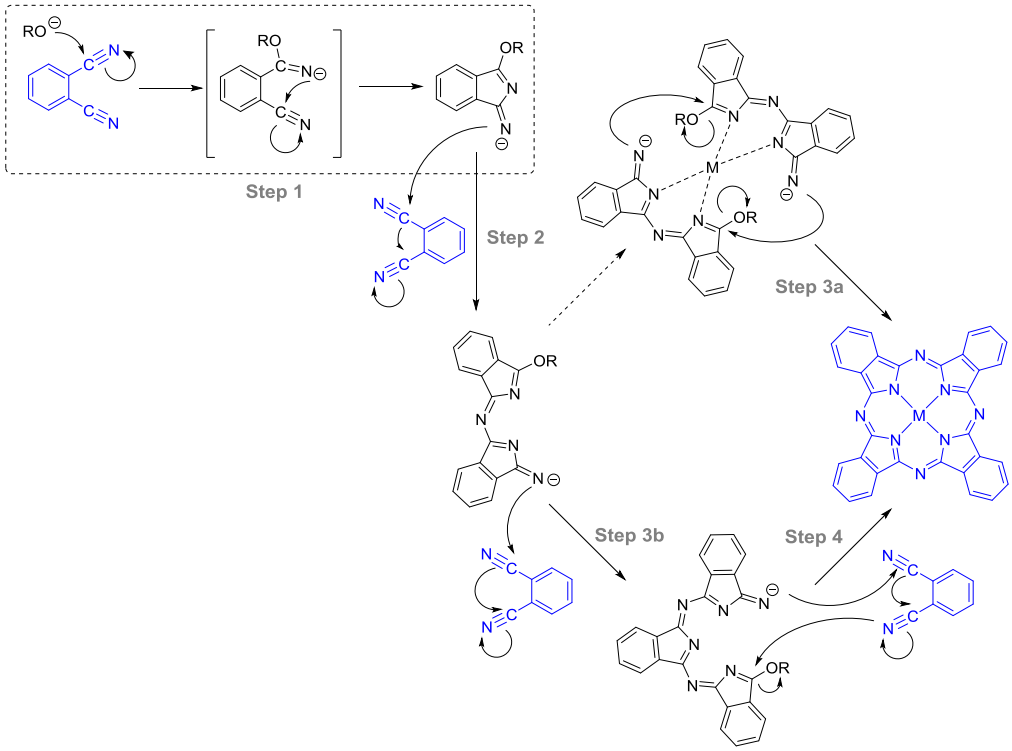

Scheme 2. Proposed mechanism for the synthesis of MPcs by cyclotetramerization of phthalonitriles by the metal templated method.

As mentioned above, the cyclotetramerization reactions are usually performed in high boiling point alcohols,[51,52] which, according to the mechanism proposed by S. W. Oliver and T. D. Smith (Scheme 2),[53] are responsible for the initiation of the reaction. In this way, when the reaction takes place in the presence of sodium or lithium alkoxides, the macrocyclization starts with the formation of 1-imido-3-alkoxyindoline corresponding salt (Step 1). This intermediate will attack as nucleophile to the nitrile group of a second phthalonitrile molecule (Step 2). The resulting dimer can either undergo self-condensation with another dimer (Step 3a), or react with a third (Step 3b) and a fourth phthalonitrile molecules (Step 4) in the same way, both steps mediated by the metallic

cation acting as template. Another possibility consists in the metal-mediated formation of the Pc ring, where a transition metal cation acts as a template to which the reacting phthalonitriles coordinate during the macrocyclization.[54]

1.5. Properties and applications

Since their first synthesis at the beginning of the last century, Pcs are an important industrial commodity, blue and green dyestuff, used primarily in inks (especially ballpoint pens), coloring for plastics or metallic surfaces, and dyes for clothing. The unique properties of Pcs, such as high optical stability, semiconductivity and excellent photophysical properties, have widen their possible applications, and therefore, their commercial utility.[17,55] Their chemical versatility makes this class of compounds applicable in different fields, ranging from nanotechnology and material science, to medicine.[17,56–58] The high extinction coefficients in the visible and near IR regions exhibited by Pcs, together to their n-type conductivities in the range of 10^{-4}-10^{-2} $\Omega^{-1}\cdot cm^{-1}$,[59] have encouraged their use in organic photovoltaics (OPV),[56] organic solar cells,[60] perovskite solar cells,[61] dye-sensitized solar cells (DSSC),[39,62,63] organic light emitting devices (OLEDs)[64] and organic thin-film transistors (OTFTs).[65] Pcs have also potential use as chemical sensors, taking advantage of the variations in their semiconducting properties produced by the interaction with different gasses (ammonia, nitrogen monoxide and dioxide, and carbon monoxide).[66,67] They have been also employed in electrochromic devices,[68] electro- and photocatalysis,[69] and as single-molecule magnets.[70] Pcs have also been widely studied as non-linear optical (NLO) materials by taking advantage of their extended two-dimensional π-electron delocalization,[71] and for liquid crystal color display applications.[72,73]

This class of molecules has attracted also great interest over the past two decades in the area of photodynamic therapy (PDT) due to their favorable photophysical and photochemical properties. In fact, this application is one of the final objectives of the present thesis and will be developed in further sections. Moreover, the ability of Pcs to produce singlet oxygen is also being used for photocatalytic degradation of pollutants[74] and catalytic oxidation in several processes.[75]

1.6. Unsimetrically substituted phthalocyanines

When using 3- or 4-substituted phthalonitriles as starting materials, the resulting tetrasubstituted Pcs are obtained as mixture of four structural isomers with C_{4h}, D_{2h}, C_{2v} and C_s symmetries (Figure 7).[4] These regioisomers sometimes can be obtained separately employing a regioselective approach,[76–78] and in some exceptional cases can be separated by chromatographic techniques.[79,80] This situation is solved by using 3,6- or 4,5-disubstituted phthalonitriles, which yield only one isomer of the corresponding

octasubstituted Pc. However, even when the Pc is constituted by a mixture of regioisomers, A_4 Pcs will be mentioned in this text as 'symmetric' whenever the four isoindole units have the same substitution pattern.

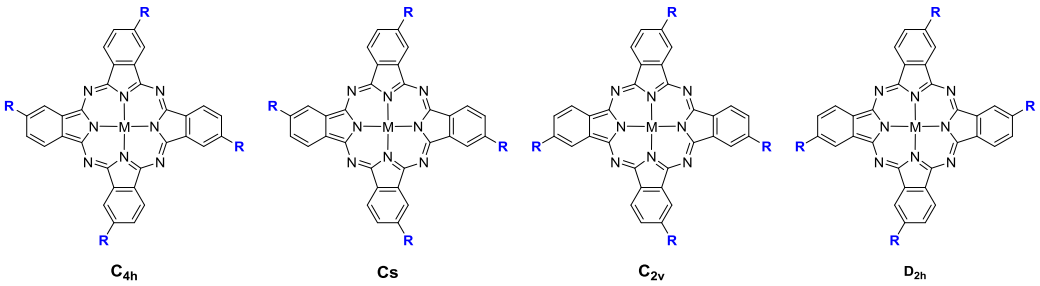

Figure 7. Constitutional isomers for A_4 tetrasubstituted Pcs.

Because of the numerous regioisomers that can be obtained from monosustituted phthalonitriles, the condensed structural formulae notation (type I, Figure 8) is most often too complex to be fully detailed. For this reason, the type II notation, though not formal, is often preferred to type I for the sake of clarity, and will be used in the thesis when necessary.

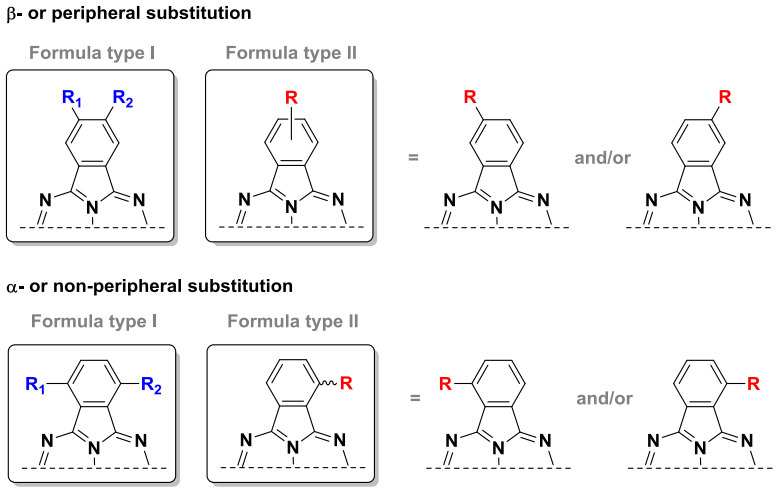

Figure 8. Condensed and simplified structural formula used for Pcs having α- and/or β-monosubstitution pattern at their isoindole units.[63]

From now, we will talk about unsymmetrically substituted Pcs when the isoindole units are differently functionalized (commonly notated as isoindoles A and B), independently of the presence of regioisomers. In this way, when using more than one different

precursor in the synthesis, the library of possible Pcs is amplified, and differently substituted systems are obtained in a statistical manner. The synthesis of unsymmetrically substituted Pcs is more difficult than the synthesis of their symmetric analogues from a statistical point of view. Even so, several synthetic approaches towards unsymmetric Pcs and their analogues have been developed.[81] First of all, the most widely employed strategy is the statistical condensation of two differently functionalized phthalonitriles, also called A and B, to produce a family of Pcs (Figure 9)[82,83] that will be separated by column chromatography.

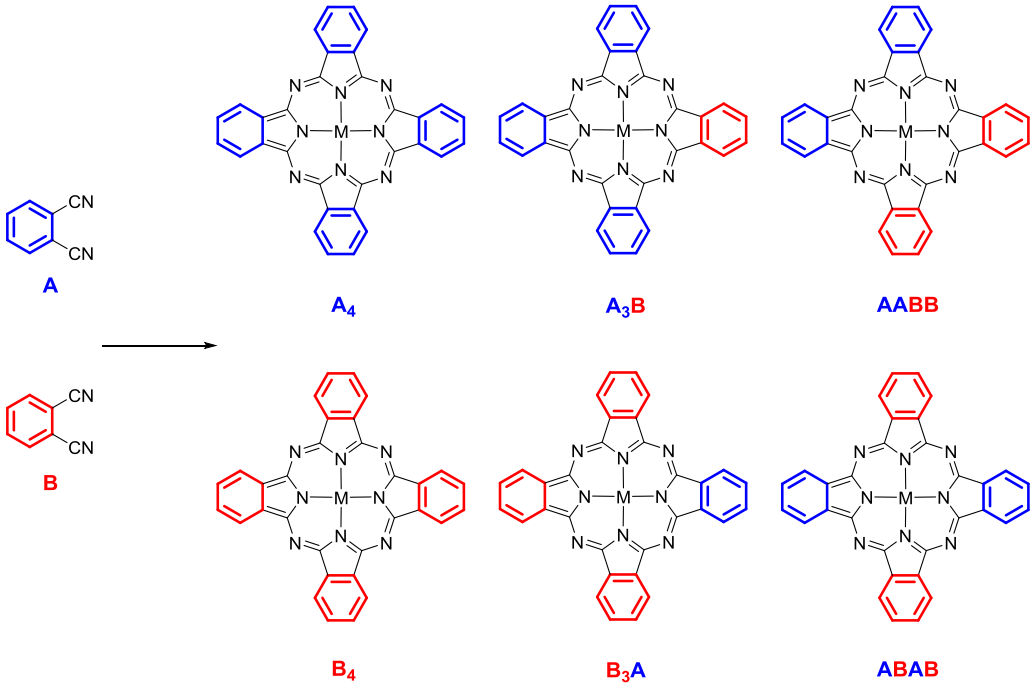

Figure 9. Mixture of Pcs obtained via statistical cyclotetramerization of two differently functionalized phthalonitriles A and B.

a) A_3B Phthalocyanines

The statistical cyclotetramerization is the most common approach to prepare A_3B Pcs, since the reaction can be directed towards the target compound by using a relatively large excess of one of the precursors (from 3:1 to 9:1 relative ratios). Controlling the stoichiometry of the phthalonitriles leads in many cases to the nearly exclusive formation of both the symmetric A_4 Pc from the most abundant precursor A, and the A_3B derivative. Some factors, such as the steric effect of the substituents or the relative reactivity of the different phthalonitriles, can also increase the yield of the desired product and facilitate its isolation. On the other hand, some chemoselective techniques for the synthesis of A_3B

Pcs have been described in the literature, but they present a great number of limitations. Therefore, A_3B Pcs can be obtained by applying the so-called Kobayashi ring expansion reaction of SubPcs.[84] The method involves treatment of a SubPc with a succinimide or a 1,3-diiminoisoindoline derivative,[85,86] but it is only compatible with certain functional groups and inefficient in terms of yield and atom economy.[85,87] Another approach for the selective preparation of A_3B Pcs is the solid-phase synthesis mainly developed by Leznoff,[88,89] which involves the linkage of one phthalonitrile precursor to a polymeric support through a cleavable linker, followed by the reaction with an excess of a second phthalonitrile in solution.[88]

Our group has strongly contributed to the synthesis of outstanding A_3B Pc derivatives for the preparation of multicomponent systems, mainly devoted to achieve materials with photoinduced charge-separation abilities.[2,90–92] The Zn(II)Pc coded as **TT1** (see Figure 10a) is a representative example of the A_3B Pcs prepared in the group. This molecules is endowed with a carboxy group as reactive or anchoring functional group, and *tert*-butyl chains in the other three isoindole units that minimize the formation of molecular aggregates and increase the solubility in organic solvents. **TT1** has been used in PDT for atherosclerotic plaques,[93] but also linked to TiO_2 for the preparation of DSSC devices.[94,95] In this context, many other Zn(II)Pcs with A_3B geometry have been also successfully implemented in DSSCs (Figure 10b).[63,96] A_3B Pcs have been also linked to carbon-based nanomaterials such as fullerene, graphene and carbon nanotubes.[90,92] In this regard, Figure 10c shows a recent example of an amphiphilic, water-soluble A_3B Zn(II)Pc, which is able to exfoliate graphene in polar media.[97]

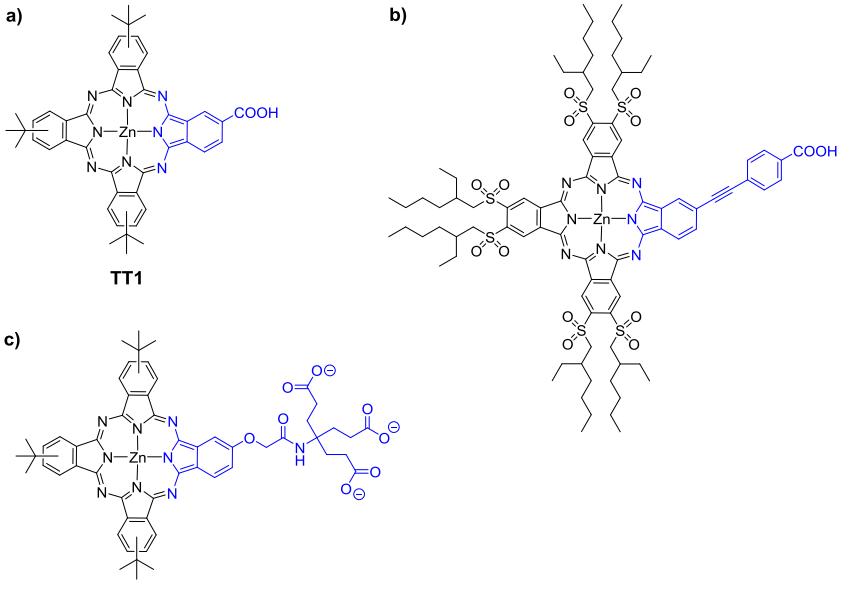

Figure 10. Examples of A_3B Zn(II)Pcs.

b) A_2B_2 Phthalocyanines

The synthesis of A_2B_2 Pcs has proved more challenging that of their A_3B counterparts. A_2B_2 Zn(II)Pcs present two different constitutional isomers, namely ABAB and AABB, which are quite difficult to separate by chromatographic techniques, although possible in some sporadic cases.[98,99] To avoid their tedious isolation, sometimes the so-called directed approach is employed to selectively obtain only one of the constitutional isomers of the A_2B_2 type.

i. *ABAB Phthalocyanines*

In 1978 Idelson reported a patent from Polaroid Corporation,[100] in which developed a new methodology to synthesize ABAB porphyrazines, that can be considered as ABAB Pc derivatives. This process was a crossed-condensation between two different precursors in which six of the eight nitrogen at the inner perimeter of the Pc can only be provided by one of them. Specifically, they patented a reaction between an amino/imino- and a trihalo-pyrroline in the presence of an acid acceptor and a hydrogen donor. Lever and Leznoff,[101] and Shirai and coworkers,[102] used this reaction in an academic setting (Scheme 3) and applied it to the synthesis of ABAB Pcs. They performed a cross condensation between 1,3-diiminoisoindoline and thiophthalimide, which is unable to self-condense. The reaction was performed at low temperature to avoid also the self-condensation of 1,3-diiminoisoindoline and favor the crossed-condensation between them, which occurs faster thanks to the marked electrophilic character of the reactive thiocarbonyl group.

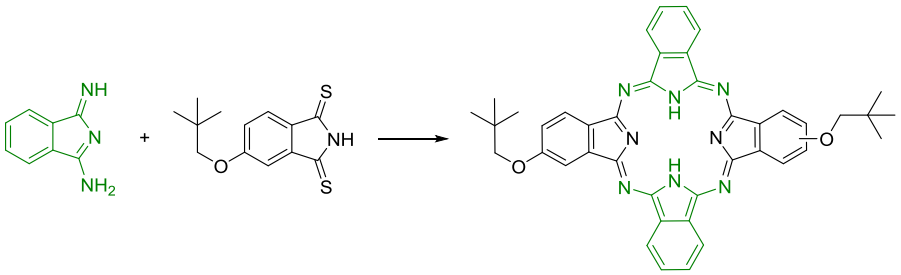

Scheme 3. Selective synthesis of ABAB Pc via cross-condensation between thiopthalimide and 1,3-isoindolediimine.

1,3,3-trichloroisoindolenine can perform as precursor, playing the same role than thiopthalimides. This reaction was discovered in 1990 by Young and Onyebuagu as a reductive coupling process using a base as reducing agent. The ABAB derivatives was obtained in very good yield, around 50%,[103] (Scheme 4a) although in other examples the A_3B product was also detected.[104] Unfortunately this method shows low tolerance to many functional groups and the synthetic routes to prepare the precursors are

difficult.[105,106] This is the reason why the method has only rarely been utilized in the literature, despite its unquestionable selectivity. Some specific examples of its application are: i) the work of Bretonnière and coworkers depicted in Scheme 4b;[107,108] ii) the publication by Youngblood in 2006 that describes an ABAB Zn(II)Pc building block for the preparation of rodlike Pc polymers (Scheme 4c);[105] and iii) the work reported by Hanack and coworkers, who prepared oxygen-bridged bicyclic ABAB Pcs (Scheme 4d) for their use in cycloaddition reactions,[104] towards the preparation of ladder-type oligomers.[109]

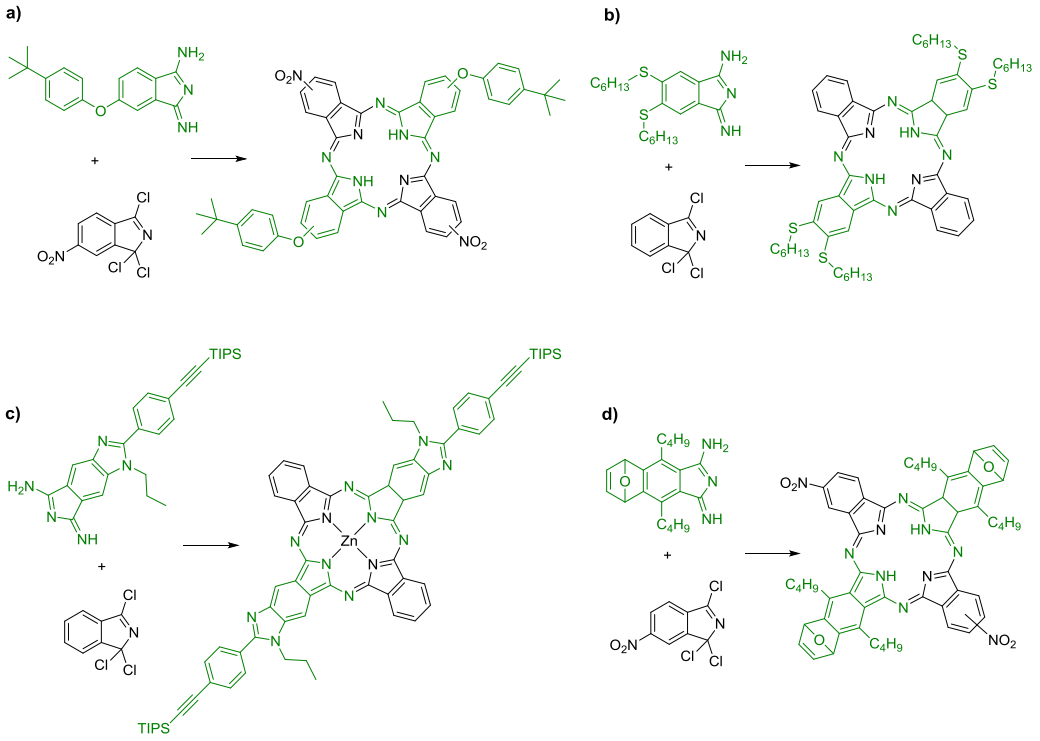

Scheme 4. Synthesis of ABAB Pcs from 1,3,3-trichloro-6-nitroisoindolenine and 1,3-diiminoisoindoline.

Particularly appealing is the possibility to create complex linear arrangements, such as Pc-containing polymers, thanks to the selective preparation of the D_{2h} ABAB geometry. In this regard, Swager's group prepared a highly conductive Pc-containing hybrid polymer that exhibited both metal-centered electroactivity as well as high conductivity (Figure 11a).[110] Yu and coworkers described the synthesis and physical study of several new photorefractive polymers, which are poly(phenylenevinylene)s copolymerized with a small amount of macrocyclic of an ABAB Zn(II)Pc (Figure 11b).[111]

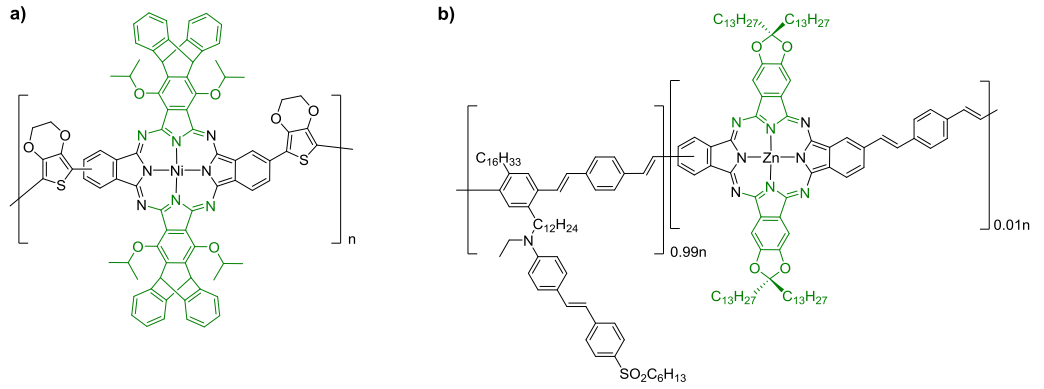

Figure 11. a) Macrocycle-linked MPc polymer; b) Poly(phenylenevinylenes) copolymerized with a small amount of ABAB Zn(II)Pc.

The most successful and extended methodology for ABAB Pc synthesis lies in the use of phthalonitriles with bulky substituents at the α-positions with equimolar amounts of other non-hindered phthalonitrile derivative in the presence of a transition metal salt. This methodology has been used to prepare ABAB Pcs (Scheme 5a) and related structural isomers of Pcs such as naphthalene-fused tetraazaporphyrins (Scheme 5b and c).[26,112–114] The hindered self-condensation of the bulky phthalonitrile (B) minimize the formation of AABB and AB_3 compounds, and the impeded aggregation capabilities of the macrocycles facilitates the chromatographic separation.

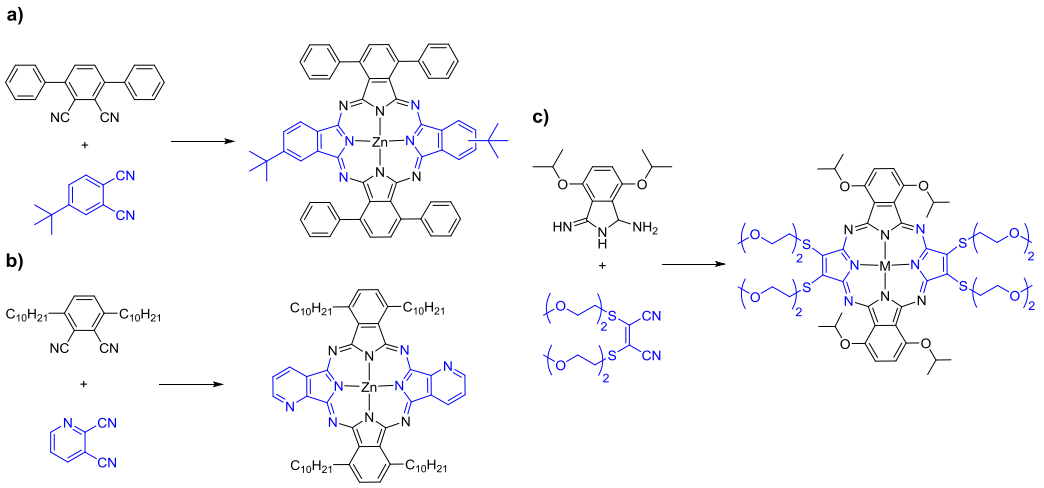

Scheme 5. Synthesis of ABAB derivatives from 3,6-substituted phthalonitriles.

ii. *AABB Phthalocyanines*

The first example on the selective preparation of AABB Pcs was reported by Leznoff and coworkers via the so-called lithium method, which involves the use of an anionic half-Pc intermediate stabilized by a lithium cation. This species, usually obtained from phthalonitriles bearing electron-withdrawing groups, can be isolated and treated with a second phthalonitrile together with a transition metal salt under soft conditions to generate the final Pc (Scheme 6a).[115] Kobayashi's group refined this method using bulky 3,6-diphenylphthalonitrile, which avoid the formation of the A_4 Pc because it is disfavored by the steric hindrance between neighboring peripheral substituents. Then, reaction with a second dinitrile resulted in the selective synthesis of the AABB targeted compound (Scheme 6b).[116,117]

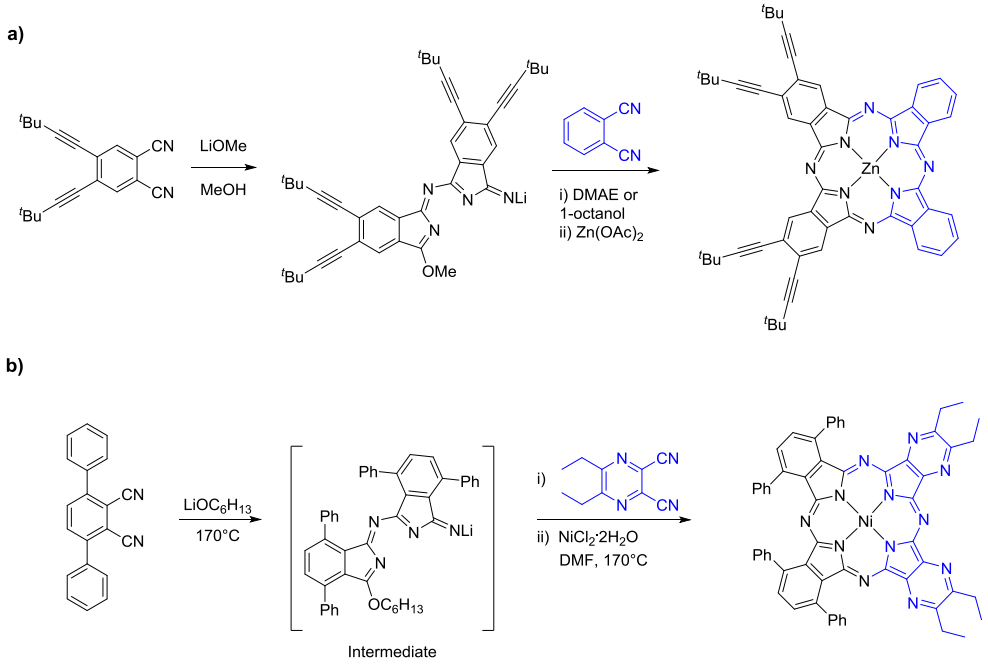

Scheme 6. a) Leznoff's selective synthesis of AABB Pcs; and b) Kobayashi's approach.

Kobayashi and coworkers described also the exclusive formation of a D_{2h} symmetrical $(AA)_2$ Pc by linking two phthalonitriles at their 4-position with proper rigid spacers. Moreover, they incorporated chirality to the system using an optically active binaphthyl-based linker (Figure 12a).[77] This strategy was reproduced by Leznoff and coworkers using a phthalonitrile dimer endowed with a propan-1,3-diol bridge (Figure 12b).[118,119]

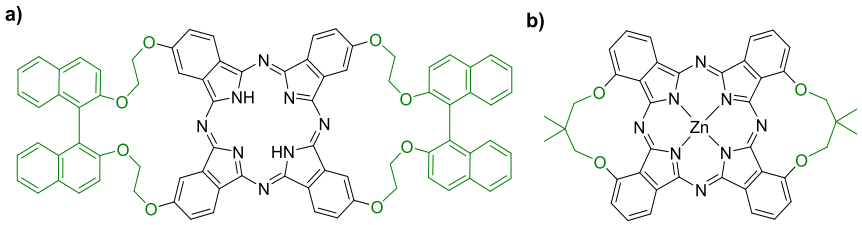

Figure 12. Structures of D_{2h} $(AA)_2$ Pcs.

Following the latter approach, that is the use of bisphthalonitriles linked through rigid spacers, a number of AABB derivatives with C_{2v} symmetry, also called *adjacent-type* Pc derivatives, have been synthesized. For instance, Kobayashi's group prepared a series of adjacent Co(II)Pc derivatives with varying number of fused benzene rings (Figure 13a).[26] They also prepared low-symmetry adjacent-type chiral MPcs endowed with branched alkyl chains that shows interesting self-organization properties, giving rise to liquid-crystalline, one dimensional columnar aggregates (Figure 13b).[120]

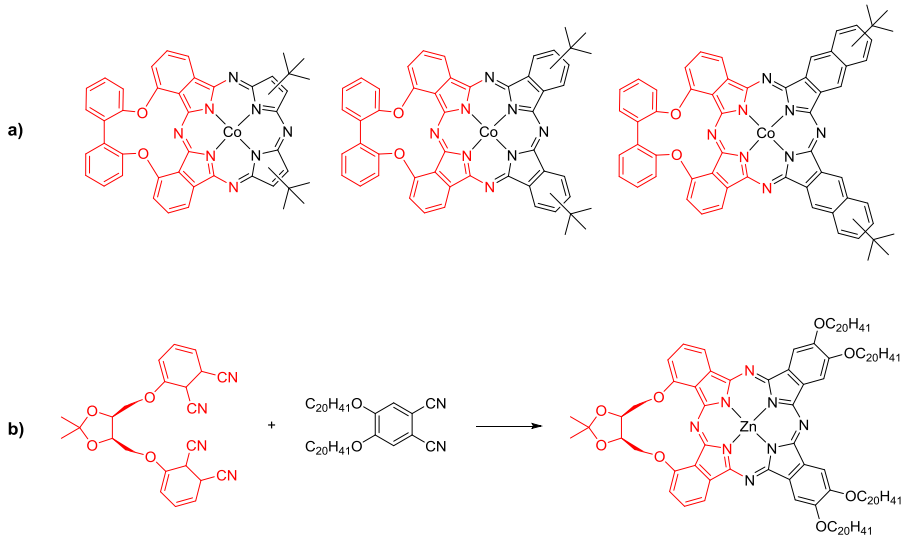

Figure 13. a) Adjacently substituted Co(II)Pc derivatives. b) Adjacent-type MPc having branched alkyl chains.

The use of bisphthalonitriles linked by constrained binding groups such as 2,29-dihydroxy-1,19-binaphthyl leads to optically active adjacent Pcs, thanks to the intrinsic atropoisomerism of the binaphtol subunit. An important feature of these bisphthalonitriles is that the binaphthol unit does not racemize under the harsh Pc synthesis conditions, because of the large steric hindrance provided by the presence of the two bulky dicyanophenoxy groups. In addition, since the distance between the two phenoxy groups

is close to the minimum to link two adjacent benzene rings in the corresponding Pc, the formation of oligomeric Pcs is suppressed. Those AABB Pcs have been synthesized in good yields in a mixed condensation with a second diminoisoindole derivative, together with the full-symmetric $(AA)_2$ Pc with two binaphtol units (Scheme 7).[121,122]

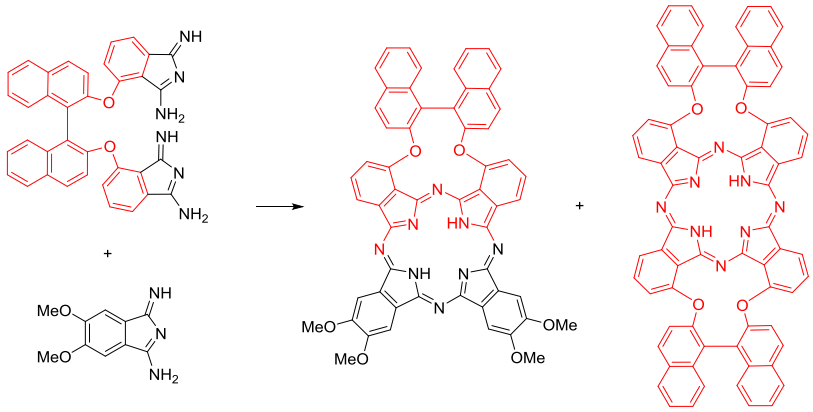

Scheme 7. Example of synthesis of AABB and $(AA)_2$ Pcs with binaphthol linkers.

One of the main advantages of Pcs with optically active binaphthyl units is that they can be spectroscopically investigated not only by absorption and emission assays, but also by circular dichroism (CD), and magnetic circular dichroism (MCD). The chiral substituents induce CD in the in-plane polarized *Q*- and Soret-bands of Pcs and, therefore, Pcs having R and S binaphthyl units show positive and negative CD, respectively.[123]

2. Photodynamic Therapy

In Section 1 of this Introduction we have discussed general concepts on phthalocyanine chemistry. In this second section we are going to focus on one of the main applications mentioned: Photodynamic Therapy.

2.1. Principles and applications

a) General concepts

The word "photodynamic" (in Greek, 'photo': light, and 'dynamo': power) refers to the energy of light as its etymology discloses. Photodynamic therapy is a promising and non-invasive form of phototherapy, using non-toxic light-sensitive compounds, called photosensitizers or photosensitizing agents (PS), which when exposed selectively to harmless visible light, become toxic to targeted diseased cells or microorganisms. Light activates the PS, which can transfer its energy to surrounding oxygen, thus resulting in the formation of reactive cytotoxic oxygen species (ROS) as e.g. singlet oxygen ($^1O_2$) that ultimately lead to an effective cell ablation.[124] This ROS triggers a phototoxic cascade, leading to cell death through apoptosis or necrosis.[125,126] In the last century, PDT is becoming widely recognized as a valuable treatment option for localized cancers and other diseased tissues, since this methodology allows for the minimally invasive, selective and localized destruction of tumor cells with reduced side effects and toxicity.[127] PDT has the advantage of selectivity, the PS can be targeted for selective accumulation in the tumor tissue, and light can be delivered only to the target area, preventing the side effects of classic systemic therapies by reducing the damage to healthy cells.[128] PDT includes the possibility to be combined with other therapies such as surgery and/or radiotherapy, and it is non-immunosuppressive.[129] This therapy was the first example of a drug-device combination approved by Food and Drug Administration (FDA),[130,131] which happened in 1993 for the use of PS Photofrin® in the prophylactic treatment of bladder cancer. After that, a large number of PS were developed and PDT was extended to other diseases.

b) Applications of PDT

Photodynamic therapy has numerous applications, which can be divided into three main fields: the photodynamic treatment of cancer, frequently referred as PDT, other non-oncological diseases, and the photodynamic inactivation of microorganisms, known as PDI.

Regarding to oncology,[132] it has been used in various branches, such as dermatology, brain malignancies, thoracic oncology, pancreatic cancer, esophageal cancer, bladder cancer, etc.[133] On the other hand, various non-oncological pathologies that go beyond the cancer malignancies can be treated with PDT, for instance, age-related macular degeneration in ophthalmology,[134] or cardiovascular diseases and atherosclerosis[135]. Photodynamic therapy has also proven ability to kill insects, parasites, and microbial cells, including bacteria, yeast, fungi, parasitic protozoa and viruses.[136,137] It has been also useful in the treatment of herpes lesions, papillomatosis, wound infections, psoriasis, acne vulgaris, superficial fungal infections of the skin and infections by Helicobacter pylori.[138,139] Authors in literature refer to the treatment as photodynamic inactivation (PDI), antimicrobial PDT (aPDT) or photodynamic antimicrobial chemotherapy (PACT). PDI has already proven its efficacy against both antibiotic-resistant and non-resistant pathogens.[140] Drug treatment and PDI are compatible since both therapies work through entirely different mechanisms. On the other hand, one of the most successful application of PDI has been in dentistry,[141] with two commercialized products (Periowave® and SaveDents®), and plays a notorious role in environmental protection in photodecomposition of pollutants through photocatalytic reactions.[142]

2.2. Active key components in PDT

PDT involves three main components: light of a specific wavelength, a PS and the presence of molecular oxygen ($^3O_2$). Only when these components are combined together, they become toxic to targeted cells.

a) Light: delivery and sources

PDT requires that sufficient light reaches the target tissue,[143,144] which is directly related with the presence of macrobiomolecules, organized cell structures and interstitial layers that make biological media turbid and inhomogeneous. For this reason, it is very important to understand how light travels through tissues, suffering either absorption or scattering processes that lead to refraction and widening of the light beam, causing changes of directionality and loss of the fluence rate. Endogenous absorption by tissue components, (e.g. nucleic acids, amino acids, etc.), affords a drastic decrease of intensity and diffusion depth of light penetration, which reduces the penetration capacity of light with wavelength <550 nm (Figure 14, left). Thus, PS absorbing light of wavelength below 700 nm are not ideal due to the presence of the endogenous light absorbers, such as oxyhemoglobin (HbO_2), deoxyhemoglobin (Hb), bilirubin and melanin. The light depth of penetration doubles from 550 to 630 nm (1-3 mm), doubles again going up to 700 nm, and a 10% increasing is observed when moving towards 800 nm. PS should not have absorption maxima at wavelengths longer than 850 nm, since such absorptions generate triplet excited states without sufficient energy to excite molecular oxygen to produce $^1O_2$

and other ROS.[145] Moreover, absorption by water and hemoglobin accounts for the low penetration of light with wavelengths above 850 nm. These facts result in an optical therapeutic window for PDT in the range from 650-850 nm (Figure 14, right),[146] which represents the range of wavelengths where light has its maximum depth of penetration in tissues.[147] Therefore, it is of high importance the development of PS able to absorb light in the phototherapeutic window in order to be effective for treatment of deeper localized tumors.[148]

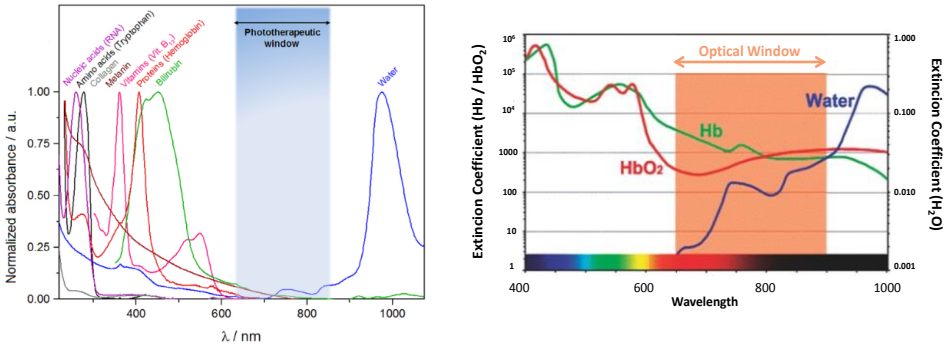

Figure 14. (Left) Phototherapeutic window: the spectral range of visible and NIR light (650–850 nm) characterized by a high penetration depth into human tissues.[148] (Right) Hemoglobin and tissue water absorb light over a broad spectral regime, creating an optical window (650-900 nm), which represents an optimal trade-off between image resolution and tissue penetration for in vivo imaging and PDT.[146]

The success of PDT relies as well in the light source that is applied to activate the PS. The increased light penetration depth at higher wavelengths is the major incentive for the development of new PS and light sources, however no single light source is ideal for all PDT applications. In general, the light source must exhibit a suitable spectral match that coincides with the maximum absorption of the PS, and the clinical efficacy of the treatment depends on total light dose, exposure time, delivery mode, and fluence rate. Non-laser sources include tungsten filament, xenon arc, metal halide, and fluorescent lamps. However, in recent times, diode lasers have been introduced as a cheap, small, automated and simple, new generation of light sources.[149] Lasers require a shorter exposition time, and produce coherent light of a specific wavelength. Light-emitting diodes (LEDs) are another alternative, which allow a narrow wavelength range and high fluence rates. Both lasers and LEDs have no significant difference regarding cytotoxicity, showing the same efficacy.[149,150]

b) Oxygen

The human body requires and regulates a specific balance of molecular oxygen in the blood and tissues by using the respiratory system. Completely essential for PDT is the

presence of $^3O_2$ in the near proximity of the site of action.[151] The unusual ground state of molecular oxygen (a triplet), has an open-shell electronic configuration with two unpaired electrons occupying separate antibonding (π*) orbitals with parallel electronic spins (Figure 15). The unique configuration of molecular oxygen is responsible for a number of important redox and photophysical interactions. $^3O_2$ can easily accept one electron at a time, as in redox reactions with other radicals or other species bearing unpaired electrons, such as transition metals. This one-electron reduction of oxygen generates superoxide radical anion ($O^{2\bullet-}$) which can undergo further successive one-electron reductions to form other ROS.[152] On the other hand, when an excited PS (also in its triplet state, $^3PS^*$) collides with $^3O_2$, a process of triplet-triplet energy transfer takes place, converting the molecular oxygen into the mentioned before, extremely short-lived and reactive $^1O_2$.[153–155] This process involves "flipping the spin" of the outermost electron and shifting it into the orbital containing the other electron, which in turn leaves one orbital entirely unoccupied (a violation of Hund's rule) (Figure 15). $^1O_2$ is considered the most reactive form of oxygen, presenting high reactivity towards organic substrates.

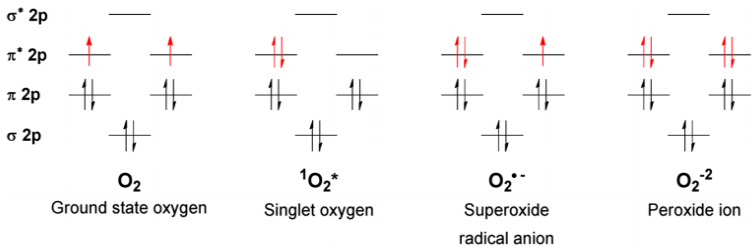

Figure 15. Molecular orbital diagrams for ground-state molecular oxygen, singlet oxygen, and ROS (superoxide radical anion and peroxide ion, deprotonated form of hydrogen peroxide).[152]

$^1O_2$ lifetime (τ) strongly depends on the solvent in which it is generated.[156] In organic solvents it is estimated to be 10-100 μs, while in water it is about 3-4 μs. This is a consequence of the strong O-H vibrations of water molecules, which facilitate relaxation and $^1O_2$ deactivation. Under physiological conditions, the lifetime of $^1O_2$ is only around 100-250 ns due to the presence of reacting molecules in the cytoplasm. Consequently, the diffusion range of $^1O_2$ is predicted to be around 45 nm,[157] and considering that the diameter of human cells ranges from 10 to 100 μm, $^1O_2$ cannot diffuse more than a single cell length. The short half-life of $^1O_2$ together with its high reactivity leads to the localized production of ROS, resulting in an oxidative damage that is limited to the irradiated areas, shrinking the probability of harming healthy cells and produce side-effects.

c) Photosensitizer

As a general definition, PS are compounds that are capable of absorbing light of a specific wavelength and transforming it into other forms of energy. In medicine, the PS is a drug, which when excited by light, can utilize and convert this energy to induce photochemical reactions and ultimately may cause lethal toxic effects in cells.[158]

i. Characteristics of ideal photosensitizers

There are many natural or synthetic dyes that can play the role of a PS for PDT applications, and in order to develop systems with high potency and selectivity, the characteristics of efficient PS must first be defined and fulfil most of the following criteria:[159]

- **Chemical composition:** The PS should be a single, pure, well-characterized substance, with a known and stable composition and good stability when stored. Also, it must have low manufacturing costs with short, inexpensive and high-yield synthetic route that can be easily translated into multigram-scale reactions.
- **Toxicity:** The PS should not show any intrinsic dark toxicity, not be mutagenic or carcinogenic, and no toxic byproducts should be generated when it is metabolized.
- **Selectivity:** The PS should preferably accumulate in the targeted tissue over healthy ones.
- **Activation:** The PS should exclusively be activated by light of a certain wavelength that provides the PS enough energy to excite $^3O_2$. The PS must present absorption with high molar extinction coefficients, in the 600-800 nm therapeutic window.
- **Functioning:** The PS should show a high triplet quantum yield (≥0.5) and triplet state energy higher than that of $^1O_2$ (~94 kJ·mol^{-1}), so that energy transfer can occur to generate singlet oxygen.
- **Aggregation:** The PS should not aggregate in the cellular media, since aggregation decreases triplet quantum yield, and therefore singlet oxygen quantum yield.
- **Imaging:** The PS should ideally produce fluorescence in order to obtain *in situ* imaging of its localization.
- **'ADME' properties:** The PS should present optimal absorption, distribution, metabolism and excretion to be effectively eliminated from the body.

ii. *Classification of photosensitizers*

PS can be categorized according to their chemical structure. In this way, three broad categories are distinguished: natural porphyrins (Por), chlorins, and synthetic dyes. The first category consists of Por, such as hematoporphyrin and its derivatives, while the second category consists of chlorophyll-like substances. The third and largest family is that of synthetic dyes, which can be subdivided in two main groups, namely porphyrinoid or non-porphyrinoid derivatives.[160–162] Non-porphyrinoid PS include phenothiazines (e.g. methylene blue and toluidine blue), xanthenes (e.g. Rose Bengal), squarines, BODIPY (boron-dipyrromethane dyes), phenalenones, anthraquinones (e.g. hypericin), cyanines, curcuminoids, chalcogenopyrylium dyes and transition metal compounds, from which ruthenium(II) polypyridyl complexes are the most studied.[163] The chemical structures of some of the most common non-porphyrinoid synthetic dyes that are used as PS are summarized in Figure 16.

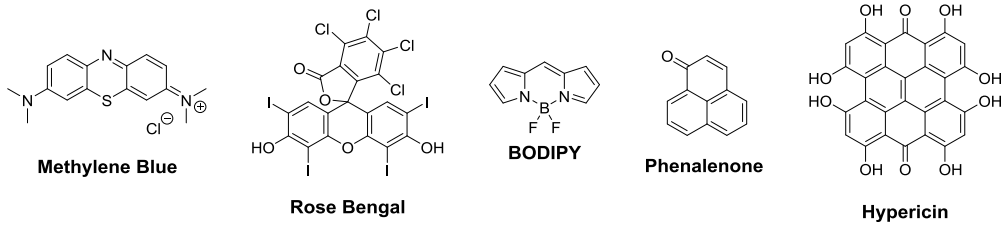

Figure 16. Chemical structures of some of the most common non-porphyrinoid synthetic dyes able to photogenerate $^1O_2$.

Porphyrinoid-based derivatives are the most used in PDT applications, because of their singular photochemical characteristics. The focus herein will be placed on this family, that historically are further classified as first, second and third generation PS.[164]

First generation PS:

Hematoporphyrin derivative (HpD), porfimer sodium (Photofrin®), and other Por made in the 1970s and 1980s are known as first generation PS.[159,165] They were the first effective PS, but showed various problematic side effects such as low selectivity and prolonged skin photosensitization. Photofrin® is the most used PS in PDT, being a reliable, activatable, pain-free and non-toxic drug. However, it presents some important disadvantages, such as its composition by an uncertain mixture of compounds, its poor selectivity, the large concentrations of compound and light that are required, and the low absorption coefficient at its absorption maximum wavelength.

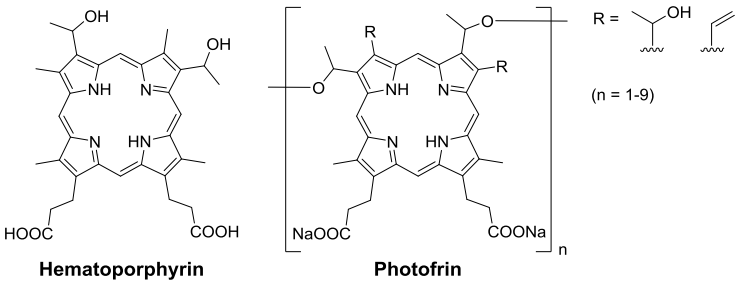

Figure 17. Chemical structures of first generation PS: Hematoporphyrin and Photofrin (a mixture of dimers and oligomers ranging from two to nine Por units connected by ether bonds).

Second generation PS:

Second generation PS are synthetic derivatives of the first generation, designed with the intention to overcome their shortcomings, absorbing at longer wavelengths and causing less skin photosensitization post-treatment. A large variety of PS has been developed over the last years, some of them being already approved for the treatment of different diseases.[160,166–168] Figure 18 shows some examples of second generation PS.[169,170]

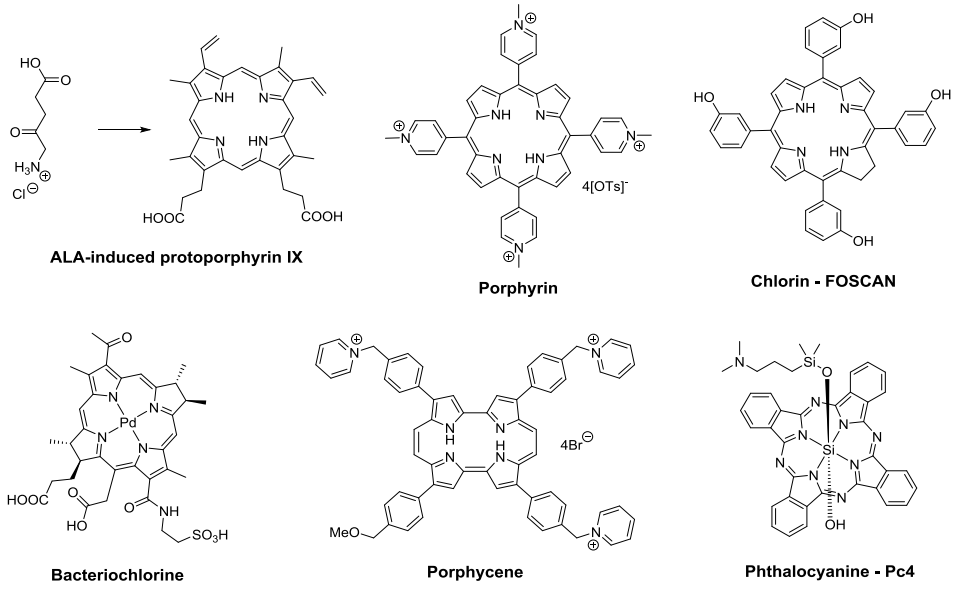

Figure 18. Examples of second generation PS.

The first one is the prodrug ALA, which is a naturally occurring amino acid that is enzymatically converted in the PS protoporphyrin, approved in 1999 by US FDA for non-oncological PDT treatment of actinic keratosis.[171] Synthetic porphyrins are also widely

used as PS in PDT since exhibit the longest wavelength absorption band around 630 nm, however with low absorption coefficients. Chlorins, which are Por analogues lacking a double bond in one of the pyrrole units and display bathochromically shifted absorptions with larger absorption coefficients, are also commonly used as PS. The same applies to bacteriochlorins, which have two pyrrole units with reduced double bonds and display more red-shifted and intense absorption bands. On the other hand, porphycenes are structural isomers of Por with strong absorptions above 600 nm and efficient production of $^1O_2$. They present a great structural versatility for improving their therapeutic properties. And last, but not least, Pcs, the compounds of interest in this thesis, are another family of second generation PS, which have a higher degree of conjugation when compared with Por, and exhibit bathochromically shifted *Q*-bands, with absorption maxima around 670 nm. Indeed, various Pcs have already been clinically approved or are under clinical trials.[172]

Third generation PS:

When second generation PS are covalently conjugated to site-specific delivery agents for selective accumulation within the targeted tissue, they are named third generation PS. Also, they are called biohybrids when the nature of the delivery agent is biological (e.g. antibodies, peptides, protein cages, low-density lipoproteins, liposomes, nucleic acids, folic acid, carbohydrates, etc.),[58] with specificity for antigens or receptors that are overexpressed or only expressed in tumor cells.[173] There are also other non-biological delivery platforms, for instance hydrogels, micelles, nanoparticles, etc.[174,175]

2.3. Molecular mechanism of action: photophysics and photochemistry

From a photochemical point of view, there are two major processes occurring between the three main components of PDT: light absorption by the PS and energy transfer to oxygen. The photophysical mechanisms of these processes are usually studied through the Jablonski scheme (Figure 19), a general 'map' for the events taking place after electronic excitation of a molecule. Jablonski energy diagram outlines the possible radiative and non-radiative transitions between electronic states of the PS (Figure 19). Usually the molecular structure of a PS is typified by a π-conjugated system with electrons that are spin paired in low energy orbitals. The total spin of the PS is therefore 0, so its ground electronic state is commonly a singlet state (S_0). Upon application of light of wavelength close to the PS absorption maximum and absorption of a photon by the PS, one electron in the highest occupied molecular orbital (HOMO) is promoted to the lowest unoccupied (higher energy) molecular orbital (LUMO), while maintaining its spin. This transition leads to the formation of a short-lived (in the range of ns) singlet excited state

(^{1}PS* or S_1), which can dissipate the absorbed energy and restore the PS ground state S_0 through two main pathways:

- **Fluorescence emission:** Spontaneous emission of a secondary photon upon transition between two electronic states with the same spin multiplicity. This process always occurs from the lowest vibrational level of S_1.[176]
- **Internal-conversion (IC) by thermal decay:** Within an excited state, an electron can decay via vibrational relaxation (VR) to the lowest vibrational level of that state, with dissipation of energy as heat (non-radiative transition).

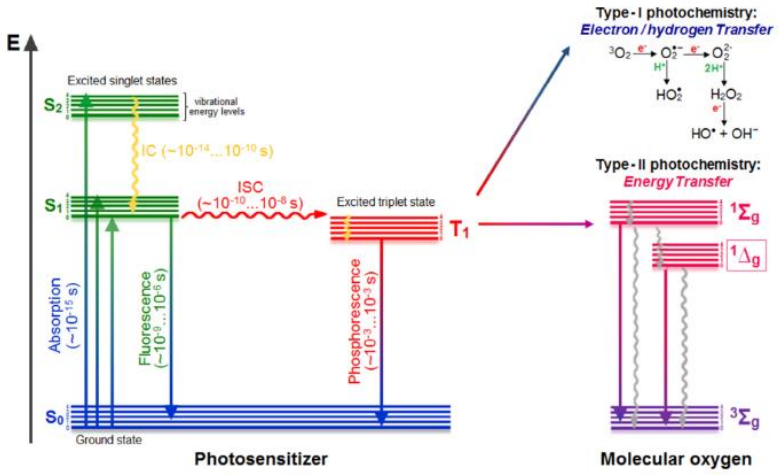

Figure 19. Jabłonski diagram illustrating the generation of excited states of PS, and triplet state photosensitized production of ROS. S indicates discrete singlet states of the PS and T indicates triplet states. IC and ISC denote internal conversion and intersystem crossing, respectively.[148]

Alternatively, and most importantly to the PDT process, the PS can undergo a reversal of the spin of the excited electron, taking the molecule to its triplet excited state T_1 (^{3}PS*) with parallel electron spins, *via* a non-radiative process called intersystem crossing (ISC). The resulting T_1 is less energetic than the singlet excited state S_1, but has a much longer lifetime (in the μs scale), since transitions from T_1 to S_0 are spin-forbidden. Nevertheless, spin-orbit coupling (SOC) makes ISC competitive against other decay routes of the S_1 state.[177] SOC is the energetic contribution arising from the interaction between the spin magnetic moment of the electron and the magnetic field that it feels as a result of orbiting around a positively charged nucleus. This interaction leads to a mixing of the singlet and triplet wave functions, making it possible for ISC to take place. Thus, heavy atoms should increase the ^{3}PS* lifetime since SOC is a function of Z^4 (where Z is the atomic number), also known as the heavy-atom effect.[178] In this way, the rate of ISC can be increased as a result of enhanced SOC by the presence of heavy atoms that are incorporated into the chromophore (internal heavy atom effect). T_1 can lose energy by phosphorescence

(spontaneous emission of radiation upon transition between two electronic states with different spin multiplicity). This occurs if after vibrational relaxation to the lowest vibrational level, T_1 decays to S_0 by changing the spin orientation of the excited electron (a relatively slow process), via emission of an electromagnetic quantum. Alternatively, T_1 may interact with molecules that are abundant in its immediate environment. Because of the selection rules that specify that triplet–triplet interactions are spin-allowed while triplet–singlet interactions are spin-forbidden, the T_1 can react readily with surrounding $^3O_2$, which is one of the few molecules that are a triplet in the ground state. This interaction constitutes two types of photodynamic reactions, schematized in Figure 20, defined as Type I and Type II:[179]

- **Type I photoreactions:** The excited PS (T_1) transfers an electron to a nearby cellular substrate (S) (i.e. lipids, proteins, nucleic acids, etc.), sometimes in concert with proton donation. Therefore, such Type I photochemical pathways trigger radical chain reactions,[180] and the direction of the electron transfer is controlled by the relative redox potentials of the PS and the substrate. The generated radicals react with $^3O_2$, yielding several different oxygen intermediates collectively called ROS, such as the superoxide anion ($O_2^{\bullet -}$), the hydroxyl radical ($OH^{\bullet}$) and hydrogen peroxide (H_2O_2). $OH^{\bullet}$ seems to be the most reactive of the three species formed since, as strong electrophile, is able to chemically attack biomolecules such as DNA, proteins and membrane lipids.[181]
- **Type II reactions:** The PS in its ^1T undergoes an electronic energy transfer upon collision with $^3O_2$, resulting in the formation of cytotoxic $^1O_2$ that provokes the oxidation of cellular substrates and eventually leads to cell dead.[180] This type of photoreaction proceeds by energy (not electron) transfer mechanism, while oxygen is the primary acceptor. Singlet oxygen is a non-radical species of electrophilic nature, highly reactive towards groups with high electron densities such as double bonds in unsaturated lipids and steroids, sulphur atoms in amino acids, aromatic and heterocyclic groups in amino acids and aromatic and heterocyclic groups in pyrimidine and purine bases.

Both type of mechanisms occur simultaneously and cause oxidative damage within the target tissues, which lead to cell death. Although the detailed mechanism of PDT and the concomitant processes are not yet fully understood, it is generally accepted that the generation of $^1O_2$ from the Type II mechanism predominates in both PDT and PDI. For this reason, $^1O_2$ quantum yield is an important parameter to take into account in the development of new PS. And the use of PS with increased ISC (high triplet-state quantum yields) is therefore of extreme importance since this allows for an efficient production of $^1O_2$ and other ROS.

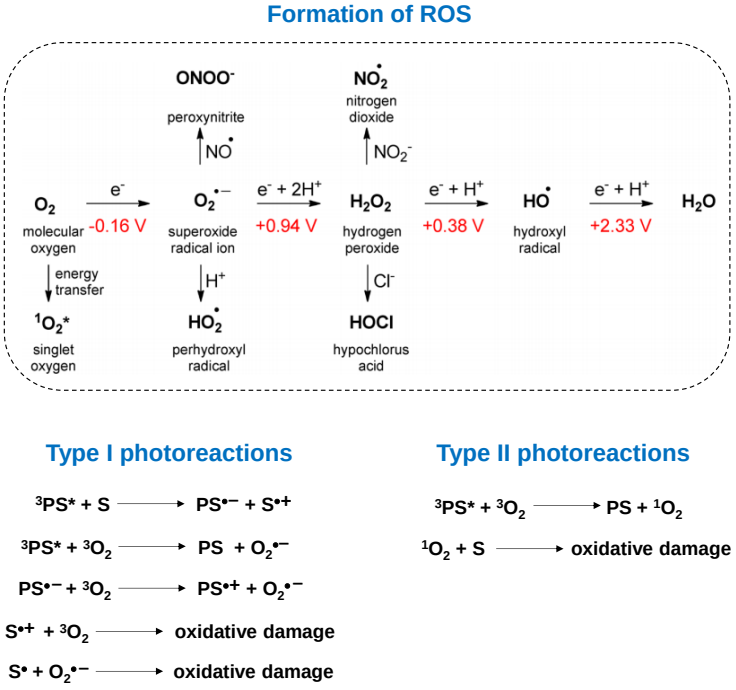

Figure 20. Formation of ROS through energy- and electron-transfer reactions,[152] and Type I and Type II photoreactions during PDT, which result in oxidative damage of biological substrates.

2.4. Reaching the tumor cells: PS location and cell destruction

a) Intracellular localization

The intracellular localization of the PS strongly determines the cellular pathways triggered by the PDT treatment. Indeed, PS that are unable to be taken by cells show a very inefficient PDT effect. Moreover, the fact that most PS are fluorescent allows for the development of an assortment of optical imaging for localization and monitoring strategies.[182] These sensitive assays quantify the amount of PS in cells, providing selectivity data. In this way, cellular PDT targets include lysosomes, plasma membrane, mitochondria, endoplasmic reticulum and the Golgi apparatus. PDT is not likely to cause DNA damage, mutations or carcinogenesis so there are scarce examples of PS that target the cell nuclei. Anionic and hydrophilic aggregated drugs are likely to enter the cell through pinocytosis or endocytosis, so that they are localized in lysosomes and endosomes. This aggregated PS state may be the explanation of the lower efficacy shown by lysosomal localization against systems located in other organelles. Mitochondria is considered the optimal target for an effective photodynamic effect. Cationic PS, even

those still hydrophobic, localize preferentially in the mitochondria, which may be related with both the membrane potential and the lipid bilayer of this organelle. This preferential accumulation of cationic drugs is more pronounced in cancer cells than in normal tissues.[147]

b) Mechanisms of tumor destruction

There are three main biological mechanisms involved in the tumor shrinkage and disappearance after PDT treatment. These three mechanisms can influence each other, and their combination is required for achieving long-term tumor control.

- **Direct damage over tumor cells:** The generated ROS during PDT can kill tumor cells directly by apoptosis and/or necrosis.[128,183] Necrosis is a violent and quick form of degeneration characterized by the destruction of organelles and disruption of the plasma membrane. In contrast, apoptosis is a mechanism of genetically programmed death characterized by a common sequence of morphological and biochemical changes.
- **Vascular destruction:** PDT can damage the tumor-associated microvasculature, leading to persistent post-PDT tumor hypoxia/anoxia and nutrient deficiency, to finally complete tumor disappearance.[130,184]
- **Immune response:** Photodynamically induced changes in the cell membranes can trigger an immune response against tumor cells by activating multiple signal transduction pathways.[185]

2.5. Photodynamic Inactivation of Microorganisms

Microbial cells display a large variety of size, sub-cellular architecture, and biochemical composition. Nevertheless, the photosensitized processes in most microorganisms occur in a similar way, which allows to define specific mechanisms of microbial inactivation.[136,137] The most frequent target of microbial cell inactivation is the cytoplasmic membrane, since it has several cofactors, proteins and enzymes, which can be inactivated by the generated ROS and $^1O_2$. This consequently leads to a massive reduction of the membrane transport capacity, which results in a shortage of essential substrates for microorganism metabolism.[186] Sometimes the PS can gradually diffuse to inner cellular districts, and a variety of non-membranous sites are also involved in the photooxidative reactions.[139] Therefore, the overall process is of multi-target nature, making it extremely difficult for microbial cells to develop resistance to PDI, which represents one of the major advantages of this treatment taking into account the current antibiotic resistance crisis.[187] In this thesis, in particular, we will focus on the deactivation of both Gram-positive and Gram-negative bacteria.

- **Gram-positive bacteria:** This kind of bacteria display a highly porous outer wall manly constituted by peptidoglycan layers, that allows the diffusion of macromolecules of about 60000 Da. Inactivation has been successfully accomplished with anionic and neutral PS.[138]
- **Gram-negative bacteria:**[188] They are characterized by an outer wall with a rigid structural element located outside the peptidoglycan compartment, which is composed by lipoproteins, lipopolysaccharides, teichoic and lipoteichoic acid. This surface is densely packed with negative charges and inhibits the penetration of macromolecules. Consequently, only relatively hydrophilic compounds with less than 600-700 Da are able to diffuse through the porin channels present at the outer wall. The presence of positive charges on the PS are required for effective PDI treatment. It is believed that they are able to penetrate the outer wall through the self-promoted uptake pathway, which consists on the displacement of divalent cations from their binding sites present on the cell surface. This mechanism can be combined with the disruption of the normal barrier features of the outer wall by the bulkiness and amphiphilicity of the polycyclic photosensitizers. Otherwise, anionic and neutral PS were ineffective in killing Gram-negative bacteria.

2.6. Phthalocyanines as photosensitizers in PDT

Pcs exhibit singular properties that have encouraged their intense study for PDT among the second-generation PS:[148,189,190]

- The Pc *Q*-band absorption can be shifted into the red/NIR region of the electromagnetic spectrum through the extension of the π-conjugation, or by introducing electron-donor substituents. This intense absorption inside the range of the therapeutic window, in general better than for Por, increases the tissue penetration depth.
- They show hardly any absorption in the range of 400–600 nm, which may possibly result in a lower photosensitization of skin when exposed to visible light.
- The main feature that converts Pcs in efficient PS is their high triplet quantum yield (Φ_t) with relatively long lifetime (τ_t), which assists in the generation of $^1O_2$ in high quantum yield (Φ_Δ).
- Lack of dark toxicity in most of the cases.
- Flexibility for their structural modifications. Pcs comprising zinc (II), aluminum (III), silicon (IV) and ruthenium (II) as atom metal in the central cavity have proved to exhibit good efficiencies. These metal Pcs can befunctionalized at their peripheral/axial positions to obtain compounds with customized properties.

The main shortcomings of Pcs are two:

- Pcs have strong tendency to aggregate, especially in aqueous media, leading to a decrease or total loss of their photophysical properties. Φ_Δ is directly related to the aggregation state of the PS, being lower when the Pc is in an aggregated form. One of the main challenges in this research field is to synthesize Pcs with a low aggregation tendency.
- Pcs are extremely hydrophobic, which decreases their solubility in polar media. This problem can be solved through the inclusion of hydrophilic groups, or by encapsulation into water-soluble nanostructures.

A large number of Pcs has been investigated as PSs for PDT applications.[167,191–193] Up to date, some Pc derivatives are available for clinical trials, namely, CGP55847 (non-substituted Zn(II)Pc), Pc4 (Figure 18), Photocyanine, and Photosense®. Third-generation PS have been developed to circumvent the deficiencies relative to all previous PS. In this respect, a large number of possible delivery vehicles have been tested, from dendrimers, micelles, liposomes, viruses and protein cages, to non-biodegradable systems such as magnetic nanoparticles, quantum dots, or carbon based nanomaterials.[58] However, for the following sections we will focus on second generation PS and the way to achieve water solubility and non-aggregated species.

a) Water soluble phthalocyanines

Aqueous solubility, which also implies solubility in buffer solutions more related to biological media, represents a desirable but challenging property for some application of Pcs in PDT. Hydrophilic drugs present improved circulation in the bloodstream, a feature that facilitates the delivery of the dye to the target site.[194] However, highly hydrophilic drugs are unable to cross the hydrophobic cellular membrane, resulting in poor cellular uptake, and have a reduced stability against proteolytic and hydrolytic degradation. These reasons combined make amphiphilic drugs the most promising compounds to be used as PS, facilitating both blood stream circulation and traversing of the cellular membrane. Thus, amphiphilic molecules are easily localized both at hydrophobic-hydrophilic interfaces of the cellular membranes eventually leading to enhanced PDT effect. For amphiphilic compounds sometimes the addition of small amounts of polar organic solvents (e.g. DMSO, DMF or MeOH) will be needed to guarantee solubility in aqueous media. Taking advantage of the synthetic versatility of Pcs, different patterns of substitution have been developed to render water-soluble derivatives, making them more bio-compatible.[3] Pcs can be classified according to the nature of the hydrophilic groups involved in their structure: Pcs with ionic functions (cationic, anionic and 'zwitterionic'),[195] or with strongly hydrophilic groups, such as peptides,[196] polyethylene

glycol (PEG)[197,198] and carbohydrates.[199,200] We will focus our attention only in cationic Pcs and those functionalized with PEG chains.

i. *Cationic phthalocyanines*

Charged functions can be covalently attached to the macrocycle to render solubility in aqueous media. The presence of charges also prevents the aggregation of the aromatic rings through electrostatic repulsion forces. Cationic Pc derivatives can be obtained by quaternization of aliphatic or aromatic nitrogen atoms in their substituents, reaction that usually takes place as the last step in the synthetic route, due to the experimental difficulty of working with charged species. This is achieved with several reactants like methyl iodide, iodoalkanes of various chain lengths and dimethyl sulfate. Below, most common cationic functional groups employed for the design of water soluble Pcs will be discussed:

- **Ammonium derivatives:** Trimethylammonium-functionalized Pcs can bear the ammonium moiety directly bounded to the Pc core,[201] or by grafting (dimethylamino)-alkyl thiols or alcohols,[202,203] either by ether or thioether linkages. Zn(II)Pc derivatives bearing ammonium groups were prepared by Petr Zimcik and coworkers and showed efficient phototoxic effect towards tumor cells, (Figure 21, left).[204] Ammonium functions were also introduced at the axial positions of Si(IV)Pcs, affording an amphiphilic Pc with high in vitro phototoxicity.[205] Our research group have reported studies with cationic Pc dendrimers as potential antimicrobial PS against bacteria and fungi.[206]
- **Pyridinium derivatives:** Pyridine, due to its synthetic versatility, is a common substituent to prepare water soluble Pcs. This heterocycle provides a lone nitrogen pair not conjugated within the aromatic ring, presenting aromaticity even after quaternization. Commonly, the linkage of pyridines to precursor phthalonitriles can be achieved through a ether or thioether bond, by nucleophilic substitution of 4,5-dichlorophthalonitrile for disubstituted derivatives, with hydroxy- or mercapto- pyridines (Figure 21, right).[207] Pcs substituted at the peripheral positions with methylpyridinium units proved to be a promising PS for PDI.[208,209]
- **Other groups:** Dimethylaminopyridine,[210] guanindinium,[211] anilinium derivatives,[212] imidazolium[213] or morpholinium substituents[214] have been also investigated.

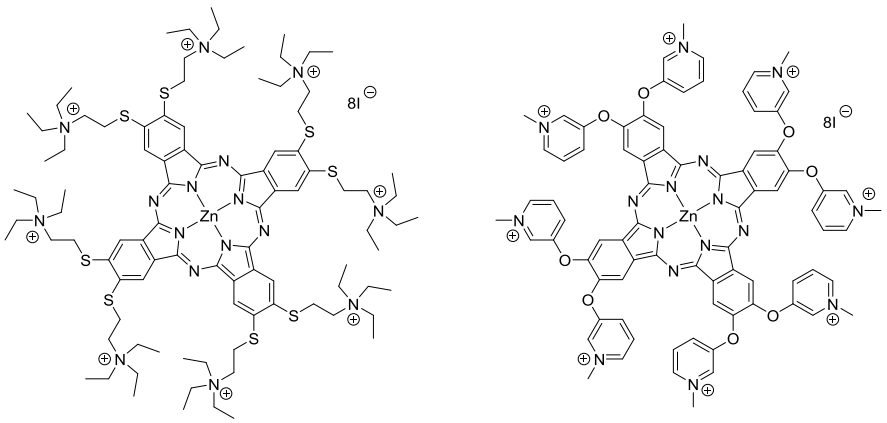

Figure 21. Chemical structures of cationic Pcs with quaternized trimethylammonium or pyridinium groups.

ii. *PEG-based phthalocyanines*

The use of PEG chains is a popular approach to enhance the biocompatibility of otherwise hydrophobic drugs, either by their direct binding to individual molecular entities or by the incorporation of PEG moieties in nanoparticles or micelles as carriers. Besides improving the hydrophilicity of the drug or nanoformulation, PEG chains lead to a prolonged blood circulating lifetime, allows for the minimization of non-specific uptake and favors the enhanced permeability and retention (EPR) effect, which result in an elevated concentration of the drug at the tumor site.[215,216] Introduction of polyether glycol chains at the Pc peripheral positions enhances the solubility in a variety of non-polar, aprotic polar, and protic polar solvents such as water. However aggregation in most solvents is commonly observed. Several Pcs functionalized with different PEG chains have been studied as PS by several groups (Figure 22).[217–222]

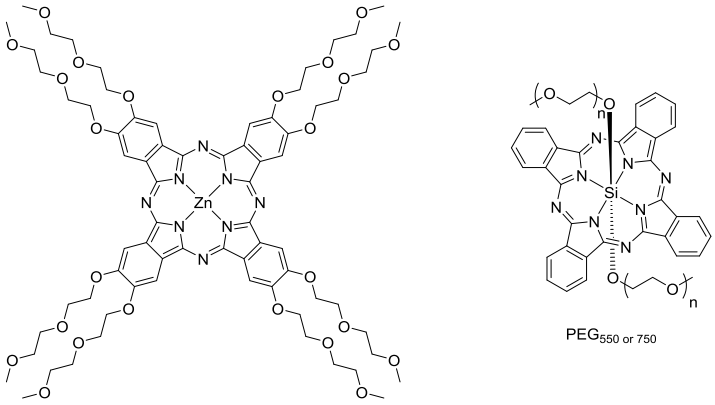

Figure 22. Examples of PEG functionalized Pcs.

b) Porphyrinoid amphiphilic photosensitizers

The synthesis of symmetrically substituted water soluble Pcs is well known. On the other hand, unsymmetrical substituted amphiphilic Pcs combining different structural motives over the isoindole units have attracted the attention of researchers only in the recent years. Molecules holding a hydrophilic and a hydrophobic part have different self-assembly behaviors in aqueous media. The self-assembly behavior of Pc amphiphiles, which can be useful also for PDT applications, is widely discussed in the next section about supramolecular chemistry. Here, we will comment on the behavior of several unsymmetrically substituted amphiphilic Pcs as molecular PS.

i. A_3B porphyrinoid photosensitizers

Several examples of A_3B amphiphilic Pcs and their use in PDT have been reported in last years. For instance, Dumoulin et al reported monoglyco-conjugated Pcs to study the effect of sugars as mannose and galactose in PDT against HT-29 human colon adenocarcinoma cells.[223] There are also examples of poly(ethylene glycol) conjugated asymmetrical Zn(II)Pcs with amphiphilic properties (Figure 23a).[197] Third generation PS based on A_3B Pcs were prepared by the groups of Ng and van Lier (Figure 23b), who synthesized peptide conjugated Pc-based PS for imaging and targeting.[196,224] Remarkable is also the work of Xue with A_3B Pcs that combine both PDT and chemotherapy features .[225]

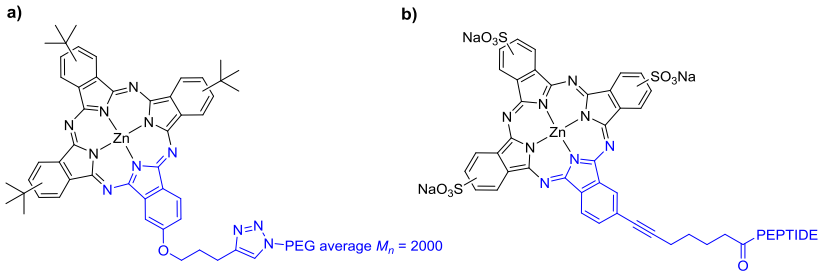

Figure 23. Examples of amphiphilic A_3B Zn(II)Pcs.

ii. A_2B_2 porphyrinoid photosensitizers

Adequately customized A_2B_2 (ABAB or AABB) Pcs, in particular, and porphyrinoids in general, may feature a well-defined amphiphilic nature that can facilitate the transport of the chromophore through the cell membrane. Unfortunately, in the case of ABAB Pcs, their difficult synthesis and isolation makes them elusive PS, and in fact, to best of our knowledge, there are no reports on PDT or PDI studies with this type of compounds. However, some porphyrinoids with ABAB-type functionalization have proved efficient PS. The group of Hamblin tested the PDT and PDI activity of several ABAB-functionalized

synthetic bacteriochlorins, holding either monoethylenglycol of alkylammonium functions (Figure 24a and b),[226,227] and T. Maisch et al. studied also the photodynamic effects of novel dicationic ABAB Por derivatives.(Figure 24c).[228]

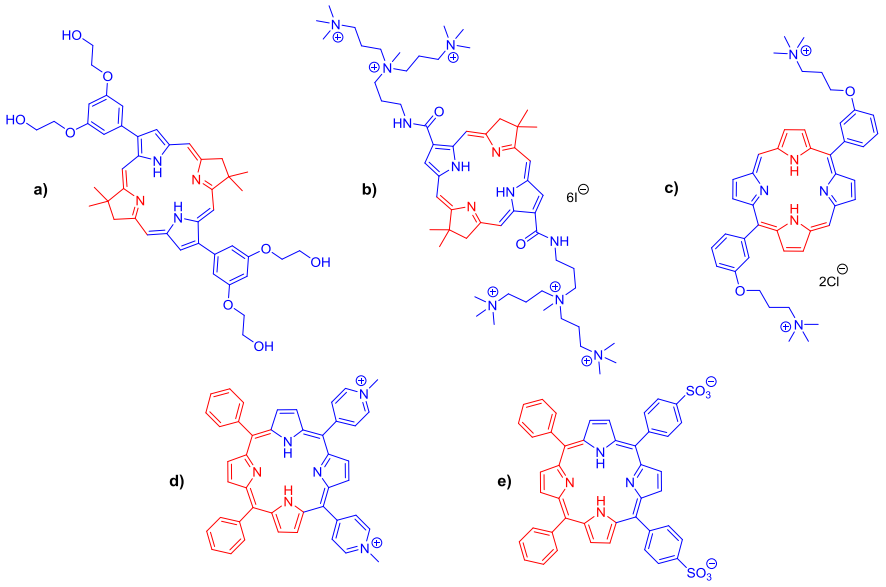

Figure 24. Examples of ABAB porphyrinoid amphiphilic PS. (a and b) Bacteriochlorins, (c) porphyrin. Examples of AABB porphyrinoid amphiphilic PS.

Regarding to AABB porphyrinoid PS, Tsubone et al. studied two asymmetric Por with opposite charges, the positively charged CisDiMPyP and the negatively charged TPPS2a in terms of photodynamic activity against HeLa cells (Figure 24d and e, respectivelt).[229] In fact, reduction product of TPPS2a, is a novel chlorin developed for clinical utilization developed by Kristian Berg et al.[230]

Unlike ABAB systems, there are some examples of AABB Pcs studied as PS, as they can be prepared with directed methods that prevent the formation of the ABAB isomer. Vicente and coworkers studied the photophysical properties and *in vitro* biological behavior in human carcinoma HEp2 cells of an AABB trimethylaminophenoxy-substituted Zn(II)Pc with a biphenyl unit linker between adjacent isoindol units (Figure 25, left).[231] A binaphthalo-Zn(II)Pcs (Figure 25, right) was prepared by the group of Nyokong that exhibited a relatively good conversion of energy from the triplet-excited state to singlet oxygen.[232]

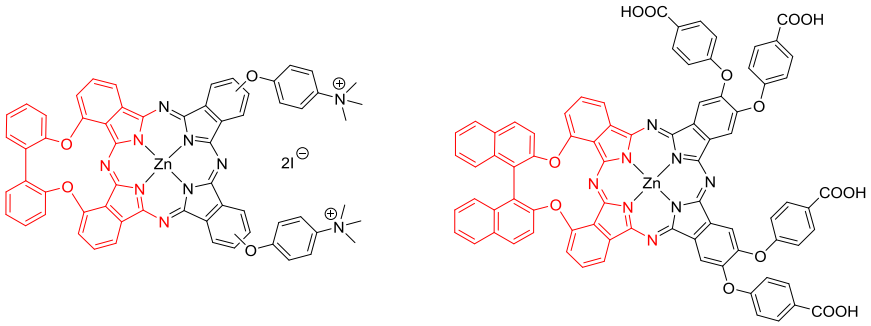

Figure 25. Examples of amphiphilic AABB Zn(II)Pcs.

Other adjacent Zn(II) Pcs reported by Vicente and coworkers are depicted in Figure 26. These compounds are cis-AABB-type Zn(II)Pcs, substituted at the α-positions of A isoindoles with tri(ethylene glycol) chains and either hydroxyl groups or a benzyloxy spacer. The latter compound was synthesized starting from the 1,2-benzyloxy-linked bisphthalonitrile (Figure 26, right), and it was then transformed into the free hydroxyl derivative (Figure 26, left). The dihydroxy Zn(II)Pc happened to be highly phototoxic to human carcinoma HEp2 cells, and was localized in multiple organelles, including mitochondria, lysosomes, Golgi apparatus and endoplasmic reticulum.[233]

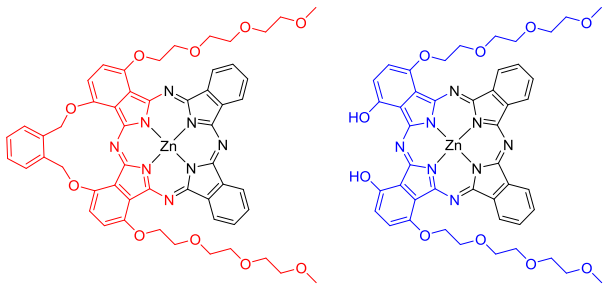

Figure 26. Structure of pegylated cis-AABB-type Zn(II)Pcs.

Regarding sugars and amphiphilic systems, Tomé's group reported amphiphilic Zn(II)Pc–cyclodextrin conjugates as third generation PS for PDT against UM-UC-3 human bladder cancer cells,[234] demonstrating how ABAB fluorinated porphyrinoids are efficient platforms for new therapeutic materials (Figure 27).[235]

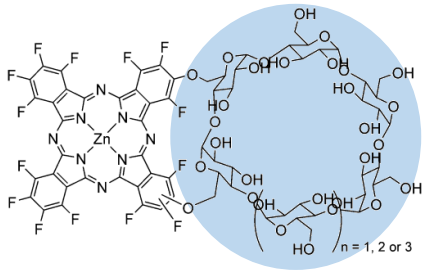

Figure 27. Amphiphilic Zn(II)Pc–cyclodextrin conjugate for cancer PDT.

Last, SuftalanZinc (trade name: Photocyanine, Figure 28) is an amphiphilic PS developed by the University of China. It is composed of a mixture of four adjacent isomers (AABB type) of di-(potassium sulfonate)-di-phthalimidomethyl Zn(II)Pc, which is in clinical trials since 2008 with the approval of State Food and Drug Administration of China. It requires a very complex procedure of purification by HPLC to separate the initial opposite (ABAB) and adjacent (AABB) isomeric mixture.[192,236]

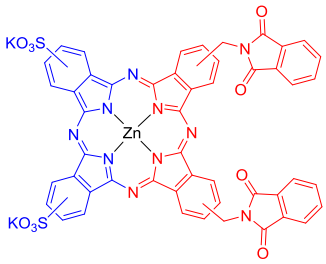

Figure 28. Structure of Photocyanine.

2.7. Aggregation vs. self-assembly: two sides of the same coin

In a previous section we have evidenced that one of the characteristics for having an efficient PS is directly related with its aggregation features. The PS should not aggregate in the cellular media, since aggregation decreases triplet quantum yield, and therefore singlet oxygen quantum yield. But a crucial question is what 'in the cellular media' means. Traditional drugs i.e., small molecules, enter the cell predominantly via passive diffusion or active transport, while nanoparticles enter into cells mainly via endocytosis. Endocytosis, that requires the production of internal membranes from the plasma membrane lipid bilayer, has been deemed the major route for the transport of nanomaterials across the membrane. On this way, our PS can be retained in the cell membrane or the bacterial wall or, on the contrary, it will be distributed in the cellular medium until it reaches specific organelles. Under these circumstances we can

differentiate two different 'cellular media' where our PS must be able to function: i) the aqueous biological medium that constitutes the cytosol and extracellular media, and ii) the cell membrane and the membranes of the corresponding organelles with a lipid composition where hydrophobia predominates. With this situation in mind, we must emphasize that the PS should not aggregate on the site of action. That is, it must remain as monomeric species to maintain its photophysical properties in hydrophobic medium.

On the other hand, the ability to self-assembly with a certain degree of order in aqueous media can represent a great advantage for transportation in a biological environment. We have previously shown how purely hydrophilic drugs present difficulties in internalizing in cells. Therefore, the best candidates to face both situations will be amphiphile compounds.

An exciting approach towards the construction of nanostructures via self-organization is the use of π-amphiphiles, because they combine the ability of planar π-systems to self-assemble and the versatility and the capacity to interact with both hydrophilic or hydrophobic environments. In the next section, we will discuss basic supramolecular chemistry concepts of π-conjugated systems, and their organization in water to facilitate the transport in aqueous medium.

3. Supramolecular chemistry of π-conjugated systems

3.1. Principles and general aspects of supramolecular chemistry

Supramolecular chemistry, originally defined by Jean-Marie Lehn as 'chemistry beyond the molecule', exploits non-covalent interactions between molecules to form ordered architectures.[237] It is one of the most active fields in chemical research, as many supramolecular arrangements have been inspired by Nature or have been designed using a biomimetic approach.[238] Hence, the self-assembly of molecules to form large clusters under equilibrium conditions is a phenomenon widely found in chemistry, physics, biology, materials, and nanoscience.[239] Supramolecular chemistry is strongly related to self-assembly, which has been defined as 'the autonomous organization of components into patterns or structures without human intervention'.[240] Both molecular self-assembly and supramolecular chemistry are connected by the formation of non-covalent bonds and/or certain nano/microsized architectures.[241] Supramolecular systems are formed through the intervention of weak intermolecular forces, including hydrogen bonds, metal-ligand coordination, electrostatic forces, interactions involving polarizable groups and hydrophobic interactions. This ensures that, in solution, there is at least some reversibility in the formation of supramolecular adducts and the component molecules can coexist in free form (unbound) and as aggregates (bound). The fact that these weak intermolecular interactions are in reversible equilibrium ensures that the system ends up in the most energetically favored state. This differs from a chemical reaction implying the formation and/or breaking of covalent bonds, where the more readily formed product is usually obtained under kinetic control. While a covalent bond normally has a homolytic dissociation energy that ranges between 100 and 400 kJ·mol^{-1}, non-covalent interactions are generally weak and vary from less than 5 kJ·mol^{-1} for van der Waals forces, through approximately 50 kJ·mol^{-1} for π-π interactions and hydrogen bonds, to 250 kJ·mol^{-1} for Coulomb interactions (Table 1).

Table 1. Strength of several non-covalent forces.[242]

type of interaction or bonding	strength (kJ mol^{-1})
covalent bond	100−400
Coulomb	250
hydrogen bond	10−65
ion−dipole	50−200
dipole−dipole	5−50
cation−π	5−80
$\pi-\pi$	0−50
van der Waals forces	<5
hydrophobic effects	difficult to assess
metal−ligand	0−400

3.2. Supramolecular polymerization

In an extensive review, Meijer and coworkers described the general principles of supramolecular polymerization,[243] which are briefly overviewed in this section. Supramolecular polymers are presented as those based on monomeric units held together by high directional, reversible non-covalent and moderately strong secondary interactions, which result in high molecular weight arrangements under diluted conditions. In the same way, the self-assembly process is called 'supramolecular polymerization', and can be classified considering four different principles. First, the physical nature of the directing force that lies at the origin of the reversible interaction. Second, the type of monomers used. Third, the evolution of the Gibbs free energy of the polymer as a function of conversion (thermodynamic classification). And finally, the dimensionality of the aggregate where the addition of a second and third dimensions will result in additional interaction energies. The third classification scheme is based on the evolution of the Gibbs free energy of the supramolecular polymer as the conversion (p) goes from zero to full conversion (p = 1). Hence, in this classification, the main concern is the mechanism by which the supramolecular polymers grow from their monomeric components into their polymeric structure as the concentration or temperature is changed. The three major growth mechanisms are isodesmic, ring-chain, and cooperative growth (Figure 29).

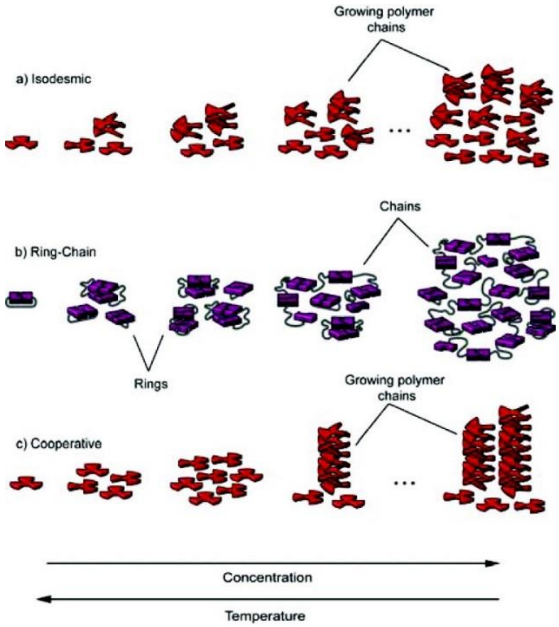

Figure 29. Graphical representation of the three growth mechanisms by which a monomer can polymerize into a supramolecular polymer: (a) isodesmic supramolecular polymerization; (b) ring-chain mediated supramolecular polymerization; (c) cooperative supramolecular polymerization.[243]

The isodesmic mechanism is characterized by a high polydispersity, and the degree of polymerization strongly depends on the association constant of the linking supramolecular units. The ring-chain of supramolecular polymerization is determined by the equilibrium between linear supramolecular polymers and their cyclic counterparts. Finally, the cooperative mechanism is characterized by non-linear growth and is often nucleated. A good example of isodesmic supramolecular polymerization is constituted by systems with electronically coupled polymerizable functionalities, namely, π-conjugated molecules where the main driving force for the supramolecular polymerization are π-π interactions.[244] The isodesmic model postulates that each addition of monomer occurs with the same equilibrium constant. This suggests that the strength of the π-π interactions should remain constant during the supramolecular polymerization. Aggregation behavior of π-conjugated systems will be discussed extensively in the following sections.

3.3. Aggregation behavior of π-conjugated systems. Supramolecular assemblies

π-Conjugated systems, for example Pcs and Pors among others, are able to interact by non-covalent interactions to build supramolecular architectures. Planar and highly conjugated aromatic molecules tend to organize through the occurrence of π–π supramolecular interactions, solvophobic effects, and enhanced Van der Waal's attractive forces.[245–247] These strong interactions grant π-conjugated systems stacking abilities,[21] forming aggregates that consist in coplanar association of rings in the form of dimers, trimers and higher order complexes. The aggregation state depends on the concentration, nature of the solvent, structure, functionalization and temperature.[248,249]

For artificial dye molecules, Stenger observed more than a century ago changes of absorption and emission properties of dye solutions upon temperature variation, and attributed such changes to aggregation–disaggregation processes.[250] In this way, the aggregation state will influence the photochemical and photophysical properties of stacking molecules, which are strongly dependent on the relative orientation and distance between them. Aggregates can be classified in two different types according to the excitonic coupling theory, developed by Kasha and co-workers (Figure 30),[251] which describes the interaction of the transition dipole moments of stacking π-conjugated systems with respect to their geometrical arrangement:

- ***H*-aggregates (face to face)**: Two or more monomers are arranged on the top of each other. The stacking direction is perpendicular to the molecular plane and the coplanar assemblies have parallel dipolar moments aligned in 90 degrees one to each other. This arrangement produces a higher energy transition that corresponds to the hypsochromic (blue) shift observed in the absorption spectra,

whit respect to the *Q*-band of the monomer. They are not photoactive and characterized, with few exceptions,[252] by loss of their fluorescent properties.[23] *H*-type aggregates are the predominant form of self-assembly for aromatic macrocycles.[245]

- ***J*-aggregates (edge to edge):**[253] Discovered in cyanine dyes by Jelley and Scheibe independently in the 1930s.[254,255] The monomers are displaced with respect to each other in a direction roughly parallel to the molecular plane. Substitution pattern leads to a shift in the columnar aggregation direction, forming staircase or brick-wall aggregates. In this kind of aggregates, the parallel dipolar moments are shifted 54.7 degrees or less, rising a lower energy transition that corresponds to a bathochromic (red) shift in the absorption spectra when compared to the corresponding monomers. *J*-type aggregates are less common,[246,256] but interestingly, they maintain the emission properties of the corresponding monomers that can be both fluorescent and triplet state photoactive.[22]

The zero-order molecular exciton model predicts that coupling of the transition dipole moments creates two new exciton states.[257] For *H*-aggregates the transition from the ground state to the higher energy exciton state is fully allowed, while the transition to the lower exciton state is forbidden.[258] For *J*-aggregates the situation is the opposite.

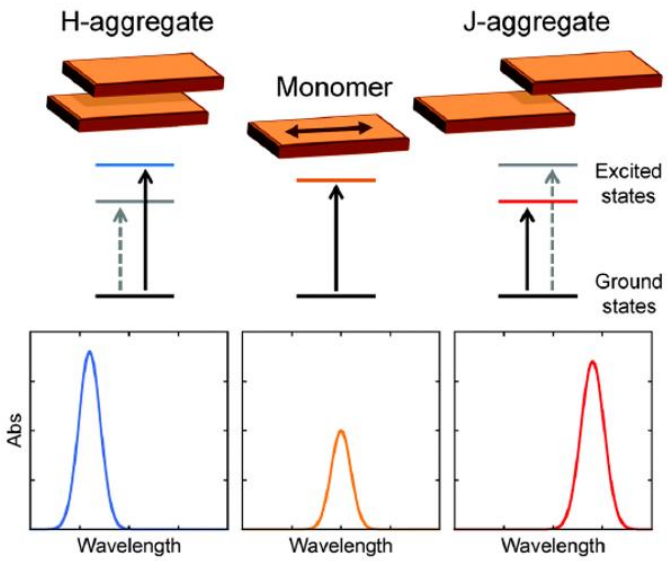

Figure 30. Typical arrangements of H- and J-aggregates (exemplified for a dimer) for a π-conjugated molecule (monomer) and corresponding spectral shift in the absorption UV-vis spectra. Full arrows depict allowed (strong) transitions, and dashed arrows forbidden (or weak) ones. The double arrow represents the transition dipole for the monomer.[238]

A more exhaustive classification in terms of the mutual orientation of molecules can be done for the nanoassemblies. They can be classified as face to face (*H*-type aggregate), slipped cofacial (*H*-aggregate for 0 < q < 54.7 or J-aggregate for 54.7 < q < 90), pure head-to-tail (*J*-type aggregate) and randomly oriented type, see Figure 31.[257]

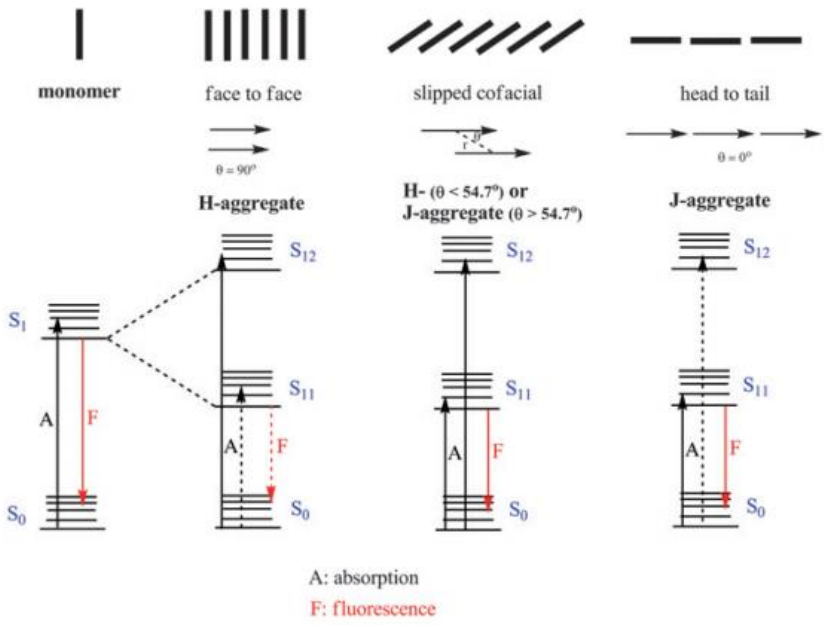

Figure 31. The mutual orientation of molecules in an aggregate, the associated energy level diagram, and the allowed or forbidden transitions.[22]

Importantly, self-aggregation interferes in excited-state processes by exciton coupling, excimer/exciplex formation, resonance energy transfer, and triplet-triplet annihilation.[259] For this reason, the formation of aggregates may be desirable or not depending on the future applications of our system. For some applications, for instance PDT,[148] the presence of aggregates presents a problem in terms of dye efficiency and properties. Otherwise, stacking can allow to obtain materials with different and improved properties related to those exhibited by the corresponding monomers.[22] Specifically, self-assembly can be extremely strong, producing an outstanding robustness. The driving force of aggregation grows with increasing size of the hydrophobic surface and results in the formation of exceedingly stable polymers.

Regarding to the size and geometry of the aromatic core, a stronger π–π interaction and concomitantly a larger aggregation constant could be expected for larger-sized π-systems in the same solvent at the same temperature. Figure 32 compares the binding constants measured for some π-systems at room temperature. Peripheral substituents attached to the π-conjugated core affect considerably to the supramolecular stacking. The electron-

withdrawing or donating nature of these groups can contribute to the electrostatic interaction of the molecules, and steric effects of bulky substituents can drastically decrease or even prevent the aggregation processes. Solvent is also crucial since solvent molecules compete with the solute to provide energetically favorable contact with the lowest overall free energy.

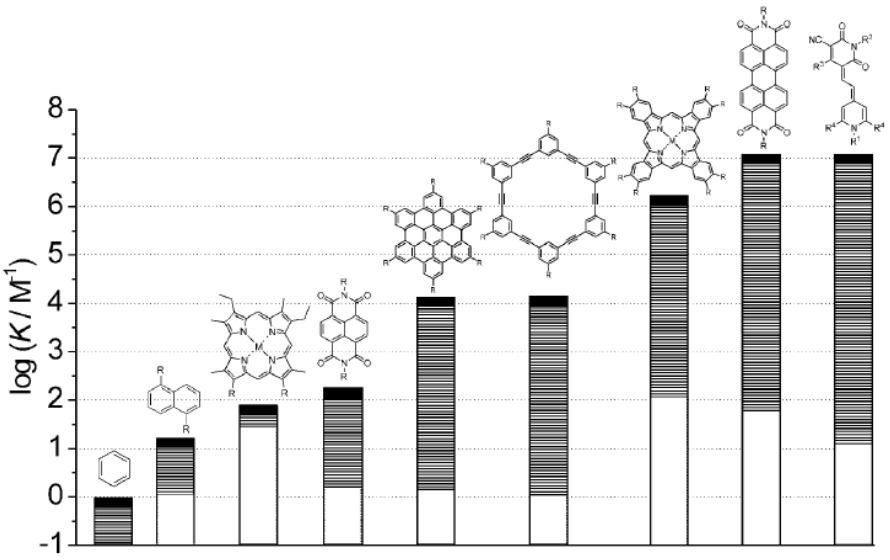

Figure 32. A comparison of the highest values (black bar) and the range (grey shaded area) of some reported aggregation constants for different π-conjugated systems.[260]

3.4. Chiral supramolecular architectures

Chirality exists as a ubiquitous phenomenon in nature in a molecular level from *L*-amino acids to *D*-sugars. Chiral supramolecular architectures also constitute crucial elements in living systems, as protein folding (α-helix/β-sheet conformations) and DNA double helix formation, and have been long mimicked by chemists to recreate their properties in artificial systems. Chirality at the supramolecular scale is an important feature of functional materials, which highly influences their applications. Supramolecular chirality can be defined as the aggregation of molecular building blocks, with or without chiral centers, which might bring asymmetric spatial stacking that further results in the appearance of non-symmetry in extended scales like helical nanofibers.[261] One of the important research topics in this field is the rational manipulation of chirality amplification and handedness. During the chiral self-assembly, the propagation of chiral information through specific interactions is generally called 'chirality transfer', and can be produced when the chiral information on a chiral center (i.e. an asymmetric carbon atom or axial chirality) is imposed to the whole assembly. When the self-assembly contains a

chromophore, the chirality can be detected by electronic circular dichroism (CD) spectroscopy.

a) Electronic circular dichroism spectroscopy

Spectroscopy provides a powerful method for detecting the chiral characteristics of supramolecular systems. CD spectroscopy is the differential absorption of left versus right circularly polarized light and represent the most widely technique used for the characterization of chiral chromophores. This spectroscopy was developed to study molecular chirality, but is also particularly useful for monitoring self-assembled systems for two reasons:[241]

- CD signals originate from the electronic transitions of the chromophore are generally sensitive to the dye packing. Many mechanisms responsible for the appearance of CD bands occur through space, and are intrinsically sensitive to intermolecular interactions and external stimuli.
- Self-assembly is usually a dynamic process, with assembly and disassembly occurring simultaneously, and generally takes place in the time scale of CD measurements.

Regarding to CD spectra interpretation, two types of spectra are generally obtained, as illustrated in Figure 33. Observation of a peak or valley in the CD spectrum is referred to as the Cotton effect, which is deemed positive if the CD first increases as the wavelength decreases, and negative if the CD decreases first. When measuring the CD spectrum, the Cotton effect generally corresponds to the absorption maximum in the UV-vis spectrum. On the other hand, the sign of the CD is determined by the handedness of the supramolecular assembly and, if enantiomers are measured, mirror images should result. The exciton-type CD spectrum, shown in Figure 33 with dashed lines, is commonly referred to as a bisignate band.[262]

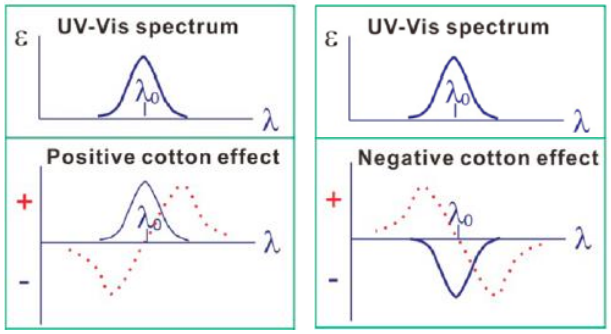

Figure 33. A) Typical CD spectra in supramolecular systems. Adapted from reference.[241]

The CD technique is typically suitable for viewing self-assembled systems in isotropic solutions, and requires the appropriate selection of the solvent, concentration, and measurement cell.[263,264] Different kinds of information can be obtained specifically when non-covalent chiral assemblies are characterized by means of CD spectroscopy,[265,266] including the simple detection of chiral aggregates or complexes, the thermodynamic and kinetic parameters such as binding and rate constants, and ultimately, the refinement of the most plausible structure of the supramolecular species. In this way, CD spectra may suggest which intermolecular forces are likely to play a role.

b) Molecular interactions: dimers, oligomers and "infinite" assemblies

Nina Berova's group reported an exhaustive study about the application of CD in the study of supramolecular systems.[238] They show how chiral supramolecular species may originate from an extensive variety of situations. When two or more identical chromophores, not conjugated to each other, are located nearby in space, they can interact through a direct dipolar interaction, which depends on the distance between them and their relative orientation. In the case of a dimer, if this couple of identical chromophores characterized by one electronic π→π* transition is irradiated, it gives rise to a delocalized excitation which results in a characteristic pair of CD bands of opposite sign, known as a couplet (Figure 33). The sequence of signs along the wavelength absorption range is diagnostic of the absolute arrangement of the electric dipole transition moments, thus a positive-negative couplet reveals that the moments define a positive exciton chirality. The sign of the exciton couplet can be directly related to the sense of twist between the two molecules participating in the assembly. Detailed analysis of the CD spectrum allows to validate geometrical models, but more quantitative information may be sought through full CD calculations on model structures.

Usually, there is little difference between dimers and oligomers spectra, and it is difficult to discriminate between them by chiroptical spectroscopy alone. Intermolecular interactions can be replicated an indefinite number of times, which leads to the formation of large aggregates, so the number of constituent units may be considered "infinite". It is common that the individual bricks of these architectures are endowed with weaker intrinsic CD than the infinite entity, which signal will actually correspond to the summation of the one associated with its small repeating units. The infinite assemblies often provide, at the mesoscopic level, twisted and threaded superstructures that can be observed by means of electron or atomic force microscopies. In order to control the aggregation process, one can change the concentration, the temperature and the solvent composition by using mixtures of a good solvent (where the molecules are well solvated and exist as monomers) with a poor solvent (where the molecules aggregate).

In the case of infinite assemblies based in conjugated monomers, both *H*- and *J*-aggregates may manifest exciton-coupled CD spectra with a more or less strong exciton

couplet depending on the exact supramolecular arrangement. According to the shape of their components, extended π-systems can be further divided into two classes (Figure 34): 'Rod-like', where the elongated chromophore has one privileged axis, and the transition dipoles of the most red-shifted transitions are aligned; and 'disk-like', as in Pors or Pcs. In both cases, the central core of the dyes are intrinsically achiral, therefore chirality must be introduced in the side groups, which are expected to provide only weak perturbations to the electronic transitions of the main chromophores and accordingly, intrinsic CD of isolated molecules is usually very weak and hardly detectable.

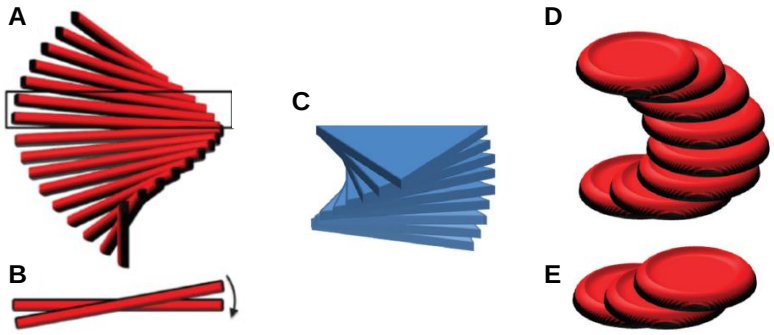

Figure 34. Twisted H-stack of rod-like molecules (A) and the twist between two adjacent molecules (B). Chiral H-stacks in disk-like systems where the center of the molecules can be aligned (C), or with certain degree of chiral tiling (D). For disk-like molecules, at least three elements to define chirality are needed (E).[238]

3.5. Supramolecular assemblies in aqueous media

a) Self-assembly of π-conjugated molecules in water

The self-assembly of large π-conjugated molecules in various solvents has been extensively studied and reviewed.[260,267–269] However, the critical component that Nature uses for achieving complexity, adaptability and robustness in its systems is water,[270] a unique medium for self-assembly,[271] where virtually all biological processes take place. In general, synthetic supramolecular systems are classified according to their formation trough hydrogen bonds,[272] large π-conjugated surfaces and host-guest interactions. Herein, only large π-conjugated surface-based systems will be discussed since this group includes Pcs.

The main advantage of aqueous supramolecular arrangements is the possibility to create biocompatible systems. π-Conjugated molecules have some features which confer advantages for the rational design and functionality of supramolecular systems in aqueous media.[273–275]. Thus, self-assembly can be extremely stable, due to a combination

of hydrophobic and π–π interactions that provide robustness.[276] In aqueous media, the strength of the hydrophobic effect often increases with rising the temperature, so that materials based on hydrophobic interactions can be extremely stable to heat. For instance, adding an organic co-solvent or introducing electrical charges may drastically weaken the hydrophobic effect, thus enabling reversible construction and destruction of self-assembled systems.[273] On the other hand, hydrophilic interactions (interactions of water molecules with polar and charged groups) are of primary importance in aqueous supramolecular arrangements,[277] since they provide solubility in water. These groups are strongly solvated, contributing to the steric bulkiness of the aqueous assemblies; however, the electrostatic repulsion between equally charged groups counterbalances the attractive interactions between hydrophobic moieties. Taking advantage of the benefits of hydrophobic interactions, together with the advantages of the hydrophilic groups contribution, amphiphiles with unique properties can be designed, topic that we will discuss in the next section.

b) Self-assembly of amphiphilic π-conjugated molecules

Conventionally, an amphiphile refers to a molecule that contains a hydrophilic and a hydrophobic part, linked by covalent bonding.[278] Amphiphiles have different self-assembly behaviors in aqueous media where the polar head group interacts with water, while the non-polar lipophilic region will migrate above the lipophilic components of other molecules. From the thermodynamic point of view, the self-association of amphiphilic molecules is driven by the competition between interfacial energy of the supramolecular system core with solvent and the conformational distortion energy of the soluble lipophilic groups emanating from the core. Control over the shapes gives a possibility to develop and manipulate the architecture of the nanostructures (Figure 35).[278] The interest in these structures arises from their self-assembly in aqueous solution to form well-defined arrangements, such as micelles, vesicles, nanotubes, nanofibers, and lamellae; which can find applications in many fields such as nanodevices,[279,280] drug delivery[281] and template synthesis.[282] Regarding biological applications, surface functional groups in these nanostructures enable multivalent binding with a cell surface and other biological targets.

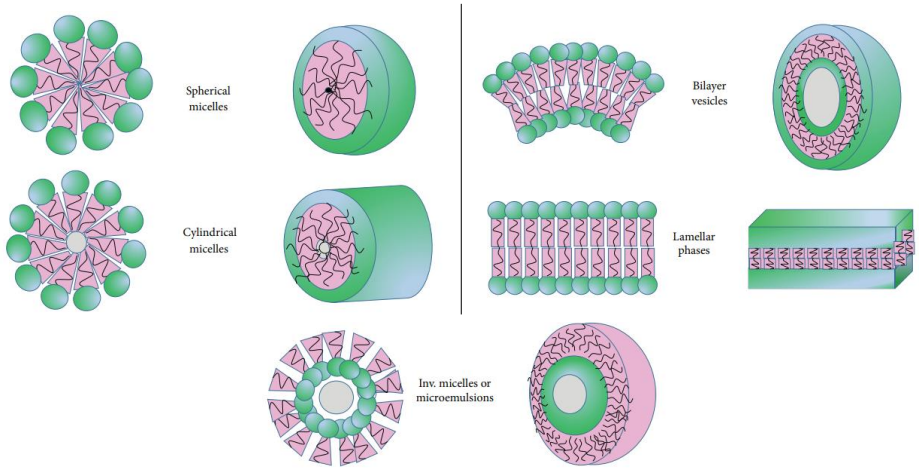

Figure 35. Summary of the possible amphiphilic aggregate structures.[278] (Adapted from the reference).

Supramolecular arrangements based on π-amphiphiles are emerging as a new class of adaptive materials that remain the ability of π-conjugated systems to self-assemble in a "programmed" fashion. In particular, their aqueous self-assembly is expected to yield a wide variety of supramolecular structures of unprecedented complexity through multiple non-covalent interactions.[283] Supramolecular polymers of π-systems in water appear promising owing to their precise internal order, stability, optical properties, and the possibility to fine tuning of the structural parameters by directional molecular interaction.[272] The literature is full of examples of complex and sophisticated self-assemblies of π-conjugated systems in water,[284] built with molecules featuring outstanding electronic properties such as boron-dipyrromethene (BODIPY),[285] azadipyrromethene (aza-BODIPY),[286] spiropyran,[287] oligo-paraphenylene,[288] hexabenzocoronene (HBC),[279,289–291] perylene bisimide (PBI),[292,293] and benzotrithiophene,[294] among others.

Remarkable are the works by Müllen and co-workers with amphiphilic coronene derivatives that form well-ordered columnar stacks in aqueous solution,[289,290] and the reports by Aida and co-workers on HBC amphiphiles endowed with triethylene glycol chains or positively charged isothiouronium groups that can polymerize into nanotubes and are uniformly dispersed in water (Figure 36A).[279,291] The latter authors also escribed an HBC molecule appended with pyridyl-terminated triethylene glycol side chains that, in combination with a platinum salt, lead to the formation of graphitic nanotubes.[295] Also remarkable are the PBI assemblies in aqueous media mostly studied by Frank Würthner's group.[292,293] They reported amphiphilic PBIs containing hydrophilic and hydrophobic imide substituents of different size and shape that are able to form a variety of supramolecular arrangements in water. For instance, dumbbell-shaped PBIs, as the shown in Figure 36B, allows the formation of rod aggregates in water with columnar

structures similar to those in organic solvents. On the other hand, the incorporation of polyglycerol dendrons to the PBI core showed to improve the water solubility and allowed a control of the aggregation behavior.

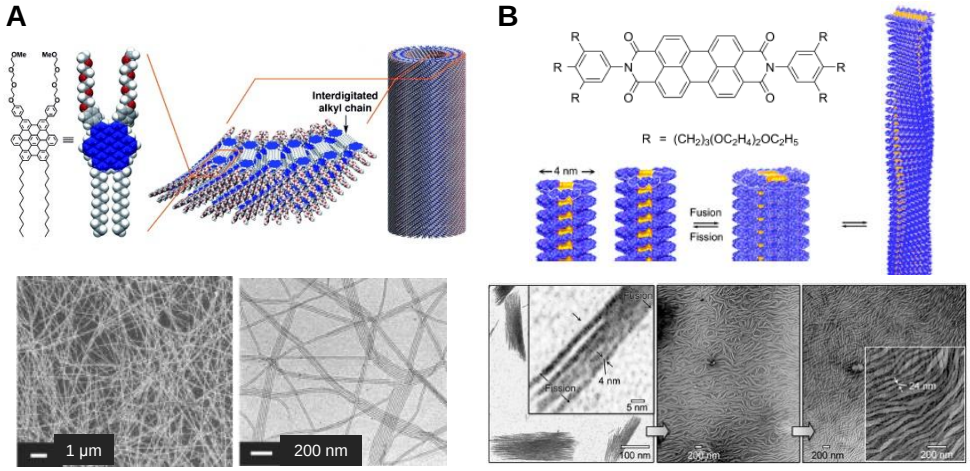

Figure 36. A) Amphiphilic hexa-peri-hexabenzocoronene, which forms tubes that can be placed between two electrodes.[279]*. B) TEM images of PBI aggregates prepared from water and schematic illustration for the hierarchical self-assembly. (Adapted from the references).*[292]

3.6. Supramolecular assemblies of porphyrinoids and phthalocyanine derivatives

Nature shows us how porphyrinoid supramolecular assemblies are able to develop a function. Chlorophyll aggregates serve as the functional units in the light-harvesting apparatus of photosynthetic organisms such as purple and green bacteria, or plants.[260] X-Ray crystallographic studies revealed how chlorophyll molecules, with the assistance of proteins, self-assemble into cyclic dye arrays of different size in purple bacteria,[296,297] and rod-like aggregates containing hundreds of π–π-stacked chromophores in green bacteria.[298] In these fascinating assemblies, the chromophores are organized in an appropriate spatial arrangement that enables efficient energy transfer between the dyes upon photoexcitation (Figure 37).

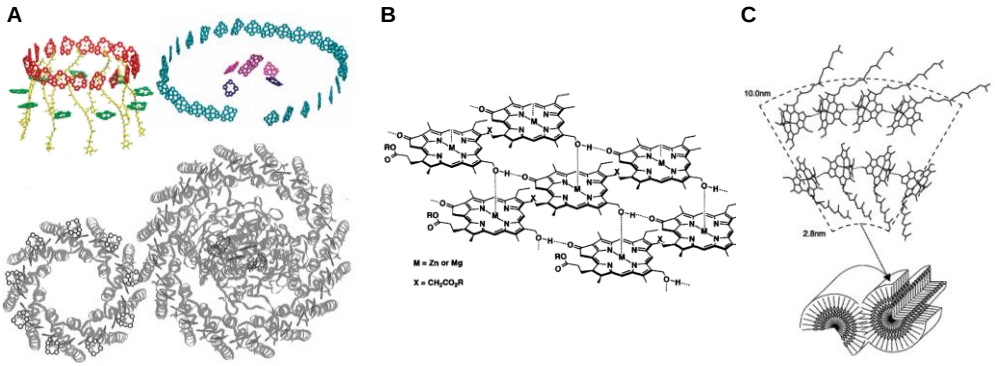

Figure 37. A) Schematic of the photosynthetic apparatus of purple non-sulfur bacteria highlighting the arrangement of chromophores (chlorophyll aggregates).[296,299] *B) Proposed supramolecular structure for self-aggregates of metallochlorin.*[298] *C) Chlorosome organization in green bacteria.*[267] *(Figure adapted from the references).*

a) Organization of synthetic dyes in organic solvents

Tetrapyrrole macrocycles (i.e. Pcs, Pors) constitute probably one of the most important classes of synthetic chromophores. Bare porphyrinoids self-assemble as one-dimensional stacks by aggregation of their π-systems through π –π interactions, described as a sum of van der Waals interactions, electrostatic interactions, and solvophobic effect, when they are in solution.[300] In general, dimerization constants of neutral Pors are in a range of 3–100 M^{-1} in organic solvents, while those for Pcs range from 100 to 10^6 M^{-1}.[245,301,302] However, the type and the extent of aggregation can be tuned controlling the substitution pattern over the molecule.[303] For instance, extension of the conjugation of the Zn(II)Pc core by attaching perylenediimide has led to strong, photoactive aggregates, as described by Wasielewski and coworkers. The tetra- perylenediimide-substituted Zn(II)Pc self-assembles in solution forming stacked heptamers, as evidenced by SAXS/WAXS, and forms long fibrous structures in the solid state.[304] On the other hand, the customized donor/acceptor character of the Pc cores has permitted the formation of π–π stacked nanoaggregates by heteroassociation between electron-rich Zn(II)Pcs and electron-deficient Ni(II)Pcs. Donor-acceptor interactions have been shown to be the main driving force for the association into one-dimensional nanoaggregates through intermolecular interactions.[305] Attachment of long alkyl chains at the periphery of the Pc macrocycle also contributes to the formation of self-organized systems. The formation of columnar liquid crystals has been deeply explored by several researchers,[306,307] but alkyl chain substitution also contributes to the organization in solution. Especially relevant examples are those in which a chiral center in the alkyl chain induces a chiral supramolecular arrangement of the Pc molecules.[120,308,309] In this regard, Nolte and coworkers were pioneers in reporting the formation of right-handed helical structures in solution with Pc

molecules functionalized with four crown ether units endowed with chiral branched alkoxy chains.[309]

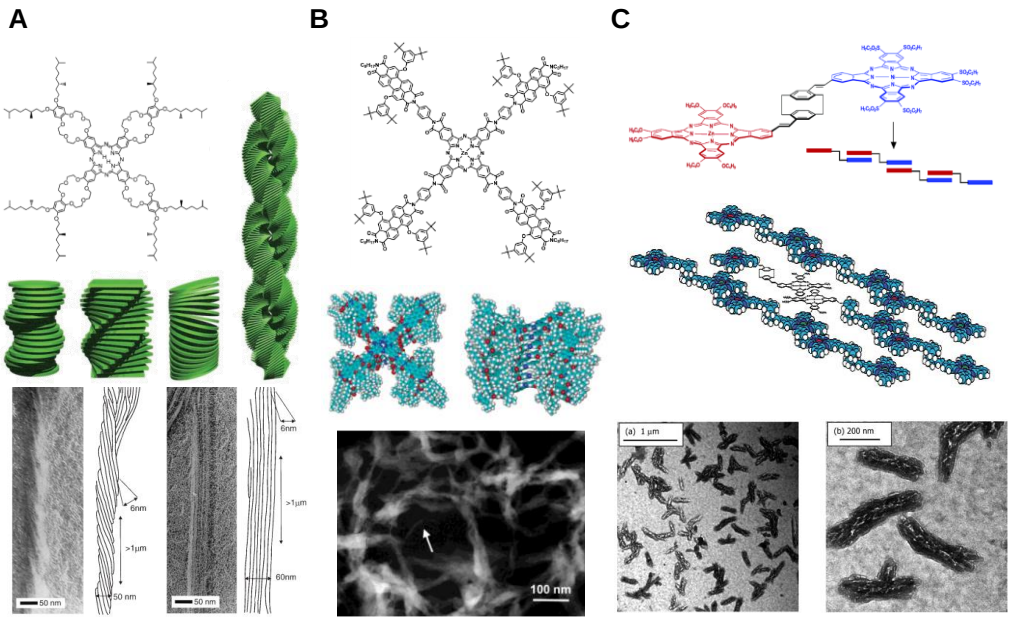

Figure 38. A) Helical structures in solution with Pc molecules functionalized with four crown ether units endowed with chiral branched alkoxy chains.[309] B) Self-assembled columns of Zn(II)Pc tetrakis(perylenediimide).[304] C) Donor-Acceptor Pc nanoaggregates and their transmission electron micrographs.[305] (Adapted from the references).

The formation of helical superstructures with Pcs has been receiving increasing research interests owing to their potential applications in catalysis, drug delivery, chemical sensors, and chiroptical devices of the macrocycle. For instance, our research group has taken benefit of the inherent chirality of C_3-monosubstituted SubPc molecules to form non-centrosymmetric homochiral columnar assemblies.[310] These assemblies (see Figure 39A) are formed through a cooperative supramolecular polymerization process driven by hydrogen-bonding between amide groups, π–π stacking, and dipolar interactions between axial B-F bonds.

By other hand, Nagao Kobayashi's review about optically active Pcs illustrates how these macrocycles can incorporate chirality in different ways in their structure and extend it to the formation of aggregates.[311] One of the most remarkable ways of introducing chirality is through the introduction of binaphthyl motifs as a chiral unit, a strategy that has been used by Kobayashi to form chiral arrangements.[312,313] For instance, chiral supramolecular arrangements are formed when the optically active symmetric metal-free Pc with two binaphthyl units, shown in Figure 39B, is decorated with four octyl chains.[314] Specifically

hollow-sphere nanostructures (*H*-aggregates) can be formed by employing a small amount of the surfactant cetyltrimethylammonium bromide (CTAB). This work, representing the first example of controllable organic nanostructures with a hollow sphere morphology fabricated from Pcs provides an effective method towards Pc hollow nanospheres.

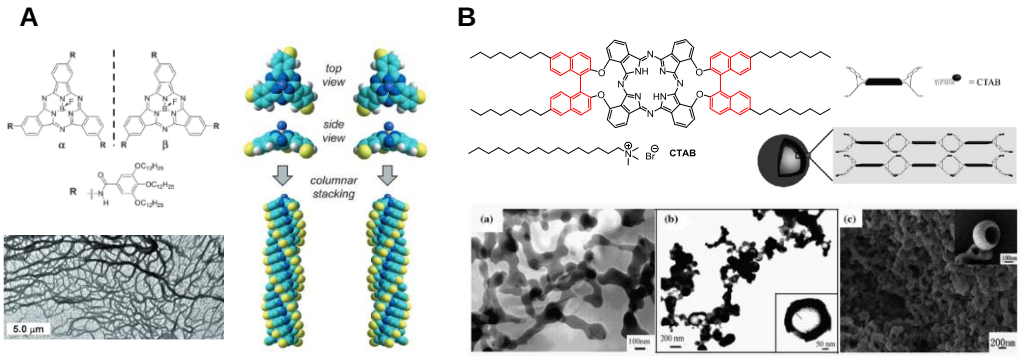

Figure 39. A) Homochiral supramolecular polymers of tetrahedral subphthalocyanine molecules.[310] *B) Schematic molecular structure of $(AA)_2$-H_2Pc and CTAB with (a) TEM image of $(AA)_2$-H_2Pc nanoparticles; TEM (b) and SEM (c) image of nanoscale hollow spheres.*[314] *(Adapted from the references).*

b) Supramolecular arrangements in aqueous media

Heme, an important molecule for life, is an amphiphilic Por possessing both hydrophilic and lipophilic groups at the opposite ends of the macrocycle. As the porphyrin skeleton is essentially hydrophobic, its transformation to an amphiphile requires introduction of hydrophilic head groups.[315] In this respect, a lot of work has been done toward develop strategies for the synthesis of amphiphilic Por to form hierarchical self-assemblies, with control on the shapes and dimensions, into nanospheres, nanorods, films, spheric micelles, vesicles or macrowires,[316–320] in some cases with application in photothermal or photodynamic therapy.[321,322]

Regarding to Pc-based systems much less examples have been reported to date. Guldi's group reported the supramolecular organization for an amphiphilic Pc–C_{60} dyad salt (Figure 40). This dyad is able to form, because of a combination of solvophobic and π–π stacking interactions, perfectly ordered 1D Pc–C_{60} nanotubules when dispersed in water, as demonstrated by transmission electron microscopy (TEM) analysis.

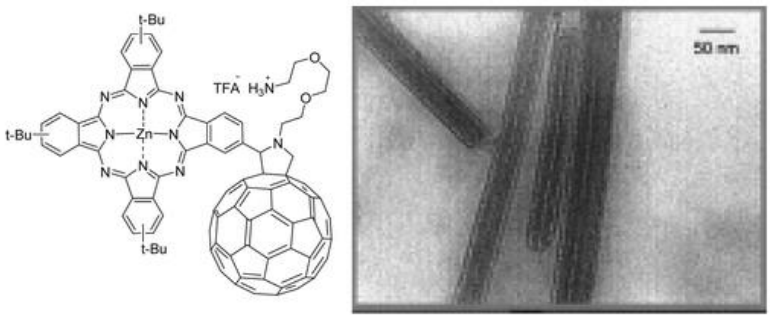

Figure 40. Nanotubules formed in water solution deposited on a TEM grid by the nanoscale organization of a Pc-Fullerene amphiphillic system.[323]

On the other hand, Li et al. (Figure 41) prepared self-assembled Zn(II)Pc-containing nanovesicles for theranostics, the Pc amphiphilic chemical structure facilitates its spontaneous assembly to form a uniform nanovesicle dispersion in aqueous solutions.[324] They also prepared Pc-assembled nanodots as PS for highly efficient Type I photoreactions in photodynamic therapy.[325] Although most nanostructured PS assemblies are super-quenched preventing their use in PDT, their new material undergo stimuli-responsive disassembly, which leads to partial recovery of PDT activity.

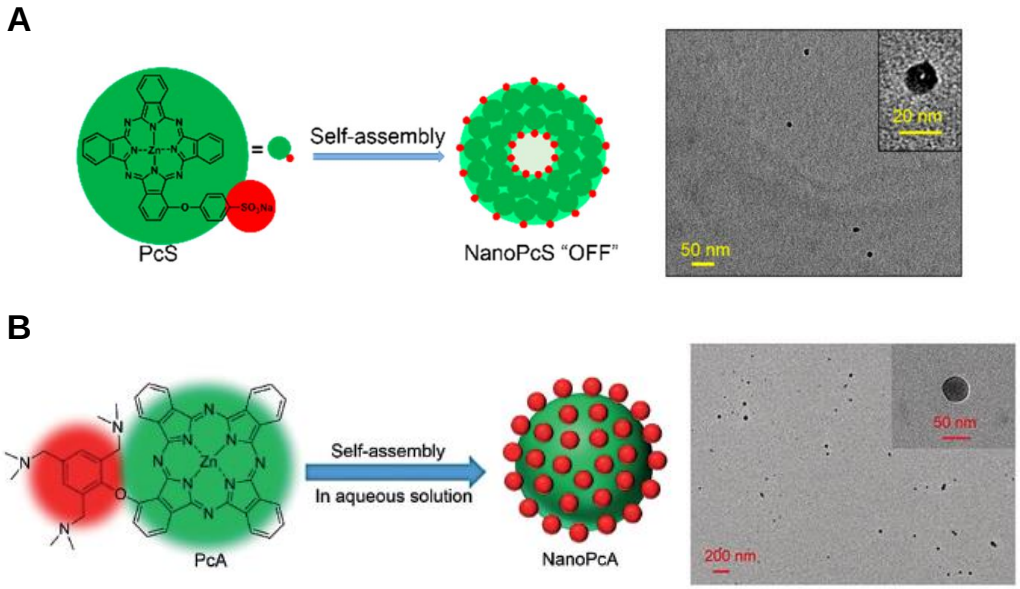

Figure 41. A and B) Zn(II)Pc nanovesicles.[324,325] *(Adapted from the references).*

4. References

(1) Claessens, C. G.; Hahn, U.; Torres, T. Phthalocyanines: From Outstanding Electronic Properties to Emerging Applications. *Chem. Rec.* **2008**, *8*, 75–97.

(2) de la Torre, G.; Bottari, G.; Hahn, U.; Torres, T. Functional Phthalocyanines: Synthesis, Nanostructuration, and Electro-Optical Applications. In *Functional Phthalocyanine Molecular Materials*; Jiang, J., Ed.; Structure and Bonding; Springer Berlin Heidelberg, 2010; Vol. 135, pp 1–44.

(3) Dumoulin, F.; Durmuş, M.; Ahsen, V.; Nyokong, T. Synthetic Pathways to Water-Soluble Phthalocyanines and Close Analogs. *Coord. Chem. Rev.* **2010**, *254* (23), 2792–2847.

(4) Mack, J.; Kobayashi, N. Low Symmetry Phthalocyanines and Their Analogues. *Chem. Rev.* **2011**, *111*, 281–321.

(5) No Title. In *Handbook of Porphyrin Science*; K. M. Kadish, K. M. Smith, R. G., Ed.; World Scientific: Singapore, 2013.

(6) McKeown, N. B. *Phthalocyanine Materials Synthesis, Structure and Function*; Cambridge University Press, Cambridge, 1998.

(7) Guillaud, G.; Simon, J.; Germain, J. P. Metallophthalocyanines: Gas Sensors, Resistors and Field Effect Transistors1In Memory of Christine Maleysson.1. *Coord. Chem. Rev.* **1998**, *178–180*, 1433–1484.

(8) Braun, A.; Tcherniac, J. Über Die Produkte Der Einwirkung von Acetanhydrid Auf Phthalamid. *Berichte der Dtsch. Chem. Gesellschaft* **1907**, *40*, 2709–2714.

(9) de Diesbach, H.; von der Weid, E. Quelques Sels Complexes Des O-Dinitriles Avec Le Cuivre et La Pyridine. *Helv. Chim. Acta* **1927**, *10*, 886–888.

(10) Dahlen, M. A. The Phthalocyanines A New Class of Synthetic Pigments and Dyes. *Ind. Eng. Chem.* **1939**, *31*, 839–847.

(11) Dent, C. E.; Linstead, R. P.; Lowe, A. R. 217. Phthalocyanines. Part VI. The Structure of the Phthalocyanines. *J. Chem. Soc.* **1934**, No. 0, 1033–1039.

(12) Robertson, J. M. 136. An X-Ray Study of the Structure of the Phthalocyanines. Part I. The Metal-Free, Nickel, Copper, and Platinum Compounds. *J. Chem. Soc.* **1935**, No. 0, 615–621.

(13) Linstead, R. P. 212. Phthalocyanines. Part I. A New Type of Synthetic Colouring Matters. *J. Chem. Soc.* **1934**, No. 0, 1016–1017.

(14) Linstead, R. P.; Lowe, A. R. 214. Phthalocyanines. Part III. Preliminary Experiments on the Preparation of Phthalocyanines from Phthalonitrile. *J. Chem. Soc.* **1934**, No. 0, 1022–1027.

(15) Ortí, E.; Brédas, J. L. Electronic Structure of Metal-free Phthalocyanine: A Valence Effective Hamiltonian Theoretical Study. *J. Chem. Phys.* **1988**, *89*, 1009–1016.

(16) Moss, G. P. Nomenclature of Tetrapyrroles. *Pure Appl. Chem.* **1987**, *59* (6), 779–832.

(17) de la Torre, G.; Claessens, C. G.; Torres, T. Phthalocyanines: Old Dyes, New Materials. Putting Color in Nanotechnology. *Chem. Commun.* **2007**, 2000–2015.

(18) van de Winckel, E.; Schneider, R. J.; de la Escosura, A.; Torres, T. Multifunctional Logic in a Photosensitizer with Triple-Mode Fluorescent and Photodynamic Activity. *Chem. – A Eur. J.* **2015**, *21*, 18551–18556.

(19) Bispo, M.; Pereira, P. M. R.; Setaro, F.; Rodríguez-Morgade, M. S.; Fernandes, R.; Torres, T.; Tomé, J. P. C. A Galactose Dendritic Silicon (IV) Phthalocyanine as a Photosensitizing Agent in Cancer Photodynamic Therapy. *Chempluschem* **2018**, *83* (9), 855–860.

(20) Teles Ferreira, J.; Pina, J.; Alberto Fontes Ribeiro, C.; Fernandes, R.; Tomé, J. P. C.;

Rodríguez-Morgade, M. S.; Torres, T. PEG-Containing Ruthenium Phthalocyanines as Photosensitizers for Photodynamic Therapy: Synthesis, Characterization and in Vitro Evaluation. *J. Mater. Chem. B* **2017**, *5* (29), 5862–5869.

(21) Hunter, C. A.; Sanders, J. K. M. The Nature of .Pi.-.Pi. Interactions. *J. Am. Chem. Soc.* **1990**, *112* (14), 5525–5534.

(22) Zhang, X. F.; Xi, Q.; Zhao, J. Fluorescent and Triplet State Photoactive J-Type Phthalocyanine Nano Assemblies: Controlled Formation and Photosensitizing Properties. *J. Mater. Chem.* **2010**, *20* (32), 6726–6733.

(23) Teixeira Tasso, T.; Yamasaki, Y.; Furuyama, T.; Kobayashi, N. An Exemplary Relationship between the Extent of Cofacial Aggregation and Fluorescence Quantum Yield as Exhibited by Quaternized Amphiphilic Phthalocyanines. *Dalt. Trans.* **2014**, *43* (15), 5886–5892.

(24) Kudrevich, S. V; van Lier, J. E. Azaanalogs of Phthalocyanine: Syntheses and Properties. *Coord. Chem. Rev.* **1996**, *156*, 163–182.

(25) Nicolau, M.; Cabezón, B.; Torres, T. Triazolephthalocyanines: Synthesis, Supramolecular Organization and Physical Properties. *Coord. Chem. Rev.* **1999**, *190–192*, 231–243.

(26) Kobayashi, N.; Miwa, H.; Nemykin, V. N. Adjacent versus Opposite Type Di-Aromatic Ring-Fused Phthalocyanine Derivatives: Synthesis, Spectroscopy, Electrochemistry, and Molecular Orbital Calculations. *J. Am. Chem. Soc.* **2002**, *124* (27), 8007–8020.

(27) Claessens, C. G.; Torres, T. Synthesis, Separation, and Characterization of the Topoisomers of Fused Bicyclic Subphthalocyanine Dimers. *Angew. Chemie Int. Ed.* **2002**, *41*, 2561–2565.

(28) Torres, T. From Subphthalocyanines to Subporphyrins. *Angew. Chemie Int. Ed.* **2006**, *45*, 2834–2837.

(29) Muranaka, A.; Yonehara, M.; Uchiyama, M. Azulenocyanine: A New Family of Phthalocyanines with Intense Near-IR Absorption. *J. Am. Chem. Soc.* **2010**, *132*, 7844–7845.

(30) Vicente, M. G. H.; Jaquinod, L.; Khoury, R. G.; Madrona, A. Y.; Smith, K. M. Synthesis and Chemistry of New Benzoporphyrins. *Tetrahedron Lett.* **1999**, *40* (50), 8763–8766.

(31) Kobayashi, N.; Nakajima, S.; Ogata, H.; Fukuda, T. Synthesis, Spectroscopy, and Electrochemistry of Tetra-Tert-Butylated Tetraazaporphyrins, Phthalocyanines, Naphthalocyanines, and Anthracocyanines, Together with Molecular Orbital Calculations. *Chem. – A Eur. J.* **2004**, *10*, 6294–6312.

(32) Alexander, V. Design and Synthesis of Macrocyclic Ligands and Their Complexes of Lanthanides and Actinides. *Chem. Rev.* **1995**, *95*, 273–342.

(33) de la Torre, G.; Martínez-Díaz, M. V.; Ashton, P. R.; Torres, T. Novel Homo- and Heterodimetallic Heterobinuclear Phthalocyaninato-Triazolehemiporphyrazinate Complexes. *J. Org. Chem.* **1998**, *63*, 8888–8893.

(34) Dubinina, T. V; Ivanov, A. V; Borisova, N. E.; Trashin, S. A.; Gurskiy, S. I.; Tomilova, L. G.; Zefirov, N. S. Synthesis and Investigation of Spectral and Electrochemical Properties of Alkyl-Substituted Planar Binuclear Phthalocyanine Complexes Sharing a Common Naphthalene Ring. *Inorganica Chim. Acta* **2010**, *363*, 1869–1878.

(35) Claessens, C. G.; González-Rodríguez, D.; Torres, T. Subphthalocyanines: Singular Nonplanar Aromatic Compounds - Synthesis, Reactivity, and Physical Properties. *Chem. Rev.* **2002**, *102*, 835–854.

(36) Claessens, C. G.; González-Rodríguez, D.; Rodríguez-Morgade, M. S.; Medina, A.; Torres, T. Subphthalocyanines, Subporphyrazines, and Subporphyrins: Singular Nonplanar Aromatic Systems. *Chem. Rev.* **2014**, *114*, 2192–2277.

(37) Mack, J.; Stillman, M. J. Assignment of the Optical Spectra of Metal Phthalocyanines through Spectral Band Deconvolution Analysis and Zindo Calculations. *Coord. Chem. Rev.*

2001, *219*, 993–1032.

(38) Rio, Y.; Salomé Rodríguez-Morgade, M.; Torres, T. Modulating the Electronic Properties of Porphyrinoids: A Voyage from the Violet to the Infrared Regions of the Electromagnetic Spectrum. *Org. Biomol. Chem.* **2008**, *6* (11), 1877–1894.

(39) Listorti, A.; López-Duarte, I.; Martínez-Díaz, M. V.; Torres, T.; DosSantos, T.; Barnes, P. R. F.; Durrant, J. R. Zn(II) versus Ru(II) Phthalocyanine-Sensitised Solar Cells. A Comparison between Singlet and Triplet Electron Injectors. *Energy Environ. Sci.* **2010**, *3* (10), 1573–1579.

(40) Zhang, X.-F.; Shao, X.; Tian, H.; Sun, X.; Han, K. Synthesis, Fluorescence, Excited Triplet State Properties and Singlet Oxygen Generation of Para-(Tert-Butylphenoxy) Substituted Phthalocyanines Containing Group IV A Central Elements. *Dye. Pigment.* **2013**, *99* (2), 480–488.

(41) Kobayashi, N.; Ogata, H.; Nonaka, N.; Luk'yanets, E. A. Effect of Peripheral Substitution on the Electronic Absorption and Fluorescence Spectra of Metal-Free and Zinc Phthalocyanines. *Chem. - A Eur. J.* **2003**, *9* (20), 5123–5134.

(42) Vannikov, A. V; Grishina, A. D.; Gorbunova, Y. G.; Zolotarevskii, V. I.; Krivenko, T. V; Laryushkin, A. S.; Lapkina, L. A.; Savel'ev, V. V; Tsivadze, A. Y. Influence of Heavy Central Atom on Photoelectric, Nonlinear Optical, and Photorefractive Properties of Metal Phthalocyanines. *High Energy Chem.* **2015**, *49* (1), 36–43.

(43) Alberto, M. E.; De Simone, B. C.; Mazzone, G.; Sicilia, E.; Russo, N. The Heavy Atom Effect on Zn(Ii) Phthalocyanine Derivatives: A Theoretical Exploration of the Photophysical Properties. *Phys. Chem. Chem. Phys.* **2015**, *17* (36), 23595–23601.

(44) Kadish, K. M.; Smith, K. M.; Guilard, R. *The Porphyrin Handbook: Phthalocyanines : Synthesis*; The Porphyrin Handbook; Academic Press, 2003.

(45) Anbarasan, P.; Schareina, T.; Beller, M. Recent Developments and Perspectives in Palladium-Catalyzed Cyanation of Aryl Halides: Synthesis of Benzonitriles. *Chem. Soc. Rev.* **2011**, *40*, 5049–5067.

(46) Leznoff, C. C.; Hu, M.; Nolan, K. J. M. The Synthesis of Phthalocyanines at Room Temperature. *Chem. Commun.* **1996**, *0*, 1245–1246.

(47) Uchida, H.; Tanaka, H.; Yoshiyama, H.; Reddy, P. Y.; Nakamura, S.; Toru, T. Novel Synthesis of Phthalocyanines from Phthalonitriles under Mild Conditions. *Synlett* **2002**, *2002*, 1649–1652.

(48) Uchida, H.; Yoshiyama, H.; Reddy, P. Y.; Nakamura, S.; Toru, T. Novel Synthesis of Metal-Free Phthalocyanines from Phthalimides and Phthalic Anhydrides with Hexamethyldisilazane. *Synlett* **2003**, *2003*, 2083–2085.

(49) Kopylovich, M. N.; Kukushkin, V. Y.; Haukka, M.; Luzyanin, K. V; Pombeiro, A. J. L. An Efficient Synthesis of Phthalocyanines Based on an Unprecedented Double-Addition of Oximes to Phthalonitriles. *J. Am. Chem. Soc.* **2004**, *126*, 15040–15041.

(50) Nas, A.; Kaya, E. Ç.; Kantekin, H.; Sökmen, A.; Çakır, V. Microwave-Assisted Synthesis and Characterization of Novel Symmetrical Substituted 19-Membered Tetrathiadiaza Metal-Free and Metallophthalocyanines and Investigation of Their Biological Activities. *J. Organomet. Chem.* **2011**, *696*, 1659–1663.

(51) Rager, C.; Schmid, G.; Hanack, M. Influence of Substituents, Reaction Conditions and Central Metals on the Isomer Distributions of 1(4)-Tetrasubstituted Phthalocyanines. *Chem. – A Eur. J.* **1999**, *5*, 280–288.

(52) Leznoff, C. C.; D'Ascanio, A. M.; Yildiz, S. Z. Phthalocyanine Formation Using Metals in Primary Alcohols at Room Temperature. *J. Porphyr. Phthalocyanines* **2000**, *4*, 103–111.

(53) Oliver, S. W.; Smith, T. D. Oligomeric Cyclization of Dinitriles in the Synthesis of Phthalocyanines and Related Compounds: The Role of the Alkoxide Anion. *J. Chem. Soc.*

Perkin Trans. 2 **1987**, No. 11, 1579–1582.

(54) Day, V. W.; Marks, T. J.; Wachter, W. A. Large Metal Ion-Centered Template Reactions. Uranyl Complex of Cyclopentakis(2-Iminoisoindoline). *J. Am. Chem. Soc.* **1975**, *97*, 4519–4527.

(55) Li, X.; Wang, H.; Wu, H. *Functional Phthalocyanine Molecular Materials*; Jiang, J., Ed.; Springer: Berlin Heidelberg, 2010.

(56) Martínez-Díaz, M. V.; de la Torre, G.; Torres, T. Lighting Porphyrins and Phthalocyanines for Molecular Photovoltaics. *Chem. Commun.* **2010**, *46* (38), 7090–7108.

(57) Bottari, G.; Trukhina, O.; Ince, M.; Torres, T. Towards Artificial Photosynthesis: Supramolecular, Donor–Acceptor, Porphyrin- and Phthalocyanine/Carbon Nanostructure Ensembles. *Coord. Chem. Rev.* **2012**, *256* (21–22), 2453–2477.

(58) Almeida-Marrero, V.; van de Winckel, E.; Anaya-Plaza, E.; Torres, T.; de la Escosura, A. Porphyrinoid Biohybrid Materials as an Emerging Toolbox for Biomedical Light Management. *Chem. Soc. Rev.* **2018**, *47* (19), 7369–7400.

(59) Craciun, M. F.; Rogge, S.; Den Boer, M. J. L.; Margadonna, S.; Prassides, K.; Iwasa, Y.; Morpurgo, A. F. Electronic Transport through Electron-Doped Metal Phthalocyanine Materials. *Adv. Mater.* **2006**, *18* (3), 320–324.

(60) Ryan, J. W.; Anaya-Plaza, E.; Escosura, A. de la; Torres, T.; Palomares, E. Small Molecule Solar Cells Based on a Series of Water-Soluble Zinc Phthalocyanine Donors. *Chem. Commun.* **2012**, *48*, 6094–6096.

(61) Urbani, M.; de la Torre, G.; Nazeeruddin, M. K.; Torres, T. Phthalocyanines and Porphyrinoid Analogues as Hole- and Electron-Transporting Materials for Perovskite Solar Cells. *Chem. Soc. Rev.* **2019**, *48* (10), 2738–2766.

(62) Ragoussi, M.-E.; Ince, M.; Torres, T. Recent Advances in Phthalocyanine-Based Sensitizers for Dye-Sensitized Solar Cells. *European J. Org. Chem.* **2013**, *2013* (29), 6475–6489.

(63) Urbani, M.; Ragoussi, M. E.; Nazeeruddin, M. K.; Torres, T. Phthalocyanines for Dye-Sensitized Solar Cells. *Coord. Chem. Rev.* **2019**, *381*, 1–64.

(64) Mativetsky, J. M.; Wang, H.; Lee, S. S.; Whittaker-Brooks, L.; Loo, Y.-L. Face-on Stacking and Enhanced out-of-Plane Hole Mobility in Graphene-Templated Copper Phthalocyanine. *Chem. Commun.* **2014**, *50* (40), 5319–5321.

(65) Melville, O. A.; Lessard, B. H.; Bender, T. P. Phthalocyanine-Based Organic Thin-Film Transistors: A Review of Recent Advances. *ACS Appl. Mater. Interfaces* **2015**, *7* (24), 13105–13118.

(66) Bohrer, F. I.; Colesniuc, C. N.; Park, J.; Schuller, I. K.; Kummel, A. C.; Trogler, W. C. Selective Detection of Vapor Phase Hydrogen Peroxide with Phthalocyanine Chemiresistors. *J. Am. Chem. Soc.* **2008**, *130* (12), 3712–3713.

(67) Snow, A. W.; Barger, W. R. Phthalocyanine Films in Chemical Sensors. In *Phthalocyanines: Properties and Applications*; Lever, A. B. P., Ed.; Wiley and Sons: New York, 1989; p 341.

(68) Leznoff, C. C.; Lever, A. B. P. *Phthalocyanines: Properties and Applications*; Phthalocyanines: Properties and Applications; VCH, 1989.

(69) Wöhrle, D. Phthalocyanines: Properties and Applications, Volume 3. Edited by C. C. Leznoff and A. B. P. Lever, VCH, Weinheim 1993, 303 Pp., Hardcover, DM 198, ISBN3-527-89638-4. *Adv. Mater.* **1993**, *5*, 943–944.

(70) Ishikawa, N.; Sugita, M.; Ishikawa, T.; Koshihara, S.; Kaizu, Y. Lanthanide Double-Decker Complexes Functioning as Magnets at the Single-Molecular Level. *J. Am. Chem. Soc.* **2003**, *125* (29), 8694–8695.

(71) de la Torre, G.; Vázquez, P.; Agulló-López, F.; Torres, T. Role of Structural Factors in the Nonlinear Optical Properties of Phthalocyanines and Related Compounds. *Chem. Rev.* **2004**, *104*, 3723–3750.

(72) Cammidge, A. N.; Gopee, H. Macrodiscotic Triphenylenophthalocyanines. *Chem. Commun.* **2002**, *0*, 966–967.

(73) Swarts, J. C.; Langner, E. H. G.; Krokeide-Hove, N.; Cook, M. J. Synthesis and Electrochemical Characterisation of Some Long Chain 1,4,8,11,15,18,22,25-Octa-Alkylated Metal-Free and Zinc Phthalocyanines Possessing Discotic Liquid Crystalline Properties. *J. Mater. Chem.* **2001**, *11* (2), 434–443.

(74) Colomban, C.; Kudrik, E. V; Afanasiev, P.; Sorokin, A. B. Degradation of Chlorinated Phenols in Water in the Presence of H2O2 and Water-Soluble μ-Nitrido Diiron Phthalocyanine. *Catal. Today* **2014**, *235*, 14–19.

(75) Çakır, V.; Saka, E. T.; Bıyıklıoğlu, Z.; Kantekin, H. Highly Selective Oxidation of Benzyl Alcohol Catalyzed by New Peripherally Tetra-Substituted Fe(II) and Co(II) Phthalocyanines. *Synth. Met.* **2014**, *197*, 233–239.

(76) Kimura, M.; Sugihara, Y.; Muto, T.; Hanabusa, K.; Shirai, H.; Kobayashi, N. Dendritic Metallophthalocyanines—Synthesis, Electrochemical Properties, and Catalytic Activities. *Chem. – A Eur. J.* **1999**, *5*, 3495–3500.

(77) Kobayashi, N.; Kobayashi, Y.; Osa, T. Optically Active Phthalocyanines and Their Circular Dichroism. *J. Am. Chem. Soc.* **1993**, *115*, 10994–10995.

(78) Iida, N.; Tanaka, K.; Tokunaga, E.; Mori, S.; Saito, N.; Shibata, N. Synthesis of Phthalocyanines with a Pentafluorosulfanyl Substituent at Peripheral Positions. *ChemistryOpen* **2015**, *4*, 698–702.

(79) Rodríguez-Morgade, S.; Hanack, M. Synthesis, Separation and Characterization of the Structural Isomers of Octa-Tert-Butylphthalocyanines and Dienophilic Phthalocyanine Derivatives. *Chem. – A Eur. J.* **1997**, *3* (7), 1042–1051.

(80) Hanack, M.; Schmid, G.; Sommerauer, M. Chromatographic Separation of the Four Possible Structural Isomers of a Tetrasubstituted Phthalocyanine: Tetrakis(2-Ethylhexyloxy)Phthalocyaninatonickel(II). *Angew. Chemie Int. Ed. English* **1993**, *32*, 1422–1424.

(81) Victor N. Nemykin; Dudkin, S. V.; Dumoulin, F.; Hirel, C.; Gürek, A. G.; Ahsen, V. Synthetic Approaches to Asymmetric Phthalocyanines and Their Analogues. *ARKIVOC* **2014**, No. 1, 142–204.

(82) Torres, T. Perspectives in the Selective Synthesis of Phthalocyanines and Related Compounds. *J. Porphyr. Phthalocyanines* **2000**, *4*, 325–330.

(83) de la Torre, G.; Claessens, C. G.; Torres, T. Phthalocyanines: The Need for Selective Synthetic Approaches. *European J. Org. Chem.* **2000**, *16*, 2821–2830.

(84) Kobayashi, N.; Kondo, R.; Nakajima, S.; Osa, T. New Route to Unsymmetrical Phthalocyanine Analogs by the Use of Structurally Distorted Subphthalocyanines. *J. Am. Chem. Soc.* **1990**, *112*, 9640–9641.

(85) Sastre, A.; Torres, T.; Hanack, M. Synthesis of Novel Unsymmetrical Monoaminated Phthalocyanines. *Tetrahedron Lett.* **1995**, *36*, 8501–8504.

(86) Kudrevich, S. V; Gilbert, S.; van Lier, J. E. Syntheses of Trisulfonated Phthalocyanines and Their Derivatives Using Boron(III) Subphthalocyanines as Intermediates. *J. Org. Chem.* **1996**, *61*, 5706–5707.

(87) Sastre, Á.; del Rey, B.; Torres, T. Synthesis of Novel Unsymmetrically Substituted Push-Pull Phthalocyanines. *J. Org. Chem.* **1996**, *61*, 8591–8597.

(88) Erdem, S. S.; Nesterova, I. V; Soper, S. A.; Hammer, R. P. Solid-Phase Synthesis of Asymmetrically Substituted "AB3-Type" Phthalocyanines. *J. Org. Chem.* **2008**, *73*, 5003–5007.

(89) Leznoff, C. C.; Hall, T. W. The Synthesis of a Soluble, Unsymmetrical Phthalocyanine on a Polymer Support. *Tetrahedron Lett.* **1982**, *23*, 3023–3026.

(90) Bottari, G.; de la Torre, G.; Guldi, D. M.; Torres, T. Covalent and Noncovalent Phthalocyanine–Carbon Nanostructure Systems: Synthesis, Photoinduced Electron Transfer, and Application to Molecular Photovoltaics. *Chem. Rev.* **2010**, *110* (11), 6768–6816.

(91) De La Torre, G.; Bottari, G.; Sekita, M.; Hausmann, A.; Guldi, D. M.; Torres, T. A Voyage into the Synthesis and Photophysics of Homo- and Heterobinuclear Ensembles of Phthalocyanines and Porphyrins. *Chem. Soc. Rev.* **2013**, *42* (20), 8049–8105.

(92) Bottari, G.; de la Torre, G.; Torres, T. Phthalocyanine–Nanocarbon Ensembles: From Discrete Molecular and Supramolecular Systems to Hybrid Nanomaterials. *Acc. Chem. Res.* **2015**, *48*, 900–910.

(93) Banerjee, S.; Sengupta, J.; Aljarilla, A. I.; Setaro, F.; Makinen, P.; Wu, L.; Holappa, L.; de la Escosura, A.; Martinelli, C.; Trohopoulos, P.; et al. Human Serum Albumin Nanoparticles Loaded with Phthalocyanine Dyes for Potential Use in Photodynamic Therapy for Atherosclerotic Plaques. *Precis. Nanomedicine* **2019**, *2* (2), 279–302.

(94) Cid, J.-J.; Yum, J.-H.; Jang, S.-R.; Nazeeruddin, M. K.; Martínez-Ferrero, E.; Palomares, E.; Ko, J.; Grätzel, M.; Torres, T. Molecular Cosensitization for Efficient Panchromatic Dye-Sensitized Solar Cells. *Angew. Chemie Int. Ed.* **2007**, *46* (44), 8358–8362.

(95) García-Iglesias, M.; Cid, J.-J.; Yum, J.-H.; Forneli, A.; Vázquez, P.; Nazeeruddin, M. K.; Palomares, E.; Grätzel, M.; Torres, T. Increasing the Efficiency of Zinc-Phthalocyanine Based Solar Cells through Modification of the Anchoring Ligand. *Energy Environ. Sci.* **2011**, *4* (1), 189–194.

(96) Langmar, O.; Fazio, E.; Schol, P.; de la Torre, G.; Costa, R. D.; Torres, T.; Guldi, D. M. Controlling Interfacial Charge Transfer and Fill Factors in CuO-Based Tandem Dye-Sensitized Solar Cells. *Angew. Chemie - Int. Ed.* **2019**, *58* (12), 4056–4060.

(97) Methfessel, C. D.; Volland, M.; Brunner, K.; Wibmer, L.; Hahn, U.; de la Torre, G.; Torres, T.; Hirsch, A.; Guldi, D. M. Exfoliation of Graphene by Dendritic Water-Soluble Zinc Phthalocyanine Amphiphiles in Polar Media. *Chem. – A Eur. J.* **2018**, *24* (70), 18696–18704.

(98) El-Nahass, M. M.; Youssef, T. E. Thin Films of Asymmetrically Substituted "ABAB-Type" Indium Phthalocyanine Chloride: Preparation, Structural Characterization and Optical Properties. *J. Lumin.* **2011**, *131*, 1419–1427.

(99) Youssef, T. E.; O'Flaherty, S.; Blau, W.; Hanack, M. Phthalocyaninatoindium(III) Acetylacetonates for Nonlinear Optics. *European J. Org. Chem.* **2004**, *2004*, 101–108.

(100) Idelson, E. M. U.S. Patent. 4.061.654, 1977.

(101) Leznoff, C. C.; Greenberg, S.; Khouw, B.; Lever, A. B. P.; Leve, A. B. P. The Syntheses of Mono- and Disubstituted Phthalocyanines Using a Dithioimide. *Can. J. Chem.* **1987**, *65*, 1705–1713.

(102) Shirai, H.; Hanabusa, K.; Kitamura, M.; Masuda, E.; Hirabaru, O.; Hojo, N. Functional Metal Porphyrazine Derivatives and Their Polymers, 14. Synthesis and Properties of [Bis- or Tetrakis(Decyloxycarbonyl)Phthalocyaninanto]Metal Complexes. *Die Makromol. Chemie* **1984**, *185*, 2537–2542.

(103) Young, J. G.; Onyebuagu, W. Synthesis and Characterization of Di-Disubstituted Phthalocyanines. *J. Org. Chem.* **1990**, *55*, 2155–2159.

(104) Stihler, P.; Hauschel, B.; Hanack, M. Synthesis of a Bisdienophilic Phthalocyanine and of Precursors for Repetitive Diels-Alder Reactions Based on Hemiporphyrazines and Phthalocyanines. *Chem. Ber.* **1997**, *130*, 801–806.

(105) Youngblood, W. J. Synthesis of a New Trans-A2B2 Phthalocyanine Motif as a Building Block for Rodlike Phthalocyanine Polymers. *J. Org. Chem.* **2006**, *71*, 3345–3356.

(106) Wang, J.-D.; Lin, M.-J.; Wu, S.-F.; Lin, Y. 1,15-Bis-(2′,2′,4′-Trimethyl-3′-

Pentoxy)Phthalocyanine, a Trans-Form Nonperipheral Di-Substituted Phthalocyanine Synthesized by the 'Cross Condensation' Method. *J. Organomet. Chem.* **2006**, *691*, 5074–5076.

(107) Ayhan, M. M.; Singh, A.; Hirel, C.; Gürek, A. G.; Ahsen, V.; Jeanneau, E.; Ledoux-Rak, I.; Zyss, J.; Andraud, C.; Bretonnière, Y. ABAB Homoleptic Bis(Phthalocyaninato)Lutetium(III) Complex: Toward the Real Octupolar Cube and Giant Quadratic Hyperpolarizability. *J. Am. Chem. Soc.* **2012**, *134*, 3655–3658.

(108) Ayhan, M. M.; Singh, A.; Jeanneau, E.; Ahsen, V.; Zyss, J.; Ledoux-Rak, I.; Gürek, A. G.; Hirel, C.; Bretonnière, Y.; Andraud, C. ABAB Homoleptic Bis(Phthalocyaninato)Lanthanide(III) Complexes: Original Octupolar Design Leading to Giant Quadratic Hyperpolarizability. *Inorg. Chem.* **2014**, *53*, 4359–4370.

(109) Hanack, M.; Stihler, P. Synthesis of Ladder-Type Oligomers Incorporating Phthalocyanine Units. *European J. Org. Chem.* **2000**, *2000* (2), 303–311.

(110) Kingsborough, R. P.; Swager, T. M. A Highly Conductive Macrocycle-Linked Metallophthalocyanine Polymer. *Angew. Chemie Int. Ed.* **2000**, *39* (16), 2897–2900.

(111) You, W.; Wang, L.; Wang, Q.; Yu, L. Synthesis and Structure/Property Correlation of Fully Functionalized Photorefractive Polymers. *Macromolecules* **2002**, *35* (12), 4636–4645.

(112) Kobayashi, N.; Ashida, T.; Osa, T.; Konami, H. Phthalocyanines of a Novel Structure: Dinaphthotetraazaporphyrins with D2h Symmetry. *Inorg. Chem.* **1994**, *33* (9), 1735–1740.

(113) Sholto, A.; Lee, S.; Hoffman, B. M.; Barrett, A. G. M.; Ehrenberg, B. Spectroscopy, Binding to Liposomes and Production of Singlet Oxygen by Porphyrazines with Modularly Variable Water Solubility. *Photochem. Photobiol.* **2008**, *84*, 764–773.

(114) Sakamoto, K.; Ohno-Okumura, E.; Kato, T.; Watanabe, M.; Cook, M. J. Investigation of Zinc Bis(1,4-Didecylbenzo)-Bis(2,3-Pyrido) Porphyrazine as an Efficient Photosensitizer by Cyclic Voltammetry. *Dye. Pigment.* **2008**, *78*, 213–218.

(115) Nolan, K. J. M.; Hu, M.; Leznoff, C. C. "Adjacent" Substituted Phthalocyanines. *Synlett* **1997**, *1997*, 593–594.

(116) Fukuda, T.; Kobayashi, N. Efficient Synthesis of a Donor-Acceptor Phthalocyanine Having Adjacently-Fused Pyrazine Rings. *Chem. Lett.* **2002**, *31*, 866–867.

(117) Kobayashi, N.; Fukuda, T. Mono-Aromatic Ring-Fused versus Adjacently Di-Aromatic Ring-Fused Tetraazaporphyrins: Regioselective Synthesis and Their Spectroscopic and Electrochemical Properties. *J. Am. Chem. Soc.* **2002**, *124*, 8021–8034.

(118) Drew, D. M.; Leznoff, C. C. The Synthesis of Pure 1,11,15,25-Tetrasubstitutedphthalocyanines as Single Isomers Using Bisphthalonitriles. *Synlett* **1994**, *1994*, 623–624.

(119) Leznoff, C. C.; Drew, D. M. The Use of Bisphthalonitriles in the Synthesis of Side-Strapped 1,11,15,25-Tetrasubstituted Phthalocyanines. *Can. J. Chem.* **1996**, *74* (3), 307–318.

(120) Kimura, M.; Ueki, H.; Ohta, K.; Shirai, H.; Kobayashi, N. Self-Organization of Low-Symmetry Adjacent-Type Metallophthalocyanines Having Branched Alkyl Chains. *Langmuir* **2006**, *22*, 5051–5056.

(121) Kobayashi, N. Optically Active 'Adjacent' Type Non-Centrosymmetrically Substituted Phthalocyanines. *Chem. Commun.* **1998**, No. 4, 487–488.

(122) Leznoff, C. C.; Marcuccio, S. M.; Greenberg, S.; Lever, A. B. P.; Tomer, K. B. Metallophthalocyanine Dimers Incorporating Five-Atom Covalent Bridges. *Can. J. Chem.* **1985**, *63* (3), 623–631.

(123) Kobayashi, N.; Higashi, R.; Titeca, B. C.; Lamote, F.; Ceulemans, A. Substituent-Induced Circular Dichroism in Phthalocyanines. *J. Am. Chem. Soc.* **1999**, *121* (51), 12018–12028.

(124) E.J.G.J. Dolmans, D.; Fukumura, D.; K. Jain, R. Photodynamic Therapy for Cancer. *Nat. Rev. Cancer* **2003**, *3* (5), 380–387.

(125) Oleinick, N. L.; Morris, R. L.; Belichenko, I. The Role of Apoptosis in Response to Photodynamic Therapy: What, Where, Why, and How. *Photochem. Photobiol. Sci.* **2002**, *1* (1), 1–21.

(126) Milla Sanabria, L.; Rodríguez, M. E.; Cogno, I. S.; Rumie Vittar, N. B.; Pansa, M. F.; Lamberti, M. J.; Rivarola, V. A. Direct and Indirect Photodynamic Therapy Effects on the Cellular and Molecular Components of the Tumor Microenvironment. *Biochim. Biophys. Acta - Rev. Cancer* **2013**, *1835* (1), 36–45.

(127) Brown, S. B.; Brown, E. A.; Walker, I. The Present and Future Role of Photodynamic Therapy in Cancer Treatment. *Lancet Oncol.* **2004**, *5* (8), 497–508.

(128) Castano, A. P.; Demidova, T. N.; Hamblin, M. R. Mechanisms in Photodynamic Therapy: Part Two—Cellular Signaling, Cell Metabolism and Modes of Cell Death. *Photodiagnosis Photodyn. Ther.* **2005**, *2* (1), 1–23.

(129) Castano, A. P.; Mroz, P.; Hamblin, M. R. Photodynamic Therapy and Anti-Tumour Immunity. *Nat. Rev. Cancer* **2006**, *6* (7), 535–545.

(130) Celli, J. P.; Spring, B. Q.; Rizvi, I.; Evans, C. L.; Samkoe, K. S.; Verma, S.; Pogue, B. W.; Hasan, T. Imaging and Photodynamic Therapy: Mechanisms, Monitoring, and Optimization. *Chem. Rev.* **2010**, *110* (5), 2795–2838.

(131) Agostinis, P.; Berg, K.; Cengel, K. A.; Foster, T. H.; Girotti, A. W.; Gollnick, S. O.; Hahn, S. M.; Hamblin, M. R.; Juzeniene, A.; Kessel, D.; et al. Photodynamic Therapy of Cancer: An Update. *CA. Cancer J. Clin.* **2011**, *61* (4), 250–281.

(132) Allison, R. R.; Bagnato, V. S.; Cuenca, R.; Downie, G. H.; Sibata, C. H. The Future of Photodynamic Therapy in Oncology. *Futur. Oncol.* **2006**, *2* (1), 53–71.

(133) Dos Santos, A. F.; De Almeida, D. R. Q.; Terra, L. F.; Baptista, M. S.; Labriola, L. Photodynamic Therapy in Cancer Treatment - an Update Review. *J. Cancer Metastasis Treat.* **2019**, *5* (25).

(134) Freund, K. B.; Mrejen, S.; Gallego-Pinazo, R. An Update on the Pharmacotherapy of Neovascular Age-Related Macular Degeneration. *Expert Opin. Pharmacother.* **2013**, *14* (8), 1017–1028.

(135) Peng, C.; Li, Y.; Liang, H.; Cheng, J.; Li, Q.; Sun, X.; Li, Z.; Wang, F.; Guo, Y.; Tian, Z.; et al. Detection and Photodynamic Therapy of Inflamed Atherosclerotic Plaques in the Carotid Artery of Rabbits. *J. Photochem. Photobiol. B Biol.* **2011**, *102* (1), 26–31.

(136) Hamblin, M. R.; Jori, G. *Photodynamic Inactivation of Microbial Pathogens*; Comprehensive Series in Photochemical & Photobiological Sciences; The Royal Society of Chemistry, 2011.

(137) Wainwright, M.; Maisch, T.; Nonell, S.; Plaetzer, K.; Almeida, A.; Tegos, G. P.; Hamblin, M. R. Photoantimicrobials—Are We Afraid of the Light? *Lancet Infect. Dis.* **2017**, *17* (2), e49–e55.

(138) Jori, G.; Camerin, M.; Soncin, M.; Guidolin, L.; Coppellotti, O. Chapter 1 Antimicrobial Photodynamic Therapy: Basic Principles. In *Photodynamic Inactivation of Microbial Pathogens: Medical and Environmental Applications*; The Royal Society of Chemistry, 2011; Vol. 11, pp 1–18.

(139) Jori, G.; Fabris, C.; Soncin, M.; Ferro, S.; Coppellotti, O.; Dei, D.; Fantetti, L.; Chiti, G.; Roncucci, G. Photodynamic Therapy in the Treatment of Microbial Infections: Basic Principles and Perspective Applications. *Lasers Surg. Med.* **2006**, *38* (5), 468–481.

(140) Grinholc, M.; Szramka, B.; Kurlenda, J.; Graczyk, A.; Bielawski, K. P. Bactericidal Effect of Photodynamic Inactivation against Methicillin-Resistant and Methicillin-Susceptible Staphylococcus Aureus Is Strain-Dependent. *J. Photochem. Photobiol. B Biol.* **2008**, *90* (1), 57–63.

(141) Bonsor, S. J.; Nichol, R.; Reid, T. M. S.; Pearson, G. J. Microbiological Evaluation of Photo-Activated Disinfection in Endodontics (An in Vivo Study). *Br. Dent. J.* **2006**, *200* (6), 337–

341.

(142) Pichat, P. *Photocatalysis and Water Purification: From Fundamentals to Recent Applications*; Lu, M., Ed.; Wiley: Weinheim, 2013.

(143) da Silva, E. F. F.; Pedersen, B. W.; Breitenbach, T.; Toftegaard, R.; Kuimova, M. K.; Arnaut, L. G.; Ogilby, P. R. Irradiation- and Sensitizer-Dependent Changes in the Lifetime of Intracellular Singlet Oxygen Produced in a Photosensitized Process. *J. Phys. Chem. B* **2012**, *116* (1), 445–461.

(144) Kuimova, M. K.; Yahioglu, G.; Ogilby, P. R. Singlet Oxygen in a Cell: Spatially Dependent Lifetimes and Quenching Rate Constants. *J. Am. Chem. Soc.* **2009**, *131* (1), 332–340.

(145) Plaetzer, K.; Krammer, B.; Berlanda, J.; Berr, F.; Kiesslich, T. Photophysics and Photochemistry of Photodynamic Therapy: Fundamental Aspects. *Lasers Med. Sci.* **2009**, *24* (2), 259–268.

(146) Kobayashi, H.; Ogawa, M.; Alford, R.; Choyke, P. L.; Urano, Y. New Strategies for Fluorescent Probe Design in Medical Diagnostic Imaging. *Chem. Rev.* **2010**, *110* (5), 2620–2640.

(147) Castano, A. P.; Demidova, T. N.; Hamblin, M. R. Mechanisms in Photodynamic Therapy: Part One—Photosensitizers, Photochemistry and Cellular Localization. *Photodiagnosis Photodyn. Ther.* **2004**, *1* (4), 279–293.

(148) Dąbrowski, J. M.; Pucelik, B.; Regiel-Futyra, A.; Brindell, M.; Mazuryk, O.; Kyzioł, A.; Stochel, G.; Macyk, W.; Arnaut, L. G. Engineering of Relevant Photodynamic Processes through Structural Modifications of Metallotetrapyrrolic Photosensitizers. *Coord. Chem. Rev.* **2016**, *325*, 67–101.

(149) Brancaleon, L.; Moseley, H. Laser and Non-Laser Light Sources for Photodynamic Therapy. *Lasers Med. Sci.* **2002**, *17* (3), 173–186.

(150) Alexiades-Armenakas, M. Laser-Mediated Photodynamic Therapy. *Clin. Dermatol.* **2006**, *24* (1), 16–25.

(151) Nonell, S.; Flors, C. *Singlet Oxygen: Applications in Biosciences and Nanosciences*; Comprehensive Series in Photochemical & Photobiological Sciences; The Royal Society of Chemistry, 2016; Vol. 1.

(152) Krumova, K.; Cosa, G. Chapter 1 Overview of Reactive Oxygen Species. In *Singlet Oxygen: Applications in Biosciences and Nanosciences, Volume 1*; The Royal Society of Chemistry, 2016; Vol. 1, pp 1–21.

(153) DeRosa, M. C.; Crutchley, R. J. Photosensitized Singlet Oxygen and Its Applications. *Coord. Chem. Rev.* **2002**, *233–234*, 351–371.

(154) Schweitzer, C.; Schmidt, R. Physical Mechanisms of Generation and Deactivation of Singlet Oxygen. *Chem. Rev.* **2003**, *103* (5), 1685–1758.

(155) Ogilby, P. R. Singlet Oxygen: There Is Indeed Something New under the Sun. *Chem. Soc. Rev.* **2010**, *39* (8), 3181–3209.

(156) Scurlock, R. D.; Nonell, S.; Braslavsky, S. E.; Ogilby, P. R. Effect of Solvent on the Radiative Decay of Singlet Molecular Oxygen (A1.DELTA.G). *J. Phys. Chem.* **1995**, *99* (11), 3521–3526.

(157) Skovsen, E.; Snyder, J. W.; Lambert, J. D. C.; Ogilby, P. R. Lifetime and Diffusion of Singlet Oxygen in a Cell. *J. Phys. Chem. B* **2005**, *109* (18), 8570–8573.

(158) Dumoulin, F. *Photosensitizers in Medicine, Environment, and Security*; Nyokong, T., Ahsen, V., Eds.; Springer: New York, 2012.

(159) Allison, R. R.; Downie, G. H.; Cuenca, R.; Hu, X.-H.; Childs, C. J. H.; Sibata, C. H. Photosensitizers in Clinical PDT. *Photodiagnosis Photodyn. Ther.* **2004**, *1* (1), 27–42.

(160) Ethirajan, M.; Chen, Y.; Joshi, P.; Pandey, R. K. The Role of Porphyrin Chemistry in Tumor Imaging and Photodynamic Therapy. *Chem. Soc. Rev.* **2011**, *40* (1), 340–362.

(161) Nyman, E. S.; Hynninen, P. H. Research Advances in the Use of Tetrapyrrolic Photosensitizers for Photodynamic Therapy. *J. Photochem. Photobiol. B Biol.* **2004**, *73* (1), 1–28.

(162) O'Connor, A. E.; Gallagher, W. M.; Byrne, A. T. Porphyrin and Nonporphyrin Photosensitizers in Oncology: Preclinical and Clinical Advances in Photodynamic Therapy. *Photochem. Photobiol.* **2009**, *85* (5), 1053–1074.

(163) Mari, C.; Pierroz, V.; Ferrari, S.; Gasser, G. Combination of Ru(II) Complexes and Light: New Frontiers in Cancer Therapy. *Chem. Sci.* **2015**, *6* (5), 2660–2686.

(164) Yoon, I.; Li, J. Z.; Shim, Y. K. Advance in Photosensitizers and Light Delivery for Photodynamic Therapy. *Clin. Endosc.* **2013**, *46* (1), 7–23.

(165) Ackroyd, R.; Kelty, C.; Brown, N.; Reed, M. The History of Photodetection and Photodynamic Therapy¶. *Photochem. Photobiol.* **2001**, *74* (5), 656–669.

(166) Gomer, C. J. Preclinical Examination of First and Second Generation Photosensitizers Used in Photodynamic Therapy. *Photochem. Photobiol.* **1991**, *54* (6), 1093–1107.

(167) Zhang, J.; Jiang, C.; Figueiró Longo, J. P.; Azevedo, R. B.; Zhang, H.; Muehlmann, L. A. An Updated Overview on the Development of New Photosensitizers for Anticancer Photodynamic Therapy. *Acta Pharm. Sin. B* **2018**, *8* (2), 137–146.

(168) Kataoka, H.; Nishie, H.; Hayashi, N.; Tanaka, M.; Nomoto, A.; Yano, S.; Joh, T. New Photodynamic Therapy with Next-Generation Photosensitizers. *Ann. Transl. Med.* **2017**, *5* (8), 183.

(169) Abrahamse, H.; Hamblin, M. R. New Photosensitizers for Photodynamic Therapy. *Biochem. J.* **2016**, *473* (4), 347–364.

(170) Ragàs, X.; Sánchez-García, D.; Ruiz-González, R.; Dai, T.; Agut, M.; Hamblin, M. R.; Nonell, S. Cationic Porphycenes as Potential Photosensitizers for Antimicrobial Photodynamic Therapy. *J. Med. Chem.* **2010**, *53* (21), 7796–7803.

(171) Wachowska, M.; Muchowicz, A.; Firczuk, M.; Gabrysiak, M.; Winiarska, M.; Wańczyk, M.; Bojarczuk, K.; Golab, J. Aminolevulinic Acid (ALA) as a Prodrug in Photodynamic Therapy of Cancer. *Molecules* **2011**, *16* (5), 4140–4164.

(172) Baskaran, R.; Lee, J.; Yang, S.-G. Clinical Development of Photodynamic Agents and Therapeutic Applications. *Biomater. Res.* **2018**, *22*, 25.

(173) Sharman, W. M.; van Lier, J. E.; Allen, C. M. Targeted Photodynamic Therapy via Receptor Mediated Delivery Systems. *Adv. Drug Deliv. Rev.* **2004**, *56* (1), 53–76.

(174) Paszko, E.; Ehrhardt, C.; Senge, M. O.; Kelleher, D. P.; Reynolds, J. V. Nanodrug Applications in Photodynamic Therapy. *Photodiagnosis Photodyn. Ther.* **2011**, *8* (1), 14–29.

(175) Calixto, G. M. F.; Bernegossi, J.; de Freitas, L. M.; Fontana, C. R.; Chorilli, M. Nanotechnology-Based Drug Delivery Systems for Photodynamic Therapy of Cancer: A Review. *Molecules* **2016**, *21* (3), 342.

(176) *Principles of Fluorescence Spectroscopy*; Lakowicz, J. R., Ed.; Springer US: Boston, MA, 2006.

(177) Marian, C. M. Spin–Orbit Coupling and Intersystem Crossing in Molecules. *Wiley Interdiscip. Rev. Comput. Mol. Sci.* **2012**, *2* (2), 187–203.

(178) Gorman, A.; Killoran, J.; O'Shea, C.; Kenna, T.; Gallagher, W. M.; O'Shea, D. F. In Vitro Demonstration of the Heavy-Atom Effect for Photodynamic Therapy. *J. Am. Chem. Soc.* **2004**, *126* (34), 10619–10631.

(179) Foote, C. S. Definition of Type I and Type II Photosensitized Oxidation. *Photochem. Photobiol.* **1991**, *54* (5), 659.

(180) Bergamini, C. M.; Gambetti, S.; Dondi, A.; Cervellati, C. Oxygen, Reactive Oxygen Species and Tissue Damage. *Curr. Pharm. Des.* **2004**, *10*, 1611.

(181) Borra, S. K.; Mahendra, J.; Gurumurthy, P.; Jayamathi; Iqbal, S. S.; Mahendra, L. Effect of Curcumin against Oxidation of Biomolecules by Hydroxyl Radicals. *J. Clin. Diagn. Res.* **2014**, *8* (10), CC01-CC5.

(182) Lovell, J. F.; Liu, T. W. B.; Chen, J.; Zheng, G. Activatable Photosensitizers for Imaging and Therapy. *Chem. Rev.* **2010**, *110* (5), 2839–2857.

(183) Agostinis, P.; Buytaert, E.; Breyssens, H.; Hendrickx, N. Regulatory Pathways in Photodynamic Therapy Induced Apoptosis. *Photochem. Photobiol. Sci.* **2004**, *3* (8), 721–729.

(184) Kawczyk-Krupka, A.; Bugaj, A. M.; Potempa, M.; Wasilewska, K.; Latos, W.; Sieroń, A. Vascular-Targeted Photodynamic Therapy in the Treatment of Neovascular Age-Related Macular Degeneration: Clinical Perspectives. *Photodiagnosis Photodyn. Ther.* **2015**, *12* (2), 161–175.

(185) Wachowska, M.; Muchowicz, A.; Demkow, U. Immunological Aspects of Antitumor Photodynamic Therapy Outcome. *Cent. Eur. J. Immunol.* **2016**, *40* (4), 481–485.

(186) Salmon-Divon, M.; Nitzan, Y.; Malik, Z. Mechanistic Aspects of Escherichia Coli Photodynamic Inactivation by Cationic Tetra-Meso(N-Methylpyridyl)Porphine. *Photochem. Photobiol. Sci.* **2004**, *3* (5), 423–429.

(187) Brown, L.; Langelier, C.; Reid, M. J. A.; Rutishauser, R. L.; Strnad, L. Antimicrobial Resistance: A Call to Action! *Clin. Infect. Dis.* **2017**, *64* (1), 106–107.

(188) Sperandio, F.; Huang, Y.-Y.; Hamblin, M. Antimicrobial Photodynamic Therapy To Kill Gram-Negative Bacteria. *Recent Pat. Antiinfect. Drug Discov.* **2013**, *8* (2), 108–120.

(189) Sekkat, N.; Van Den Bergh, H.; Nyokong, T.; Lange, N. Like a Bolt from the Blue: Phthalocyanines in Biomedical Optics. *Molecules* **2012**, *17* (1), 98–144.

(190) Nyokong, T. Desired Properties of New Phthalocyanines for Photodynamic Therapy. *Pure Appl. Chem.* **2011**, *83* (9), 1763–1779.

(191) Josefsen, L. B.; Boyle, R. W. Unique Diagnostic and Therapeutic Roles of Porphyrins and Phthalocyanines in Photodynamic Therapy, Imaging and Theranostics. *Theranostics* **2012**, *2* (9), 916–966.

(192) Jiang, Z.; Shao, J.; Yang, T.; Wang, J.; Jia, L. Pharmaceutical Development, Composition and Quantitative Analysis of Phthalocyanine as the Photosensitizer for Cancer Photodynamic Therapy. *J. Pharm. Biomed. Anal.* **2014**, *87*, 98–104.

(193) Lo, P.-C.; Chow, S. Y. S.; Ng, D. K. P. Molecular Phthalocyanine-Based Photosensitizers for Photodynamic Therapy. In *Handbook of Photodynamic Therapy*; WORLD SCIENTIFIC, 2015; pp 237–272.

(194) Sun, T.; Zhang, Y. S.; Pang, B.; Hyun, D. C.; Yang, M.; Xia, Y. Engineered Nanoparticles for Drug Delivery in Cancer Therapy. *Angew. Chemie Int. Ed.* **2014**, *53* (46), 12320–12364.

(195) Çamur, M.; Ahsen, V.; Durmuş, M. The First Comparison of Photophysical and Photochemical Properties of Non-Ionic, Ionic and Zwitterionic Gallium (III) and Indium (III) Phthalocyanines. *J. Photochem. Photobiol. A Chem.* **2011**, *219* (2), 217–227.

(196) Ranyuk, E.; Cauchon, N.; Klarskov, K.; Guérin, B.; van Lier, J. E. Phthalocyanine–Peptide Conjugates: Receptor-Targeting Bifunctional Agents for Imaging and Photodynamic Therapy. *J. Med. Chem.* **2013**, *56* (4), 1520–1534.

(197) Dinçer, H.; Mert, H.; Çalışkan, E.; Atmaca, G. Y.; Erdoğmuş, A. Synthesis and Photophysicochemical Studies of Poly(Ethylene Glycol) Conjugated Symmetrical and Asymmetrical Zinc Phthalocyanines. *J. Mol. Struct.* **2015**, *1102*, 190–196.

(198) Uslan, C.; İşleyen, N. D.; Öztürk, Y.; Yıldız, B. T.; Çakar, Z. P.; Göksel, M.; Durmuş, M.; Gürsel, Y. H.; Sesalan, B. Ş. A Novel of PEG-Conjugated Phthalocyanine and Evaluation of Its Photocytotoxicity and Antibacterial Properties for Photodynamic Therapy. *J. Porphyr.*

Phthalocyanines **2018**, *22* (01n03), 10–24.

(199) Singh, S.; Aggarwal, A.; Bhupathiraju, N. V. S. D. K.; Arianna, G.; Tiwari, K.; Drain, C. M. Glycosylated Porphyrins, Phthalocyanines, and Other Porphyrinoids for Diagnostics and Therapeutics. *Chem. Rev.* **2015**, *115* (18), 10261–10306.

(200) Aggarwal, A.; Singh, S.; Zhang, Y.; Anthes, M.; Samaroo, D.; Gao, R.; Drain, C. M. Synthesis and Photophysics of an Octathioglycosylated Zinc(II) Phthalocyanine. *Tetrahedron Lett.* **2011**, *52* (42), 5456–5459.

(201) Rocha, D. M. G. C.; Venkatramaiah, N.; Gomes, M. C.; Almeida, A.; Faustino, M. A. F.; Almeida Paz, F. A.; Cunha, Â.; Tomé, J. P. C. Photodynamic Inactivation of Escherichia Coli with Cationic Ammonium Zn(Ii) Phthalocyanines. *Photochem. Photobiol. Sci.* **2015**, *14* (10), 1872–1879.

(202) Arslanoğlu, Y.; Hamuryudan, E. Synthesis and Derivatization of Near-IR Absorbing Titanylphthalocyanines with Dimethylaminoethylsulfanyl Substituents. *Dye. Pigment.* **2007**, *75* (1), 150–155.

(203) Arslanoğlu, Y.; Hayran, E.; Hamuryudan, E. Synthesis, Electrochemical and Photophysical Studies of Axially Substituted Quarternizable Titanyl Phthalocyanines. *Dye. Pigment.* **2013**, *97* (2), 340–346.

(204) Machacek, M.; Cidlina, A.; Novakova, V.; Svec, J.; Rudolf, E.; Miletin, M.; Kučera, R.; Simunek, T.; Zimcik, P. Far-Red-Absorbing Cationic Phthalocyanine Photosensitizers: Synthesis and Evaluation of the Photodynamic Anticancer Activity and the Mode of Cell Death Induction. *J. Med. Chem.* **2015**, *58* (4), 1736–1749.

(205) Lo, P.-C.; Huang, J.-D.; Cheng, D. Y. Y.; Chan, E. Y. M.; Fong, W.-P.; Ko, W.-H.; Ng, D. K. P. New Amphiphilic Silicon(IV) Phthalocyanines as Efficient Photosensitizers for Photodynamic Therapy: Synthesis, Photophysical Properties, and in Vitro Photodynamic Activities. *Chem. – A Eur. J.* **2004**, *10* (19), 4831–4838.

(206) Ruiz-González, R.; Setaro, F.; Gulías, Ò.; Agut, M.; Hahn, U.; Torres, T.; Nonell, S. Cationic Phthalocyanine Dendrimers as Potential Antimicrobial Photosensitisers. *Org. Biomol. Chem.* **2017**, *15* (42), 9008–9017.

(207) Li, H.; Jensen, T. J.; Fronczek, F. R.; Vicente, M. G. H. Syntheses and Properties of a Series of Cationic Water-Soluble Phthalocyanines. *J. Med. Chem.* **2008**, *51* (3), 502–511.

(208) van de Winckel, E.; David, B.; Simoni, M. M.; González-Delgado, J. A.; de la Escosura, A.; Cunha, Â.; Torres, T. Octacationic and Axially Di-Substituted Silicon (IV) Phthalocyanines for Photodynamic Inactivation of Bacteria. *Dye. Pigment.* **2017**, *145*, 239–245.

(209) Lourenço, L. M. O.; Sousa, A.; Gomes, M. C.; Faustino, M. A. F.; Almeida, A.; Silva, A. M. S.; Neves, M. G. P. M. S.; Cavaleiro, J. A. S.; Cunha, Â.; Tomé, J. P. C. Inverted Methoxypyridinium Phthalocyanines for PDI of Pathogenic Bacteria. *Photochem. Photobiol. Sci.* **2015**, *14* (10), 1853–1863.

(210) Lourenço, L. M. O.; Rocha, D. M. G. C.; Ramos, C. I. V; Gomes, M. C.; Almeida, A.; Faustino, M. A. F.; Almeida Paz, F. A.; Neves, M. G. P. M. S.; Cunha, Â.; Tomé, J. P. C. Photoinactivation of Planktonic and Biofilm Forms of Escherichia Coli through the Action of Cationic Zinc(II) Phthalocyanines. *ChemPhotoChem* **2019**, *3* (5), 251–260.

(211) Membrino, A.; Paramasivam, M.; Cogoi, S.; Alzeer, J.; Luedtke, N. W.; Xodo, L. E. Cellular Uptake and Binding of Guanidine-Modified Phthalocyanines to KRAS/HRAS G-Quadruplexes. *Chem. Commun.* **2010**, *46* (4), 625–627.

(212) Sugimori, T.; Nojima, J.; Ozawa, T.; Handa, M.; Kasuga, K. Preparation and Properties of Tetra- and Octa-Substituted Phthalocyanines with Cationic Trimethylaniliniumyl Groups. *Chem. Lett.* **2004**, *33* (8), 1014–1015.

(213) Makhseed, S.; Machacek, M.; Alfadly, W.; Tuhl, A.; Vinodh, M.; Simunek, T.; Novakova, V.; Kubat, P.; Rudolf, E.; Zimcik, P. Water-Soluble Non-Aggregating Zinc Phthalocyanine and in Vitro Studies for Photodynamic Therapy. *Chem. Commun.* **2013**, *49* (95), 11149–

11151.

(214) Zheng, B.-Y.; Ke, M.-R.; Lan, W.-L.; Hou, L.; Guo, J.; Wan, D.-H.; Cheong, L.-Z.; Huang, J.-D. Mono- and Tetra-Substituted Zinc(II) Phthalocyanines Containing Morpholinyl Moieties: Synthesis, Antifungal Photodynamic Activities, and Structure-Activity Relationships. *Eur. J. Med. Chem.* **2016**, *114*, 380–389.

(215) van Vlerken, L. E.; Vyas, T. K.; Amiji, M. M. Poly(Ethylene Glycol)-Modified Nanocarriers for Tumor-Targeted and Intracellular Delivery. *Pharm. Res.* **2007**, *24* (8), 1405–1414.

(216) Liu, J.-Y.; Jiang, X.-J.; Fong, W.-P.; Ng, D. K. P. Highly Photocytotoxic 1,4-Dipegylated Zinc (II) Phthalocyanines. Effects of the Chain Length on the in Vitro Photodynamic Activities. *Org. Biomol. Chem.* **2008**, *6* (24), 4560–4566.

(217) Li, H.; Fronczek, F. R.; Vicente, M. G. H. Pegylated Phthalocyanines: Synthesis and Spectroscopic Properties. *Tetrahedron Lett.* **2011**, *52* (50), 6675–6678.

(218) Hahn, U.; Torres, T. Amphiphilic Zinc Phthalocyanine Dendrimers by the Click Chemistry Approach. *J. Porphyr. Phthalocyanines* **2011**, *15* (5–6), 364–372.

(219) Li, M.; Khoshdel, E.; Haddleton, D. M. Synthesis of Water Soluble PEGylated (Copper) Phthalocyanines via Mitsunobu Reaction and Cu(I)-Catalysed Azide–Alkyne Cycloaddition (CuAAC) "Click" Chemistry. *Polym. Chem.* **2013**, *4* (16), 4405–4411.

(220) Huang, J.-D.; Wang, S.; Lo, P.-C.; Fong, W.-P.; Ko, W.-H.; Ng, D. K. P. Halogenated Silicon (IV) Phthalocyanines with Axial Poly(Ethylene Glycol) Chains. Synthesis, Spectroscopic Properties, Complexation with Bovine Serum Albumin and in Vitro Photodynamic Activities. *New J. Chem.* **2004**, *28* (3), 348–354.

(221) Çakır, D.; Göksel, M.; Çakır, V.; Durmuş, M.; Biyiklioglu, Z.; Kantekin, H. Amphiphilic Zinc Phthalocyanine Photosensitizers: Synthesis, Photophysicochemical Properties and in Vitro Studies for Photodynamic Therapy. *Dalt. Trans.* **2015**, *44* (20), 9646–9658.

(222) Foley, S.; Jones, G.; Liuzzi, R.; J. McGarvey, D.; H. Perry, M.; George Truscott, T. The Synthesis and Photophysical Properties of Polyether Substituted Phthalocyanines of Potential Use in Photodynamic Therapy. *J. Chem. Soc. Perkin Trans. 2* **1997**, No. 9, 1725–1730.

(223) Lafont, D.; Zorlu, Y.; Savoie, H.; Albrieux, F.; Ahsen, V.; Boyle, R. W.; Dumoulin, F. Monoglycoconjugated Phthalocyanines: Effect of Sugar and Linkage on Photodynamic Activity. *Photodiagnosis Photodyn. Ther.* **2013**, *10* (3), 252–259.

(224) Xue, E. Y.; Wong, R. C. H.; Wong, C. T. T.; Fong, W.-P.; Ng, D. K. P. Synthesis and Biological Evaluation of an Epidermal Growth Factor Receptor-Targeted Peptide-Conjugated Phthalocyanine-Based Photosensitiser. *RSC Adv.* **2019**, *9* (36), 20652–20662.

(225) Zhou, X.-Q.; Meng, L.-B.; Huang, Q.; Li, J.; Zheng, K.; Zhang, F.-L.; Liu, J.-Y.; Xue, J.-P. Synthesis and in Vitro Anticancer Activity of Zinc(II) Phthalocyanines Conjugated with Coumarin Derivatives for Dual Photodynamic and Chemotherapy. *ChemMedChem* **2015**, *10* (2), 304–311.

(226) Huang, Y.-Y.; Mroz, P.; Zhiyentayev, T.; Sharma, S. K.; Balasubramanian, T.; Ruzié, C.; Krayer, M.; Fan, D.; Borbas, K. E.; Yang, E.; et al. In Vitro Photodynamic Therapy and Quantitative Structure–Activity Relationship Studies with Stable Synthetic Near-Infrared-Absorbing Bacteriochlorin Photosensitizers. *J. Med. Chem.* **2010**, *53* (10), 4018–4027.

(227) Huang, L.; Huang, Y.-Y.; Mroz, P.; Tegos, G. P.; Zhiyentayev, T.; Sharma, S. K.; Lu, Z.; Balasubramanian, T.; Krayer, M.; Ruzié, C.; et al. Stable Synthetic Cationic Bacteriochlorins as Selective Antimicrobial Photosensitizers. *Antimicrob. Agents Chemother.* **2010**, *54* (9), 3834 LP – 3841.

(228) Maisch, T.; Bosl, C.; Szeimies, R.-M.; Lehn, N.; Abels, C. Photodynamic Effects of Novel XF Porphyrin Derivatives on Prokaryotic and Eukaryotic Cells. *Antimicrob. Agents Chemother.* **2005**, *49* (4), 1542–1552.

(229) Tsubone, T. M.; Martins, W. K.; Pavani, C.; Junqueira, H. C.; Itri, R.; Baptista, M. S. Enhanced Efficiency of Cell Death by Lysosome-Specific Photodamage. *Sci. Rep.* **2017**, *7* (1), 6734.

(230) Berg, K.; Nordstrand, S.; Selbo, P. K.; Tran, D. T. T.; Angell-Petersen, E.; Høgset, A. Disulfonated Tetraphenyl Chlorin (TPCS2a), a Novel Photosensitizer Developed for Clinical Utilization of Photochemical Internalization. *Photochem. Photobiol. Sci.* **2011**, *10* (10), 1637–1651.

(231) Ongarora, B. G.; Hu, X.; Li, H.; Fronczek, F. R.; Vicente, M. G. H. Syntheses and Properties of Trimethylaminophenoxy-Substituted Zn(Ii)-Phthalocyanines. *Medchemcomm* **2012**, *3* (2), 179–194.

(232) Seotsanyana-Mokhosi, I.; Chen, J.-Y.; Nyokong, T. Synthesis, Photophysicochemical Studies of Adjacently Tetrasubstituted Binaphthalo-Phthalocyanines. *J. Porphyr. Phthalocyanines* **2005**, *09* (05), 316–325.

(233) Ongarora, B. G.; Zhou, Z.; Okoth, E. A.; Kolesnichenko, I.; Smith, K. M.; Vicente, M. G. H. Synthesis, Spectroscopic, and Cellular Properties of α-Pegylated Cis-A(2)B(2)- and A(3)B-Types ZnPcs. *J. Porphyr. Phthalocyanines* **2014**, *18* (10–11), 1021–1033.

(234) Lourenço, L. M. O.; Pereira, P. M. R.; Maciel, E.; Válega, M.; Domingues, F. M. J.; Domingues, M. R. M.; Neves, M. G. P. M. S.; Cavaleiro, J. A. S.; Fernandes, R.; Tomé, J. P. C. Amphiphilic Phthalocyanine–Cyclodextrin Conjugates for Cancer Photodynamic Therapy. *Chem. Commun.* **2014**, *50* (61), 8363–8366.

(235) Bhupathiraju, N. V. S. D. K.; Rizvi, W.; Batteas, J. D.; Drain, C. M. Fluorinated Porphyrinoids as Efficient Platforms for New Photonic Materials, Sensors, and Therapeutics. *Org. Biomol. Chem.* **2016**, *14* (2), 389–408.

(236) Wong, R. C. H.; Lo, P.-C.; Ng, D. K. P. Stimuli Responsive Phthalocyanine-Based Fluorescent Probes and Photosensitizers. *Coord. Chem. Rev.* **2019**, *379*, 30–46.

(237) Lehn, J.-M. Perspectives in Chemistry—Aspects of Adaptive Chemistry and Materials. *Angew. Chemie Int. Ed.* **2015**, *54* (11), 3276–3289.

(238) Pescitelli, G.; Di Bari, L.; Berova, N. Application of Electronic Circular Dichroism in the Study of Supramolecular Systems. *Chem. Soc. Rev.* **2014**, *43* (15), 5211–5233.

(239) Bai, C.; Liu, M. From Chemistry to Nanoscience: Not Just a Matter of Size. *Angew. Chemie Int. Ed.* **2013**, *52* (10), 2678–2683.

(240) Whitesides, G. M.; Boncheva, M. Beyond Molecules: Self-Assembly of Mesoscopic and Macroscopic Components. *Proc. Natl. Acad. Sci.* **2002**, *99* (8), 4769 LP – 4774.

(241) Liu, M.; Zhang, L.; Wang, T. Supramolecular Chirality in Self-Assembled Systems. *Chem. Rev.* **2015**, *115* (15), 7304–7397.

(242) Steed, J. W.; Atwood, J. L. *Supramolecular Chemistry*; Wiley & Sons: Chichester, 2000.

(243) De Greef, T. F. A.; Smulders, M. M. J.; Wolffs, M.; Schenning, A. P. H. J.; Sijbesma, R. P.; Meijer, E. W. Supramolecular Polymerization. *Chem. Rev.* **2009**, *109* (11), 5687–5754.

(244) Grimme, S. Do Special Noncovalent π–π Stacking Interactions Really Exist? *Angew. Chemie Int. Ed.* **2008**, *47* (18), 3430–3434.

(245) Snow, A. W. Phthalocyanine Aggregation. In *The Porphyrin Handbook*; K. Kadish, R. Guilard, K. M. S., Ed.; Academic Press: Amsterdam, 2003; pp 129–176.

(246) Kameyama, K.; Morisue, M.; Satake, A.; Kobuke, Y. Highly Fluorescent Self-Coordinated Phthalocyanine Dimers. *Angew. Chemie Int. Ed.* **2005**, *44*, 4763–4766.

(247) Esenpınar, A. A.; Durmuş, M.; Bulut, M. Tetra-3-[(2-Diethylamino)Ethyl]-7-Oxo-4-Methylcoumarin-Substituted Zinc Phthalocyanines: Synthesis, Characterization and Aggregation Effects on Photophysical/Photochemical Properties. *J. Photochem. Photobiol. A Chem.* **2010**, *213* (2), 171–179.

(248) Choi, M. T. M.; Li, P. P. S.; Ng, D. K. P. A Direct Comparison of the Aggregation Behavior

of Phthalocyanines and 2,3-Naphthalocyanines. *Tetrahedron* **2000**, *56* (24), 3881–3887.

(249) Sinnokrot, M. O.; Sherrill, C. D. Substituent Effects in Π−π Interactions: Sandwich and T-Shaped Configurations. *J. Am. Chem. Soc.* **2004**, *126* (24), 7690–7697.

(250) Stenger, F. No Title. *Ann. Phys. Chem.* **1888**, *269*, 577–586.

(251) McRae, E. G.; Kasha, M. Enhancement of Phosphorescence Ability upon Aggregation of Dye Molecules. *J. Chem. Phys.* **1958**, *28* (4), 721–722.

(252) Bayda, M.; Dumoulin, F.; Hug, G. L.; Koput, J.; Gorniak, R.; Wojcik, A. Fluorescent H-Aggregates of an Asymmetrically Substituted Mono-Amino Zn(Ii) Phthalocyanine. *Dalt. Trans.* **2017**, *46* (6), 1914–1926.

(253) Würthner, F.; Kaiser, T. E.; Saha-Möller, C. R. J-Aggregates: From Serendipitous Discovery to Supramolecular Engineering of Functional Dye Materials. *Angew. Chemie Int. Ed.* **2011**, *50* (15), 3376–3410.

(254) Scheibe, G. Über Die Veränderlichkeit Der Absorptionsspektren in Lösungen Und Die Nebenvalenzen Als Ihre Ursache. *Angew. Chemie* **1937**, *50* (11), 212–219.

(255) JELLEY, E. E. Spectral Absorption and Fluorescence of Dyes in the Molecular State. *Nature* **1936**, *138* (3502), 1009–1010.

(256) FitzGerald, S.; Farren, C.; Stanley, C. F.; Beeby, A.; Bryce, M. R. Fluorescent Phthalocyanine Dimers—a Steady State and Flash Photolysis Study. *Photochem. Photobiol. Sci.* **2002**, *1* (8), 581–587.

(257) Kasha, M.; Rawls, H. R.; El-Bayoumi, M. A. The Exciton Model in Molecular Spectroscpy. *Pure Appl. Chem.* **1965**, *11*, 371–392.

(258) Wasielewski, M. R. Self-Assembly Strategies for Integrating Light Harvesting and Charge Separation in Artificial Photosynthetic Systems. *Acc. Chem. Res.* **2009**, *42* (12), 1910–1921.

(259) Ng, K. K.; Zheng, G. Molecular Interactions in Organic Nanoparticles for Phototheranostic Applications. *Chem. Rev.* **2015**, *115* (19), 11012–11042.

(260) Chen, Z.; Lohr, A.; Saha-Möller, C. R.; Würthner, F. Self-Assembled π-Stacks of Functional Dyes in Solution: Structural and Thermodynamic Features. *Chem. Soc. Rev.* **2009**, *38* (2), 564–584.

(261) Xing, P.; Zhao, Y. Controlling Supramolecular Chirality in Multicomponent Self-Assembled Systems. *Acc. Chem. Res.* **2018**, *51* (9), 2324–2334.

(262) Arteaga, O.; Canillas, A.; Purrello, R.; Ribó, J. M. Evidence of Induced Chirality in Stirred Solutions of Supramolecular Nanofibers. *Opt. Lett.* **2009**, *34* (14), 2177–2179.

(263) Gottarelli, G.; Lena, S.; Masiero, S.; Pieraccini, S.; Spada, G. P. The Use of Circular Dichroism Spectroscopy for Studying the Chiral Molecular Self-Assembly: An Overview. *Chirality* **2008**, *20* (3-4), 471–485.

(264) Taniguchi, T.; Usuki, T. Supramolecular Chemistry: From Molecules to Nanomaterials. In *Circular Dichroism Spectroscopy.*; John Wiley & Sons, Ltd.: New York, 2012.

(265) Berova, N.; Bari, L. Di; Pescitelli, G. Application of Electronic Circular Dichroism in Configurational and Conformational Analysis of Organic Compounds. *Chem. Soc. Rev.* **2007**, *36* (6), 914–931.

(266) Pescitelli, G.; Di Bari, L.; Berova, N. Conformational Aspects in the Studies of Organic Compounds by Electronic Circular Dichroism. *Chem. Soc. Rev.* **2011**, *40* (9), 4603–4625.

(267) Hoeben, F. J. M.; Jonkheijm, P.; Meijer, E. W.; Schenning, A. P. H. J. About Supramolecular Assemblies of π-Conjugated Systems. *Chem. Rev.* **2005**, *105* (4), 1491–1546.

(268) Ryu, J.-H.; Hong, D.-J.; Lee, M. Aqueous Self-Assembly of Aromatic Rod Building Blocks. *Chem. Commun.* **2008**, No. 9, 1043–1054.

(269) Kim, F. S.; Ren, G.; Jenekhe, S. A. One-Dimensional Nanostructures of π-Conjugated

Molecular Systems: Assembly, Properties, and Applications from Photovoltaics, Sensors, and Nanophotonics to Nanoelectronics. *Chem. Mater.* **2011**, *23* (3), 682–732.

(270) Ball, P. Water as an Active Constituent in Cell Biology. *Chem. Rev.* **2008**, *108* (1), 74–108.

(271) Oshovsky, G. V.; Reinhoudt, D. N.; Verboom, W. Supramolecular Chemistry in Water. *Angew. Chemie Int. Ed.* **2007**, *46* (14), 2366–2393.

(272) Sikder, A.; Ray, D.; Aswal, V. K.; Ghosh, S. Hydrogen-Bonding-Regulated Supramolecular Nanostructures and Impact on Multivalent Binding. *Angew. Chemie - Int. Ed.* **2019**, *58* (6), 1606–1611.

(273) Krieg, E.; Bastings, M. M. C.; Besenius, P.; Rybtchinski, B. Supramolecular Polymers in Aqueous Media. *Chem. Rev.* **2016**, *116* (4), 2414–2477.

(274) Krieg, E.; Rybtchinski, B. Noncovalent Water-Based Materials: Robust yet Adaptive. *Chem. – A Eur. J.* **2011**, *17* (33), 9016–9026.

(275) Rybtchinski, B. Aqueous Supramolecular Polymers Based on Aromatic Amphiphiles: Rational Design, Complexity, and Functional Materials. In *Hierarchical Macromolecular Structures: 60 Years after the Staudinger Nobel Prize I*; Percec, V., Ed.; Springer International Publishing: Berlin, 2013; p 363–387.

(276) Rybtchinski, B. Adaptive Supramolecular Nanomaterials Based on Strong Noncovalent Interactions. *ACS Nano* **2011**, *5* (9), 6791–6818.

(277) Israelachvili, J. N. *Intermolecular and Surface Forces*, 3rd ed.; Academic Press: Amsterdam, 2011.

(278) Lombardo, D.; Kiselev, M. A.; Magazù, S.; Calandra, P. Amphiphiles Self-Assembly: Basic Concepts and Future Perspectives of Supramolecular Approaches. *Adv. Condens. Matter Phys.* **2015**, *2015*.

(279) Hill, J. P.; Jin, W.; Kosaka, A.; Fukushima, T.; Ichihara, H.; Shimomura, T.; Ito, K.; Hashizume, T.; Ishii, N.; Aida, T. Self-Assembled Hexa-Peri-Hexabenzocoronene Graphitic Nanotube. *Science (80-.).* **2004**, *304* (5676), 1481–1483.

(280) Claussen, R. C.; Rabatic, B. M.; Stupp, S. I. Aqueous Self-Assembly of Unsymmetric Peptide Bolaamphiphiles into Nanofibers with Hydrophilic Cores and Surfaces. *J. Am. Chem. Soc.* **2003**, *125* (42), 12680–12681.

(281) Rösler, A.; Vandermeulen, G. W. M.; Klok, H.-A. Advanced Drug Delivery Devices via Self-Assembly of Amphiphilic Block Copolymers. *Adv. Drug Deliv. Rev.* **2001**, *53* (1), 95–108.

(282) Zhang, Q.; Ariga, K.; Okabe, A.; Aida, T. A Condensable Amphiphile with a Cleavable Tail as a "Lizard" Template for the Sol−Gel Synthesis of Functionalized Mesoporous Silica. *J. Am. Chem. Soc.* **2004**, *126* (4), 988–989.

(283) Mayoral Muñoz, M. J.; Fernández, G. Metallosupramolecular Amphiphilic π-Systems. *Chem. Sci.* **2012**, *3* (5), 1395–1398.

(284) Kondo, K.; Klosterman, J. K.; Yoshizawa, M. Aromatic Micelles as a New Class of Aqueous Molecular Flasks. *Chem. - A Eur. J.* **2017**, *23* (66), 16710–16721.

(285) Yang, L.; Fan, G.; Ren, X.; Zhao, L.; Wang, J.; Chen, Z. Aqueous Self-Assembly of a Charged BODIPY Amphiphile via Nucleation-Growth Mechanism. *Phys. Chem. Chem. Phys.* **2015**, *17* (14), 9167–9172.

(286) Chen, Z.; Liu, Y.; Wagner, W.; Stepanenko, V.; Ren, X.; Ogi, S.; Würthner, F. Near-IR Absorbing J-Aggregate of an Amphiphilic BF 2 -Azadipyrromethene Dye by Kinetic Cooperative Self-Assembly. *Angew. Chemie - Int. Ed.* **2017**, *56* (21), 5729–5733.

(287) Kwangmettatam, S.; Kudernac, T. Light-Fuelled Reversible Expansion of Spiropyran-Based Vesicles in Water. *Chem. Commun.* **2018**, *54* (42), 5311–5314.

(288) Kim, H.-J.; Kang, S.-K.; Lee, Y.-K.; Seok, C.; Lee, J.-K.; Zin, W.-C.; Lee, M. Self-Dissociating Tubules from Helical Stacking of Noncovalent Macrocycles. *Angew. Chemie Int. Ed.* **2010**, *49* (45), 8471–8475.

(289) El Hamaoui, B.; Zhi, L.; Pisula, W.; Kolb, U.; Wu, J.; Müllen, K. Self-Assembly of Amphiphilic Imidazolium-Based Hexa-Peri-Hexabenzo-Coronenes into Fibreous Aggregates. *Chem. Commun.* **2007**, No. 23, 2384–2386.

(290) Wu, J.; Li, J.; Kolb, U.; Müllen, K. A Water-Soluble Hexa-Peri-Hexabenzocoronene: Synthesis, Self-Assembly and Role as Template for Porous Silica with Aligned Nanochannels. *Chem. Commun.* **2006**, No. 1, 48–50.

(291) Zhang, G.; Jin, W.; Fukushima, T.; Kosaka, A.; Ishii, N.; Aida, T. Formation of Water-Dispersible Nanotubular Graphitic Assembly Decorated with Isothiouronium Ion Groups and Its Supramolecular Functionalization. *J. Am. Chem. Soc.* **2007**, *129* (3), 719–722.

(292) Würthner, F.; Saha-Möller, C. R.; Fimmel, B.; Ogi, S.; Leowanawat, P.; Schmidt, D. Perylene Bisimide Dye Assemblies as Archetype Functional Supramolecular Materials. *Chem. Rev.* **2016**, *116* (3), 962–1052.

(293) Grande, V.; Soberats, B.; Herbst, S.; Stepanenko, V.; Würthner, F. Hydrogen-Bonded Perylene Bisimide J-Aggregate Aqua Material. *Chem. Sci.* **2018**, *9* (34), 6904–6911.

(294) Casellas, N. M.; Pujals, S.; Bochicchio, D.; Pavan, G. M.; Torres, T.; Albertazzi, L.; García-Iglesias, M. From Isodesmic to Highly Cooperative: Reverting the Supramolecular Polymerization Mechanism in Water by Fine Monomer Design. *Chem. Commun.* **2018**, *54* (33), 4112–4115.

(295) Zhang, W.; Jin, W.; Fukushima, T.; Ishii, N.; Aida, T. Metal-Ion-Coated Graphitic Nanotubes: Controlled Self-Assembly of a Pyridyl-Appended Gemini-Shaped Hexabenzocoronene Amphiphile. *Angew. Chemie Int. Ed.* **2009**, *48* (26), 4747–4750.

(296) Pullerits, T.; Sundström, V. Photosynthetic Light-Harvesting Pigment−Protein Complexes: Toward Understanding How and Why. *Acc. Chem. Res.* **1996**, *29* (8), 381–389.

(297) Hu, X.; Ritz, T.; Damjanović, A.; Autenrieth, F.; Schulten, K. Photosynthetic Apparatus of Purple Bacteria. *Q. Rev. Biophys.* **2002**, *35* (1), 1–62.

(298) Tamiaki, H. Supramolecular Structure in Extramembraneous Antennae of Green Photosynthetic Bacteria. *Coord. Chem. Rev.* **1996**, *148*, 183–197.

(299) Frischmann, P. D.; Mahata, K.; Würthner, F. Powering the Future of Molecular Artificial Photosynthesis with Light-Harvesting Metallosupramolecular Dye Assemblies. *Chem. Soc. Rev.* **2013**, *42* (4), 1847–1870.

(300) Elemans, J. A. A. W.; van Hameren, R.; Nolte, R. J. M.; Rowan, A. E. Molecular Materials by Self-Assembly of Porphyrins, Phthalocyanines, and Perylenes. *Adv. Mater.* **2006**, *18* (10), 1251–1266.

(301) Scheer, H.; Katz, J. J. *Porphyrins and Metalloporphyrins*; Smith, K. M., Ed.; Elsevier: Amsterdam, 1975.

(302) White, W. I. *The Porphyrins*; Dolphin, D., Ed.; Academic Press: New York, 1978.

(303) Claessens, C. G.; Martínez-Díaz, M. V.; Torres, T. Supramolecular Phthalocyanine-Based Systems. In *Supramolecular Chemistry*; Major Reference Works; John Wiley & Sons, Ltd: Chichester, UK, 2012.

(304) Li, X.; Sinks, L. E.; Rybtchinski, B.; Wasielewski, M. R. Ultrafast Aggregate-to-Aggregate Energy Transfer within Self-Assembled Light-Harvesting Columns of Zinc Phthalocyanine Tetrakis(Perylenediimide). *J. Am. Chem. Soc.* **2004**, *126* (35), 10810–10811.

(305) de la Escosura, A.; Martínez-Díaz, M. V.; Thordarson, P.; Rowan, A. E.; Nolte, R. J. M.; Torres, T. Donor−Acceptor Phthalocyanine Nanoaggregates. *J. Am. Chem. Soc.* **2003**, *125* (40), 12300–12308.

(306) Duro, J. A.; de la Torre, G.; Barberá, J.; Serrano, J. L.; Torres, T. Synthesis and Liquid-Crystal Behavior of Metal-Free and Metal-Containing Phthalocyanines Substituted with Long-Chain Amide Groups. *Chem. Mater.* **1996**, *8* (5), 1061–1066.

(307) Tant, J.; Geerts, Y. H.; Lehmann, M.; De Cupere, V.; Zucchi, G.; Laursen, B. W.; Bjørnholm,

T.; Lemaur, V.; Marcq, V.; Burquel, A.; et al. Liquid Crystalline Metal-Free Phthalocyanines Designed for Charge and Exciton Transport. *J. Phys. Chem. B* **2005**, *109* (43), 20315–20323.

(308) Rai, R.; Saxena, A.; Ohira, A.; Fujiki, M. Programmed Hyperhelical Supramolecular Assembly of Nickel Phthalocyanine Bearing Enantiopure 1-(p-Tolyl)Ethylaminocarbonyl Groups. *Langmuir* **2005**, *21* (9), 3957–3962.

(309) Engelkamp, H.; Middelbeek, S.; Nolte, R. J. M. Self-Assembly of Disk-Shaped Molecules to Coiled-Coil Aggregates with Tunable Helicity. *Science (80-.).* **1999**, *284* (5415), 785–788.

(310) Guilleme, J.; Mayoral, M. J.; Calbo, J.; Aragó, J.; Viruela, P. M.; Ortí, E.; Torres, T.; González-Rodríguez, D. Non-Centrosymmetric Homochiral Supramolecular Polymers of Tetrahedral Subphthalocyanine Molecules. *Angew. Chemie Int. Ed.* **2015**, *54* (8), 2543–2547.

(311) Kobayashi, N. Optically Active Phthalocyanines. *Coord. Chem. Rev.* **2001**, *219–221*, 99–123.

(312) Wu, L.; Wang, Q.; Lu, J.; Bian, Y.; Jiang, J.; Zhang, X. Helical Nanostructures Self-Assembled from Optically Active Phthalocyanine Derivatives Bearing Four Optically Active Binaphthyl Moieties: Effect of Metal-Ligand Coordination on the Morphology, Dimension, and Helical Pitch of Self-Assembled Nanostructures. *Langmuir* **2010**, *26* (10), 7489–7497.

(313) Liu, H.; Liu, Y.; Liu, M.; Chen, C.; Xi, F. Synthesis and Properties of Optically Active 6,6′-Didodecyl-1,1′-Binaphthyl-Phthalocyanine Linked through Crown Ether Units. *Tetrahedron Lett.* **2001**, *42* (40), 7083–7086.

(314) Lv, W.; Zhang, X.; Lu, J.; Zhang, Y.; Li, X.; Jiang, J. Synthesis and Hollow-Sphere Nanostructures of Optically Active Metal-Free Phthalocyanine. *Eur. J. Inorg. Chem.* **2008**, *27*, 4255–4261.

(315) Pisarek, S.; Maximova, K.; Gryko, D. Strategies toward the Synthesis of Amphiphilic Porphyrins. *Tetrahedron* **2014**, *70* (38), 6685–6715.

(316) Lovell, J. F.; Jin, C. S.; Huynh, E.; Jin, H.; Kim, C.; Rubinstein, J. L.; Chan, W. C. W.; Cao, W.; Wang, L. V; Zheng, G. Porphysome Nanovesicles Generated by Porphyrin Bilayers for Use as Multimodal Biophotonic Contrast Agents. *Nat. Mater.* **2011**, *10* (4), 324–332.

(317) Komatsu, T.; Moritake, M.; Tsuchida, E. Molecular Energy and Electron Transfer Assemblies Made of Self-Organized Lipid-Porphyrin Bilayer Vesicles. *Chem. – A Eur. J.* **2003**, *9* (19), 4626–4633.

(318) Wang, S.-P.; Lin, W.; Wang, X.; Cen, T.-Y.; Xie, H.; Huang, J.; Zhu, B.-Y.; Zhang, Z.; Song, A.; Hao, J.; et al. Controllable Hierarchical Self-Assembly of Porphyrin-Derived Supra-Amphiphiles. *Nat. Commun.* **2019**, *10* (1), 1399.

(319) Liu, K.; Yuan, C.; Zou, Q.; Xie, Z.; Yan, X. Self-Assembled Zinc/Cystine-Based Chloroplast Mimics Capable of Photoenzymatic Reactions for Sustainable Fuel Synthesis. *Angew. Chemie Int. Ed.* **2017**, *56* (27), 7876–7880.

(320) Moriishi, M.; Kitayama, Y.; Ooya, T.; Takeuchi, T. Amphiphilic Polymerizable Porphyrins Conjugated to a Polyglycerol Dendron Moiety as Functional Surfactants for Multifunctional Polymer Particles. *Langmuir* **2015**, *31* (47), 12903–12910.

(321) Zou, Q.; Abbas, M.; Zhao, L.; Li, S.; Shen, G.; Yan, X. Biological Photothermal Nanodots Based on Self-Assembly of Peptide–Porphyrin Conjugates for Antitumor Therapy. *J. Am. Chem. Soc.* **2017**, *139* (5), 1921–1927.

(322) Liu, K.; Liu, Y.; Yao, Y.; Yuan, H.; Wang, S.; Wang, Z.; Zhang, X. Supramolecular Photosensitizers with Enhanced Antibacterial Efficiency. *Angew. Chemie - Int. Ed.* **2013**, *52* (32), 8285–8289.

(323) Guldi, D. M.; Gouloumis, A.; Vázquez, P.; Torres, T.; Georgakilas, V.; Prato, M. Nanoscale Organization of a Phthalocyanine−Fullerene System: Remarkable Stabilization of Charges

in Photoactive 1-D Nanotubules. *J. Am. Chem. Soc.* **2005**, *127* (16), 5811–5813.

(324) Li, X.; Yu, S.; Lee, Y.; Guo, T.; Kwon, N.; Lee, D.; Yeom, S. C.; Cho, Y.; Kim, G.; Huang, J. D.; et al. In Vivo Albumin Traps Photosensitizer Monomers from Self-Assembled Phthalocyanine Nanovesicles: A Facile and Switchable Theranostic Approach. *J. Am. Chem. Soc.* **2019**, *141* (3), 1366–1372.

(325) Li, X.; Lee, D.; Huang, J. D.; Yoon, J. Phthalocyanine-Assembled Nanodots as Photosensitizers for Highly Efficient Type I Photoreactions in Photodynamic Therapy. *Angew. Chemie - Int. Ed.* **2018**, *57* (31), 9885–9890.

BACKGROUND AND OBJECTIVES

1. Background of our research group in photosensitizers for PDT

Our research group has wide experience on the preparation and biological evaluation of porphyrinoid-based second and third generation PS. Some examples of Pc-based PS are shown below, paying special attention to the structural approaches to prevent aggregation and provide solubility in aqueous medium.

Our group has worked on dendrimer-encased Zn(II)Pcs[1,2] as an approach to achieve successful biomedical applications because the inner chromophores are partially shielded from media thanks to the spatial distribution of the dendrimers. This allows maintaining the PS photoactive, since the bulky substituents prevent the aggregation of the Zn(II)Pcs macrocycles. Specifically, these symmetric A_4 substituted Pcs, are highly water-soluble compounds presenting either positive or negative charges at the end of the dendrimer branches (see Figure 1). In particular, cationic dendrimers were employed successfully as antimicrobial agents.

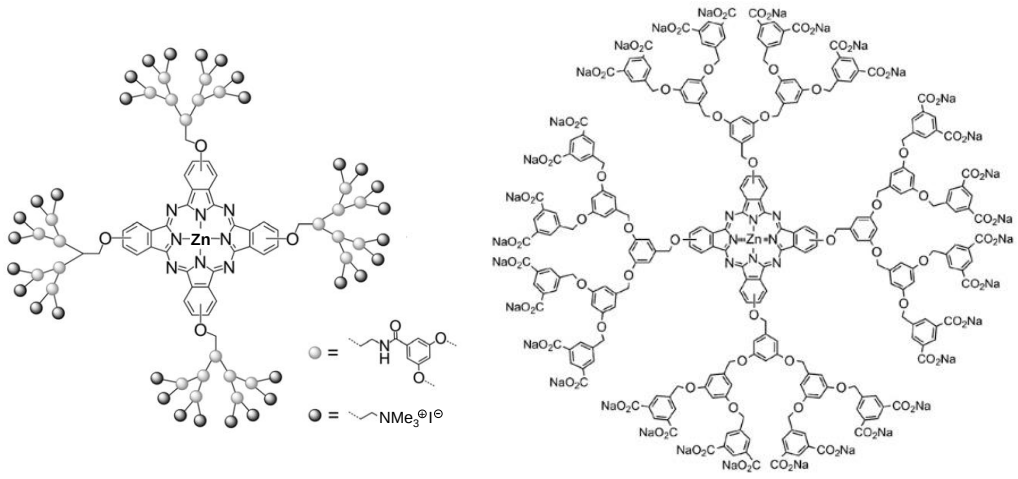

Figure 1. Ionic terminated Zn(II)Pcs dendrimers.

Another approach to avoid aggregation is to place metals in the central cavity that are able to coordinate axial ligands. For instance, the coordination of two pyridine ligands at the ruthenium axial positions in Ru(II)Pc compounds prevents, to a great extent, the aggregation often encountered for Pcs. In these compounds, the substituents that afford solubility, can be attached either at the Pc periphery or can be located in the axial substituent itself. Our group has reported A_4 cationic Ru(II)Pcs with alkyl amines[2] or PEG[3]

in the periphery, and/or with PEG or carbohydrate-based substituents at the pyridine axial ligand as shown in Figure 2.[4]

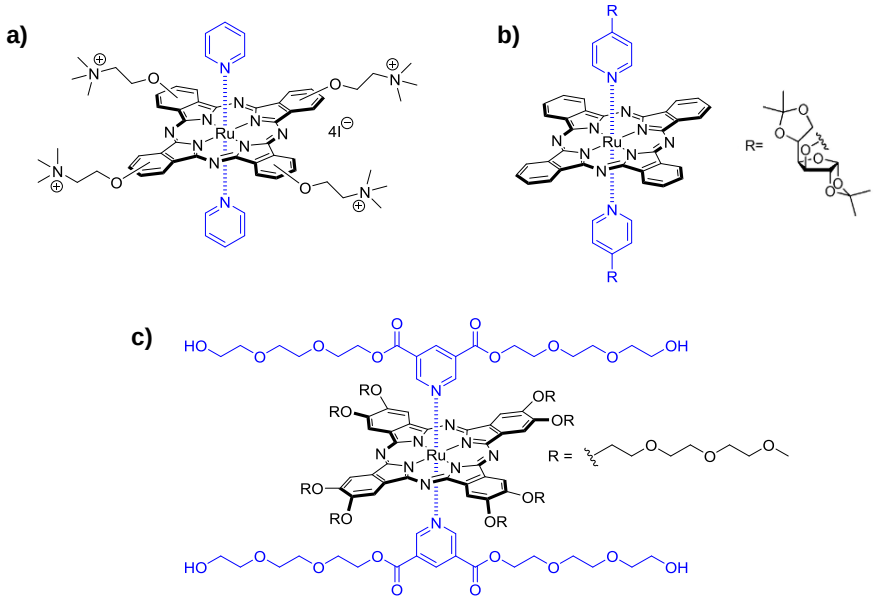

Figure 2. Ru(II)Pcs with different substituion patterns.

Similarly, the axial substituent strategy to avoid aggregation also applies to Si(IV)Pcs, which form covalent Si-O bonds with axial substituents. As an example, symmetrically substituted, octacationic Si(IV)Pc shown in Figure 3a was used for the photodynamic inactivation of bacteria.[5] More recently (Figure 3b), amphiphilic Si(IV)Pcs in polymeric were incorporated into micelles in a supramolecular approach toward efficient third-generation PS.[6]

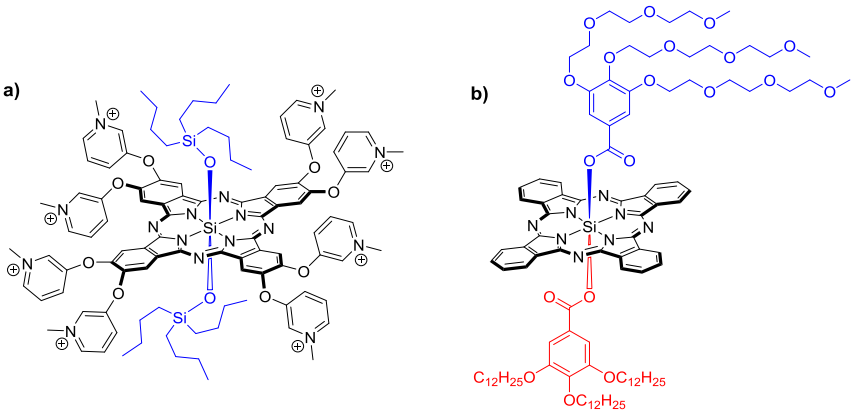

Figure 3. Axially di-substituted Si(IV)Pcs.

Zn(II)Pcs are excellent candidates for PDT and PDI applications, but as long as they are not able to stablish strong axial coordination, the strategy to avoid aggregation consist in the incorporation of bulky substituents in the periphery to prevent π-π stacking. An example of a bulky Zn(II)Pc PS reported in our group is the compound coded as **TT1** (mentioned in Introduction – PDT section) with three *tert*-butyl substituents playing this role. We also reported photo-antimicrobial biohybrids based on the supramolecular immobilization of cationic Zn(II)Pcs onto cellulose nanocrystals.[7] In this case, pyridyloxy peripheral substituents responsible of the cationic character of the molecule include also *p-tert*-butylphenyl groups in position 3 to hinder the aggregation of the macrocycles (see Figure 4).

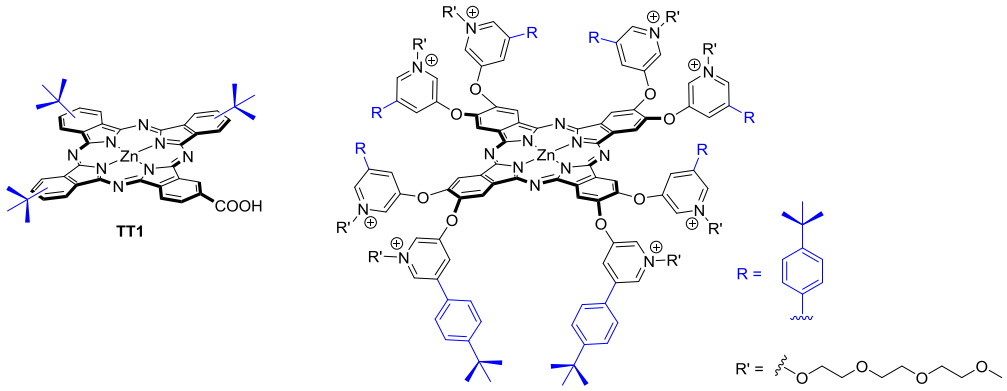

Figure 4. Zn(II)Pcs with bulky peripheral substituents.

For this doctoral thesis we will focus our attention in Zn(II)Pcs as PS due to their high singlet oxygen quantum yields. However, to date there are no reports on A_2B_2 substituted Zn(II)Pcs for PDT. As we will explain in the Objectives section, we are interested in this type of substitution because it provides high directionality, (Figure 5) feature that is ideal to build amphiphiles. In the next section, previous work from our research group on ABAB Zn(II)Pcs for application in photoelectronics, which establishes a new successful methodology to prepare this kind of compounds, is summarized.

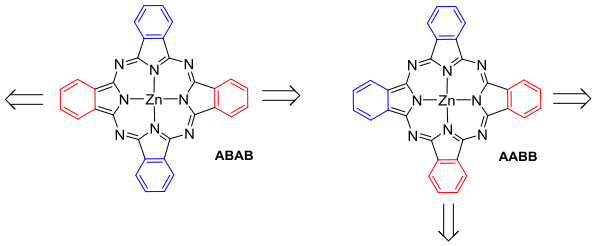

Figure 5. Representation of the directionality imposed in the A_2B_2 substitution pattern.

2. Background of our research group in ABAB Pcs

Our group has been involved for many years in the synthesis of A_3B Pcs targeted to the preparation of multicomponent materials for optoelectronic applications. However, in recent years, we have selected A_2B_2 Pcs as challenging targets towards the preparation of more complex Pc-based systems. In particular, we have developed some work on the preparation of ABAB Pcs for several purposes, but the selective synthesis of AABB Pcs has not been explored yet. The following lines show a summary of the most relevant work on ABAB Zn(II)Pcs, which constitute one of the pillars in which this doctoral thesis is based on. First of all, the group developed an efficient method for the synthesis of ABAB functionalized Pcs.[8] Although the selective crossed condensation of different precursors, namely trichloroisoindolenine and diiminoisoindoline derivatives, has led to a number of ABAB Pcs, (Introduction section 1.6.), this method is only feasible when the trichloroisoindolenine is either functionalized with NO_2 moieties or lacks any functional group. On the other hand, functionalization at the diiminoisoindoline precursor is usually devoted to impart solubility to the target compound. Although some of the reported ABAB Pcs exhibit crossed functionality that permits further derivatization towards more complex systems,[9,10] the synthesis of the precursors requires elaborated procedures. Therefore, in our former work, we described a method to prepare ABAB Zn(II)Pcs crosswise-functionalized with two or four iodine atoms (Scheme 1), programmed for their further implementation into more complex structures. Key to the selective preparation of the opposite ABAB isomers versus the adjacent AABB ones is the use of a bulky 3,6-(3′,5′-bis(trifluoromethyl)-phenyl)phthalonitrile with hampered self-condensation capabilities, and therefore, AABB Pcs containing adjacent bis(trifluoromethyl)phenyl moieties were not formed during the cyclization process. Importantly, although different bulky phthalonitriles were tested as precursors to direct the reaction towards the formation of ABAB products, only 3,6-bis-(3,5-bistrifluoromethylphenyl)phthalonitrile proved to be effective in providing the corresponding ABAB Pcs with selectivity and in reasonable yields.[11]

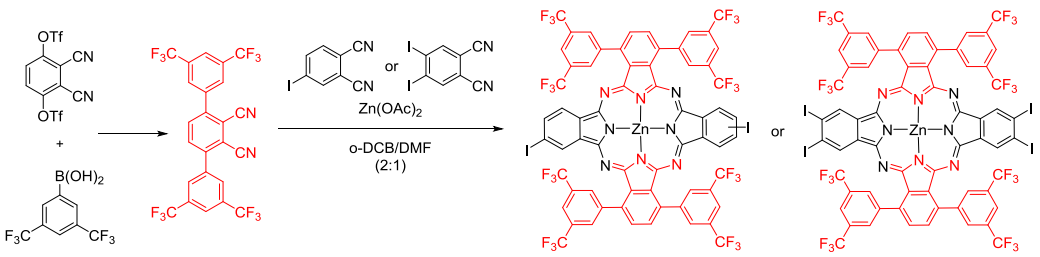

Scheme 1. Statistical synthesis of diiodo- or tetraiodo-ABAB Zn(II)Pcs under optimized conditions from bulky 3,6-(3′,5′-bis(trifluoromethyl)phenyl)phthalonitrile.

As mentioned above, the most relevant feature of these Pcs is the crosswise functionalization with iodine atoms, which can lead to unprecedented multicomponent systems based on ABAB Pcs through reliable cross-coupling methodologies. Therefore, these compounds were employed as scaffolds for building unprecedented donor–π–acceptor chromophores,[11] through the asymmetric functionalization of the two iodine atoms using Pd-catalyzed cross-coupling reactions with adequate electron-donor and electron-acceptor moieties (Figure 6). The new push–pull molecules were tested for dye-sensitized solar cells (DSSCs).

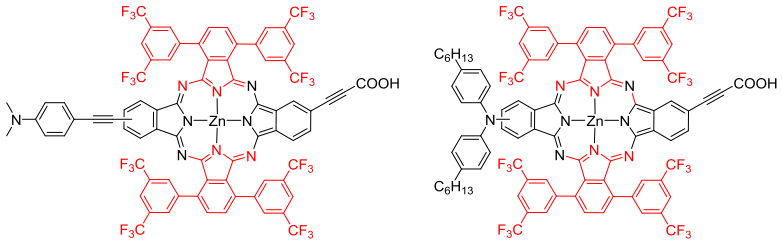

Figure 6. Donor–π–acceptor ABAB Zn(II)Pc chromophores.

Within the same field, the next milestone with increased complexity was the preparation of a panchromatic, charge-stabilizing electron donor–acceptor conjugate (Figure 7) comprising (biphenyl)phenylamine units linked to Zn(II) porphyrin (ZnPor) that is bound to a ZnPc-SubPc dyad.[12]. The combination of the three porphyrinoids in a covalent linear conjugate followed a rational design towards an appropriate energy level alignment, which led to a cascade of energy and charge transfer processes from the electron-donating (biphenyl)phenylamine-ZnPor system to the SubPc termini, the central Zn(II)Pc operating as energy/electron transfer funnel between the ZnPor and the SubPc.

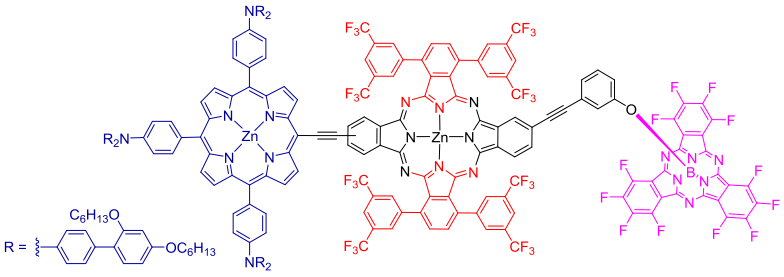

Figure 7. Structure of $(BBPA)_3$–ZnPor–ZnPc–SubPc triad.

Our ABAB-type diiodo-substituted Pc has been also used by other authors to prepare Pc-diketopyrrolopyrrole conjugated alternating polymers, which present promising applications in electronic and optoelectronic devices.[13]

Finally, the diiodo-ABAB Zn(II)Pc was also employed as precursor to assemble an unprecedented Fe_2Pc_3 metallo-organic helicate using a bidentate Pc ligand, 2-formylpyridine and $Fe(OTf)_2$ (Figure 8). This giant helicate has proved itself as a host for large redox-active guests such as fullerene and naphthalenediimide derivatives, where photoactivated electronic interactions between components occur in the host–guest complex.[14]

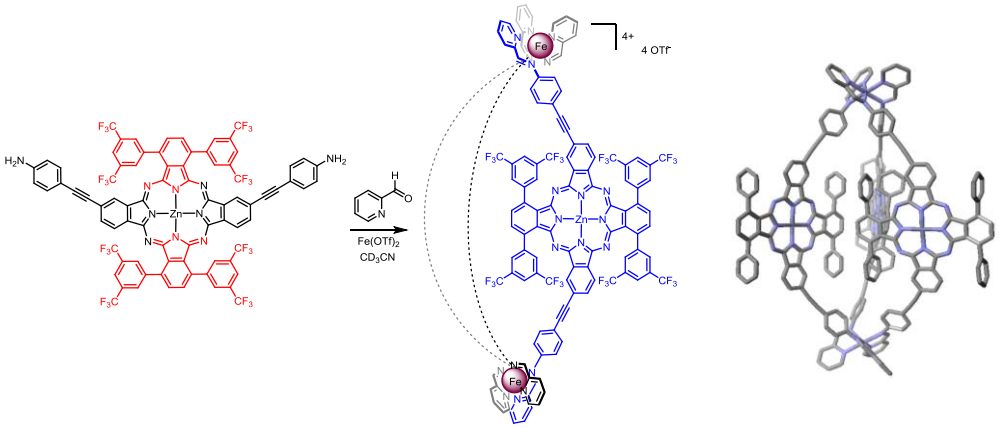

Figure 8. $Fe(II)_2L_3(OTf)_4$ helicate synthesis together with a side view of an energy-minimized structure.

3. General Objectives

The main goal of this doctoral thesis is the synthesis of unprecedented A_2B_2 Pcs for their application as photosensitizers in photodynamic therapy. Specifically for **Part 1**, we aim to prepare different ABAB Zn(II)Pcs with a linear, face-to-face arrangement of the functional groups anchored to the aromatic core, which can provide the molecule with non-aggregating features and amphiphilicity, being both important requirements for this application. **Part 2** is devoted to the synthesis of amphiphilic AABB Zn(II)Pcs endowed with chiral binaphtol units, and the exploration of their photosensitizing abilities and supramolecular self-assembly behaviour in solution.

3.1. Objectives – Part 1

In **Part 1**, the preparation of ABAB Pcs with crosswise functionalization will be carried out by using a bulky phthalonitrile with appropriate functionalization in the α-positions to hamper its self-condensation (Scheme 2). This approach prevents the formation of the undesired AABB isomer, and allow us to direct the synthesis towards the formation of the target ABAB Pcs. Therefore, this bulky phthalonitrile will be reacted under statistical conditions with phthalonitriles endowed with different functionalities for specific purposes, as detailed below.

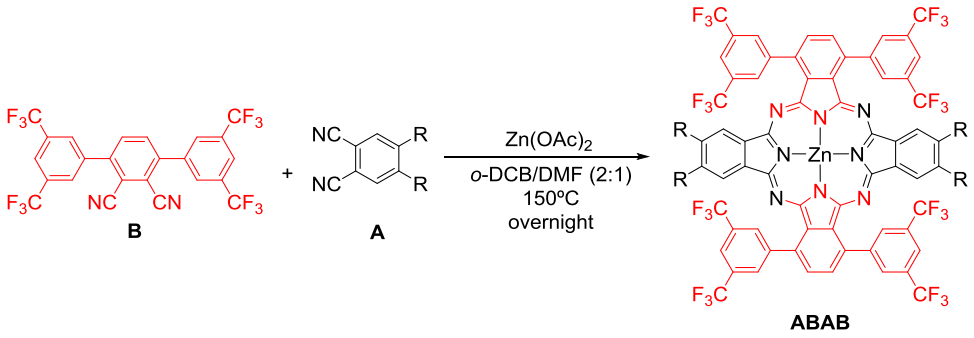

Scheme 2. Planned synthesis of generic ABAB Zn(II)Pc from bulky phthalonitrile B.

More in detail, the objectives of this section are defined as follows:

Chapter 1 is devoted to determine the influence of the substitution pattern on the aggregation features, fluorescence quantum yields and $^1O_2$ generation abilities of a family of ABAB, A_3B and A_4 Zn(II)Pcs, functionalized with a varying number of bis(trifluoromethyl)phenyl units (i.e. at the B isoindoles) and other electron-withdrawing/electron-donating moieties (i.e. at the A isoindoles). The final goal is to find

out if the ABAB substitution is advantageous *versus* other already explored substitution patterns (i.e. A_3B and A_4) in the search of efficient photosensitizers.

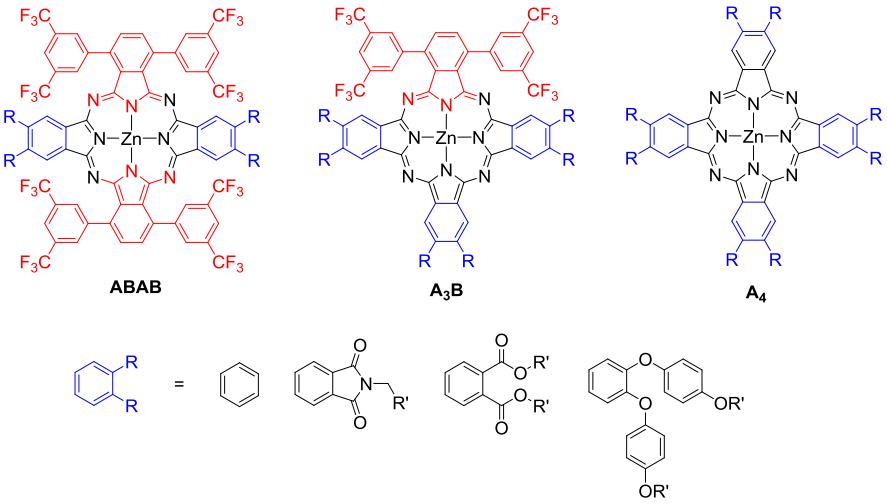

Figure 9. Targeted ABAB, A_3B and A_4 Zn(II)Pcs in Chapter 1.

The aim of **Chapter 2** is the synthesis of collinearly functionalized systems based on the ABAB Zn(II)Pc design. For that purpose, extra-annulated phthalimide units will be attached to the A isoindoles (A), bearing different substituents in the nitrogen positions (i.e. ethynyl, vinyl, amine and carboxylic acid) that may allow for the further construction of 1D multi-Pc arrays, and also permits to build third-generation PS, where the Zn(II)Pc can be covalently conjugated to two site-specific delivery agents.

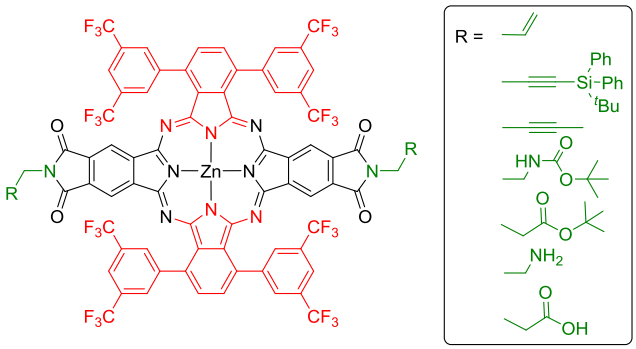

Figure 10. Structure of Zn(II)Pcs bearing different collinear functional groups for further functionalization.

Chapter 3 is focused on the synthesis and evaluation as PS of a Zn(II)Pc with the ABAB substitution pattern developed in Chapters 1 and 2, but endowed with hydrophilic

triethylene glycol monomethyl ether (i.e. at the A isoindoles) to provide solubility in aqueous media. The aim here is to compare its ability as a real PS for PDT treatments with regard to those exhibited by its A_3B and A_4 counterpartners. For that purpose, *in vitro* biological assays in cell cultures of different human cancer cells will be performed.

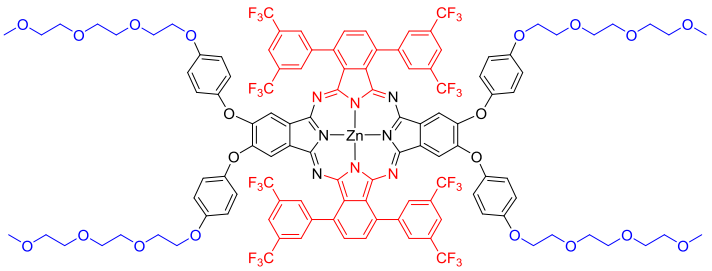

Figure 11. Structure of amphiphilic peglilated ABAB Zn(II)Pc for PDT studies.

Finally, regarding to **Chapter 4**, we aim to prepare novel PS showing abilities towards the inactivation of Gram-positive and Gram-negative bacteria. To this end, the preparation of cationic ABAB Zn(II)Pc following different approaches will be tackled, in order to determine the influence of the type of positively charged groups and its separation from the aromatic core in the photosensitizing properties of the Zn(II)Pcs.

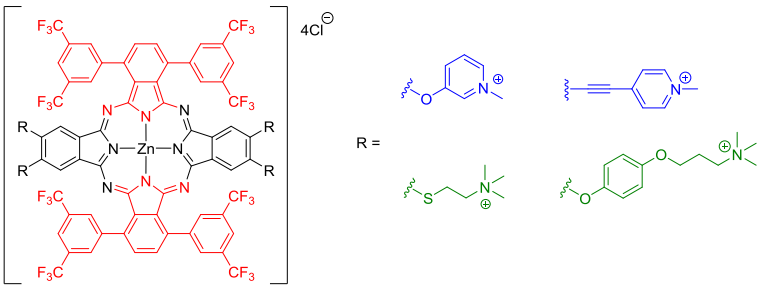

Figure 12. Structure of aimed amphiphilic, tetracationic ABAB Zn(II)Pcs for PDI.

3.2. Objectives – Part 2

In Part 2, the development of novel unprecedented amphiphiles based on adjacent AABB Zn(II)Pcs will be undertaken. To this end, we aim to use chiral binaphthyloxy-linked bisphthalonitriles (Scheme 3), which prevent the formation of the undesired ABAB isomer, and reduce to three the number of expected products formed during the condensation. These bisphthalonitriles will be cross-reacted with other phthalonitriles with specific functionalization, giving rise to AABB Zn(II)Pcs that can be further derivatized to provide them with hydrophilic properties and, therefore, develop structurally new PS. As this type of Pcs do no present hindered aggregation, we aim to exploit their self-assembly behaviour in water media, trying to control the formation of Zn(II)Pcs nanostructures that could present improved delivery properties through the bloodstream in photodynamic treatments, but remaining non-aggregated in less polar environments as the interior of the cell.

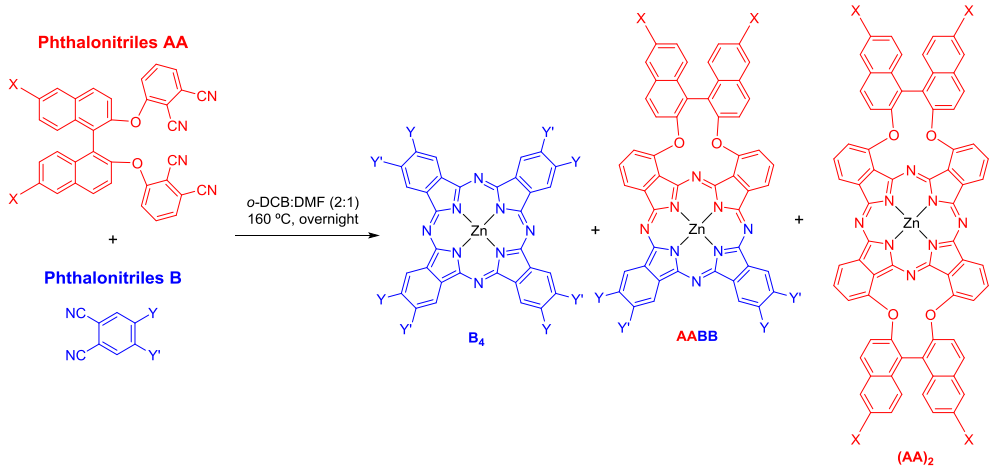

Scheme 3. General synthetic scheme towards AABB Zn(II)Pcs from bisphthalonitriles AA.

More in detail, the objectives of this section are defined as follows:

In **Chapter 5** we aim to explore the crossed reactivity of binaphthyloxy-linked bisphthalonitriles with differently substituted phthalonitriles, following simpler synthetic protocols than those previously reported in the literature. In such a way, we intend to effectively produce a battery of chiral, binaphthyl-functionalized AABB Zn(II)Pcs, endowed with functional groups that can be further transformed to obtain a variety of customized compounds, particularly amphiphilic water soluble compounds (see Objectives of Chapter 7). The presence of the chiral binaphthyl unit could allow us to explore the formation of chiral assemblies in solution.

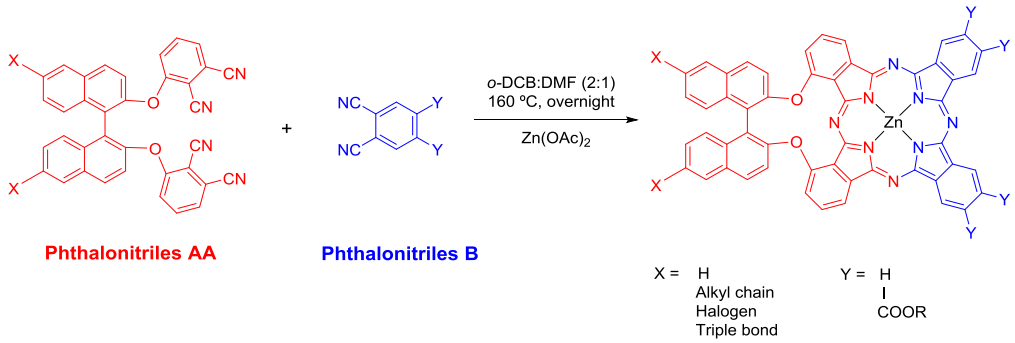

Scheme 4. AABB Zn(II)Pcs with reactive groups for further functionalization.

The aim of **Chapter 6** is to explore the abilities of binaphthyloxy-linked AABB Zn(II)Pcs as PS. For that purpose, we aim to prepare a series of cationic ABAB Zn(II)Pcs with a customized amphiphilic character, to explore their ability to self-assemble in water, and to test the efficiency of this approach in the photoinactivation of Gram-positive and Gram-negative bacteria.

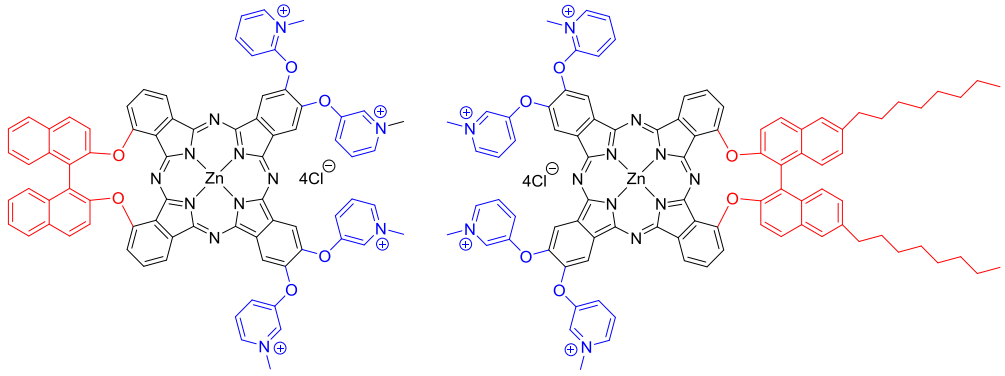

Figure 13. Structure of amphiphilic, cationic AABB Zn(II)Pcs designed for the inactivation of bacteria

Chapter 7 aims also to obtain AABB Zn(II)Pc amphiphiles, but following a different approach, that is incorporating polyethylene glycol chains directly over a Pc synthon or a properly functionalized phthalonitrile. Also in this case, the molecules will be programmed to self-assemble in aqueous media and, therefore, aggregation studies and evaluation of their photosensitizing abilities will be carried out.

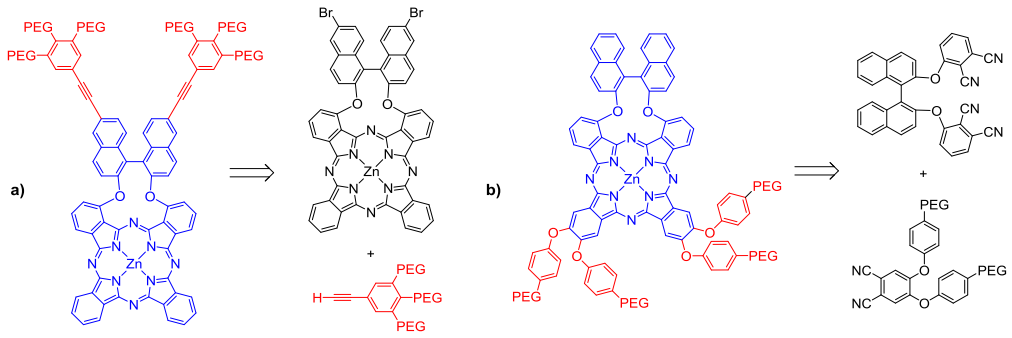

Figure 14. Structure of amphiphilic peglilated AABB Zn(II)Pc.

4. References

(1) Setaro, F.; Ruiz-González, R.; Nonell, S.; Hahn, U.; Torres, T. Synthesis, Photophysical Studies and 1O2 Generation of Carboxylate-Terminated Zinc Phthalocyanine Dendrimers. *J. Inorg. Biochem.* **2014**, *136*, 170–176.

(2) Ruiz-González, R.; Setaro, F.; Gulías, Ò.; Agut, M.; Hahn, U.; Torres, T.; Nonell, S. Cationic Phthalocyanine Dendrimers as Potential Antimicrobial Photosensitisers. *Org. Biomol. Chem.* **2017**, *15* (42), 9008–9017.

(3) Ferreira, J. T.; Pina, J.; Ribeiro, C. A. F.; Fernandes, R.; Tomé, J. P. C.; Rodríguez-Morgade, M. S.; Torres, T. Synthesis, Characterization and In Vitro Evaluation of Carbohydrate-Containing Ruthenium Phthalocyanines as Third Generation Photosensitizers for Photodynamic Therapy. *ChemPhotoChem* **2018**, *2* (7), 640–654.

(4) Teles Ferreira, J.; Pina, J.; Alberto Fontes Ribeiro, C.; Fernandes, R.; Tomé, J. P. C.; Rodríguez-Morgade, M. S.; Torres, T. PEG-Containing Ruthenium Phthalocyanines as Photosensitizers for Photodynamic Therapy: Synthesis, Characterization and in Vitro Evaluation. *J. Mater. Chem. B* **2017**, *5* (29), 5862–5869.

(5) van de Winckel, E.; David, B.; Simoni, M. M.; González-Delgado, J. A.; de la Escosura, A.; Cunha, Â.; Torres, T. Octacationic and Axially Di-Substituted Silicon (IV) Phthalocyanines for Photodynamic Inactivation of Bacteria. *Dye. Pigment.* **2017**, *145*, 239–245.

(6) Setaro, F.; Wennink, J. W. H.; Mäkinen, P. I.; Holappa, L.; Trohopoulos, P. N.; Ylä-Herttuala, S.; van Nostrum, C. F.; de la Escosura, A.; Torres, T. Amphiphilic Phthalocyanines in Polymeric Micelles: A Supramolecular Approach toward Efficient Third-Generation Photosensitizers. *J. Mater. Chem. B* **2020**.

(7) Anaya-Plaza, E.; van de Winckel, E.; Mikkilä, J.; Malho, J.-M.; Ikkala, O.; Gulías, O.; Bresolí-Obach, R.; Agut, M.; Nonell, S.; Torres, T.; et al. Photoantimicrobial Biohybrids by Supramolecular Immobilization of Cationic Phthalocyanines onto Cellulose Nanocrystals. *Chem. – A Eur. J.* **2017**, *23* (18), 4320–4326.

(8) Fazio, E.; Jaramillo-García, J.; de La Torre, G.; Torres, T. Efficient Synthesis of ABAB Functionalized Phthalocyanines. *Org. Lett.* **2014**, *16*, 4706–4709.

(9) Stihler, P.; Hauschel, B.; Hanack, M. Synthesis of a Bisdienophilic Phthalocyanine and of Precursors for Repetitive Diels-Alder Reactions Based on Hemiporphyrazines and Phthalocyanines. *Chem. Ber.* **1997**, *130*, 801–806.

(10) Youngblood, W. J. Synthesis of a New Trans-A2B2 Phthalocyanine Motif as a Building Block for Rodlike Phthalocyanine Polymers. *J. Org. Chem.* **2006**, *71*, 3345–3356.

(11) Fazio, E.; Nazeerudin, M. K.; de la Torre, G.; Medel, M.; Grätzel, M.; Jaramillo-García, J.; Urbani, M.; Torres, T. ABAB Phthalocyanines: Scaffolds for Building Unprecedented Donor-π-Acceptor Chromophores. *ChemistryOpen* **2016**, *6* (1), 121–127.

(12) Fazio, E.; Winterfeld, K. A.; López-Pérez, A.; Torres, T.; Guldi, D. M.; de la Torre, G. Synergy of Light Harvesting and Energy Transfer as Well as Short-Range Charge Shift Reactions in Multicomponent Conjugates. *Nanoscale* **2018**, *10* (47), 22400–22408.

(13) Mutyala, A. K.; Hong, S.-M.; Namgoong, J. W.; Kim, J. P.; Park, J. S. Low Bandgap Poly(Fluorinated Metallophthalocyanine-Alt-Diketopyrrolopyrrole)s with Outstanding Thermal Stability. *Dye. Pigment.* **2017**, *142*, 237–242.

(14) Fazio, E.; Haynes, C. J. E.; de la Torre, G.; Nitschke, J. R.; Torres, T. A Giant M2L3 Metallo-Organic Helicate Based on Phthalocyanines as a Host for Electroactive Molecules. *Chem. Commun.* **2018**, *54* (21), 2651–2654.

- PART 1 -

ABAB

PHTHALOCYANINES

Chapter 1 – Boosting the $^1O_2$ photosensitization abilities of Zn(II)Pcs through functionalization with bulky fluorinated substituents

Organic & Biomolecular Chemistry

PAPER

View Article Online
View Journal | View Issue

Check for updates

Cite this: Org. Biomol. Chem., 2019, 17, 7448

Boosting the singlet oxygen photosensitization abilities of Zn(II) phthalocyanines through functionalization with bulky fluorinated substituents†

Miguel A. Revuelta-Maza,[a] Santi Nonell,[b] Gema de la Torre[a,c] and Tomás Torres[a,c,d]

Received 15th April 2019,
Accepted 11th July 2019

DOI: 10.1039/c9ob00872a

rsc.li/obc

In-depth, systematic photophysical studies have been performed on a series of **ABAB**, A_2B and A_4 ZnPcs functionalized with a varying number of bis(trifluoromethyl)phenyl units (i.e. at the B isoindoles) and other electron-withdrawing/electron-donating moieties (i.e. at the A isoindoles), to determine the influence of the substitution pattern on the aggregation features, fluorescence quantum yields and singlet oxygen ($^1O_2$) generation abilities of these molecules. As a general trend, the larger the number of bis(trifluoromethyl)phenyl units (*i.e.* **ABAB** crosswise functionalized ZnPcs), the lower the fluorescence quantum yield and the higher the $^1O_2$ photosensitization. On the other hand, the electronic character of the substituents at the A isoindoles do not seem to have a clear effect on the photophysical properties of these **ABAB** ZnPcs. Overall, $^1O_2$ quantum yields determined by the direct observation of the $^1O_2$ phosphorescence are very high, with values ranging from 1 to 0.74 in THF solutions.

Introduction

Phthalocyanines (Pcs) represent the most prominent family of second-generation synthetic photosensitizers (PS),[1–4] mainly due to their strong absorption in the phototherapeutic window and the efficient sensitization of triplet oxygen ($^3O_2$) to form highly reactive singlet oxygen ($^1O_2$). Owing to their extended π-conjugation, Pcs exhibit a strong tendency to aggregate that drives the formation of oligomers in solution.[5] The formation of stacked aggregates affects their photochemical and photophysical properties, and hence their use as PS, because aggregation-induced fast radiationless deactivation detracts from $^1O_2$ generation. In aqueous media, aggregation of Pcs is facilitated by their inherent insolubility. In this context, hydrophilic groups can be introduced to render an amphiphilic character and water-solubility to the Pcs,[6–8] but they do not bring about the elimination of the aggregation tendency of Pcs in this medium. A means to circumvent the aggregation derived from the π–π stacking of Pcs arises from the complexation of closed shell, diamagnetic metal ions such as Si(IV)[6,9] or Ru(IV),[10] which can be axially functionalized with the required hydrophilic moieties.

On the other hand, ZnPcs are very interesting PS as they present, in general, higher efficiencies in the generation of $^1O_2$ than the abovementioned Ru(IV)Pcs or Si(IV)Pcs.[11] However, an important shortcoming of ZnPcs is that they cannot circumvent the π–π stacking issues by covalent axial functionalization. In this regard, our research group has recently described a new strategy to prepare ZnPcs showing both hindered aggregation and water solubility, that is, by introducing two types of peripheral substituents into the Pc in a crosswise, **ABAB** architecture[12,13] (A and B coding for the two differently functionalized isoindole constituents). Within this architecture, π–π interactions between the Pc cores are prevented by endowing two facing isoindoles (B) of the ZnPc with bulky bis(trifluoromethyl)phenyl units, while the other two isoindoles (A) can provide the necessary water-solubility if they are properly functionalized with hydrophilic substituents. Interestingly, **ABAB** ZnPcs with extra-annulated phthalimide units containing different moieties in the nitrogen positions gave rise to $^1O_2$ quantum yields (ϕ_Δ) that are higher than the average values reported in the literature for other functionalized ZnPcs, which proved our **ABAB** ZnPcs to be very interesting motifs for the preparation of PS.[13]

[a]Universidad Autónoma de Madrid, c/Francisco Tomás y Valiente 7, 28049 Madrid, Spain. E-mail: tomas.torres@uam.es, gema.delatorre@uam.es
[b]Institut Químic de Sarrià, Universitat Ramon Llull, 08017 Barcelona, Spain
[c]Institute for Advanced Research in Chemical Sciences (IAdChem), Universidad Autónoma de Madrid, 28049 Madrid, Spain
[d]Institute Madrileño de Estudios Avanzados (IMDEA)-Nanociencia, c/Faraday 9, Cantoblanco, 28049 Madrid, Spain

†Electronic supplementary information (ESI) available: Synthetic details and spectroscopic and photophysical characterization. See DOI: 10.1039/c9ob00872a

1.1. Citation and contribution

Revuelta-Maza, M.A.; Nonell, S.; de la Torre, G.; Torres, T. Boosting the singlet oxygen photosensitization abilities of Zn(II) phthalocyanines through functionalization with bulky fluorinated substituents. *Org. Biomol. Chem.* **2019**, *17*, 7448–7454.

Contribution: Revuelta-Maza, M.A.: Synthesis, characterization, and photophysical studies. Preparation of the manuscript.

Funding and supervision: Nonell, S.; de la Torre, G.; Torres, T. This work was supported by MINECO (CTQ2017-85393-P and CTQ2016-78454-C2-1-R) and ERA-NET/MINECO EuroNanoMed2017-191/PCIN-2017-042.

Abstract:

In-depth, systematic photophysical studies have been performed on a series of ABAB, A_3B and A_4 Zn(II)Pcs functionalized with a varying number of bis(trifluoromethyl)phenyl units (i.e. at the B isoindoles) and other electron-withdrawing/electron-donating moieties (i.e. at the A isoindoles), to determine the influence of the susbtitution pattern on the aggregation features, fluorescence quantum yields and singlet oxygen ($^1O_2$) generation abilities of these molecules. As a general trend, the larger the number of bis(trifluoromethyl) phenyl units (i.e. ABAB crosswise functionalized Zn(II)Pcs), the lower the fluorescence quantum yield and the higher the $^1O_2$ photosensitization. On the other hand, the electronic character of the substituents at the A isoindoles do not seem to have a clear effect on the photophysical properties of these ABAB ZnPcs. Overall, $^1O_2$ quantum yields determined by the direct observation of the $^1O_2$ phosphorescence are very high, with values ranging from 1 to 0.74 in THF solutions.

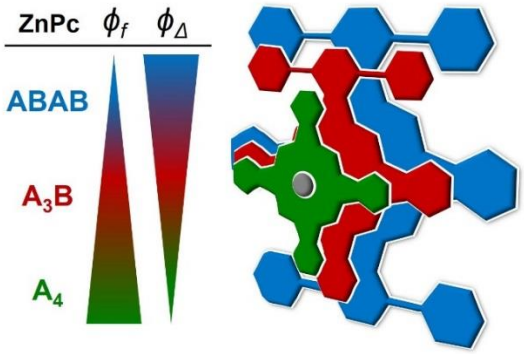

1.2. Introduction and Objectives

As showed before in the General Introduction Section, Pcs represent one of the most prominent families of second-generation synthetic PS,[1–4] mainly due to their strong absorption in the phototherapeutic window and the efficient sensitization of $^3O_2$ to form highly reactive $^1O_2$. Thus, owing to their extended π-conjugation, Pcs exhibit a strong tendency to aggregate that drives the formation of oligomers in solution.[5] The formation of stacked aggregates affects their photochemical and photophysical properties, and hence their use as PS, because aggregation-induced fast radiationless deactivation detracts from $^1O_2$ generation. In aqueous media, aggregation of Pcs is facilitated by their inherent insolubility. In this context, hydrophilic groups can be introduced to render an amphiphilic character and water-solubility to the Pcs,[6–8] but they do not bring about the elimination of the aggregation tendency of Pcs in this medium. A means to circumvent the aggregation derived from the π–π stacking of Pcs arises from the complexation of closed shell, diamagnetic metal ions such as Si(IV)[6,9,10] or Ru(II),[11,12] which can be axially functionalized with the required hydrophilic moieties.

On the other hand, Zn(II)Pcs are very interesting PS as they present, in general, higher efficiencies in the generation of $^1O_2$ than the above mentioned Ru(II)Pcs or Si(IV)Pcs.[13] However, an important shortcoming of Zn(II)Pcs is that they cannot circumvent the π–π stacking issues by covalent axial functionalization. In this regard, our research group has recently described a new strategy to prepare Zn(II)Pcs showing hindered aggregation by introducing two types of peripheral substituents into the Pc in a crosswise, ABAB architecture,[14,15] (A and B coding for the two differently functionalized isoindole constituents). Within this architecture, π–π interactions between the Pc cores are prevented by endowing two facing isoindoles (B) of the Zn(II)Pc with bulky bis(trifluoromethyl)phenyl units, while the other two isoindoles (A) can provide the necessary water-solubility if they are properly functionalized with hydrophilic substituents.

Before using this ABAB Zn(II)Pc skeleton to build amphiphilic, water-soluble chromophores with plausible application as PS, we have tackled an in-depth study to establish structure/activity relationships that can help us to design and prepare Zn(II)Pcs with maximized ϕ_Δ. From previous studies performed over different types of fluorinated Pcs,[16–20] we can expect that the functionalization with bis(trifluoromethyl)phenyl units at the alpha position of the outer benzene rings of the Pc could produce high $^1O_2$ generation efficiencies as a result of: (i) the position of the fluorinated substituents, since alpha-substitution is usually preferable versus beta functionalization at the Zn(II)Pc;[21] (ii) the enhanced photostability that fluorine-functionalization affords to the Zn(II)Pc,[22] due to the electron-withdrawing character of the CF_3 groups that results in energetically low-lying highest occupied molecular orbitals (HOMOs);[23] and/or the heavy atom effect that favors intersystem crossing and, therefore, high triplet lifetimes.[16–18]

Then, we aim here to verify the effect of the functionalization with bis(trifluoromethyl)phenyl units by preparing and studying the photophysical features of a series of Zn(II)Pcs endowed with a different number of fluorinated substituents (i.e. **ABAB 1a–d**, **A_3B 1a–d** and **A_4 1a** and **c**) (Scheme 1. 1). Moreover, to determine the effect that the nature of the substituents at the A isoindoles exerts on the electronic structure, and therefore, on the photophysical properties of the compounds, we have synthesized a series of Zn(II)Pcs with A units lacking any functional group (**1a** series), or endowed with either electron-withdrawing functional groups, such as extraannulated phthalimides (**1b** series) and ester moieties (**1c** series), or electron-donating *p*-methoxyphenoxy substituents (**1d** series). Importantly, the functionalization incorporated into Zn(II)Pcs **ABAB 1b–d** would enable further chemical modifications to convert these series of compounds into real water-soluble molecules, with a balanced hydrophilicity/lipophilicity,[17,18] for their use as PS. Therefore, this systematic study would allow us to establish optimal Zn(II)Pc cores for the divergent preparation of a number of amphiphilic PS.

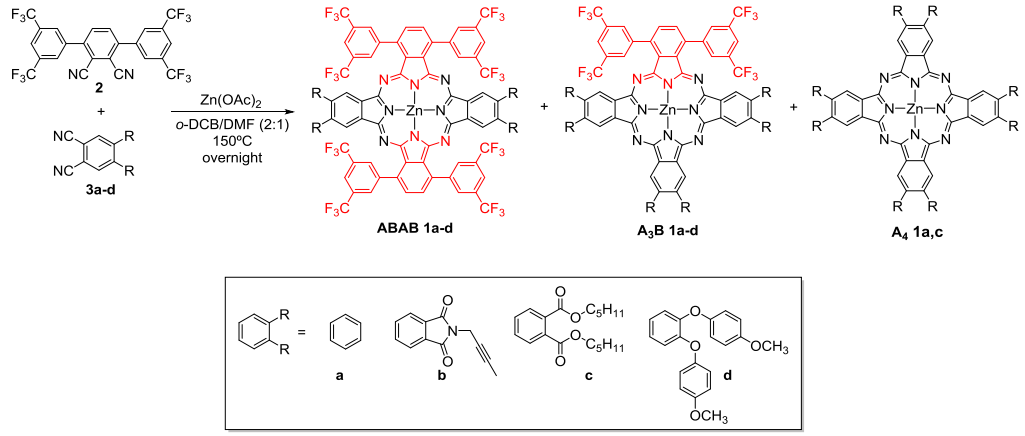

*Scheme 1. 1. Synthesis of Zn(II)Pcs **ABAB 1a–d**, **A_3B 1a–d** and **A_4 1a,c**.*

1.3. Results and discussion

a) Synthesis

The synthesis of the target Zn(II)Pcs was carried out by cross-condensation between equimolecular amounts of bulky phthalonitrile **2** (B) and phthalonitriles **3a–d** (A). In all the reactions, the corresponding Zn(II)Pcs **ABAB 1a–d** were formed, together with the related **A_3B 1a–d** and **A_4 1a–d** derivatives. As previously observed in preceding studies,[14,15] no traces of Pcs with two adjacent B units were observed, due to the presence of rigid phenyl groups in the 3,6-positions of the corresponding phthalonitrile

that hampers its self-condensation. All ABAB and A_3B derivatives were easily isolated by chromatographic means, in yields ranging from 2% to 9% for the ABAB series, and from 5% to 12% for the A_3B Zn(II)Pcs. In contrast, A_4-type compounds could not be isolated in appropriate quantities and purities, mainly due to their low solubility and their manifest aggregation tendency, with the exception of **A_4 1c**, which was isolated and characterized. For that reason, only **A_4 1c** and the commercially available **A_4 1a** (that is, non-functionalized Zn(II)Pc) could be included in the photophysical study. Apart from the rather insoluble unsubstituted **A_4 1a**, the rest of the synthesized Zn(II)Pcs have in common good solubility features. This fact, together with the high symmetry exhibited by all the derivatives, results in extremely well-resolved ^1H and ^{13}C NMR spectra, which is infrequent for Zn(II)Pcs. As an example, the ^1H NMR spectra of compounds **ABAB 1d** and **A_3B 1a** are shown in Figure 1. 1. The good resolution observed in the spectrum of **A_3B 1a** points out the ability of the bis(trifluoromethyl)phenyl moieties to hamper aggregation in solution, even if only one isoindole is functionalized with bulky groups.

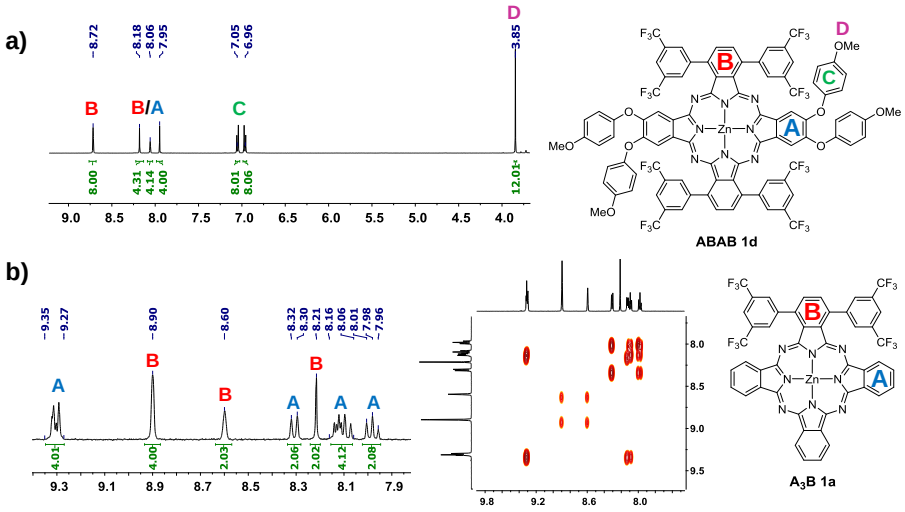

*Figure 1. 1. a) ^1H-NMR (500 MHz, THF-d_8) of **ABAB 1d**. b) ^1H-NMR and COSY (500 MHz, THF-d_8) of **A_3B 1a.***

Geometry optimization of **ABAB 1a** and **A_3B 1a** structures performed with SCIGRESS (FJ 2.8.1 EU 3.3.1) well-illustrates how bis(trifluoromethyl)phenyl substituents hamper the stacking of the Zn(II)Pc macrocycles (Figure 1. 2).

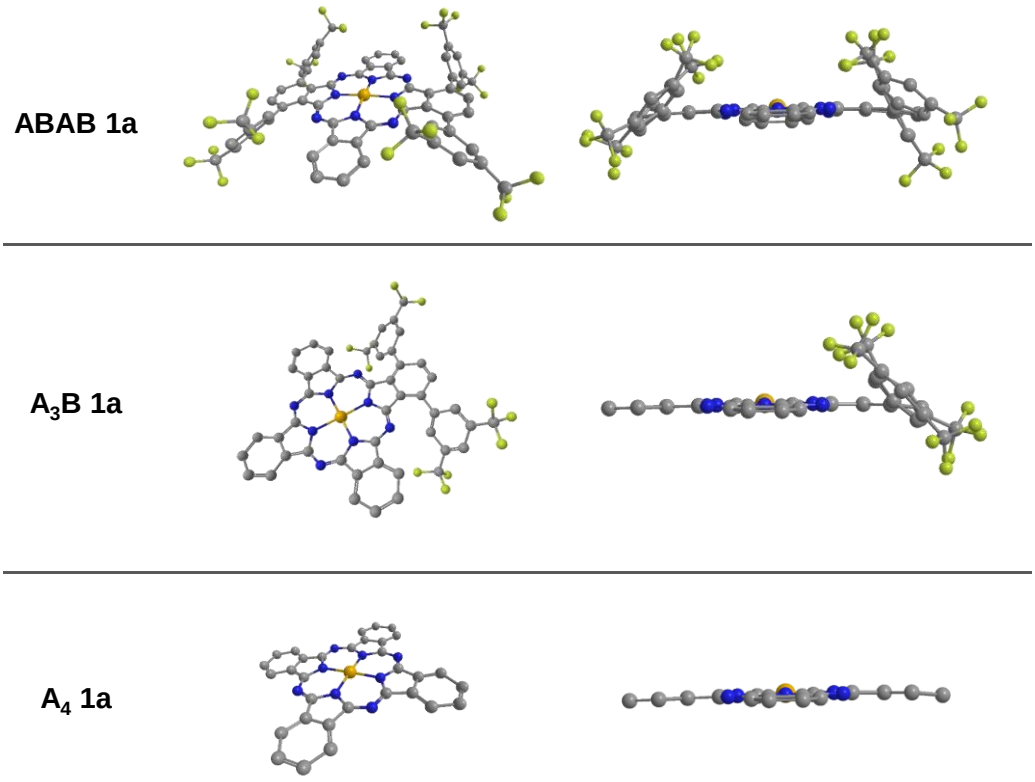

*Figure 1. 2. Geometry optimization of Zn(II)Pcs **1a** with SCIGRESS (FJ 2.8.1 EU 3.3.1) MM2 geometry optimization.*

b) Photophysical studies

First, ground-state absorption experiments were performed for all the Zn(II)Pcs, showing the typical *Q*-band and *B*-band transitions.[24] UV-vis absorption spectra were first recorded in THF, a solvent that is able to coordinate the Zn(II) metal centre, hampering the aggregation of Zn(II)Pcs independently of the substitution pattern. As an example to visualize the absorption changes along the ABAB, A_3B and A_4 series, the UV-vis spectra of all the members of the **1a** family in THF are depicted in Figure 1. 3.

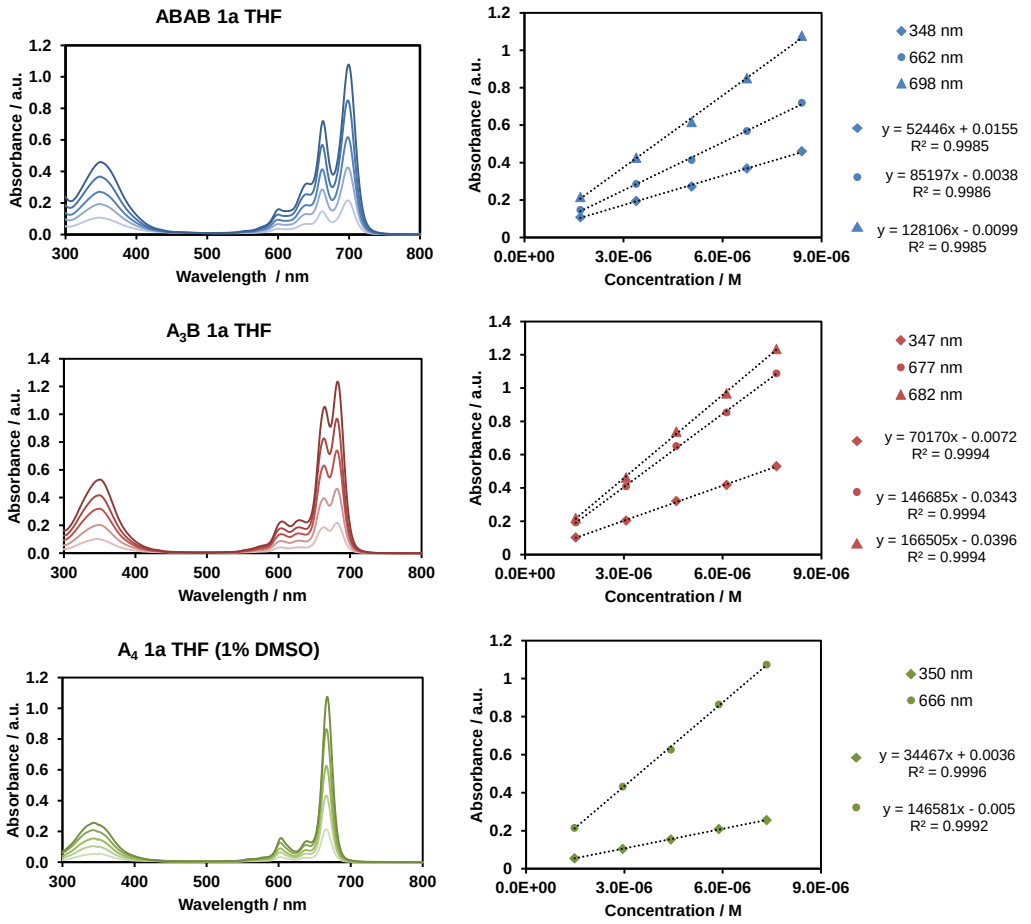

*Figure 1. 3. Concentration-dependent UV-vis experiments for Zn(II)Pcs **1a** in THF (between ~1·10^{-6} - 9·10^{-6} M).*

On the other hand, when the UV-vis experiments were performed in toluene, hints of aggregation were observed for **A_3B 1c** and **A_4 1c**, with *Q*-bands featuring shoulders at longer wavelengths. Aggregation in toluene solutions of these compounds was confirmed in concentration-dependent studies (Figure 1. 4). Importantly, in the case of non-functionalized Zn(II)Pc **A_4 1a**, the solutions in both THF and toluene had to be prepared from a stock solution in DMSO (1% final content), which also contributed to the disaggregation of the Pc.

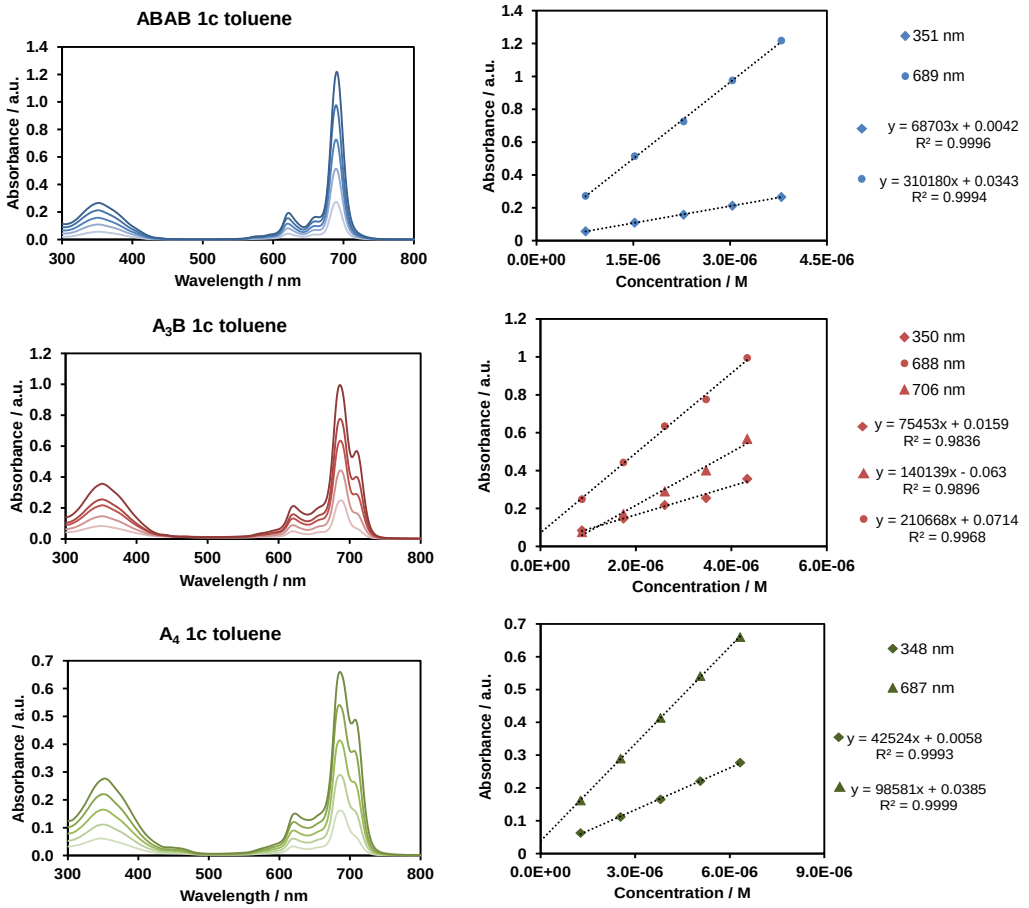

*Figure 1. 4. Concentration-dependent UV-vis experiments for Zn(II)Pcs **1c** in THF (between ~1·10^{-6} - 5·10^{-6} M).*

The ABAB and A_3B derivatives show split *Q*-bands both in toluene and THF, accompanied by the typical vibrational absorptions, although splitting is much more pronounced in **ABAB 1a**, which is consistent with its D_{2h} symmetry. Increasing the number of α-bis (trifluoromethyl)phenyl substituents produces a red-shift of the *Q*-band maximum, namely, from 666 nm for **A_4 1a** to 698 nm for **ABAB 1a** in THF solutions (Table 1. 1). The other three families (**1b–d**), with different types of substituents in the A isoindole units, showed similar behaviour when the different members of each family are compared, with the exception of the **1c** series, which show a single *Q*-band in THF for the three ABAB, A_3B and A_4 members.

*Table 1. 1. Photophysical properties of Zn(II)Pcs **1a-d** in THF solution. Estimated uncertainties in the quantum yields are ±10%.*

ZnPc	logε (λ)	λ_f / nm	ϕ_f	τ_S / ns	τ_T / μs[a]	ϕ_Δ
ABAB 1a	4.72 (348), 4.93 (662), 5.11 (698)[b]	705	0.05	1.7	0.32	~1
A_3B 1a	4.85 (347), 5.17 (677), 5.22 (682)[b]	686	0.11	2.5	0.18	0.92
A_4 1a[c]	4.54 (350), 5.17 (666)[b]	669	0.17	3.4	0.28	0.79
ABAB 1b	4.73 (349), 5.03 (676), 5.16 (712)[b]	717	0.06	2.1	0.13	0.74
A_3B 1b	4.73 (359), 5.10 (698)[b]	711	0.08	2.4	0.46	0.74
ABAB 1c	4.90 (350), 5.50 (687)[b]	693	0.08	3.0	0.23	0.80
A_3B 1c	4.87 (348), 5.46 (684)[b]	691	0.12	3.1	0.22	0.78
A_4 1c	4.49 (350), 5.05 (682)[b]	687	0.09	3.2	0.25	0.73
ABAB 1d	4.80 (358), 5.13 (671)[b], 5.15 (704)	711	0.06	1.8	0.27	0.86
A_3B1d	4.82 (358), 5.08 (674)[b], 5.15 (693)	695	0.09	2.1	0.17	0.84

[a] In air-saturated solutions. [b] Q-band maximum. [c] Prepared from a stock solution of the ZnPc in DMSO (Final content: 1% DMSO).

*Table 1. 2. Photophysical properties of Zn(II)Pcs **1a-d** in toluene solution. Estimated uncertainties in the quantum yields are ±10%.*

ZnPc	logε (λ)	λ_f / nm	ϕ_f	τ_S / ns	τ_T / μs[a]	ϕ_Δ
ABAB 1a	4.54 (350), 4.75 (664), 5.00 (705)[b]	709	0.13	1.8	0.12	0.76
A_3B 1a	4.86 (349), 5.22 (664), 5.30 (687)[b]	690	0.23	2.1	0.27	0.69
A_4 1a[c]	4.53 (340), 5.22 (669)[b]	673	0.53	2.4	0.21	0.66
ABAB 1b	4.81 (359), 5.11 (682), 5.28 (707)[b]	711	0.24	2.3	0.22	0.65
A_3B 1b	4.71 (365), 5.29 (698)[b]	706	0.23	2.6	0.30	0.65
ABAB 1c	4.84 (351), 5.49 (689)[b]	695	0.16	3.0	0.22	0.69
A_3B 1c	aggregation	693	0.29	3.2	0.20	0.62
A_4 1c	aggregation	691	0.20	3.2	0.20	0.49
ABAB 1d	4.99 (349), 5.37 (673), 5.39 (712)[b]	716	0.11	1.7	0.30	0.62
A_3B1d	4.89 (349), 5.28 (676)[b], 5.28 (695)	699	0.20	2.0	0.20	0.57

[a] In air-saturated solutions. [b] Q-band maximum. [c] Prepared from a stock solution of the ZnPc in DMSO (Final content: 1% DMSO).

The spectra of the ABAB and A_3B members of the four series of Zn(II)Pcs **1a–d** are superimposed in Figure 1. 5. In both the ABAB and the A_3B series, Zn(II)Pcs **1d** with facing *N*-functionalized phthalimides display the largest red shift.

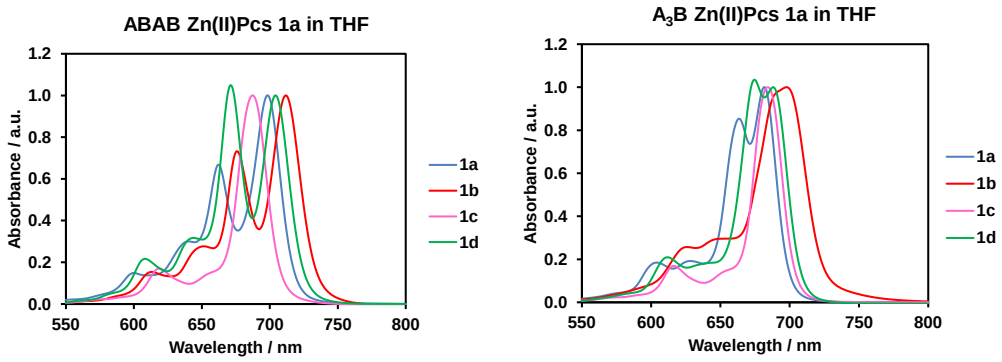

*Figure 1. 5. UV-vis spectra for **ABAB 1a-d** and **A$_3$B 1a-d** in THF (Q-band normalized).*

From this initial comparison, a first conclusion arises regarding the merits of these compounds as PS. In principle, the red-shifted absorption of ABAB Zn(II)Pcs is an advantage for photodynamic therapy, which, together with their wider range of absorption wavelengths (i.e. covering approximately 190 nm, while only 140 nm for A_4 derivatives), render ABAB compounds more outstanding than their counterparts.

The lack of aggregation in THF and toluene solutions for most of these Zn(II)Pcs was proven by the absorption studies performed in a range of concentrations as in Figure 1. 3 and Figure 1. 4. For the verification of the Lambert–Beer law, an analysis of linear regression between the intensity of the *Q*-band and the concentration of the Zn(II)Pcs was performed. Under the conditions of our concentration-dependent studies, only **A$_3$B 1c** and **A$_4$ 1c** showed aggregation evidence in toluene solutions (namely, the linear fitting in this solvent does not pass through the origin of coordinates, see Figure 1. 4) thus confirming our previous assumption. Further demonstration was achieved upon the addition of 1% THF over the solutions of the two compounds in toluene. The spectra recorded in the presence of the coordinative solvent showed relevant changes in the form of a single *Q*-band with no traces of the red–shifted shoulder (Figure 1. 6a). Also in ^{1}H NMR experiments, the addition of 1% THF-d_6 over a toluene-d_8 solution improves the resolution of the aromatic signals (Figure 1. 6b). The fact that **A$_3$B 1c** is the only compound of the A_3B series displaying aggregation, can be rationalized on the basis of the presence of ester functions, which can coordinate the Zn(II) centre of a vicinal Zn(II)Pc to give *J*-type aggregates (Figure 1. 6c).[5]

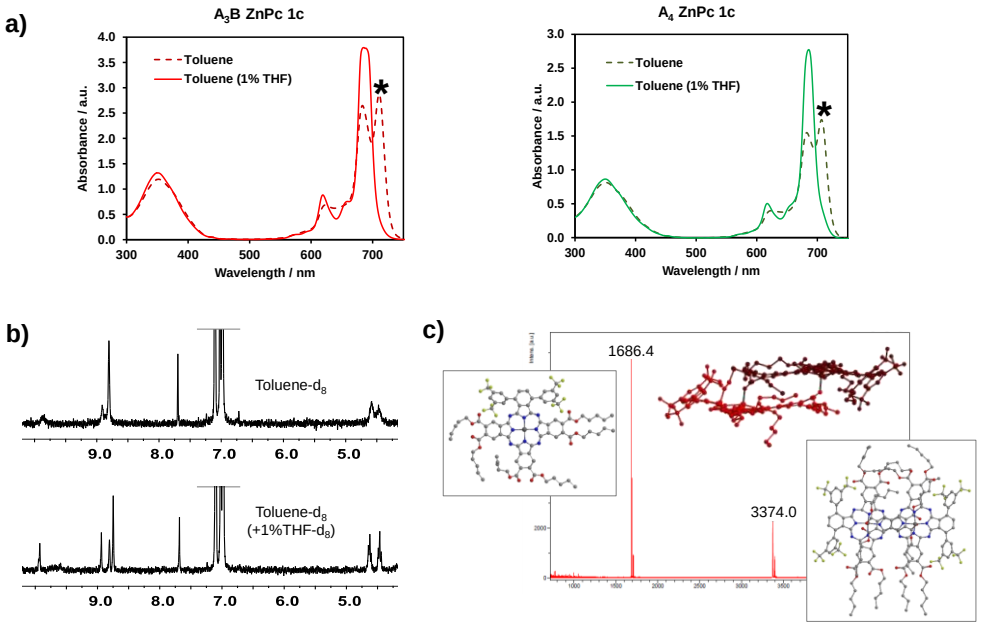

*Figure 1. 6. a) Qualitative UV-Vis spectra of **A_3B** and **A_4 1c** in toluene at ~$2 \cdot 10^{-5}$ M, before and after addition of 1% THF. Please, notice the disappearance of aggregation bands (*) and Q-bands recovery. b) MS (MALDI) of **A_3B 1c** with identified peaks for monomer and dimer modelized with SCIGRESS (FJ 2.8.1 EU 3.3.1) MM2 geometry optimization; c) ^{1}H NMR in toluene-d_8 of **A_3B 1c**, before and after 1% THF-d_8 addition for disaggregation.*

Fluorescence experiments (Figure 1. 7a) are in line with absorption assays: a shift to longer wavelengths takes place when increasing the number of bis(trifluoromethyl)phenyl units over the Pc core. In contrast, fluorescence quantum yields (ϕ_f) increase in the opposite direction, (i.e. ϕ_f: A_4 > A_3B > ABAB derivatives) (see Table 1. 1, Table 1. 2 and Figure 1. 8).

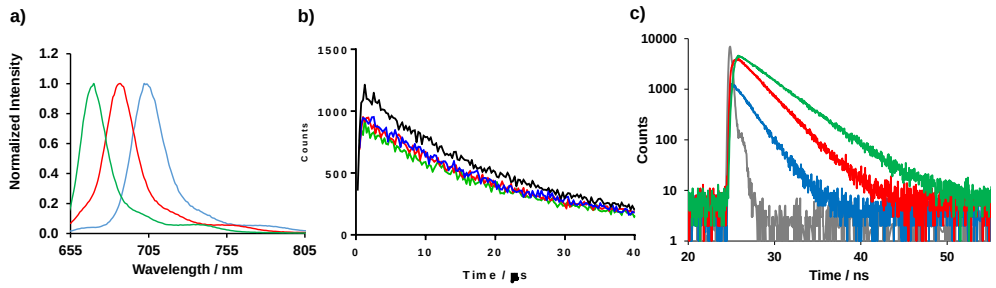

*Figure 1. 7. a) Fluorescence spectra of Zn(II)Pcs **1a**; b) $^1O_2$ production of Zn(II)Pcs **1c** against phenalenone (black line) and c) time resolved fluorescence for Zn(II)Pcs **1a** with IRF (Instrument response fluorescence, LUDOX®, grey line);for ABAB (blue lines), A_3B (red lines) and A_4 (green lines) Zn(II)Pcs in THF.*

Also, the quantification of the ϕ_Δ was performed for these series of compounds, by direct observation of the $^1O_2$ phosphorescence at 1275 nm after excitation at 355 nm, both in THF and toluene solutions (see Table 1. 1, Table 1. 2 and Figure 1. 7b). Regardless of the solvent, the same trend was observed for the four families of compounds, namely, an increase of the ϕ_Δ takes place when adding bis(trifluoromethyl)phenyl units to the Zn(II)Pc core (i.e. A_4- < A_3B- < ABAB-derivatives) concomitantly with a ϕ_f decrease, as depicted in Figure 1. 8 for the **ABAB 1a**, **A_3B 1a** and **A_4 1a** series. Also, time resolved fluorescence decays pointed in the same direction, showing singlet excited-state lifetimes decreasing from A_4 to ABAB Zn(II)Pcs. These observations support our previous hypothesis that pointed to the alpha-substitution with these fluorinated aromatic groups as the driving force that pushes up $^1O_2$ generation abilities of Zn(II)Pcs.

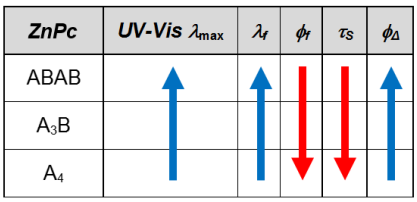

*Figure 1. 8. Trends observed in the photophysical properties for each family of Zn(II)Pcs **1a-d**.*

On the other hand, the impact of the substitution in the A isoindole on the photosensitization abilities of the Zn(II)Pc has been also analyzed. The first remark concerns the very high ϕ_Δ values observed in the **1a** series, lacking functionalization in the A isoindole, especially that of **ABAB 1a**, which is very close to 1 in THF (Table 1. 1). Beyond this remarkable value, when one compares the other three substituted ABAB derivatives, ϕ_Δ values in THF are all between 0.86 and 0.74, which are still far above average. In THF, the ϕ_Δ of the ABAB series follows the trend **1a** > **1d** > **1c** > **1b**. However, in toluene solutions (Table 1. 2), all the ϕ_Δ values of the ABAB Zn(II)Pcs decrease in comparison with those in THF, and vary in the **1a** > **1c** > **1b** > **1d** direction, ranging from 0.76 for **ABAB 1a** to 0.62 for **ABAB 1d**. These results point to a minor impact of the substitution at the A isoindole on the photophysical properties of the analysed Zn(II)Pc derivatives.

1.4. Conclusions

The study of a number of Zn(II)Pcs with an iterating substitution pattern, that is, a varying number of B isoindoles containing bis(trifluoromethyl)phenyl substituents (i.e. **ABAB**, **A_3B** and **A_4 1** series), and with different functionalization in the A isoindole (i.e. **1a–d** series), has allowed us to ascertain the determinant role of the bulky, fluorinated substituents in the photophysical properties and $^1O_2$ generation capabilities of these compounds. For all the **1a–d** series, the ABAB substitution provides the Zn(II)Pcs with

the most red-shifted absorptions and non-aggregating features that are independent of the solvent employed, as well as the highest $^1O_2$ quantum yields. These are outstanding characteristics, not easy to gather in Zn(II)Pcs, and that are all fundamental for using them as PS in therapeutic applications. Remarkable data found in these studies are the ϕ_Δ close to 1 obtained for compound **ABAB 1a**, with no functionalization at the A isoindoles, which evidences the relevant function of bis(trifluoromethyl)phenyl moieties on the $^1O_2$ production. On the other hand, adding substituents at the A isoindole produces a slightly detrimental effect on the ϕ_Δ, although the values are still very high, above the average of the figures of merit reported for Zn(II)Pc PS. We did not find a clear relationship between the electronic character of the substituents at the A isoindole and the $^1O_2$ production, since the trends change with the solvent employed. However, **ABAB 1d** is, with its ϕ_Δ of 0.86 in polar THF, a candidate of choice for further derivatization of the four phenolic positions with hydrophilic substituents in the search for efficient PS, considering also that **ABAB 1d** is the compound of the ABAB series that was isolated in better chemical yield. Therefore, our rational study will allow us to develop efficient ABAB Zn(II)Pc derivatives with balanced hydrophilicity and lipophilicity, in the search of non-aggregated chromophores, soluble in water media and with high ϕ_Δ, which can find application in PDT.

1.5. Experimental section

a) Synthesis

Chemicals were purchased from commercial suppliers and used without further purification unless stated otherwise. 3,3″,5,5″-tetrakis(trifluoromethyl)-[1,1′:4′,1″-terphenyl]-2′,3′- dicarbonitrile (**2**),[14] 2-(but-2-yn-1-yl)-1,3-dioxoisoindoline-5,6-dicarbonitrile (**3b**), [detailed in **Chapter 2** for the sake of consistency] dipentyl 4,5-dicyanophthalate (**3c**),[25] 4,5-bis(4-methoxyphenoxy)phthalonitrile (**3d**),[26] and **A_4 1c**,[27] have been prepared according to published procedures. ^{13}C NMR spectra for A_3B-Zn(II)Pcs are not detailed due to the great complexity and high number of overlapped signals.

General procedure for the synthesis of Zn(II)Pcs 1a–d:

2 (0.27 mmol, 150 mg), phthalonitrile **3a–d** (0.27 mmol) and anhydrous $Zn(AcO)_2$ (0.27 mmol, 50 mg) were placed in a 5 mL high pressure resistant flask equipped with a magnetic stirrer, and then 2.7 mL ([**2**] = 0.1 M) of dry *o*-dichlorobenzene/DMF (dried over 4 Å molecular sieves) 2:1 were added. The mixture was heated to 150–160 °C overnight under an argon atmosphere. After cooling, the solvent was removed under vacuum. The mixture of products was purified by column chromatography on SiO_2.

i. *Synthesis of Zn(II)Pcs **1a**:*

Column chromatography on SiO_2 (dioxane/heptane in gradient from 1:4 to 1:2) was performed. The first fraction to elute contained the desired product ABAB, followed by compound A_3B. Non-functionalized Zn(II)Pc (**A_4 1a**) is commercially available.

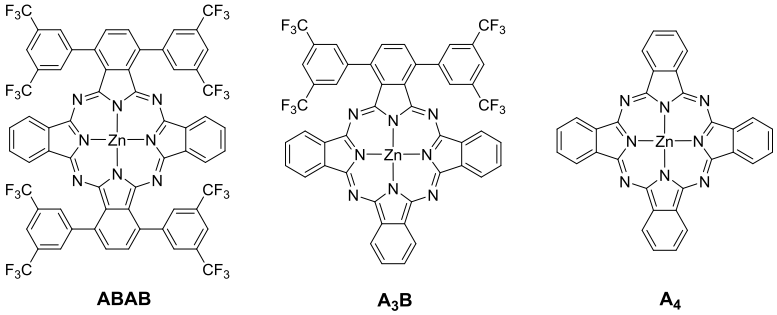

ABAB 1a. The product was further purified by additional column chromatography on Bio-Beads using $CHCl_3$ as the eluent. After evaporation of the solvent, a blue solid was obtained, which was washed with MeOH. Yield: 15.2 mg, (8%). ^{1}H NMR (500 MHz, acetone-d_6): δ 8.00 (br s, 4H, HAr), 8.28 (br s, 4H, HAr), 8.35 (s, 4H, HAr), 8.62 (s, 4H, HAr), 8.89 (s, 4H, HAr); ^{13}C NMR (125 MHz, acetone-d_6): δ 122.7 (C Ar), 123.2 (C Ar), 125.0 (q, J = 275.5 Hz, CF_3), 130.2 (C Ar), 132.0 (br s, C*CF_3), 132.3 (C Ar), 132.7 (C Ar), 136.3 (CH Ar), 137.7 (CH Ar), 139.3 (CH Ar), 144.2 (CH Ar), 153.4 (C=N), 154.4 (C=N); IR (ATR) v^{-1} (cm^{-1}): 1374, 1273, 1167, 1123, 896, 838; HR-MS (MALDI ULTRAFLEX, matrix DCTB + PPG 1000 + 2000): *m/z* 1424.1019 (calculated for $C_{64}H_{24}F_{24}N_8Zn$: 1424.1027).

A_3B 1a. The product was further purified by additional column chromatography on Bio-Beads using THF as the eluent. After evaporation of the solvent a blue solid was obtained, which was washed with MeOH. Yield: 10.1 mg, (11%). ^{1}H NMR (500 MHz, THF-d_8): δ 7.95–8.02 (m, 2H, HAr), 8.06–8.16 (m, 4H, HAr), 8.21 (s, 2H, HAr), 8.31 (d, J = 7.37 Hz, 2H, HAr), 8.60 (s, 2H, HAr), 8.90 (s, 4H, HAr), 9.27–9.35 (m, 4H, HAr); IR (ATR) v^{-1} (cm^{-1}): 1376, 1332, 1271, 1119, 893, 830; HR-MS (MALDI ULTRAFLEX III, matrix DCTB + PPG 1000): *m/z* 1000.0900 (calculated for $C_{48}H_{20}F_{12}N_8Zn$: 1000.0905).

A_4 1a. Comercially available.

ii. *Synthesis of Zn(II)Pcs **1b**:*

Column chromatography on SiO_2 (THF/heptane in gradient from 2:1 to 1:1) was performed. The first fraction to elute contained the desired product ABAB followed by compounds A_3B and A_4.

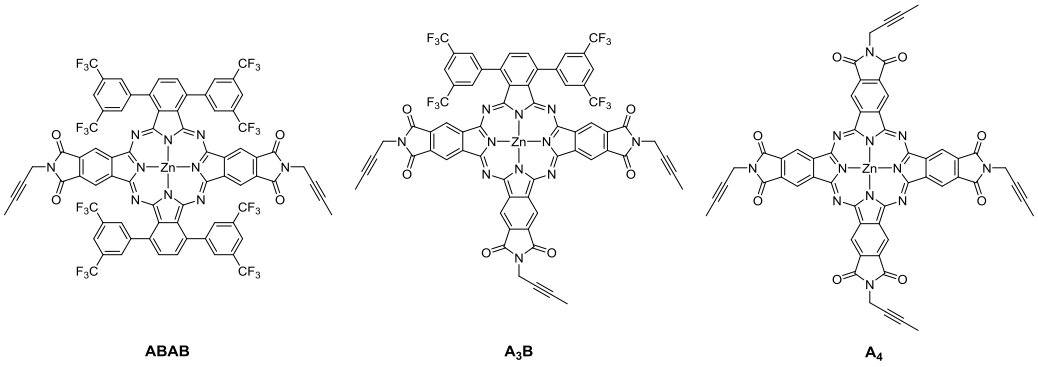

ABAB 1b. The product was further purified by an additional column chromatography on Bio-Beads using $CHCl_3$ as eluent. After evaporation of the solvent a blue solid was obtained, which was washed with heptane. Yield: 5.6 mg, (2%). ^{1}H NMR (300 MHz, THF-d_8): δ 8.81 (s, 8H, Ar), 8.73 (s, 4H, Ar), 8.56 (s, 4H, Ar), 8.38 (s, 4H, Ar), 4.49 (s, 4H, CH_2), 1.84 (s, 6H, CH_3); ^{13}C NMR (75 MHz, THF-d_8): δ 3.2 (CH_2), 28.2 (CH_3), 74.1 (C≡C), 79.2 (C≡C), 118.3 (C Ar), 125.0 (q, *J* = 270. 8 Hz, CF_3), 131. (br s, C*CF_3), 132.5 (C Ar), 133.0 (C Ar), 133.0 (C Ar), 134.0 (C Ar), 136.8 (CH Ar), 138.4 (CH Ar), 142.7 (CH Ar), 143.8 (CH Ar), 153.6 (C=N), 155.1 (C=N), 166.8 (C=O); IR(ATR) v^{-1} (cm^{-1}): 2359, 1771, 1708, 1384, 1384, 1277, 1178, 1136; HR-MS (MALDI, matrix DCTB + PPGNa 2000): *m/z* 1666.1343 [M^+] (calculated: 1666.1354).

A_3B 1b. The product was further purified by additional column chromatography on Bio-Beads using $CHCl_3$ as the eluent. After evaporation of the solvent a blue-green solid was obtained, which was washed with heptane. Yield: 6.3 mg, (5%). ^{1}H NMR (300 MHz, DMSO-d_6): δ 1.86–2.06 (m, 9H, CH_3), 4.58–4.83 (m, 6H, CH_2), 8.21–8.66 (m, 6H, CHAr), 8.79 (br s, 4H, CHAr), 8.87–9.32 (m, 4H, CHAr); IR (ATR) v^{-1} (cm^{-1}): 2914, 2845, 2301, 1769, 1717, 1421, 1379, 1341, 1211, 1165, 1126; HR-MS (MALDI ULTRAFLEX III, matrix DCTB + PPGNa 1000 + PPGNa 2000): *m/z* 1363.1356 (calculated for $C_{66}H_{29}F_{12}N_{11}O_6Zn$: 1363.1397).

A_4 1b. MS (MALDI, matrix DCTB): *m/z* 1060.3 (calculated for $C_{56}H_{28}N_{12}O_8Zn$: 1060.1).

iii. *Synthesis of Zn(II)Pcs **1c**:*

Column chromatography on SiO_2 (THF/heptane in gradient from 1:4 to 1:1). The first fraction to elute contained the desired product ABAB followed by compounds A_3B and A_4.

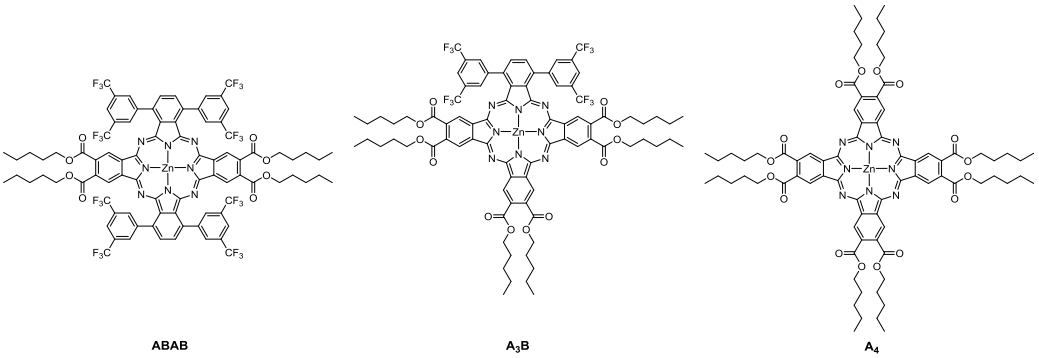

ABAB 1c. The product was further purified by an additional column chromatography on Bio-Beads using $CHCl_3$ as eluent. After evaporation of the solvent a blue solid was obtained, which was washed with MeOH. Yield: 13.5 mg, (5%). ^{1}H NMR (500 MHz, THF-d_8): δ 8.79 (s, 8H, Ar); 8.57 (s, 4H, Ar); 8.52 (s, 4H, Ar); 8.31 (s, 4H, Ar); 4.56 (t, 8H, J = 6.99 Hz, CH_2); 1.92-1.98 (m, 8H, CH_2); 1.46-1.58 (m, 16H, CH_2), 1.02 (t, 12H, J = 7.04 Hz, CH_3); ^{13}C NMR (125 MHz, THF-d_8): δ 14.4 (CH_3), 23.4(CH_2), 29.2(CH_2), 29.5(CH_2), 66.7 (COOC*H_2), 124.3 (C Ar), 125.0 (q, *J* = 272.7 Hz, CF_3), 131.9 (br s, C*CF_3), 132.6 (C Ar), 132.7 (C Ar),134.6 (C Ar), 136.7 (CH Ar), 138.2 (CH Ar), 140.0 (CH Ar), 143.9 (CH Ar), 153.5 (C=N), 154.5 (C=N), 167.9 (C=O); IR(ATR) v^{-1} (cm^{-1}): 1716, 1380, 1277, 1217, 1176, 1134, 1092 ; HR-MS (MALDI, matrix DCTB + PPGNa 2100): *m/z* 1903.3676 $[M+Na]^+$ (calculated: 1903.3648).

A_3B 1c. The product was further purified by additional column chromatography on Bio-Beads using $CHCl_3$ as the eluent. After evaporation of the solvent a blue solid was obtained, which was washed with MeOH. Yield: 18.5 mg, (12%). ^{1}H NMR (300 MHz, acetone-d_6): δ 0.97–1.17 (m, 18H, CH_3), 1.47–1.71 (m, 24H, CH_2), 2.67–2.87 (m, 12H, CH_2), 4.47–4.73 (m, 12H, CH_2), 8.40 (s, 2H, CHAr), 8.50 (s, 2H, CHAr), 8.63 (s, 2H, CHAr), 8.97 (s, 4H, CHAr), 9.38 (s, 2H, CHAr), 9.49 (s, 2H, CHAr); IR (ATR) v^{-1} (cm^{-1}): 2954, 2928, 2858, 1718, 1464, 1377, 1334, 1263, 1172, 1127, 1091; HR-MS (MALDI ULTRAFLEX III, matrix DCTB + PPG 1000 + 2000): *m/z* 1684.5043 (calculated for $C_{84}H_{80}F_{12}N_8O_{12}Zn$: 1684.4990).

A_4B 1c. Previously reported and characterized.[27]

iv. *Synthesis of Zn(II)Pcs **1d**:*

Column chromatography on SiO_2 (heptane/EtOAc 1:1 as the eluent) was performed. The first fraction to elute contained the desired product ABAB, followed by compounds A_3B and A_4.

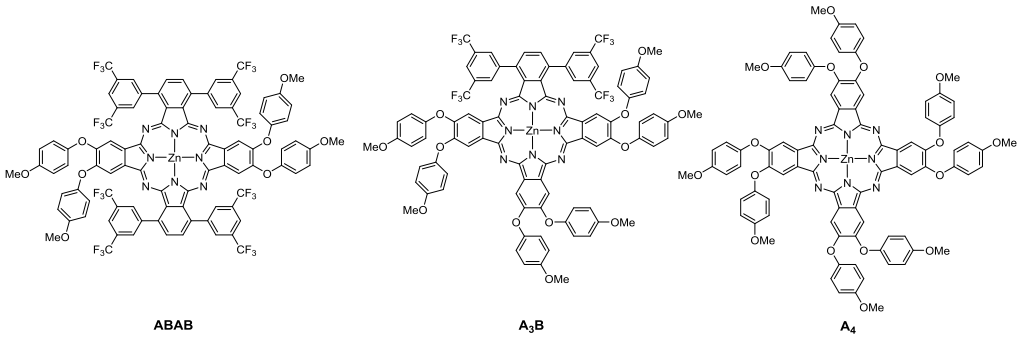

ABAB 1d. The product was further purified by additional column chromatography on Bio-Beads using $CHCl_3$ as the eluent. After evaporation of the solvent a blue solid was obtained, which was washed with MeOH. Yield: 23 mg (9%). ^{1}H NMR (300 MHz, DMSO-d_6): δ 3.8 (s, 12H, OMe), 7.03 (d, *J* = 9.10 Hz, 8H, O–Ph–O), 7.12 (d, *J* = 9.10 Hz, 8H, O–Ph–O), 7.76 (s, 4H, CHAr), 7.99 (s, 4H, CHAr), 8.25 (s, 4H, CHAr), 8.78 (s, 8H, CHAr); ^{1}H NMR (500 MHz, THF-d_8): δ 3.8 (s, 12H, OMe), 6.96 (d, *J* = 9.18 Hz, 8H, O–Ph–O), 7.05 (d, *J* = 9.18 Hz, 8H, O–Ph–O), 7.95 (s, 4H, CHAr), 8.06 (s, 4H, CHAr), 8.18 (s, 4H, CHAr), 8.72 (s, 8H, CHAr); ^{13}C NMR (125 MHz, THF-d_8): δ 55.7 (CH_3), 115.5 (CHAr PhOMe), 115.7 (CHAr), 119.4 (CHAr PhOMe), 122.4 (C Ar), 126.8 (q, *J* = 273.6 Hz, CF_3), 131.9 (br s, C*CF_3), 132.0 (C Ar), 132.2 (C Ar), 132.6 (C Ar), 135.6 (CH Ar), 136.2 (CH Ar), 137.9 (CH Ar), 144.0, 152.3, 152.9, 153.3, 154.0, 156.9 (C Ar); IR (ATR) v^{-1} (cm^{-1}): 2925, 1502, 1410, 1376, 1276, 1198, 1177, 1133; HR-MS (MALDI ULTRAFLEX III, matrix: DCTB): *m/z* 1912.2488 (calculated for $C_{92}H_{48}F_{24}N_8O_8Zn$: 1912.2498).

A_3B 1d. The product was further purified by additional column chromatography on Bio-Beads using $CHCl_3$ as the eluent. After evaporation of the solvent a blue solid was obtained, which was washed with MeOH. Yield: 9.4 mg (6%). ^{1}H NMR (300 MHz, DMSO-d_6): δ 3.81 (s, 6H, OMe), 3.82 (s, 6H, OMe), 3.83 (s, 6H, OMe), 6.97–7.08 (m, 8H, O–Ph–O), 7.10–7.17 (m, 8H, O–Ph–O), 7.17–7.28 (m, 8H, O–Ph–O), 7.77 (s, 2H, CHAr), 8.00 (s, 2H, CHAr), 8.22 (s, 2H, CHAr), 8.54 (s, 2H, CHAr), 8.59 (s, 2H, CHAr), 8.78 (s, 4H, CHAr); IR (ATR) v^{-1} (cm^{-1}): 2954, 2883, 1723, 1507, 1449, 1362, 1279, 1182, 1134, 1034; HR-MS (MALDI ULTRAFLEX III, matrix: DCTB): *m/z* 1732.3115 (calculated for $C_{90}H_{56}F_{12}N_8O_{12}Zn$: 1732.3112).

A_4 1d. HR-MS (MALDI ULTRAFLEX III, matrix DCTB + PEGNa 1500): *m/z* 1552.3741 (calculated for $C_{88}H_{64}N_8O_{16}Zn$: 1552.3726).

b) Photophysical studies

i. *Fluorescence spectra:*

The samples were excited at: **ABAB** (THF), 690 (**1a**), 692 (**1b**), 677 (**1c**) and 694 nm (**1d**); **ABAB** (toluene), 690 (**1a**), 687 (**1b**), 679 (**1c**) and 700 nm (**1d**); **A_3B** (THF), 662 (**1a**), 678 (**1b**), 674 (**1c**) and 685 nm (**1d**); **A_3B** (toluene), 667 (**1a**), 678 (**1b**), 674 (**1c**) and 687 nm (**1d**); **A_4** (THF), 672 nm (**1c**); **A_4** (toluene), 677 nm (**1c**).

ii. *Fluorescence Quantum Yields:*

The samples were excited at: ABAB (THF), 638 (**1a**), 636 (**1b**), 630 (**1c**) and 632 nm (**1d**); ABAB (toluene), 644 (**1a**), 611 (**1b**), 632.5 (**1c**) and 634 nm (**1d**); A_3B (THF), 632 (**1a**), 635 (**1b**), 630.5 (**1c**) and 636 nm (**1d**); A_3B (toluene), 636 (**1a**), 634.5 (**1b**), 627.5 (**1c**) and 632 nm (**1d**); A_4 (THF), 631.5 nm (**1c**); A_4 (toluene), 629.5 nm (**1c**).

1.6. References

(1) Roznyatovskiy, V. V; Lee, C.-H.; Sessler, J. L. π-Extended Isomeric and Expanded Porphyrins. *Chem. Soc. Rev.* **2013**, *42* (5), 1921–1933.

(2) Lu, H.; Kobayashi, N. Optically Active Porphyrin and Phthalocyanine Systems. *Chem. Rev.* **2016**, *116* (10), 6184–6261.

(3) Basova, T.; Hassan, A.; Durmuſ, M.; Gürek, A. G.; Ahsen, V. Liquid Crystalline Metal Phthalocyanines: Structural Organization on the Substrate Surface. *Coord. Chem. Rev.* **2016**, *310*, 131–153.

(4) Almeida-Marrero, V.; van de Winckel, E.; Anaya-Plaza, E.; Torres, T.; de la Escosura, A. Porphyrinoid Biohybrid Materials as an Emerging Toolbox for Biomedical Light Management. *Chem. Soc. Rev.* **2018**, *47* (19), 7369–7400.

(5) Zhang, X. F.; Xi, Q.; Zhao, J. Fluorescent and Triplet State Photoactive J-Type Phthalocyanine Nano Assemblies: Controlled Formation and Photosensitizing Properties. *J. Mater. Chem.* **2010**, *20* (32), 6726–6733.

(6) van de Winckel, E.; David, B.; Simoni, M. M.; González-Delgado, J. A.; de la Escosura, A.; Cunha, Â.; Torres, T. Octacationic and Axially Di-Substituted Silicon (IV) Phthalocyanines for Photodynamic Inactivation of Bacteria. *Dye. Pigment.* **2017**, *145*, 239–245.

(7) Li, Y.; Wang, J.; Zhang, X.; Guo, W.; Li, F.; Yu, M.; Kong, X.; Wu, W.; Hong, Z. Highly Water-Soluble and Tumor-Targeted Photosensitizers for Photodynamic Therapy. *Org. Biomol. Chem.* **2015**, *13* (28), 7681–7694.

(8) Koç, V.; Topal, S. Z.; Aydın Tekdaş, D.; Ateş, Ö. D.; Önal, E.; Dumoulin, F.; Gürek, A. G.; Ahsen, V. Assessment of the Relevance of GaPc Substituted with Azido-Polyethylene Glycol Chains for Photodynamic Therapy. Design, Synthetic Strategy, Fluorescence, Singlet Oxygen Generation, and PH-Dependent Spectroscopic Behaviour. *New J. Chem.* **2017**, *41* (18), 10027–10036.

(9) Bispo, M.; Pereira, P. M. R.; Setaro, F.; Rodríguez-Morgade, M. S.; Fernandes, R.; Torres, T.; Tomé, J. P. C. A Galactose Dendritic Silicon (IV) Phthalocyanine as a Photosensitizing Agent in Cancer Photodynamic Therapy. *Chempluschem* **2018**, *83* (9), 855–860.

(10) van de Winckel, E.; Schneider, R. J.; de la Escosura, A.; Torres, T. Multifunctional Logic in a Photosensitizer with Triple-Mode Fluorescent and Photodynamic Activity. *Chem. – A Eur. J.* **2015**, *21*, 18551–18556.

(11) Ferreira, J. T.; Pina, J.; Ribeiro, C. A. F.; Fernandes, R.; Tomé, J. P. C.; Rodríguez-Morgade, M. S.; Torres, T. Synthesis, Characterization and In Vitro Evaluation of Carbohydrate-Containing Ruthenium Phthalocyanines as Third Generation Photosensitizers for Photodynamic Therapy. *ChemPhotoChem* **2018**, *2* (7), 640–654.

(12) Teles Ferreira, J.; Pina, J.; Alberto Fontes Ribeiro, C.; Fernandes, R.; Tomé, J. P. C.; Rodríguez-Morgade, M. S.; Torres, T. PEG-Containing Ruthenium Phthalocyanines as Photosensitizers for Photodynamic Therapy: Synthesis, Characterization and in Vitro Evaluation. *J. Mater. Chem. B* **2017**, *5* (29), 5862–5869.

(13) Li, X.; Zheng, B.-D.; Peng, X.-H.; Li, S.-Z.; Ying, J.-W.; Zhao, Y.; Huang, J.-D.; Yoon, J. Phthalocyanines as Medicinal Photosensitizers: Developments in the Last Five Years. *Coord. Chem. Rev.* **2019**, *379*, 147–160.

(14) Fazio, E.; Jaramillo-García, J.; de La Torre, G.; Torres, T. Efficient Synthesis of ABAB Functionalized Phthalocyanines. *Org. Lett.* **2014**, *16* (18), 4706–4709.
(15) Fazio, E.; Nazeerudin, M. K.; de la Torre, G.; Medel, M.; Grätzel, M.; Jaramillo-García, J.; Urbani, M.; Torres, T. ABAB Phthalocyanines: Scaffolds for Building Unprecedented Donor-π-Acceptor Chromophores. *ChemistryOpen* **2016**, *6* (1), 121–127.
(16) Erdoğmuş, A.; Nyokong, T. Novel, Soluble, FluXoro Functional Substituted Zinc Phthalocyanines; Synthesis, Characterization and Photophysicochemical Properties. *Dye. Pigment.* **2010**, *86* (2), 174–181.
(17) Pucelik, B.; Gürol, I.; Ahsen, V.; Dumoulin, F.; Dąbrowski, J. M. Fluorination of Phthalocyanine Substituents: Improved Photoproperties and Enhanced Photodynamic Efficacy after Optimal Micellar Formulations. *Eur. J. Med. Chem.* **2016**, *124*, 284–298.
(18) Oda, K.; Ogura, S.; Okura, I. Preparation of a Water-Soluble Fluorinated Zinc Phthalocyanine and Its Effect for Photodynamic Therapy. *J. Photochem. Photobiol. B Biol.* **2000**, *59* (1), 20–25.
(19) Erdoğmuş, A.; Arıcı, M. Novel Soluble Octa-Substituted Phthalocyanines Bearing Chloro and Long Alkyl Chain Containing Fluorine: Synthesis, Characterization and Photophysical and Photochemical Properties. *J. Fluor. Chem.* **2014**, *166*, 127–133.
(20) Erdoğmuş, A.; Moeno, S.; Litwinski, C.; Nyokong, T. Photophysical Properties of Newly Synthesized Fluorinated Zinc Phthalocyanines in the Presence of CdTe Quantum Dots and the Accompanying Energy Transfer Processes. *J. Photochem. Photobiol. A Chem.* **2010**, *210* (2), 200–208.
(21) Ongarora, B. G.; Hu, X.; Li, H.; Fronczek, F. R.; Vicente, M. G. H. Syntheses and Properties of Trimethylaminophenoxy-Substituted Zn(Ii)-Phthalocyanines. *Medchemcomm* **2012**, *3* (2), 179–194.
(22) Bhupathiraju, N. V. S. D. K.; Rizvi, W.; Batteas, J. D.; Drain, C. M. Fluorinated Porphyrinoids as Efficient Platforms for New Photonic Materials, Sensors, and Therapeutics. *Org. Biomol. Chem.* **2016**, *14* (2), 389–408.
(23) Furuyama, T.; Miyaji, Y.; Maeda, K.; Maeda, H.; Segi, M. Extremely Photostable Electron-Deficient Phthalocyanines That Generate High Levels of Singlet Oxygen. *Chem. – A Eur. J.* **2019**, *25* (7), 1678–1682.
(24) Günsel, A.; Güzel, E.; Bilgiçli, A. T.; Atmaca, G. Y.; Erdoğmuş, A.; Yarasir, M. N. Synthesis and Investigation of Photophysicochemical Properties of Novel Ketone-Substituted Gallium (III) and Indium (III) Phthalocyanines with High Singlet Oxygen Yield for Photodynamic Therapy. *J. Lumin.* **2017**, *192*, 888–892.
(25) Tylleman, B.; Gómez-Aspe, R.; Gbabode, G.; Geerts, Y. H.; Sergeyev, S. Ester-Functionalized Phthalonitriles and Zinc Phthalocyanines via Palladium-Catalyzed Cyanation of 4,5-Dichlorophthalates. *Tetrahedron* **2008**, *64* (19), 4155–4161.
(26) Yoshioka, M.; Ohta, K.; Yasutake, M. Flying-Seed-like Liquid Crystals. Part 4: A Novel Series of Bulky Substituents Inducing Mesomorphism Instead of Using Long Alkyl Chains. *RSC Adv.* **2015**, *5* (18), 13828–13839.
(27) Opris, D. M.; Nüesch, F.; Löwe, C.; Molberg, M.; Nagel, M. Synthesis, Characterization, and Dielectric Properties of Phthalocyanines with Ester and Carboxylic Acid Functionalities. *Chem. Mater.* **2008**, *20* (21), 6889–6896.

Chapter 2 – Crosswise Zn(II)Pcs with collinear functionalization

ChemPubSoc Europe
DOI: 10.1002/cplu.201800631
CHEMPLUSCHEM Full Papers

Crosswise Phthalocyanines with Collinear Functionalization: New Paradigmatic Derivatives for Efficient Singlet Oxygen Photosensitization

Miguel A. Revuelta-Maza,[a] Cormac Hally,[d] Santi Nonell,[d] Gema de la Torre,*[a, b] and Tomás Torres*[a, b, c]

We describe here the preparation of a series of *trans*-ABAB Zn (II) phthalocyanines (ZnPcs, which combine several interesting features. First, these compounds present high solubility and hindered aggregation, due to the functionalization of two facing isoindole constituents (B) of the ZnPc with bis(trifluoromethylphenyl) units. Second, the other two isoindoles (A) bear extra-annulated phthalimide units containing different substituents in the nitrogen positions, this feature results in a collinear arrangement of a variety of functional groups. Some of these collinearly functionalized ZnPcs are interesting building blocks for constructing either homo- or heteroarrays containing ZnPc units. Furthermore, the amphiphilic nature of some members of the series renders them interesting candidates for photosensitization of singlet oxygen. Photophysical studies on a model compound of the series have shown that these molecules are efficient singlet oxygen photosensitizers in both polar and apolar media, with $^1O_2$ quantum yields (ϕ_Δ) as high as 0.74.

Introduction

Phthalocyanines (Pcs) are focus of research because of their exceptional electronic properties and their stability under a wide range of environmental conditions.[1] These chromophores are appealing targets for many different applications, as a result of their strong absorption in the visible/near infrared ranges of the electromagnetic spectrum, and their extraordinary robustness. Moreover, Pcs can form complexes with a large variety of metal atoms, and can be endowed with a range of substituents at axial and/or peripheral positions. This structural versatility has a strong impact on their electronic properties, such as molar absorption coefficients, redox potentials and excited-state lifetimes, among others. All these interesting features have driven their use in two broad scientific areas: i) biological applications,[2] namely, for therapeutic treatments as anticancer and antimicrobial agents, taking advantage of the ability of some Pc derivatives to sensitize singlet oxygen ($^1O_2$) due to their long-lived triplet excited states; and ii) as functional materials, for instance, as catalytic systems[3] or dyes for energy conversion schemes.[4] For most of these applications, the formation of well-defined nanoassemblies offers a route to improve the function of the Pc molecules. In this regard, the presence of certain functional groups on the periphery of the Pcs provides a tool for the engineering of outstanding supramolecular arrays. For instance, the incorporation of Pcs in 2D or 3D ensembles of different shapes and sizes relies on the preparation of macrocycles with highly directional binding motifs. Particularly, an angular orientation of the binding sites of 180° permits to create complex linear arrangements, such as Pc-containing polymers,[5] or to use Pcs as subcomponents for the self-assembly of metalloorganic cavities for host-guest interactions.[6] On the other hand, appropriate functionalization of the Pcs with collinear lipophilic/hydrophilic substituents may lead to nanovesicles in water media, which can be envisioned as delivery systems for photodynamic and photothermal therapies (PDT).[7,8] In this regard, we have recently described the preparation of *trans*-A_2B_2 Pcs[7b] containing: i) two crosswise isoindoles functionalized with bulky bis(trifluoromethyl)phenyl groups at the non-peripheral positions, which provide solubility and hinder the aggregation between macrocycles; and ii) two crosswise isoindoles endowed with iodine atoms.[7b,c] Importantly, the presence of opposite iodine atoms has allowed us to prepare amino-containing, ditopic Pc ligands able to self-assemble into supramolecular cages by metal-ligand coordination with iron(II) salts.[8] However, the fact that each of the iodine atoms in the starting Pc is offset with respect to one of the central N–N axes by a 30° angle results in the presence of two positional isomers (i.e. syn and anti) with the same ratio. Therefore, to obtain Pc ligands with well-defined coordination geometries,[8] it was necessary to separate the corresponding isomers.

[a] M. A. Revuelta-Maza, Dr. G. de la Torre, Prof. T. Torres
Universidad Autónoma de Madrid,
c/Francisco Tomás y Valiente 7, 28049 Madrid (Spain)
E-mail: tomas.torres@uam.es
gema.delatorre@uam.es
[b] Dr. G. de la Torre, Prof. T. Torres
Institute for Advanced Research in Chemical Sciences (IAdChem)
Universidad Autónoma de Madrid
28049 Madrid (Spain)
[c] Prof. T. Torres
Instituto Madrileño de Estudios Avanzados (IMDEA)-Nanociencia
c/ Faraday 9, Cantoblanco, 28049 Madrid (Spain)
[d] C. Hally, Prof. S. Nonell
Institut Químic de Sarrià
Universitat Ramon Llull
08017 Barcelona (Spain)

Supporting information for this article is available on the WWW under https://doi.org/10.1002/cplu.201800631

This article is part of a Special Issue on "Novel Aromatics".

2.1. Citation and contribution

Revuelta-Maza, M.A.; Hally, C.; Nonell, S.; de la Torre, G.; Torres, T. Crosswise phthalocyanines with collinear functionalization: New paradigmatic derivatives for efficient singlet oxygen photosensitization. *Chempluschem* **2019**, *84*, 673–679.

Contribution: Revuelta-Maza, M. A.: Synthesis, characterization, and photophysical studies (together with C. H.). Preparation of the manuscript.

Funding and supervision: Nonell, S.; de la Torre, G. and Torres, T. This work has been supported by Comunidad de Madrid, Spain (S2013/MIT-2841, FOTOCARBON), MINECO, Spain (CTQ2017-85393-P and CTQ2016-78454-C2-1-R), and the "Solar Energy goes Hybrid" Initiative of the Bavarian Ministry for Science, Culture and Education (SolTech).

Abstract:

We describe here the preparation of a series of trans-ABAB Zn(II)Pcs, which combine several interesting features. First, these compounds present high solubility and hindered aggregation, due to the functionalization of two facing isoindole constituents (B) of the Zn(II)Pc with bis(trifluoromethylphenyl) units. Second, the other two isoindoles (A) bear extra-annulated phthalimide units containing different substituents in the nitrogen positions, this feature results in a collinear arrangement of a variety of functional groups. Some of these collinearly functionalized Zn(II)Pcs are interesting building blocks for constructing either homo- or heteroarrays containing Zn(II)Pc units. Furthermore, the amphiphilic nature of some members of the series renders them interesting candidates for photosensitization of $^1O_2$. Photophysical studies on a model compound of the series have shown that these molecules are efficient $^1O_2$ PS in both polar and apolar media, with ϕ_Δ as high as 0.74.

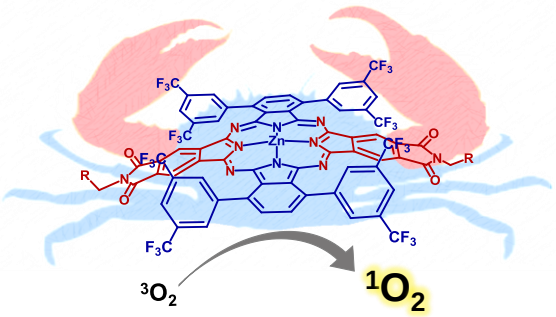

2.2. Introduction and Objectives

In **Chapter 1** (**C1**) we have proved the efficiency of ABAB Zn(II)Pcs for $^1O_2$ photosensitization. Taking advantage of the outstanding photophysical properties of these family of compounds, in this second chapter we have selected compound **ABAB 1b** from **Chapter 1** with phthalimide-based substitution pattern in isoindol units A (Figure 2. 1), as a head of series to perform modifications directed to enlarge the versatility of the system by replacement of the 2-(but-2-yn-1-yl) substituent by other reactive functional groups that afford further modifications.

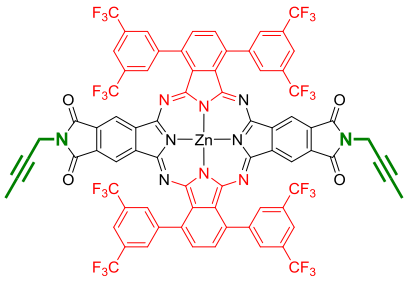

*Figure 2. 1. Structure of compound **ABAB 1b–C1**.*

Let's first analyze why we have selected this compound among those available in **Chapter 1**. As mentioned in the Introduction section, the interesting features of Pcs have driven their use in two broad scientific areas: i) biological applications,[1,2] namely, for therapeutic treatments as anticancer and antimicrobial agents, taking advantage of the ability of some Pc derivatives to sensitize $^1O_2$ due to their long-lived triplet excited states; and ii) as functional materials, for instance, as catalytic systems[3] or dyes for energy conversion schemes.[4–6] For most of these applications, the formation of well-defined nanoassemblies offers a route to improve the function of the Pc molecules. In this regard, the presence of certain functional groups on the periphery of the Pcs provides a tool for the engineering of outstanding supramolecular arrays. For instance, the incorporation of Pcs in 2D or 3D ensembles of different shapes and sizes relies on the preparation of macrocycles with highly directional binding motifs. Particularly, an angular orientation of the binding sites of 180° permits to create complex linear arrangements, such as Pc-containing polymers,[7] or to use Pcs as subcomponents for the self-assembly of metalloorganic cavities for host-guest interactions.[8] On the other hand, as we have explained in **Chapter 1**, appropriate functionalization of the Pcs with collinear lipophilic/hydrophilic substituents may lead to amphiphiles in water media, which can be envisioned as delivery systems after nanostructured self-organization for photodynamic and photothermal therapies.[9–13]

The first *trans*-ABAB Zn(II)Pc reported by our group [14] was one containing two crosswise isoindoles functionalized with bulky bis(trifluoromethyl)phenyl groups at the non-peripheral positions, and two crosswise isoindoles endowed with one iodine atom each.[14,15]However, the fact that each of the iodine atoms in the starting Pc is offset with respect to one of the central N-N axes by a 30° angle results in the presence of two positional isomers (i.e *syn* and *anti*) with the same ratio that could not be separated by chromatographic means. In a following report, we described the preparation of a diamino-containing, ditopic Pc ligand able to self-assemble into supramolecular cages by metal-ligand coordination with iron(II) salts.[8] To obtain this Pc ligand with well-defined coordination geometries, it was necessary to separate the corresponding isomers of a bis(hydroxymethylethynyl) intermediate (Figure 2. 2), which proved a complex and tedious procedure.

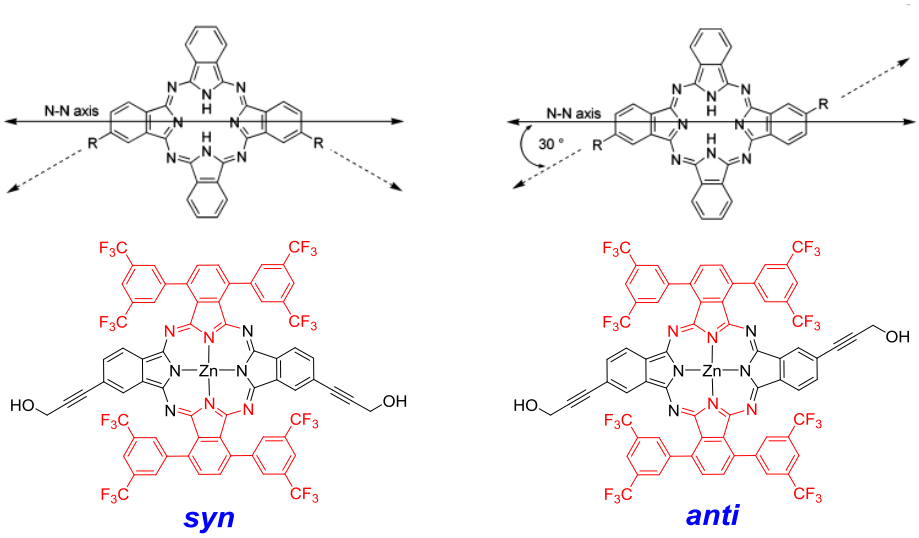

Figure 2. 2. (Top) Structures of two disubstituted phthalocyanines. The N-N axis bisects two inner nitrogen atoms and two opposing benzo rings. The axis equally can be displayed bisecting the NH-NH atoms.[16] *(Down) Example of syn and anti ABAB Zn(II)Pcs liable to be separated by chromatographic means.*[8]

In the previous context, it is indeed challenging to achieve a truly linear arrangement of the functional groups at the Pc core. However, this task is not trivial because of the limitations imposed by the geometry of Pcs and the methodology for their synthesis. An approach to prepare Pc derivatives holding substituents that are collinear with the N-N axes of the macrocycles is to use phthalonitrile derivatives endowed with fused five membered rings, which give rise to extra-annulated Pc derivatives. Several examples of Pc derivatives endowed with one or more fused imidazole and/or thiophene units have been reported.[17–20] A relevant work was reported by Youngblood, who prepared trans-ABAB bis(benzimidazole)phthalocyanines holding alkyl, phenyl or ethynylphenyl moieties

linked to the 2- position of the benzimidazole unit, resulting in compounds with a linear arrangement of the substituents.[16] However, *N*-alkylation at the imidazole ring was necessary, rendering a mixture of two positional isomers with different orientations of the *N*-alkyl chains.

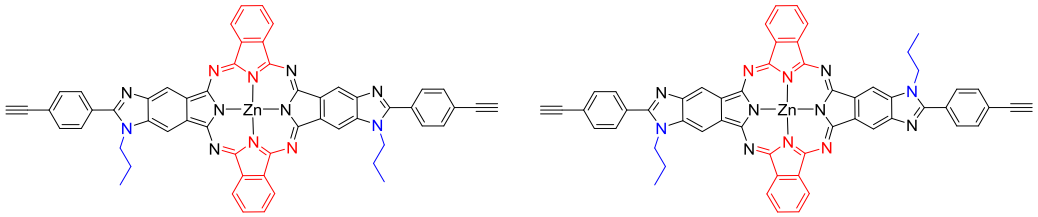

Figure 2. 3. Example of trans-ABAB Zn(II)Pc, mixture of two isomers.[16]

On the other hand, extra-annulation with phthalimide units containing substituents in the N position has been also described as a route to obtain highly symmetrical, isomerically pure, D_{4h} tetrafunctionalized Pcs.[21–24] This type of phthalimide derivatives have been synthesized either from the tetraanhydrides of 2,3,9,10,16,17,23,24-octacarboxyPcs and the corresponding amines,[21,23] or by cyclotetramerization of imidephthalonitriles.[22] However, to the best of our knowledge, ABAB Pcs with a collinear arrangement of *N*-functionalized phthalimide outer rings have not been described yet. In this Chapter, we report a unique family of ABAB Zn(II)Pcs (**1a–g**) with a collinear arrangement of the binding moieties located at the N position of facing phthalimide outer rings, (Scheme 2. 1). As explained in Chapter 1, the synthesis of of ABAB Zn(II)Pcs relies on the use of bulky 2,5-bis(trifluoromethyl)phenylphthalonitrile to direct the reaction towards the cross-condensation product. The extraannulation with the phthalimide rings has been attempted by the formation of a tetracarboxy-Zn(II)Pc, which could be further reacted with different amines to form the targeted compounds, and also by cross-condensation of differently functionalized imido-phthalonitriles with the bulky phthalonitrile.

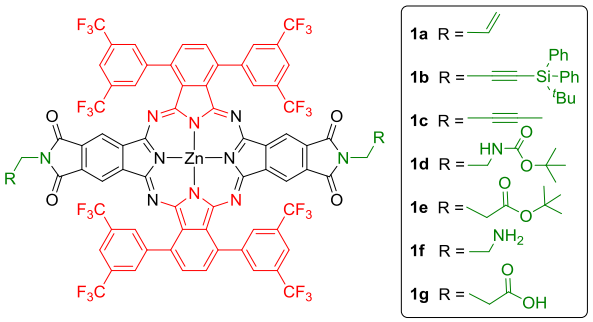

*Scheme 2. 1. Structure of Zn(II)Pcs **1a-g** synthesized in this chapter.*

The prepared Zn(II)Pc derivatives can be considered as motifs for building either linear or macrocyclic assemblies of Pcs, through efficient click thiol-ene (**1a**), Pd-catalyzed Sonogashira Sonogashira coupling (**1b**) or alkyne-metathesis (**1c**) reactions. On the other hand, the amphiphilic nature of some members of the series (**1f,g**), combined with hindered aggregation, renders them interesting for photosensitization of $^1O_2$.[25] Importantly, the presence of trifluoromethylphenyl units at the alfa position of the outer benzene rings of the Pc is expected to enhance the photostability and lipophilicity,[26] and also the photosensitization ability, as demontrated in **Chapter 1**. In fact, these ABAB-type ZnPcs have shown to be a new paradigm for PDT photosensitizers. Moreover, the geometry of these derivatives and the presence of amino, carboxylic acid, vinyl or ethynyl moieties will permit to build third-generation PS, where the Zn(II)Pc can be covalently conjugated to two-site specific delivery agents affording solubility in physiological media and selective accumulation within the targeted tissue.[2] Therefore, it appears of interest to establish the $^1O_2$ generation capabilities of this family of compounds. To this end, photophysical studies have been realized on Zn(II)Pc **1c** as model compound, which have been already shown in **Chapter 1** as compound **AABB 1b-C1**.

2.3. Results and discussion

a) Synthesis

The preparation of Zn(II)Pcs **1a–g** was undertaken by two different approaches. First, a most convergent route was attempted, which consisted in the preparation of tetracarboxy-Zn(II)Pc **2**, (Scheme 2. 2), as a synthon for the preparation of the targeted *N*-functionalized phthalimide-Zn(II)Pcs.

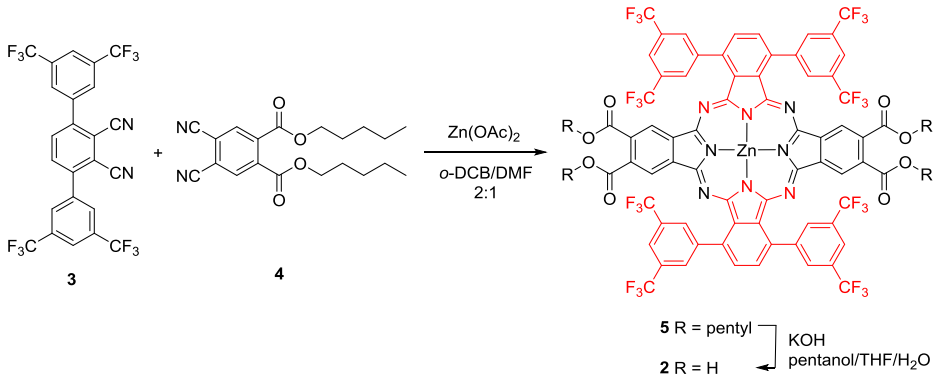

*Scheme 2. 2. Synthesis of tetracarboxy-Zn(II)Pc **2**.*

For the sake of obtaining a soluble precursor of **2** that could be easily purified by column chromatography, we performed a cross-condensation reaction between the bulky 2,5-

bis(trifluoromethyl)phenylphthalonitrile (**3**) (B unit),[14] and 4,5-bis(pentyloxycarbonyl)phthalonitrile (**4**) (A unit)[27] to obtain Zn(II)Pc **5**, which could be hydrolyzed in a second step to the tetracarboxy-derivative **2**. As previously established in **Chapter 1**, yields in the cross-condensation towards ABAB Zn(II)Pcs are maximized when a mixture of dry *o*-DCB and DMF is used as solvent, and $Zn(OAc)_2$ as source of metal. Moreover, in this particular case, avoiding the use of alcoholic solvents is crucial to circumvent substitutions of the alkoxy moieties at the ester functions. Yet, the reaction yielded Zn(II)Pc **3** in only 5%, probably due to the strong tendency of phthalonitriles functionalized with electron-withdrawing groups to give self-condensation instead of the crossed condensation with the bulky phthalonitrile. In fact, **A_3B 5** and **A_4 5** Zn(II)Pcs (Figure 2. 4) were isolated in 9 and 10% yield, respectively.

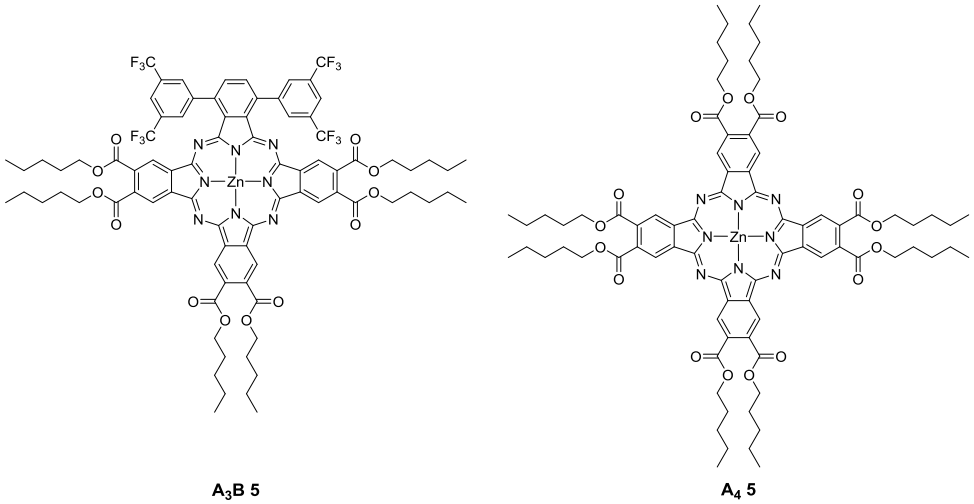

*Figure 2. 4. Structures of **A_3B** and **A_4 5** Zn(II)Pcs.*

The next step was to carry out the hydrolysis of the ester function. Although several conditions were tested, most of them failed to yield the tetracarboxy-Zn(II)Pc **2**. When using KOH in a pentanol/THF/water mixture, only traces of **2** were obtained. These results compelled us to direct our synthetic efforts towards the preparation of appropriately functionalized phthalimide-derived phthalonitriles, for the straightforward cross-condensation with bulky phthalonitrile **3**.

As mentioned in the **Background and Objectives Section**, one of the aims of the work is to establish a synthetic approach that allows to prepare differently substituted ABAB Zn(II)Pcs, all of them with a linear arrangement of functional groups at the Pc core. These geometrically well-defined disposition of the functional groups can be exploited for the preparation of Pc assemblies, and also to impart a marked amphiphilic character to the Pc molecule, when it is functionalized with facing lipophilic and hydrophilic

substituents in the same Pc ring. To this end, different *N*-substituted 5,6-dichloroisoindoline-1,3-diones (Scheme 2. 3) were envisioned, endowed either with reactive vinyl/acetylene moieties that can further give rise to efficient chemical transformations (**6a–c**), or with protected amino or carboxy moieties (**6d,e**) that can be deprotected (**6f,g**) towards the final preparation of a novel archetype of amphiphilic photosensitizers for PDT.

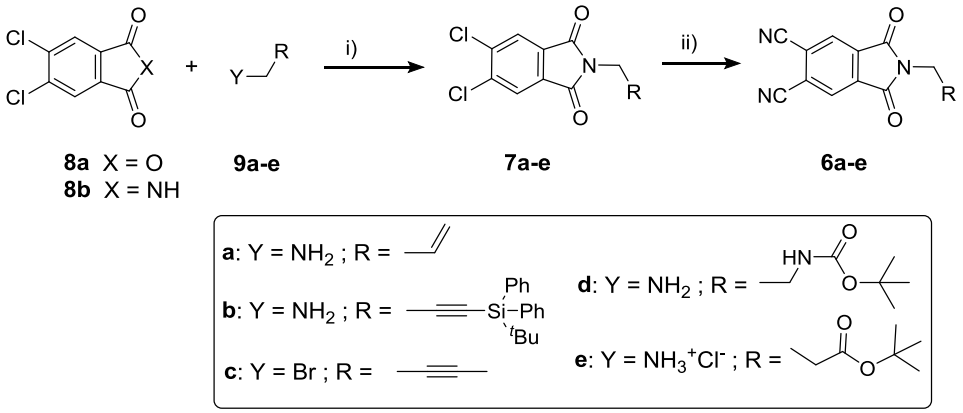

*Scheme 2. 3. Reagents and conditions. i) for **7a** (83%) and **7b** (68 %): **8a**, **9a** or **9b**, acetic acid, MW, 150°C, 2 h; for **7c** (70 %): **8b**, **9c**, N,N-diisopropylethylamine, acetonitrile, Ar, rt; for **7d** (84 %): **8a**, **9d**, acetic acid, 100 °C, 1.5 h; for **7e** (91 %): **8a**, **9e**, N,N-diisopropylethylamine, anhydrous toluene, Dean-Stark trap. ii) $Pd_2(dba)_3$, dppf, Zn powder, $Zn(CN)_2$, N,N-dimethylacetamide, Ar, 120°C, 2–4 h.*

The synthesis of 5,6-dicyano-1,3-dioxoisoindoline derivatives **6a–g** was accomplished by the initial preparation of *N*-substituted- 5,6-dichlorophthalimides (**7a–e**) followed by Pd-catalyzed cyanation reactions. Two general methods were applied for the synthesis of **7a–e** depending on the availability of the reactants, namely, the condensation reaction between 5,6-dichlorophthalic anhydride (**8a**) and the corresponding alkylamine (**9a,b,d**) or alkylamine hydrochloride (**9e**), and the *N*-alkylation of 5,6-dichlorophthalimide (**8b**) with the bromopropargyl derivative **9c** (Scheme 2. 3). The reaction of 5,6-dichlorophthalic anhydride and the corresponding alkylamine or alkylamine hydrochloride was performed either by thermal (reaction with **9d,e**) or microwave (reaction with **9a,b**) activation. All these reactions proceeded in good yields, ranging from 68 to 91%. However, the corresponding cyanations rendered phthalonitriles **6a–e** in moderate yields (31–53 %), with the exception of phthalonitrile **6a** that was isolated in a poor 5% yield. It is worth mentioning that, although we envisioned the preparation of 5,6-dicyano-1,3-dioxoisoindoline derivatives with aromatic *N*-substituents, this type of precursors proved very unstable and could not be utilized to prepare ABAB Zn(II)Pcs.

Next, we undertook the synthesis of the target ABAB Zn(II)Pcs, which was carried out by cross condensation between equimolecular amounts of bulky phthalonitrile **3** (B) and 5,6- dicyano-1,3-dioxoisoindoline derivatives **6a–e** (A). In all the reactions, trans-ABAB Zn(II)Pcs were formed, together with the related A_3B and A_4 Zn(II)Pcs, but with no traces of Pcs holding two adjacent B units. Nevertheless, the target compounds were isolated in low yields. Additionally, the carbamate and ester functions of compounds **1d** and **1e**, respectively, were easily removed using trifluoroacetic acid, yielding the diamino (**1f**) and dicarboxylic acid (**1g**) amphiphilic Zn(II)Pcs in good yields (Scheme 2. 4).

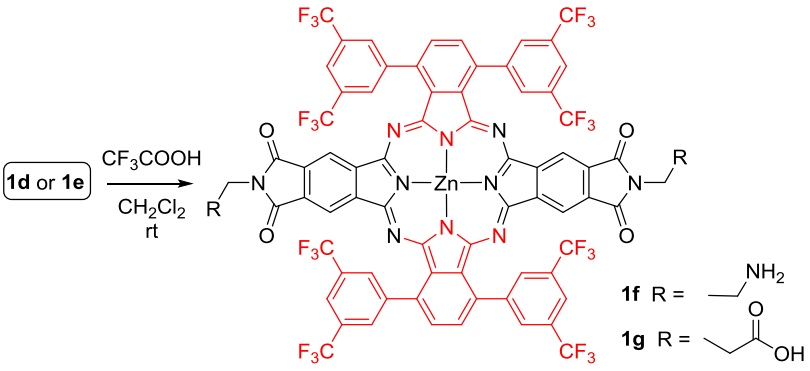

*Scheme 2. 4. Synthesis of amphiphilic Zn(II)Pcs **1f** and **1g**.*

All the Zn(II)Pcs have in common good solubility features and hindered aggregation in solution imparted by the bis(trifluoromethyl) phenyl moieties. These facts, together with the high symmetry exhibited by all the derivatives, result in extremely well-resolved ^{1}H and ^{13}C NMR spectra. As an example, the ^{1}H NMR spectra of compounds **1a-d** is shown in Figure 2. 5.

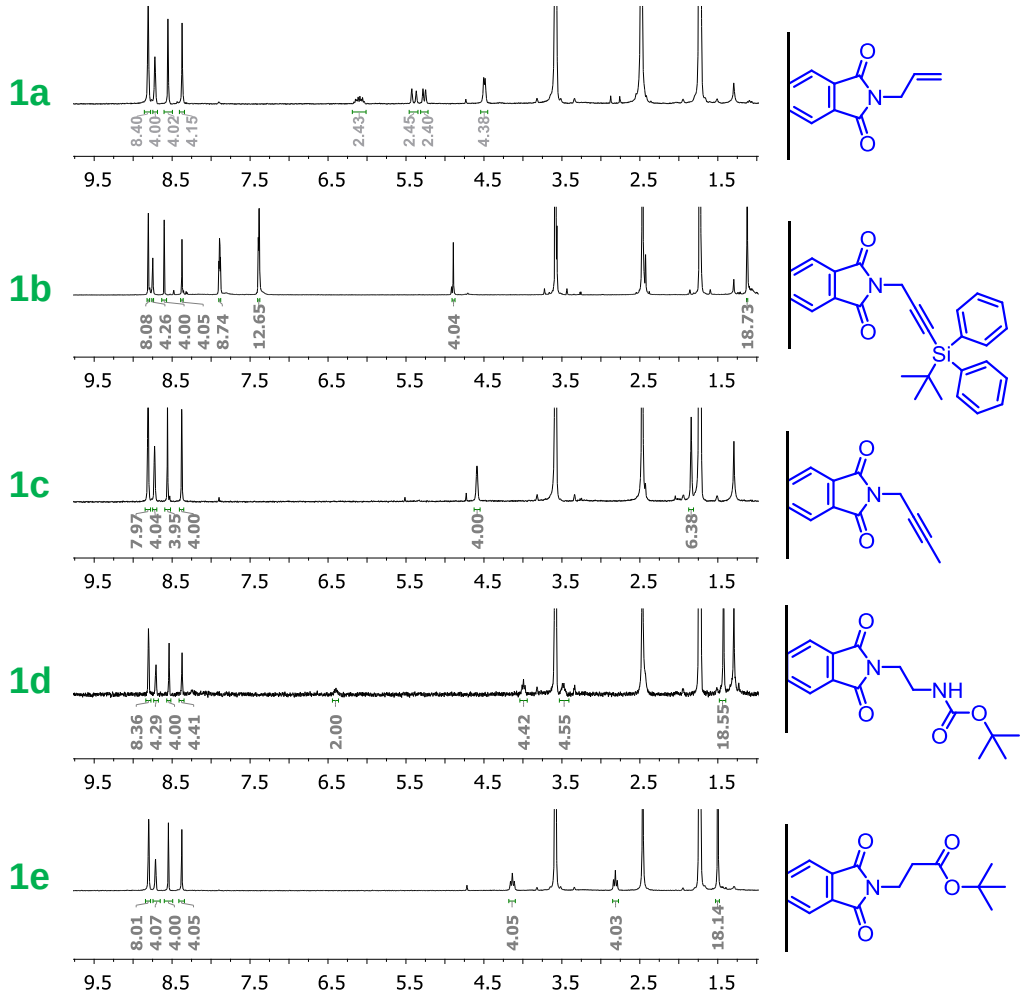

*Figure 2. 5. ^{1}H NMR spectra in THF-d_8 for **ABAB 1a-d**.*

b) Photophysical studies

UV-vis spectra of ABAB Zn(II)Pcs **1a–g** shows symmetric, split *Q*-bands with any evidence of aggregation in THF or toluene, as otherwise expected for these compounds. In Figure 2. 6, concentration dependent experiments are shown for compound **1c**. The UV-vis spectra of the other compounds of the series resemble that of **1c**, which is consistent with the nearly identical substitution at the Pc cores.

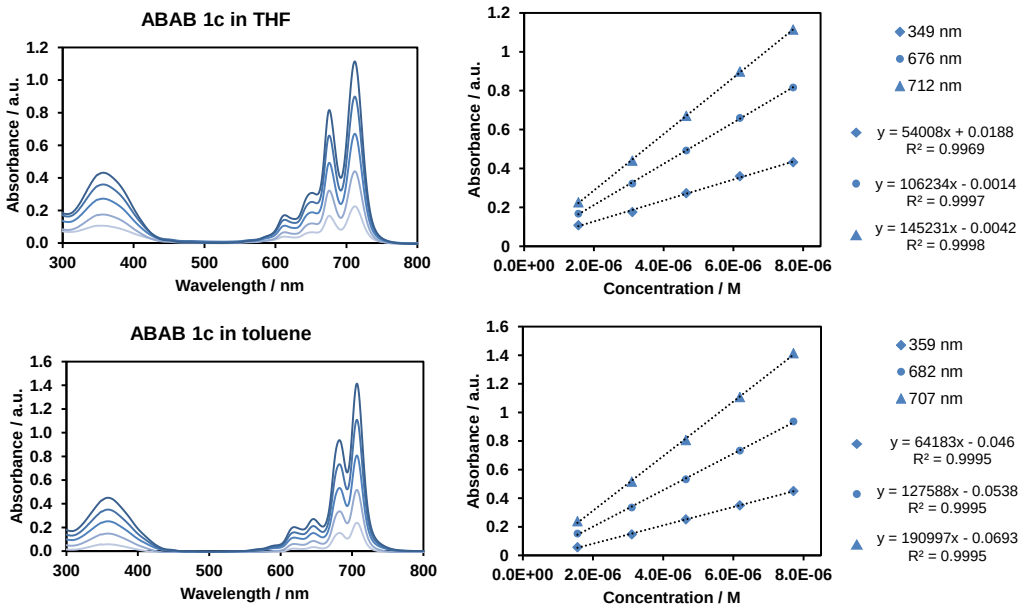

*Figure 2. 6. Concentration-dependent UV-vis experiments for Zn(II)Pc **1c** in THF and toluene (between ~$1 \cdot 10^{-6}$ - $8 \cdot 10^{-6}$ M).*

Next, we tackled the evaluation of the ϕ_Δ of some representatives of the series. First, it is necessary to bring back that the complete photophysical characterization of compound **1c** has been previously shown in **Chapter 1** (compound **ABAB-1b-C1**). ϕ_Δ was determined for **1c** by the straightforward measurement of the $^1O_2$ phosphorescence, both in THF and toluene solutions (see **Chapter 1**, Tables 1.1 and 1.2), giving a value of 0.80. We have also determined the ϕ_Δ in DMSO by the same method, obtaining a similar value (0.67), which indicates a low solvent-dependence. It is expected that, due to the structural similarity, the other members of the series show similar photophysical behaviour. To confirm this hypothesis, $^1O_2$ generation studies have been performed on compounds **1c**, **1d** and **1e** by an indirect method, that is measuring the photoinduced decomposition of 1,3-diphenylisobenzofuran (DPBF) in DMSO solutions, under the irradiation of the corresponding Zn(II)Pcs (see Figure 2. 7). Although the indirect method is quantitatively less accurate than the measurement of the $^1O_2$ phosphorescence, it can be useful for comparative purposes. In fact, we observed that the three compounds gave similar ϕ_Δ values, which is consistent with their similar substitution nearby the Pc core, with only slight changes in the *N*-functionalization of the extra-annulated phthalimide.

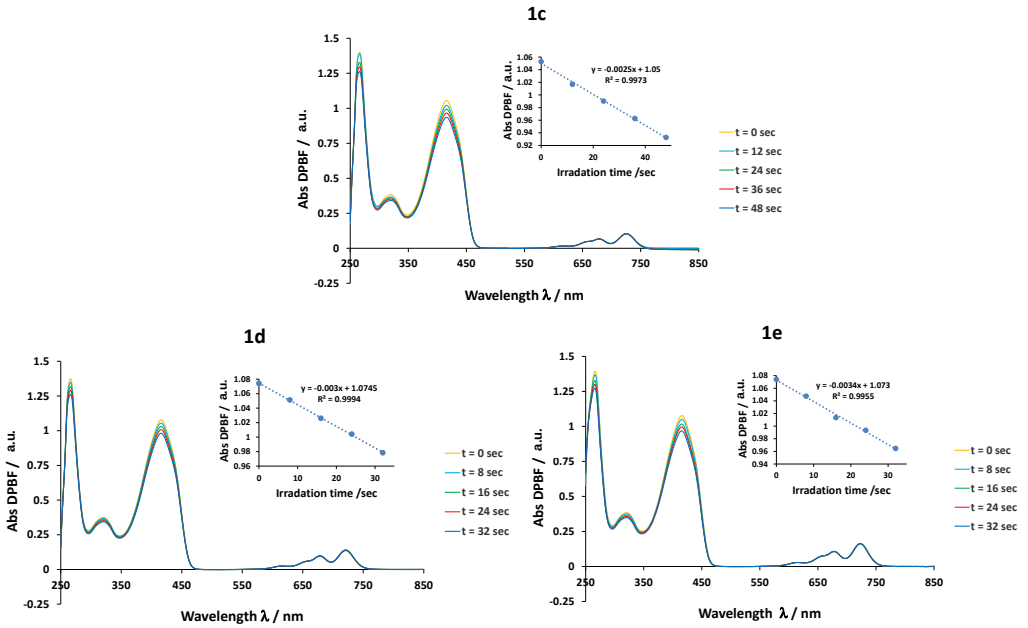

*Figure 2. 7. Time dependent photobleaching of DPBF-absorption in the presence of **1c**, **1d** and **1e** in DMSO, which is directly related to the photoinduced generation of $^1O_2$ by the PS: (Inset: detail of DPBF absorption decrease).*

2.4. Conclusions

In this Chapter, we describe the preparation of a series of *trans*-ABAB Zn(II)Pcs **1a–g** featuring high solubility, hindered aggregation and a collinear arrangement of a variety of functional groups. These compounds constitute a paradigmatic type of Zn(II)Pcs that can be exploited for the construction of multi-Pc arrays. Importantly, this substitution pattern permits to obtain amphiphilic Zn(II)Pcs with inherent non-aggregating features that are independent of the solvent employed. This is an outstanding characteristic, not easy to achieve in Zn(II)Pcs, and that is fundamental for using them as PS for the production of $^1O_2$ in therapeutic applications, together with their high singlet oxygen photosensitization capabilities.

2.5. Experimental section

Chemicals were purchased from commercial suppliers and used without further purification unless stated otherwise. 3,3″,5,5″-tetrakis(trifluoromethyl)-[1,1′ :4′,1″-terphenyl]-2′,3′-dicarbonitrile (**3**)[14] dipentyl 4,5-dicyanophthalate (**4**),[28] 5,6-dichloroisoindoline-1,3-dione (**8b**),[29] 4,5-dichlorophthalic anhydride (**8a**),[28] 3-(tert-

butyl(diphenyl) silyl)prop-2-yn-1-amine (**9b**),[30] and compound **5-ABAB (Chapter 1)** have been prepared according to published procedures.

i. *Synthesis of N-substituted 5,6-dichloroisoindoline-1,3-diones (**7a-e**):*

Method A: MW assisted reaction: To a microwave test tube were added **8a** (300 mg, 1.38 mmol), acetic acid (2 mL), and alkyl amine (**9a** or **9b**) (1.52 mmol). The reaction was stirred in a microwave reactor, at 150°C for 2 h. After that time, the crude reaction mixture was diluted with EtOAc (50 mL), poured carefully in aqueous solution of $NaHCO_3$ (sat) (50 mL) to neutralize the acetic acid. The organic phase was washed with the $NaHCO_3$ (sat) (50 mL) solution, and with H_2O (2x20 mL). The organic phase was separated and dried over $MgSO_4$, and the solvent was removed under reduced pressure to give the corresponding product. **Thermal reaction: 9d** (369 mg, 2.30 mmol) was added to a solution of **8a** (500 mg, 2.30 mmol) in 11 mL acetic acid. The mixture was stirred for 1.5 h at 100°C and after being cooled to rt, it was treated with H_2O (20 mL). The solid was filtered and washed several times with H_2O (20 mL), $NaHCO_3$ (sat) (2x20 mL) and H_2O (20 mL).

Method B: 8b (500 mg, 2.31 mmol), *N,N*-diisopropylethylamine (605 µL, 3.47 mmol), alkyl bromide (**9c**) (230 µL, 2.55 mmol) and acetonitrile (5 mL) were placed in a round bottom flask and stirred at rt under argon atmosphere. After completion of the reaction (monitored by TLC), the reaction mixture was filtered, the solid was washed with H_2O (10 mL) and dried in a vacuum oven overnight.

Method C: Alkyl amine hydrochloride (**9e**) (1.38 mmol), *N,N*-diisopropylethylamine (503 µL, 2.89 mmol), **8a** (300 mg, 1.38 mmol), and anhydrous toluene (150 mL) were added. The apparatus was equipped with a Dean–Stark trap, and the mixture was refluxed overnight. Finally, toluene was removed under reduced pressure.

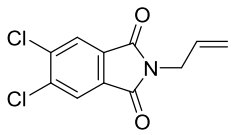

2-Allyl-5,6-dichloroisoindoline-1,3-dione (7a): Compound **7a** was synthesized from **9a** following **method A (MW assisted reaction)**. No further purification was required, affording **4a** as a white solid which was dried in a vacuum oven overnight. Yield: 294 mg, (83%). ^{1}H NMR (300 MHz, $CDCl_3$): δ 7.93 (s, 2H, Ar), 5.93-5.79 (m, 1H, HC=C), 5.30-5.18 (m, 2H, C=CH_2), 4.29 (d, 2H, *J* = 5.78 Hz, CH_2); ^{13}C NMR (75 MHz, $CDCl_3$): δ 40.4 (CH_2), 118.0 (CH=C*H_2), 125.3 (CH Ar), 131.0 (C Ar), 131.2 (C Ar), 138.8 (C*H=CH_2), 165.7 (C=O); IR(ATR) v^{-1} (cm^{-1}): 3083 (=CH_2 st), 3021 (=CH st), 1766 (C=O st), 1698 (C=O st), 1642 (C=C st), 1075 (C-Cl st), 927 (=CH δ oop);HR-MS (FAB, matrix m-NBA) *m/z*: 255.9928 $[M+H]^+$ (calculated: 255.9932).

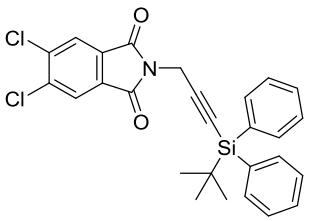

2-(3-(*tert*-Butyldiphenylsilyl)prop-2-yn-1-yl)-5,6-dichloroisoindoline-1,3-dione (7b): Compound **7b** was synthesized from **9b** following **method A (MW assisted reaction)**. The crude product was purified by filtration over silica gel in EtOAc:heptane (1:1), affording **7b** as a brown oil which crystalizes by standing. Yield: 571 mg, (84%). ^{1}H NMR (300 MHz, $CDCl_3$): δ 7.98 (s, 2H, Ar), 7.81-7.71 (m, 4H, Ar), 7.44-7.31 (m, 6H, Ar), 4.62 (s, 2H, CH_2), 1.05 (s, 9H, CH_3); ^{13}C NMR (75 MHz, $CDCl_3$): δ 18.6 (C*(CH_3)$_3$), 27.1 (C(C*H_3)$_3$), 28.8 (CH_2), 102.1 (C≡C), 125.8 (CH Ar), 127.9 (CH Ar), 129.7 (CH Ar), 131.3 (C Ar), 132.9 (C Ar), 135.7 (CH Ar), 139.4 (C Ar), 165.1(C=O); IR(ATR) v^{-1} (cm^{-1}): 2184 (C≡C st), 1782 (C=O st), 1725 (C=O st), 1414 (CH_3 δ as/CH_2 δ), 1382 (CH_3 δ sim), 1110 (C-Cl st); HR-MS (APCI+) *m/z*: 492.0952 $[M+H]^+$ (calculated: 492.0948).

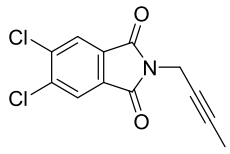

2-(But-2-yn-1-yl)-5,6-dichloroisoindoline-1,3-dione (7c): Compound **7c** was synthesized from **9c** following **method B**. No further purification was required, affording **7c** as a brown solid. Yield: 430 mg, (70%). ^{1}H NMR (300 MHz, $CDCl_3$): δ 7.95 (s, 2H, Ar), 4.38 (q, 2H, *J* = 2.41 Hz, CH_2), 1.77 (t, 3H, *J* = 2.41 Hz, CH_3); ^{13}C-APT NMR (75 MHz, $CDCl_3$): δ 3.6 (CH_2), 28.0 (CH_3), 72.2 (C≡C), 79.9 (C≡C), 125.7 (CH Ar), 131.4 (C Ar), 139.2 (C Ar), 165.4 (C=O); IR(ATR) v^{-1} (cm^{-1}): 2295 (C≡C st), 1773 (C=O st), 1725 (C=O st), 1705 (C=O st), 1418 (CH_3 δ as/CH_2 δ), 1380 (CH_3 δ sim), 1101 (C-Cl st);HR-MS (APCI) *m/z*: 267.9918 $[M+H]^+$ (calculated: 267.9927).

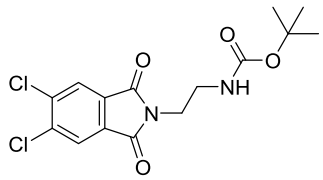

***tert*-Butyl-(2-(5,6-dichloro-1,3-dioxoisoindolin-2-yl)ethyl)carbamate (7d):** Compound **7d** was synthesized from **9d** following **method A (thermal reaction)**. No further purification was required, affording **7d** as a white solid. Yield: 750 mg, (91%). ^{1}H NMR (300 MHz, $CDCl_3$): δ 7.92 (s, 2H, Ar), 4.75 (s, 1H, NH), 3.82 (t, 2H, *J* = 5.55 Hz, CH_2), 3.46-3.33 (m, 2H, CH_2), 1.33 (s, 9H, CH_3); ^{13}C NMR (75 MHz, $CDCl_3$): δ 28.2 (C(C*H_3)$_3$), 38.7 (CH_2), 39.1 (CH_2), 79.4 (C*(CH_3)$_3$), 125.3 (CH Ar), 131.2 (C Ar), 138.8 (C Ar), 156.0 (C=O), 166.4 (C=O); IR(ATR) v^{-1} (cm^{-1}): 3369 (N-H st), 1771 (C=O st), 1703 (C=O st), 1684 (C=O st), 1521 (N-H δ), 1450 (CH_3 δ as/CH_2 δ), 1383 (CH_3 δ sim), 1288 (C-O st as/ N-CO-O st as), 1273 (C-O st as/ N-CO-O st as), 1250 (C-O st as/ N-CO-O st as), 1171 (C-Cl st); HR-MS (ESI) *m/z*: 381.0380 $[M+Na]^+$ (calculated: 381.0379).

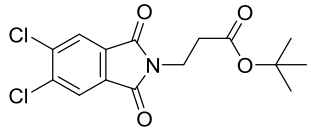

***tert*-Butyl 3-(5,6-dichloro-1,3-dioxoisoindolin-2-yl)propanoate (7e):** Compound **7e** was synthesized from **9e** following **method C**. The crude product was purified by filtration over silica gel in $CHCl_3$ and washed with heptane,

affording **7e** as a white solid. Yield: 324 mg, (68%). ^{1}H NMR (300 MHz, $CDCl_3$): δ 7.93 (s, 2H, Ar), 2.38 (t, 2H, *J* = 7.23 Hz, CH_2), 2.38 (t, 2H, *J* = 7.23 Hz, CH_2), 1.41 (s, 9H, CH_3); ^{13}C NMR (75 MHz, $CDCl_3$): δ 28.1 ($C(C^*H_3)_3$, 34.0 (CH_2), 34.6 (CH_2), 81.4 ($C^*(CH_3)_3$), 125.6 (CH Ar), 131.3 (C Ar), 139.1 (C Ar), 166.2 (C=O), 169.9 (C=O); IR(ATR) v^{-1} (cm^{-1}): 1777 (C=O st), 1710 (C=O st), 1443 (CH_3 δ as/CH_2 δ), 1400 (CH_3 δ sim), 1365 (C-O st), 1322 (C-O st), 1139 (C-O st as), 1017 (C-Cl st); HR-MS (ESI) *m/z*: $[M+Na]^+$ 366.0281 (calculated: 366.0270), $[2M+Na]^+$ 711.0642.

ii. *General procedure for the synthesis of N-substituted 1,3-dioxoisoindoline-5,6-dicarbonitriles (**6a-e**):*

N-Substituted 1,3-dioxoisoindoline-5,6-dicarbonitriles were prepared from *N*-substituted 5,6-dichloroisoindoline-1,3-diones **6a-e** via Pd-catalyzed cyanation reactions.[28] All of them were performed in oven-dry glassware under dry argon atmosphere. Dry *N,N*-dimethylacetamide was kept over 4 Å molecular sieves. 5,6-Dichloroisoindoline-1,3-dione **6a-e** (0.70 mmol), $Pd_2(dba)_3$ (27 mg, 0.03 mmol), dppf (22 mg, 0.04 mmol), Zn powder (9 mg, 0.14 mmol), and $Zn(CN)_2$ (99 mg, 0.84 mmol) were placed in a dry flask flushed with argon. *N,N*-Dimethylacetamide (3.6 mL) was added via syringe. The resulting mixture was heated at 120°C for 2-4h (monitorized by TLC), then cooled to rt, and diluted with EtOAc (50 mL). The resulting mixture was filtered and mixed with H_2O (50 mL). The organic layer was separated, and the aqueous layer was extracted with EtOAc (50 mL). The combined organic extracts were washed with H_2O (50 mL), dried over $MgSO_4$, and concentrated in vacuum.

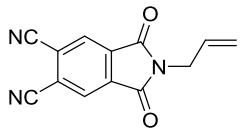

2-Allyl-1,3-dioxoisoindoline-5,6-dicarbonitrile (6a): Compound **6a** was synthesized from 5,6-dichloroisoindoline-1,3-dione **7a**. It was further purified by column chromatography on SiO_2 (in gradient from EtOAc/heptane 4:1 to 1:1) affording **6a** as a yellow solid. Yield: 8.3 mg, (5%). ^{1}H NMR (300 MHz, $CDCl_3$): δ 8.28 (s, 2H, Ar), 5.95-5.78 (m, 1H, HC=C), 5.36-5.23 (m, 2H, $C=CH_2$), 4.35 (d, 2H, *J* = 5.97 Hz, CH_2); ^{13}C NMR (75 MHz, $CDCl_3$): δ 41.2 (CH_2), 114.1 (C Ar), 119.5 ($CH=C^*H_2$), 121.4 (C≡N), 128.1 (CH Ar), 130.3 (C Ar), 135.4 ($C^*H=CH_2$), 164.3 (C=O); IR(ATR) v^{-1} (cm^{-1}): 3049 (=CH_2 st), 2238 (C≡N st), 1780 (C=O st), 1714 (C=O st), 1428 (CH_2 δ); HR-MS (GC-EI) *m/z*: 237.0535 $[M+H]^+$ (calculated: 237.10538).

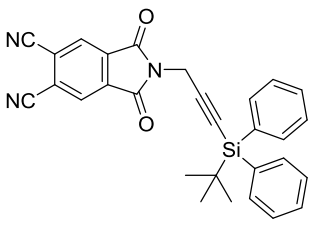

2-(3-(*tert*-Butyldiphenylsilyl)prop-2-yn-1-yl)-1,3-dioxoisoindoline-5,6-dicarbonitrile (6b): Compound **6b** was synthesized from 5,6-dichloroisoindoline-1,3-dione **7b**. It was further purified by column chromatography on SiO_2 (EtOAc/heptane, 1:3) affording **6b** as a white-brown solid. Yield: 123 mg, (36%). ^{1}H NMR (300 MHz, $CDCl_3$): δ 8.31 (s, 2H, Ar), 7.84-7.69 (m, 4H,

Ar), 7.50-7.30 (m, 6H, Ar), 4.69 (s, 2H, CH_2), 1.05 (s, 9H, CH_3); ^{13}C NMR (75 MHz, $CDCl_3$): 18.7 (C*(CH_3)$_3$), 27.1 (C(C*H_3)$_3$), 29.4 (CH_2), 85.8 (C≡C), 100.9 (C≡C), 114.0 (C Ar), 121.6 (C≡N), 127.9 (CH Ar), 128.4 (CH Ar), 129.9 (CH Ar), 132.6 (C Ar), 135.4 (C Ar), 135.7 (CH Ar), 163.4 (C=O); IR(ATR) v^{-1} (cm^{-1}): 2236 (C≡N st), 2184 (C≡C st), 1791 (C=O st), 1721 (C=O st), 1425 (CH_3 δ as/CH_2 δ), 1388 (CH_3 δ sim); HR-MS (APCI+) *m/z*: 474.1633 (calculated: 474.1632).

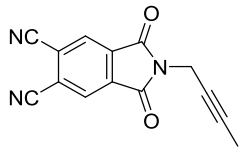

2-(But-2-yn-1-yl)-1,3-dioxoisoindoline-5,6-dicarbonitrile (6c): Compound **6c** was synthesized from 5,6-dichloroisoindoline-1,3-dione **7c**. It was further purified by column chromatography on SiO_2 (EtOAc/heptane, 1:1) affording **6c** as a yellow solid. Yield: 63 mg, (37%). ^1H NMR (300 MHz, $CDCl_3$): δ 8.29 (s, 2H, Ar), 4.45 (s, 2H, CH_2) 1.78 (s, 3H, CH_3); ^{13}C-APT NMR (75 MHz, $CDCl_3$): δ 3.6 (CH_2), 28.7 (CH_3), 71.4 (C≡C), 80.8 (C≡C), 114.1 (C Ar), 121.5 (C≡N), 128.3 (CH Ar), 135.4 (C Ar), 163.7 (C=O); IR(ATR) v^{-1} (cm^{-1}): 2235 (C≡N st), 2111 (C≡C st), 1773 (C=O st), 1711 (C=O st), 1420 (CH_3 δ as/CH_2 δ), 1390 (CH_3 δ sim); HR-MS (APCI) *m/z*: 250.0601 $[M+H]^+$ (calculated 250.0601).

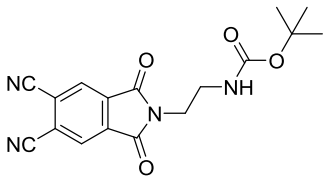

***tert*-Butyl (2-(5,6-dicyano-1,3-dioxoisoindolin-2-yl)ethyl)carbamate (6d):** Compound **6d** was synthesized from 5,6-dichloroisoindoline-1,3-dione **7d**. It was further purified by column chromatography on SiO_2 (EtOAc/heptane, 1:1) affording **6d** as a white solid. Yield: 81 mg, (34%). ^1H NMR (300 MHz, $CDCl_3$): δ 8.28 (s, 2H, Ar), 4.77 (s, 1H, NH), 3.88 (t, 2H, *J* = 5.23 Hz, CH_2), 3.53-3.39 (m, 2H, CH_2), 1.27 (s, 9H, CH_3); ^{13}C NMR (75 MHz, $CDCl_3$): δ 28.3 (C(C*H_3)$_3$), 39.0 (CH_2), 39.8 (CH_2), 79.9 (C*(CH_3)$_3$), 114.2 (C Ar), 121.2 (C≡N), 128.0 (CH Ar), 135.6 (C Ar), 156.4 (C=O), 165.0 (C=O); IR(ATR) v^{-1} (cm^{-1}): 3391 (N-H st), 2233 (C≡N st), 1777 (C=O st), 1711 (C=O st), 1686 (C=O st), 1523 (N-H δ), 1437 (CH_3 δ as/CH_2 δ), 1390 (CH_3 δ sim), 1249 (C-O st as/ N-CO-O st as), 1162 (C-O st as/ N-CO-O st as); HR-MS (ESI) *m/z*: $[M+Na]^+$ 363.1056 (calculated: 363.1063).

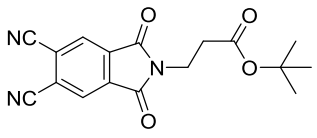

***tert*-Butyl 3-(5,6-dicyano-1,3-dioxoisoindolin-2-yl)propanoate (6e):** Compound **6e** was synthesized from 5,6-dichloroisoindoline-1,3-dione **7e**. It was further purified by column chromatography on SiO_2 (EtOAc/heptane, 1:3) and wash with heptane affording **6e** as a yellow solid. Yield: 121 mg, (53%). ^1H NMR (300 MHz, $CDCl_3$): δ 8.27 (s, 2H, Ar), 4.01 (t, 2H, *J* = 7.04 Hz, CH_2), 2.66 (t, 2H, *J* = 7.04 Hz, CH_2), 1.40 (s, 9H, CH_3); ^{13}C NMR (75 MHz, $CDCl_3$): δ 28.1 (C(C*H_3)$_3$), 33.6 (CH_2), 35.1 (CH_2), 81.7 (C*(CH_3)$_3$), 114.1 (C Ar), 121.4 (C≡N), 128.1 (CH Ar), 135.4 (C Ar), 164.5 (C=O), 169.6 (C=O); IR(ATR) v^{-1} (cm^{-1}): 2235 (C≡N st),

1786 (C=O st), 1697 (C=O st), 1152 (C-O st), 1120 (C-O st); HR-MS (FAB, matrix m-NBA) *m/z*: 326.1143 $[M+H]^+$ (calculated: 326.1141), 651.2 $[2M+H]^+$.

iii. *Synthesis of compound **2-ABAB**:*

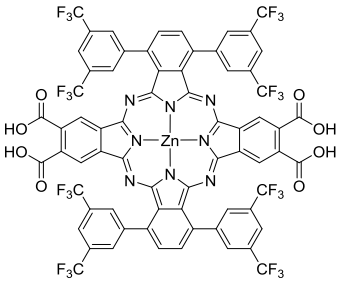

A solution of **5-ABAB** (12.5 mg, 0.00664 mmol) and KOH (1N) in a mixture of pentanol (2 mL) and tetrahydrofurane (2 mL) was refluxed for 10 min. Water (2 mL) was then added and the reaction was refluxed for another 10 min. The change of color from blue to green and the loss of mass indicates some kind of decomposition. The mixture was treated with an aqueous HCl (5% w/w) to pH 2. The organic layer was separated and washed with water (2x10 mL) and brine (10 mL). Finally, the volatiles were removed under reduced pressure. The product was treated with a cation exchange resin (Bio-Rad resin, AG® 50W-X8 and AG MP-50). MS (MALDI, matrix DCTB): 1600.0 $[M]^+$ (calculated: 1600.1). The low amount of product prevented the complete characterization of the product.

iv. *General procedure for the synthesis of ABAB phthalocyanines **1a-e**:*

7 (0.27 mmol, 150 mg), phthalonitrile **6a-e** (0.27 mmol) and anhydrous $Zn(AcO)_2$ (0.27 mmol, 50 mg) were placed in a 5 mL high pressure resistant flask equipped with a magnetic stirrer, and then 2.7 mL ([**7**]=0.1 M) of dry *o*-diclorobenzene/DMF (dried over 4Å molecular sieves) 2:1 was added. The mixture was heated to 150-160°C overnight under an argon atmosphere. After cooling the solvent was removed under vacuum.

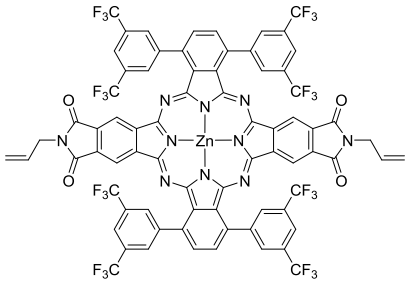

Compound 1a-ABAB: Compound **1a-ABAB** was synthesized from **6a**. The product was purified by column chromatography on SiO_2 (dioxane/heptane in gradient from 4:1 to 1:0) where the first fraction to elute containing the desired product **1a-ABAB**, followed by compounds **1a-A_3B**, and **1a-A_4**. The product was further purified by an additional column chromatography on Bio-Beads using $CHCl_3$ as eluent. After evaporation of the solvent a blue solid was obtained, which was washed with heptane. Yield: 6 mg, (3%). ^{1}H NMR (300 MHz, THF-d_8): δ 8.81 (s, 8H, Ar), 8.72 (s, 4H, Ar), 8.55 (s, 4H, Ar), 8.37 (s, 4H, Ar), 6.18-6.02 (m, 2H, HC=C), 5.40 (d, 2H, *J* = 17.12 Hz, C=CH_2), 5.26 (d, 2H, *J* = 10.27 Hz, C=CH_2), 4.50 (d, 4H, *J* = 5.27 Hz, CH_2); ^{13}C NMR (75 MHz, THF-d_8): 41.3 (CH_2), 117.8 (C Ar), 118.2 (CH=C*H_2), 125.0 (q, *J*= 274.3 Hz, CF_3), 132.0 (br s, C*CF_3), 132.5 (C Ar), 132.9 (C Ar), 133.0 (C Ar), 133.4 (C*H=CH_2), 134.1 (C Ar), 136.8 (CH Ar), 138.4 (CH Ar), 142.7 (CH Ar), 143.8 (CH Ar), 153.7 (C=N), 155.0 (C=N), 167.5 (C=O); IR(ATR) v^{-1} (cm^{-1}): 3085, 3044, 1768, 1700,

1618, 1382, 1274, 1179, 1128; HR-MS (MALDI, matrix DCTB + PPGNa 2000): First fraction, **1a-ABAB**, *m/z* 1642.1380 [M^+] (calculated: 1642.1354); MS (MALDI, matrix DCTB): Second fraction, **1a-A$_3$B**, *m/z* 1327.1 (calculated: 1327.1); third fraction: **1a-A$_4$**, *m/z*, 1012.2 (calculated: 1012.1); UV-vis (THF), λ_{max} (log ε): 710 (4.90), 676 (4.79), 649 (sh), 613 (sh), 356 (4.44) nm.

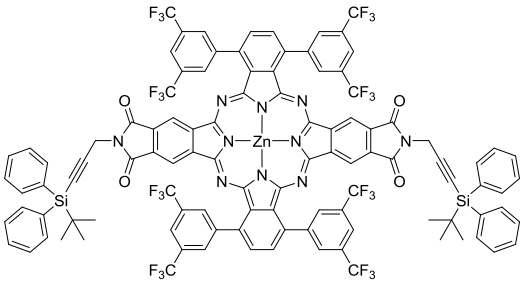

Compound 1b-ABAB: Compound **1b-ABAB** was synthesized from **7b**. The product was purified by column chromatography on SiO_2 (THF/heptane 1:1) where the first fraction to elute contained the desired product **1b-ABAB**, followed by compounds **1b-A$_3$B**, and **1b-A$_4$**. The product was further purified by an additional column chromatography on Bio-Beads using $CHCl_3$ as eluent. After evaporation of the solvent a blue solid was obtained, which was washed with heptane. Yield: 8.6 mg, 3%. ^{1}H NMR (500 MHz, THF-d_8): δ 1.12 (s, 18H, CH_3), 4.88-4.90 (s, 4H, CH_2), 7.35-7.41 (m, 12H, Ar), 7.86-7.92 (m, 8H, Ar), 8.37 (s, 4H, Ar), 8.60 (s, 4H, Ar), 8.75 (s, 4H, Ar), 8.81 (s, 8H, Ar); ^{13}C NMR (125 MHz, THF-d_8): 19.2 (C*(CH_3)$_3$), 27.5 (C(C*H_3)$_3$), 29.1 (CH_2), 84.0 (C≡C), 105.3 (C≡C), 118.5 (C Ar), 125.0 (q, *J* = 273.5 Hz, CF_3), 130.4 (CH Ar-TBDPS), 132.0 (br s, C*CF_3), 132.6 (C Ar), 132.9 (C Ar), 133.0 (C Ar), 134.0 (C Ar), 136.6 (CH Ar-TBDPS), 136.8 (CH Ar),138.4 (CH Ar), 142.7 (CH Ar), 143.8 (CH Ar), 153.6 (C=N), 155.1 (C=N), 166.8 (C=O); IR(ATR) v^{-1} (cm^{-1}): 2920, 2851, 2184, 1772, 1720, 1276, 1381, 1136; HR-MS (MALDI, matrix DCTB + PPGNa 2000): First fraction, **1b-ABAB**, *m/z* 2114.3486 [M^+] (calculated: 2114.3397), 2137.3334 [M+Na]$^+$ (calculated: 2137.3294); MS (MALDI, matrix DCTB + NaI): Second fraction, **1b-A$_3$B**, *m/z* 2058.5 [M+Na]$^+$ (calculated: 2058.4); MS (MALDI, matrix ditranol): Third fraction: **1b-A$_4$**, *m/z*, 1960.6 (calculated: 1960.6); UV-vis (THF), λmax (log ε): 713 (3.97), 676 (3.84), 653 (sh), 613 (sh), 357 (3.49) nm.

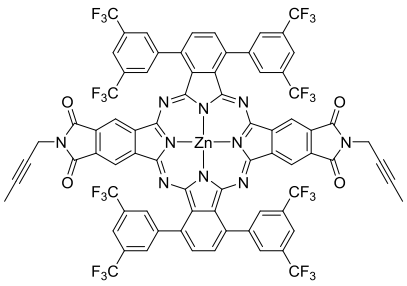

Compound 1c-ABAB: See **Chapter 1**.

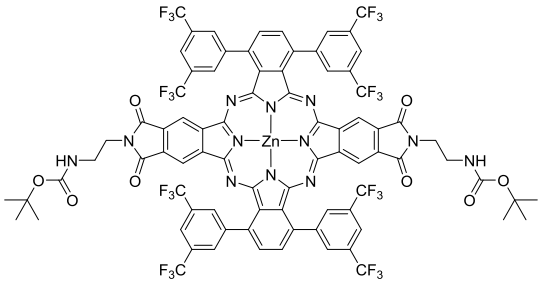

Compound 1d-ABAB: Compound **1d-ABAB** was synthesized from **6d**. The product was purified by column chromatography on SiO_2 (THF/heptane in gradient from 1:2 to 3:1) where the first fraction to elute containing the desired product **1d-ABAB**, followed by compounds **1d-A$_3$B**, and **1d-A$_4$**. The product was further purified by an additional column chromatography on Bio-Beads using $CHCl_3$ as eluent. After evaporation of the solvent a blue solid was obtained, which was washed with heptane. Yield: 6.3 mg, (3%). ^{1}H NMR (300 MHz, THF-d_8): δ 1.43 (s, 18H, CH_3), 3.42-3.53 (m, 4H, CH_2), 3.99 (t, 4H, *J* = 5.24 Hz, CH_2), 6.40 (br s, 2H, NH), 8.37 (s, 4H, Ar), 8.54 (s, 4H, Ar), 8.71 (s, 4H, Ar), 8.80 (s, 8H, Ar); ^{13}C NMR (75 MHz, THF-d_8): 28.7 (CH_3), 39.3 (CH_2), 39.9 (CH_2), 78.6 (C*(CH_3)$_3$), 117.9 (C Ar), 125.0 (q, *J* = 277.2 Hz, CF_3), 131.9 (br s, C*CF_3), 132.5 (C Ar), 132.8 (C Ar), 132.9 (C Ar), 134.2 (C Ar), 136.8 (CH Ar), 138.3 (CH Ar), 142.6 (CH Ar), 143.9 (CH Ar), 153.8 (C=N), 155.0 (C=O), 156.9 (C=N), 168.1 (C=O); IR(ATR) v^{-1} (cm^{-1}): 1770, 1717, 1384, 1276, 1180, 1133; HR-MS (MALDI, matrix DCTB + PPGNa 2000): First fraction, **1d-ABAB**, *m/z* 1848.2635 [M^+] (calculated: 1848.2621); second fraction, **1d-A$_3$B**, *m/z* 1636.3289 (calculated: 1636.3296); UV-vis (THF), λ_{max} (log ε): 709 (4.75), 676 (4.66), 648 (sh), 614 (sh), 355 (4.29) nm.

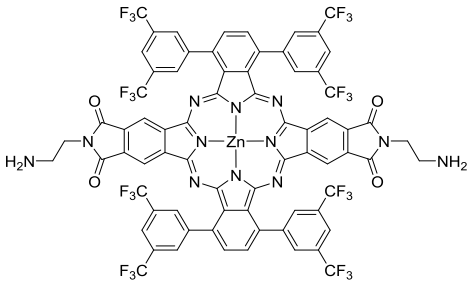

Compound 1f-ABAB: A mixture of **1d-ABAB** (4 mg, 0.0022 mmol) and trifluoroacetic acid (4 x 19 μL, every 30 minutes) in dry CH_2Cl_2 (1 mL) was stirred at rt in an argon atmosphere and monitored by TLC. After the reaction was completed the volatiles were removed under reduced pressure, then the residue was dissolved in CH_2Cl_2 (15 mL), washed with H_2O (3x15 mL) and concentrated in vacuum. Yield: 3.1 mg, (87%). ^{1}H NMR (300 MHz, THF-d_8): δ 8.81 (s, 8H, Ar), 8.60 (s, 4H, Ar), 8.53 (s, 4H, Ar), 8.26 (s, 4H, Ar), 4.22 (br s, 4H, CH_2), 3.52 (br s, 4H, CH_2); IR(ATR) v^{-1} (cm^{-1}): 3283, 1770, 1716, 1690, 1386, 1278, 1182, 1133;HR-MS (ESI Positive TOF_MS-500-4000.m): 1649.1644 $[M+H]^+$ (calculated: 1649.1650); UV-vis (THF), λmax (log ε): 709 (4.48), 676 (4.39), 649 (sh), 614 (sh), 357 (4.09) nm.

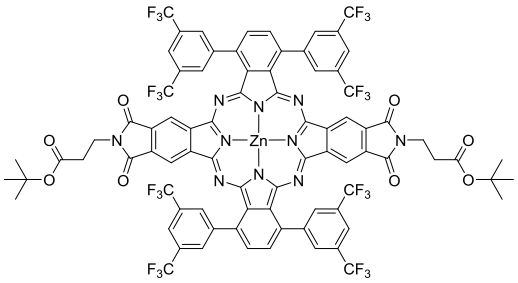

Compound 1e-ABAB: Compound **1e-ABAB** was synthesized from **6e**. The product was purified by column chromatography on SiO_2 (dioxane/heptane in gradient from 1:1 to 1:0) where the first fraction to elute containing the desired product **1e-ABAB**, followed by compounds **1e-A$_3$B**, and **1e-A$_4$**. The product was further purified by an additional column chromatography on Bio-Beads using $CHCl_3$ as eluent. After evaporation of the solvent a blue solid was obtained, which was washed with heptane. Yield: 5.2 mg, (2%). ^{1}H NMR (300 MHz, THF-d$_8$): δ 8.80 (s, 8H, Ar), 8.71 (s, 4H, Ar), 8.54 (s, 4H, Ar), 8.37 (s, 4H, Ar), 4.13 (t, 4H, *J* = 7.53 Hz, CH_2), 2.81 (t, 4H, *J* = 7.53 Hz, CH_2), 1.50 (s, 18H, CH_3); ^{13}C NMR (75 MHz, THF-d$_8$): δ 28.3 (CH_3), 34.9 (CH_2), 35.3 (CH_2), 81.0 (C*(CH_3)$_3$), 118.2 (C Ar), 125.0 (q, *J* = 272.7 Hz, CF_3), 131.9 (br s, C*CF_3), 132.5 (C Ar), 133.0 (C Ar), 134.1 (C Ar), 136.8 (CH Ar), 138.4 (CH Ar), 142.6 (CH Ar), 143.8 (CH Ar), 153.7 (C=N), 155.0 (C=N), 167.7 (C=O), 170.5 (C=O); IR(ATR) v^{-1} (cm^{-1}): 1766, 1714, 1386, 1277, 1178, 1128, 1094, 1040; HR-MS (MALDI, matrix DCTB + PPGNa 2000): First fraction, **1e-ABAB**, *m/z* 1818.2439 [M^+] (calculated: 1818.2403), 1840.2975 [$M+Na^+$]; MS (MALDI, matrix DCTB): Second fraction, **1e-A$_3$B**, *m/z* 1591.2 (calculated: 1591.3); third fraction: **1e-A$_4$**, *m/z*, 1364.3 (calculated: 1364.4); UV-vis (THF), λ_{max} (log ε): 711 (5.09), 676 (4.99), 650 (sh), 613 (sh), 356 (4.67) nm.

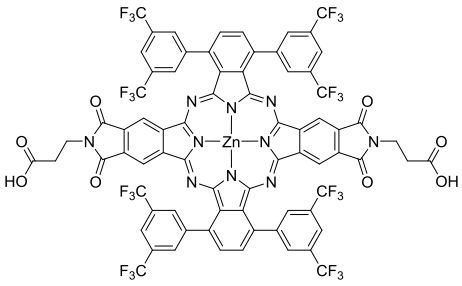

Compound 1g-ABAB: A mixture of **1e-ABAB** (3 mg, 0.0016 mmol) and trifluoroacetic acid (0.14 mL) in dry CH_2Cl_2 (0.40 mL) was stirred at rt for 30 minutes in an argon atmosphere. The volatiles were removed under reduced pressure, then the residue was dissolved in CH_2Cl_2 (15 mL), washed with H_2O (15 mL x3) and concentrated in vacuum. Yield: 2.5 mg, (90%). ^{1}H NMR (300 MHz, THF-d$_8$): δ 8.80 (s, 8H, Ar), 8.72 (s, 4H, Ar), 8.54 (s, 4H, Ar), 8.36 (s, 4H, Ar), 4.14 (t, 4H, *J* = 7.45 Hz, CH_2), 2.86 (t, 4H, *J* = 7.45 Hz, CH_2); IR(ATR) v^{-1} (cm^{-1}): 3281 (O-H st), 2919 (O-H st), 2851 (O-H st), 1690 (C=O st); HR-MS (MALDI, matrix DCTB + PEGNa 1500): *m/z* 1706.1114 [M^+] (calculated: 1706.1151), 1729.9667 [$M+Na^+$]; UV-vis (THF), λmax (log ε): 710 (4.23), 676 (4.14), 650 (sh), 613 (sh), 357 (3.79) nm.

2.6. References

(1) Singh, S.; Aggarwal, A.; Bhupathiraju, N. V. S. D. K.; Arianna, G.; Tiwari, K.; Drain, C. M. Glycosylated Porphyrins, Phthalocyanines, and Other Porphyrinoids for Diagnostics and Therapeutics. *Chem. Rev.* **2015**, *115* (18), 10261–10306.

(2) Almeida-Marrero, V.; van de Winckel, E.; Anaya-Plaza, E.; Torres, T.; de la Escosura, A. Porphyrinoid Biohybrid Materials as an Emerging Toolbox for Biomedical Light Management. *Chem. Soc. Rev.* **2018**, *47* (19), 7369–7400.

(3) Sorokin, A. B. Phthalocyanine Metal Complexes in Catalysis. *Chem. Rev.* **2013**, *113* (10), 8152–8191.

(4) Martínez-Díaz, M. V.; de la Torre, G.; Torres, T. Lighting Porphyrins and Phthalocyanines for Molecular Photovoltaics. *Chem. Commun.* **2010**, *46* (38), 7090–7108.

(5) Imahori, H.; Umeyama, T.; Kurotobi, K.; Takano, Y. Self-Assembling Porphyrins and Phthalocyanines for Photoinduced Charge Separation and Charge Transport. *Chem. Commun.* **2012**, *48* (34), 4032–4045.

(6) de la Torre, G.; Bottari, G.; Torres, T. Phthalocyanines and Subphthalocyanines: Perfect Partners for Fullerenes and Carbon Nanotubes in Molecular Photovoltaics. *Adv. Energy Mater.* **2016**, 1601700.

(7) Kingsborough, R. P.; Swager, T. M. A Highly Conductive Macrocycle-Linked Metallophthalocyanine Polymer. *Angew. Chemie Int. Ed.* **2000**, *39* (16), 2897–2900.

(8) Fazio, E.; Haynes, C. J. E.; de la Torre, G.; Nitschke, J. R.; Torres, T. A Giant M2L3 Metallo-Organic Helicate Based on Phthalocyanines as a Host for Electroactive Molecules. *Chem. Commun.* **2018**, *54* (21), 2651–2654.

(9) Lucky, S. S.; Soo, K. C.; Zhang, Y. Nanoparticles in Photodynamic Therapy. *Chem. Rev.* **2015**, *115* (4), 1990–2042.

(10) Li, X.; Lee, S.; Yoon, J. Supramolecular Photosensitizers Rejuvenate Photodynamic Therapy. *Chem. Soc. Rev.* **2018**, *47* (4), 1174–1188.

(11) Lovell, J. F.; Jin, C. S.; Huynh, E.; Jin, H.; Kim, C.; Rubinstein, J. L.; Chan, W. C. W.; Cao, W.; Wang, L. V; Zheng, G. Porphysome Nanovesicles Generated by Porphyrin Bilayers for Use as Multimodal Biophotonic Contrast Agents. *Nat. Mater.* **2011**, *10* (4), 324–332.

(12) Zou, Q.; Abbas, M.; Zhao, L.; Li, S.; Shen, G.; Yan, X. Biological Photothermal Nanodots Based on Self-Assembly of Peptide–Porphyrin Conjugates for Antitumor Therapy. *J. Am. Chem. Soc.* **2017**, *139* (5), 1921–1927.

(13) Li, X.; Lee, D.; Huang, J.-D.; Yoon, J. Phthalocyanine-Assembled Nanodots as Photosensitizers for Highly Efficient Type I Photoreactions in Photodynamic Therapy. *Angew. Chemie* **2018**, *130* (31), 10033–10038.

(14) Fazio, E.; Jaramillo-García, J.; de La Torre, G.; Torres, T. Efficient Synthesis of ABAB Functionalized Phthalocyanines. *Org. Lett.* **2014**, *16* (18), 4706–4709.

(15) Fazio, E.; Nazeerudin, M. K.; de la Torre, G.; Medel, M.; Grätzel, M.; Jaramillo-García, J.; Urbani, M.; Torres, T. ABAB Phthalocyanines: Scaffolds for Building Unprecedented Donor-π-Acceptor Chromophores. *ChemistryOpen* **2016**, *6* (1), 121–127.

(16) Youngblood, W. J. Synthesis of a New Trans-A2B2 Phthalocyanine Motif as a Building Block for Rodlike Phthalocyanine Polymers. *J. Org. Chem.* **2006**, *71*,

3345–3356.

(17) P. A. Stuzhin, C. E. The Porphyrin Handbook. In *The Porphyrin Handbook*; Kadish, K. M., K. M. Smith, R. G., Eds.; Academic Press: San Diego, 2003; pp 263–364.

(18) Bakboord, J. V.; Cook, M. J.; Hamuryudan, E. Non-Uniformly Substituted Phthalocyanines and Related Compounds: Alkylated Tribenzo-Imidazolo[4,5]-Porphyrazines. *J. Porphyr. Phthalocyanines* **2000**, *04* (05), 510–517.

(19) Knawby, D. M.; Swager, T. M. Liquid-Crystalline Heterocyclic Phthalocyanine Analogues Based on Thiophene. *Chem. Mater.* **1997**, *9* (2), 535–538.

(20) Pardo, C.; Yuste, Ma.; Elguero, J. Tetraimidazophthalocyanines. *J. Porphyr. Phthalocyanines* **2000**, *04* (05), 505–509.

(21) Kobayashi, N.; Ohya, T.; Sato, M.; Nakajima, S. Synthesis and Spectroscopic Properties of Symmetrically Tetrasubstituted Phthalocyanines with Four Alkyl or Aryl Chains or Porphyrin, Adamantane, Crown, or Quinone Units Attached. *Inorg. Chem.* **1993**, *32* (9), 1803–1808.

(22) Gonidec, M.; Amabilino, D. B.; Veciana, J. Novel Double-Decker Phthalocyaninato Terbium(Iii) Single Molecule Magnets with Stabilised Redox States. *Dalt. Trans.* **2012**, *41* (44), 13632–13639.

(23) Li, X.; Sinks, L. E.; Rybtchinski, B.; Wasielewski, M. R. Ultrafast Aggregate-to-Aggregate Energy Transfer within Self-Assembled Light-Harvesting Columns of Zinc Phthalocyanine Tetrakis(Perylenediimide). *J. Am. Chem. Soc.* **2004**, *126* (35), 10810–10811.

(24) Mezei, G.; Venter, A. R.; Kreft, J. W.; Urech, A. A.; Mouch, N. R. Monomeric, Not Tetrameric Species Are Responsible for the Colossal Dielectric Constant of Copper Phthalocyanine Derived from Pyromellitic Dianhydride. *RSC Adv.* **2012**, *2* (28), 10466–10469.

(25) Macdonald, I. J.; Dougherty, T. J. Basic Principles of Photodynamic Therapy. *J. Porphyr. Phthalocyanines* **2001**, *05* (02), 105–129.

(26) Bhupathiraju, N. V. S. D. K.; Rizvi, W.; Batteas, J. D.; Drain, C. M. Fluorinated Porphyrinoids as Efficient Platforms for New Photonic Materials, Sensors, and Therapeutics. *Org. Biomol. Chem.* **2016**, *14* (2), 389–408.

(27) Opris, D. M.; Nüesch, F.; Löwe, C.; Molberg, M.; Nagel, M. Synthesis, Characterization, and Dielectric Properties of Phthalocyanines with Ester and Carboxylic Acid Functionalities. *Chem. Mater.* **2008**, *20* (21), 6889–6896.

(28) Tylleman, B.; Gómez-Aspe, R.; Gbabode, G.; Geerts, Y. H.; Sergeyev, S. Ester-Functionalized Phthalonitriles and Zinc Phthalocyanines via Palladium-Catalyzed Cyanation of 4,5-Dichlorophthalates. *Tetrahedron* **2008**, *64* (19), 4155–4161.

(29) Wöhrle, D.; Eskes, M.; Shigehara, K.; Yamada, A. A Simple Synthesis of 4,5-Disubstituted 1,2-Dicyanobenzenes and 2,3,9,10,16,17,23,24-Octasubstituted Phthalocyanines. *Synthesis (Stuttg).* **1993**, *2*, 194–196.

(30) Valverde, I. E.; Delmas, A. F.; Aucagne, V. Click à La Carte: Robust Semi-Orthogonal Alkyne Protecting Groups for Multiple Successive Azide/Alkyne Cycloadditions. *Tetrahedron* **2009**, *65* (36), 7597–7602.

Chapter 3 – Assessing amphiphilic ABAB Zn(II)Pcs with enhanced photosensitization abilities in *in vitro* PDT studies against cancer

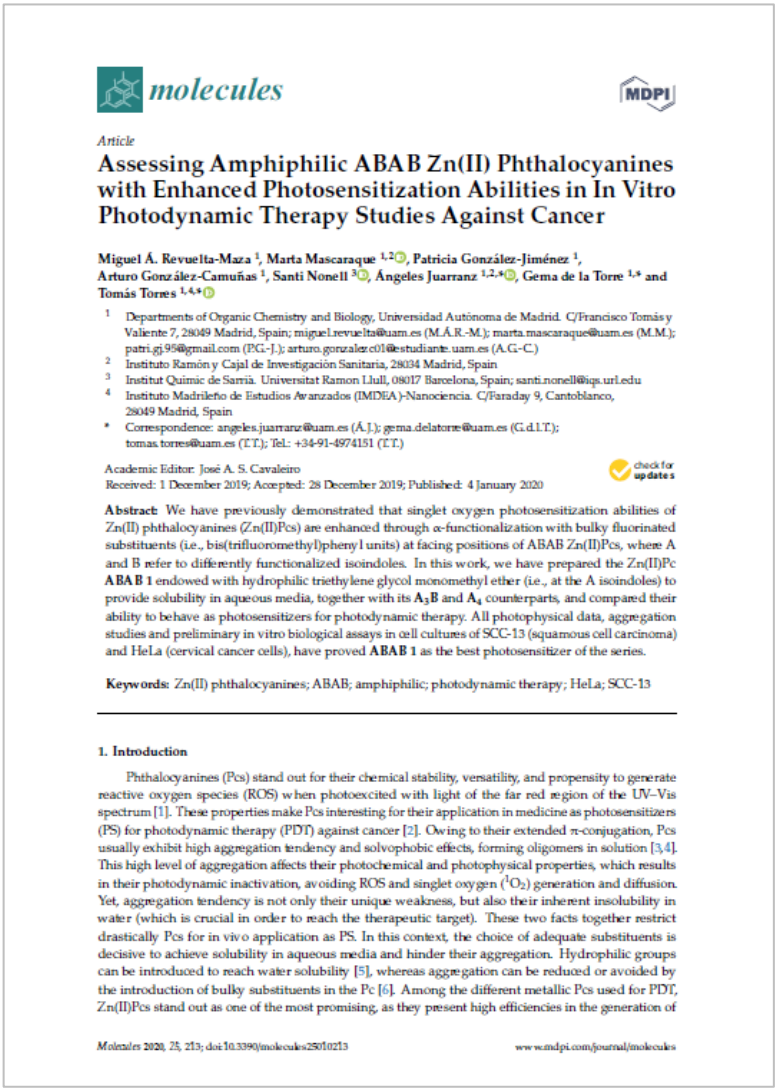

molecules

MDPI

Article

Assessing Amphiphilic ABAB Zn(II) Phthalocyanines with Enhanced Photosensitization Abilities in In Vitro Photodynamic Therapy Studies Against Cancer

Miguel Á. Revuelta-Maza [1], Marta Mascaraque [1,2], Patricia González-Jiménez [1], Arturo González-Camuñas [1], Santi Nonell [3], Ángeles Juarranz [1,2,*], Gema de la Torre [1,*] and Tomás Torres [1,4,*]

1 Departments of Organic Chemistry and Biology, Universidad Autónoma de Madrid. C/Francisco Tomás y Valiente 7, 28049 Madrid, Spain; miguel.revuelta@uam.es (M.Á.R.-M.); marta.mascaraque@uam.es (M.M.); patri.gj.95@gmail.com (P.G.-J.); arturo.gonzalezc01@estudiante.uam.es (A.G.-C.)
2 Instituto Ramón y Cajal de Investigación Sanitaria, 28034 Madrid, Spain
3 Institut Químic de Sarrià. Universitat Ramon Llull, 08017 Barcelona, Spain; santi.nonell@iqs.url.edu
4 Instituto Madrileño de Estudios Avanzados (IMDEA)-Nanociencia. C/Faraday 9, Cantoblanco, 28049 Madrid, Spain
* Correspondence: angeles.juarranz@uam.es (Á.J.); gema.delatorre@uam.es (G.d.l.T.); tomas.torres@uam.es (T.T.); Tel.: +34-91-4974151 (T.T.)

Academic Editor: José A. S. Cavaleiro
Received: 1 December 2019; Accepted: 28 December 2019; Published: 4 January 2020

check for updates

Abstract: We have previously demonstrated that singlet oxygen photosensitization abilities of Zn(II) phthalocyanines (Zn(II)Pcs) are enhanced through α-functionalization with bulky fluorinated substituents (i.e., bis(trifluoromethyl)phenyl units) at facing positions of ABAB Zn(II)Pcs, where A and B refer to differently functionalized isoindoles. In this work, we have prepared the Zn(II)Pc **ABAB 1** endowed with hydrophilic triethylene glycol monomethyl ether (i.e., at the A isoindoles) to provide solubility in aqueous media, together with its $\mathbf{A_3B}$ and $\mathbf{A_4}$ counterparts, and compared their ability to behave as photosensitizers for photodynamic therapy. All photophysical data, aggregation studies and preliminary in vitro biological assays in cell cultures of SCC-13 (squamous cell carcinoma) and HeLa (cervical cancer cells), have proved **ABAB 1** as the best photosensitizer of the series.

Keywords: Zn(II) phthalocyanines; ABAB; amphiphilic; photodynamic therapy; HeLa; SCC-13

1. Introduction

Phthalocyanines (Pcs) stand out for their chemical stability, versatility, and propensity to generate reactive oxygen species (ROS) when photoexcited with light of the far red region of the UV–Vis spectrum [1]. These properties make Pcs interesting for their application in medicine as photosensitizers (PS) for photodynamic therapy (PDT) against cancer [2]. Owing to their extended π-conjugation, Pcs usually exhibit high aggregation tendency and solvophobic effects, forming oligomers in solution [3,4]. This high level of aggregation affects their photochemical and photophysical properties, which results in their photodynamic inactivation, avoiding ROS and singlet oxygen ($^1O_2$) generation and diffusion. Yet, aggregation tendency is not only their unique weakness, but also their inherent insolubility in water (which is crucial in order to reach the therapeutic target). These two facts together restrict drastically Pcs for in vivo application as PS. In this context, the choice of adequate substituents is decisive to achieve solubility in aqueous media and hinder their aggregation. Hydrophilic groups can be introduced to reach water solubility [5], whereas aggregation can be reduced or avoided by the introduction of bulky substituents in the Pc [6]. Among the different metallic Pcs used for PDT, Zn(II)Pcs stand out as one of the most promising, as they present high efficiencies in the generation of

3.1. Citation and contribution

Revuelta-Maza, M. A.; Mascaraque, M.; González-Jiménez, P.; González-Camuñas, A.; Nonell, S.; Juarranz, A.; de la Torre, G. and Torres, T. Assessing amphiphilic ABAB Zn(II) phthalocyanines with enhanced photosensitization abilities in in vitro photodynamic therapy studies against cancer. *Molecules* **2020**, *25*, 213; https://doi.org/10.3390/molecules25010213

Contribution: Revuelta-Maza, M. A.: Synthesis and characterization (together with P. G.-J. and A. G.-C.), photophysical and aggregation studies. Preparation of the manuscript.

Funding and supervision: Nonell, S.; Juarranz, A.; de la Torre, G. and Torres, T. This research was funded by MINECO, Spain (CTQ2017-85393-P and CTQ2016-78454-C2-1-R).

Abstract:

Singlet oxygen photosensitization abilities of Zn(II) phthalocyanines have been previously shown to be enhanced through α-functionalization with bulky fluorinated substituents (i.e. bis(trifluoromethyl)phenyl units) at facing positions of ABAB Zn(II)Pcs, where A and B refer to differently functionalized isoindoles. In this work, we have prepared the Zn(II)Pc **ABAB 1** endowed with hydrophilic triethylene glycol monomethyl ether (i.e. at the A isoindoles) to provide solubility in aqueous media, and compared its ability to behave as photosensitizer in photodynamic therapy with regard to those exhibited by its **A_3B** and **A_4** counterpartners. All photophysical data, aggregation studies and preliminary *in vitro* biological assays in cell cultures of SCC-13 (squamous cell carcinoma) and HeLa (cervical cancer cells), have proved **ABAB 1** as the best photosensitizer of the series.

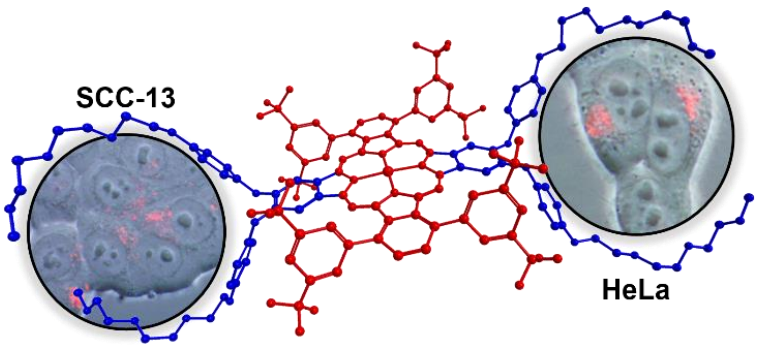

3.2. Introduction and Objectives

The use of polyethylene glycol (PEG) chains is a popular approach to enhance the biocompatibility of hydrophobic drugs in general,[1] and of PDT agents in particular. Among other advantages, PEG chains lead to a prolonged blood-circulating lifetime, allows for the minimization of non-specific uptake, and favors the enhanced permeability and retention (EPR) effect. All that features combined can result in an elevated concentration of the drug at the tumor site.[2] From a chemical point of view, PEG chains have proven to enhance the solubility in a variety of solvents, including non-polar solvents, aprotic polar solvents like DMSO, and protic polar solvents such as water.[3,4] Several Pcs functionalized with PEG chains of different length as peripheral[2,4–6] or axial groups[7,8] have shown solubility in biological media, and some of them have been studied as PS for PDT.[9,10] Herein, we report on the synthesis and characterization of a series of triethylene glycol (TEG)-containing Zn(II)Pcs, namely **ABAB, A_3B** and **A_4** Zn(II)Pcs **1**, the study of their $^1O_2$ generation capabilities, and preliminary biological assays to determine their potential as PS for PDT. The main objective, in connection with **Chapters 1 and 2**, is to confirm whether the presence of trifluoromethylphenyl groups that enhance the photophysical properties of PS, maintain these benefits when testing them *in vitro*.

For that purpose, we have undertaken two synthetic pathways: i) a convergent route that allows to obtain generic ABAB or A_3B Zn(II)Pcs functionalized with free phenolic groups (**ABAB-2** and **A_3B-2** Zn(II)Pcs in Scheme 3. 1), which represent synthons over which it is possible to add hydrophilic groups such as PEG chains; and ii) the straightforward preparation of **ABAB-1** and **A_3B-1** (and also **A_4-1**) starting from adequately functionalized phthalonitriles. We have performed aggregation and photophysical studies in solution, over this family of compounds in order to ratify our previous results regarding the enhanced $^1O_2$ generation abilities of the non-aggregated ABAB-type Zn(II)Pc compounds with regard to A_3B and A_4 counterparts (see **Chapter 1**).[11] Going one step further, we have performed *in vitro* assays in order to examine the toxicity of **ABAB-1**, **A_3B-1** and **A_4-1** in different tumor cells, i.e. SCC-13 and HeLa, as well as their cell localization. The final goal here is to demonstrate the benefits of bis(trifluoromethyl)phenyl-containing Zn(II)Pcs versus other substitution patterns.

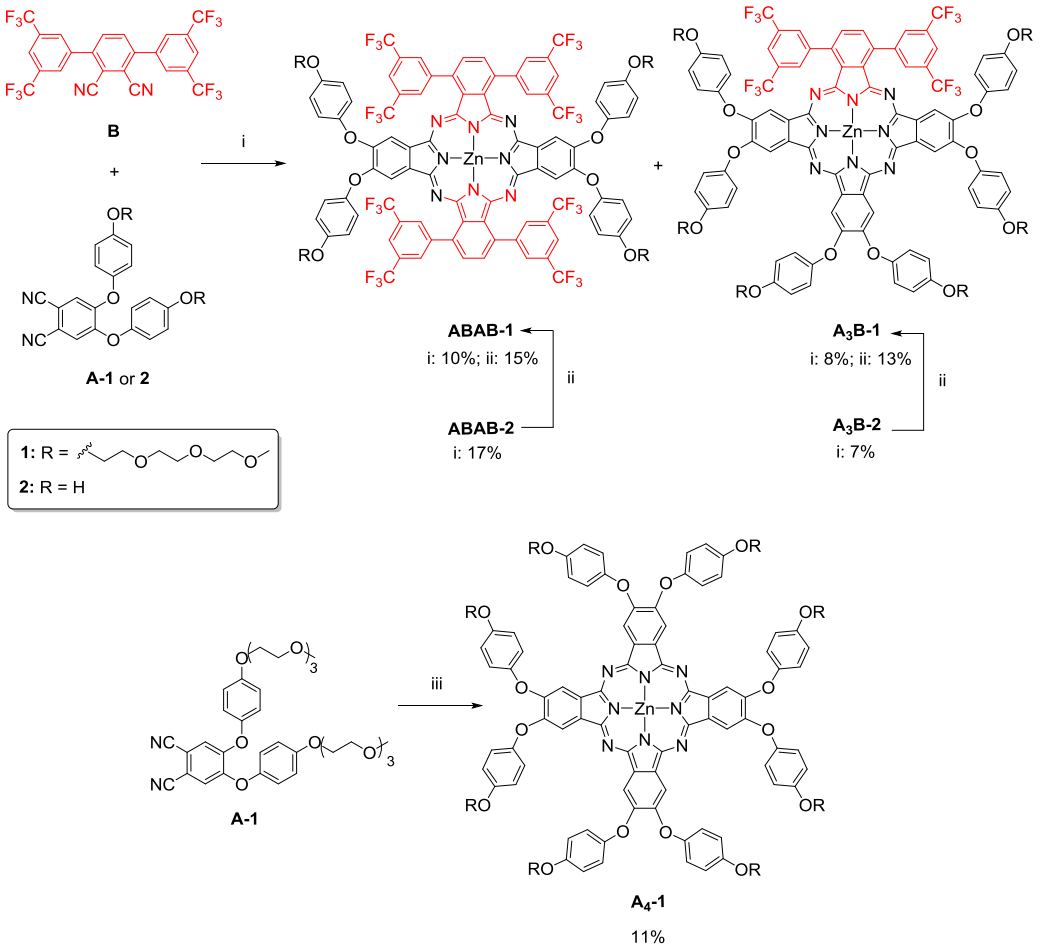

*Scheme 3. 1. Synthesis of triethylene glycol monomethyl ether substituted **ABAB-1**, **A_3B-1** and **A_4-1** Zn(II)Pcs. i) $Zn(OAc)_2$, o-DCB/DMF (2:1), 150 °C, 15 h; ii) TEG-Ts, K_2CO_3, DMF, 50°C, overnight; iii) $Zn(OAc)_2$, pentanol, DBU, 150 °C, 1h.*

3.3. Results and discussion

a) Synthesis

For the preparation of our targeted Zn(II)Pcs, in particular **ABAB-1** and **A_3B-1,** endowed with both bulky groups over B isoindolic rings and hydrophilic TEG substituents over the A positions, we have performed cross-condensation reactions with the bulky phthalonitrile **B**, and either **A-1**, already containing the TEG moieties, or 4,5-bis(4-hydroxyphenoxy)phthalonitrile **A-2** (see Scheme 3. 1).[12] The latter approach, yielding the intermediate Zn(II)Pcs **ABAB-2** and **A_3B-2,** that should be further *O*-alkylated, was tackled on the basis of previous studies, which had shown that the crossed condensation

between **B** and the protected form of **A-2** is a highly efficient process (see **Chapter 1**).[13] Phthalonitrile **A-1** was thus prepared by *O*-alkylation of **A-2**[12] with the tosyl derivative of triethylene glycol monomethyl ether (**TEG-Ts**)[14] in 53% yield (see Scheme 3. 2).

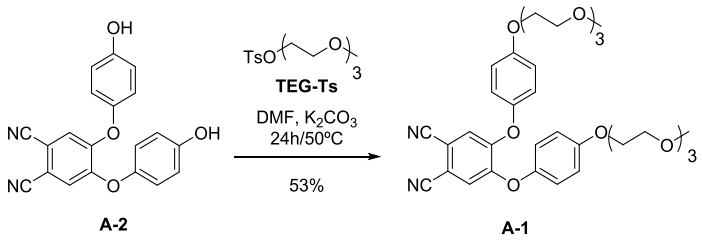

*Scheme 3. 2. Synthesis of ftalonitrile **A-1** from **A-2**.*

Then, the reaction between phthalonitriles **A** and **B** was carried out by heating at 150 °C an equimolar mixture of them in *o*-DCB/DMF and in the presence of $Zn(OAc)_2$. For the selected **A**:**B** ratio, the yield in A_3B Zn(II)Pcs is lower (8% for **A_3B-1** and 7% for **A_3B-2**,) than those obtained for their corresponding ABAB Zn(II)Pcs (10% for **ABAB-1** and 17%, for **ABAB-2**). The *O*-alkylation reaction of **ABAB-2** and **A_3B-2** with **TEG-Ts** to give, respectively, **ABAB-1** and **A_3B-1** took place in poor yields (15% and 13%, respectively), making this linear approach less efficient than the preparation of **A-1** and its condensation with **B**. It is worth mentioning that the symmetric A_4 Zn(II)Pc is not detected quantitatively in any reaction mixture. This symmetric octasubstituted TEG-Zn(II)Pc **A_4-1** is useful to perform a full comparative study of the influence of the bulky fluorinated substituents and the TEG moieties on the solubility, aggregation and $^1O_2$ generation studies of this family of Zn(II)Pcs. In this context, this molecule was synthesized through a direct self-condensation of **A-1** phthalonitrile, using in this case the classical pentanol/DBU conditions, which gave rise to **A_4-1** in 11% yield.

Figure 3. 1 shows the ^{1}H NMR spectra of **ABAB-1**, **A_3B-1** and **A_4-1**. The signal pattern for each compound arises from the molecular symmetry group these compounds belong to, namely, D_{2h} for **ABAB-1,** C_{2h} for **A_3B-1** and D_{4h} for **A_4-1**.Thus, highly symmetrical **A_4-1** presents less signals than **ABAB-1**, which at the same time exhibits a simpler spectrum than **A_3B-1**. The ^{1}H NMR of **ABAB-1**, shows 4 singlets for the aromatic protons of the isoindole units and the bulky groups, two doublets for the phenoxy substituents, and a set of signals for the TEG chains with a chemical shift between 3.0 and 4.5 ppm. **A_3B-1** produces 6 singlets for the isoindole units and the trifluoromethylphenyl substituents, and a multiplet that corresponds to the presence of three types of phenoxy groups. Figure 3. 1 also shows structural models for the three compounds, where the molecular amphiphilic nature is represented in blue (hydrophilic zone) and yellow (hydrophobic zone). The products show good solubility in polar media, and, although

they are no soluble directly in water due to the strong amphiphilic character, they are soluble in DMSO/water or MeOH/water (1:99) mixtures.

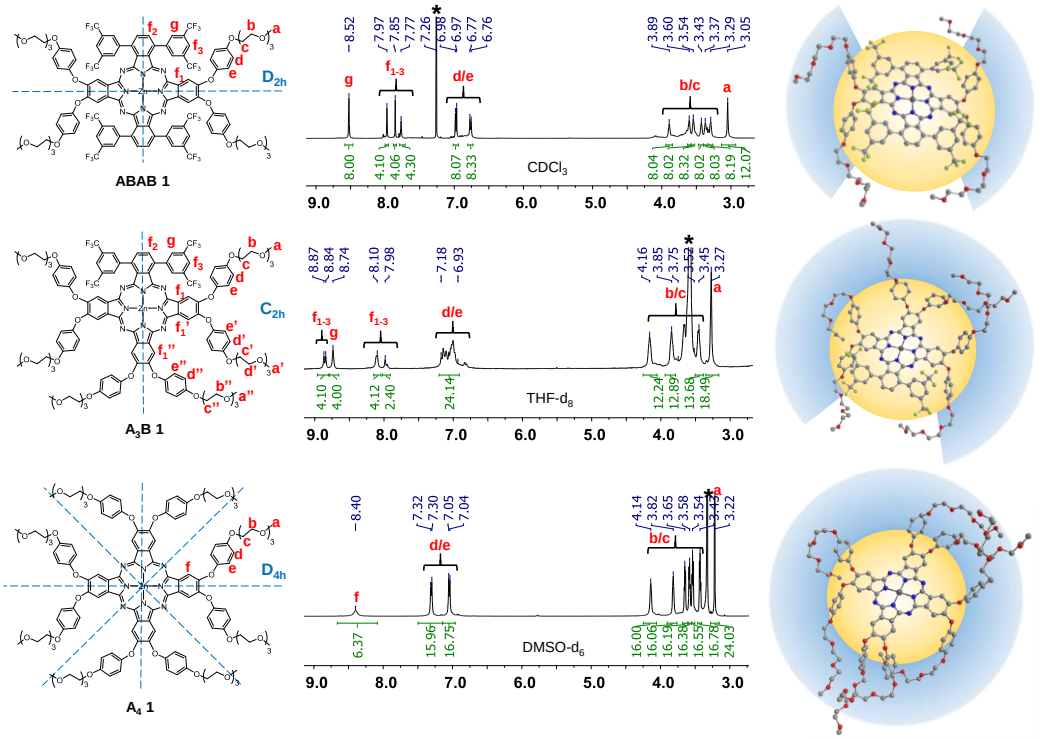

*Figure 3. 1. ^{1}H NMR spectra for **ABAB-1** (in $CDCl_3$), **A_3B-1** (in THF-d_8) and **A_4-1** (in DMSO-d_6). Geometry optimization (MM2, SCIGRESS (FJ 2.8.1 EU 3.3.1)) for each molecule is shown, with a representation of their molecular amphiphilic character: hydrophobic area (yellow), hydrophilic area (blue).*

b) Photophysical studies

The UV-vis spectra of **ABAB-1** and **A_3B-1**, in both non-coordinating toluene and coordinating THF, show split *Q*-bands, accompanied by the typical vibrational absorptions, although splitting is much more pronounced in **ABAB-1**, which is consistent with its D_{2h} symmetry (e.g. Figure 3. 2 and Table 3. 1). Indeed, the absorption spectra of thesecompounds (i.e. in THF and toluene solutions) do not show any evidence of aggregation, as otherwise expected due to the presence of rather bulky substituents at the non-peripheral positions of the Pc core. Further confirmation of the lack of aggregation for these Zn(II)Pc results from absorption studies performed at a range of concentrations (between ~$0.5\cdot10^{-6}$ M – $5\cdot10^{-6}$ M in toluene) (e.g. Figure 3. 2), with an analysis of linear regression between the intensity of the *Q*-band and the concentration giving R^2 values of ~0.999. **A_4-1**, with a regular single *Q*-band in its UV-vis spectrum in

toluene, does not show evidence of aggregation either,. Increasing the number of α-bis(trifluoromethyl)phenyl substituents produces a red-shift of the *Q*-band maximum, namely, from 682 nm for **A_4-1** to 712 nm for **ABAB-1** in toluene solutions (Table 3. 1).

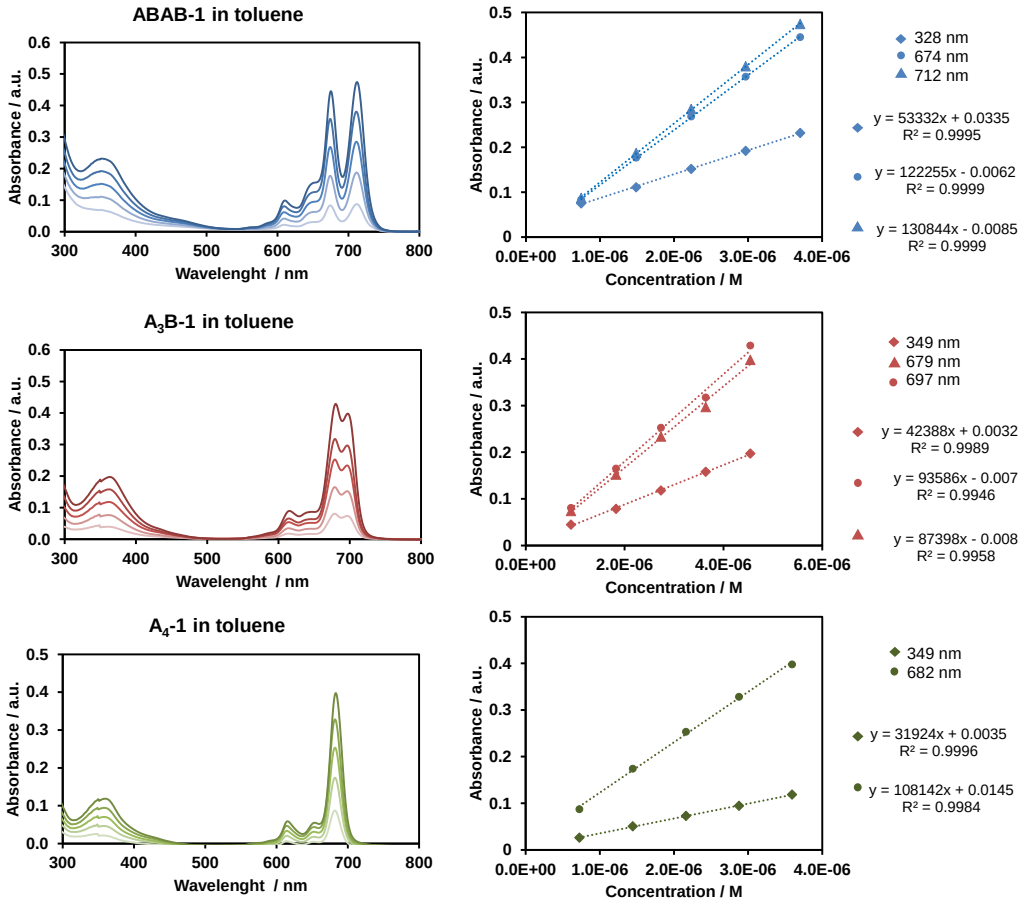

*Figure 3. 2. UV-vis spectra for concentration-dependent studies of **ABAB-1**, **A_3B-1** and **A_4-1** in toluene. Linear regression between maxima intensity and concentration.*

On the other hand, fluorescence studies have been also performed in toluene and THF solutions of **ABAB-1**, **A_3B-1** and **A_4-1,** which showed an increase in the Stokes shift as the number of bis(trifluoromethyl)phenyl units attached to the Zn(II)Pc increases. Fluorescence quantum yield (Φ_F), and singlet state (τ_S) and triplet state (τ_T) lifetimes (extracted from Time-Resolved Fluorescence -TRF- experiments) are also included in Table 3. 1. The results are consistent with those of non-aggregated Zn(II)Pcs, and show a modest solvent dependence. The mono-exponential fluorescence decay kinetics confirm that **ABAB-1**, **A_3B-1** and **A_4-1** are in monomeric form in THF and toluene solutions, and the singlet excited-state lifetimes are similar between for the two solvents.

The quantification of the Φ_Δ, for **ABAB-1**, **A$_3$B-1** and **A$_4$-1** has been performed by two different methods. The first one entail the measurement of the photoinduced decomposition of DPBF in DMSO solutions. The spectroscopic data obtained from these measurements are shown in Figure 3. 3. For the three compunds, the DPBF absorption decrease was completely linear (R^2 = 0.99), while no change was observed in the absorption of Zn(II)Pcs during the measurement, which evidences that photobleaching is not taking place under the irradiation conditions. **ABAB-1**, **A$_3$B-1** and **A$_4$-1** showed Φ_Δ values of 93%, 85% and 53%, respectively. These values should be considered with caution since indirect methods could be subjected to different variables, but are useful for comparative purposes. From those results we can infer that the larger the number of bulky groups at α-positions, the better in the $^1O_2$ generation efficiency, as otherwise expected considering previous studies detailed in **Chapter 1**.[11] It is important to mention that aggregation is not considered to evaluate these results since the three compounds are non-aggregated in DMSO.

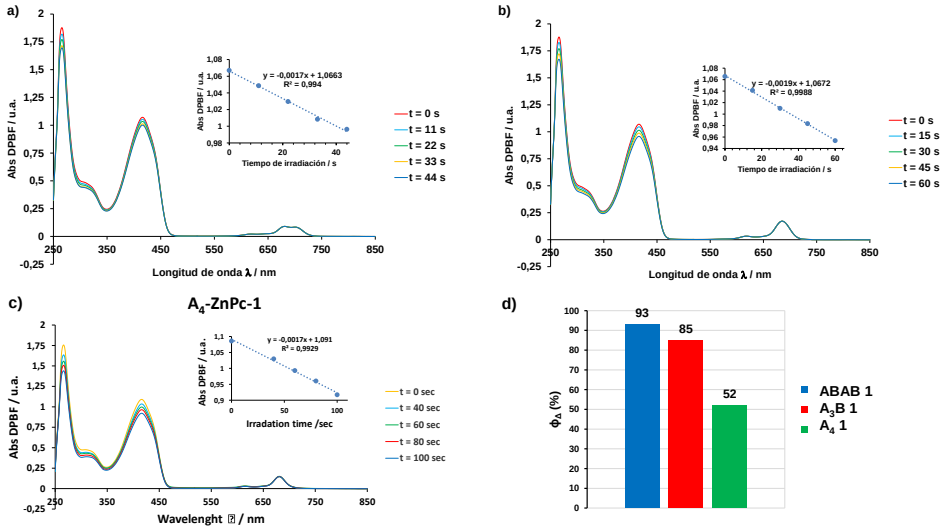

*Figure 3. 3. a-c) Absorbance decrease of DPBF over time due to $^1O_2$ photoinduced generation by **ABAB-1**, **A$_3$B-1** and **A$_4$-1** in DMSO. d) Representation of the relative $^1O_2$ efficiency of **ABAB-1** (93%), **A$_3$B-1** (85%) and **A$_4$-1** (52%).*

On the other hand, we have evaluated the Φ_Δ for **ABAB-1**, **A$_3$B-1** and **A$_4$-1** via the direct detection of $^1O_2$ phosphorescence at 1275 nm exciting at 355 nm, both in toluene and THF solutions (Table 3. 1).This method is detailed in Chapter 1. The Φ_Δ values show the same trend observed in the indirect measurements, namely, a parallel increase with the number of bulky fluorinated substituents and, indeed, Φ_F and Φ_Δ change concomitantly in the opposite direction. Overall, the measured Φ_Δ values are moderately higher than those reported for other amphiphilic Zn(II)Pcs, which confirms that the substitution pattern of

this family of compounds improves the photoproperties of the dye core, rendering them adequate for PDT applications.

*Table 3. 1. Photophysical properties of **ABAB**, **A_3B** and **A_4** Zn(II)Pcs 1 in toluene and THF.*

ZnPc	Solvent	logε (λ)	λ_f / nm	ϕ_f	τ_S / ns	τ_T / μs[a]	ϕ_Δ
ABAB-1	toluene	4.73 (328), 5.09 (674), 5.12 (712)[1]	715	0.13	1.7	0.35	0.77
A_3B-1	toluene	4.63 (349), 4.97 (679)[1], 4.94 (697)	702	0.17	2.1	0.47	0.71
A_4-1	toluene	4.50 (349), 5.03 (682)[1]	684	0.43	3.0	0.45	0.61
ABAB-1	THF	4.82 (349), 5.08 (671), 5.09 (703)[1]	709	0.13	1.7	0.30	0.83
A_3B-1	THF	4.71 (348), 5.03 (675)[1]	692	0.28	2.2	0.23	0.74
A_4-1	THF	4.61 (349), 5.12 (676)[1]	682	0.25	3.0	0.37	0.68

[1] λ absorption maxima

c) Aggregation experiments

Aggregation studies are fundamental for the former evaluation the potential application *in vitro* of the PS. Absorption and emission experiments were carried out over solutions of TEG-functionalized **ABAB-1**, **A_3B-1** and **A_4-1**. Although they are not soluble in pure water, they appear to be soluble upon addition from stock DMSO solutions to Milli-*Q* water until a 99:1 DMSO/water ratio is reached, what is admissible for further *in vitro* assays. Therefore, we performed aggregation studies by registering UV-vis and fluorescence spectra of the three Zn(II)Pcs in different mixtures of DMSO/water, in order to compare the specific behavior derived from the presence of two substituted isoindole units with bulky groups (**ABAB-1**) versus one (**A_3B-1**) or none of them (**A_4-1**). Mixed solutions of DMSO/water ranging from 100:0 to 1:99 were measured, in both absorption (Figure 3. 4) and emission (Figure 3. 5) experiments. Importantly, initial measurements in pure DMSO correspond to a fully non-aggregated state for the three compounds. Looking at absorbance spectra we can determine that from 100% to 80% DMSO, **ABAB-1** presents an almost constant absorption for the *Q*-band, whereas **A_3B-1** shows a gradual decrease of its intensity and broadening, as well as a rise of a band with shorter wavelength, compatible with the formation of cofacial *H*-type aggregated species. Furthermore, in the case of **ABAB-1**, when a 70:30 DMSO/water ratio is reached, the spectrum shows a sudden decrease of the *Q*-band intensity, and the concomitant emergence of a shoulder at lower wavelength. Below 70% of DMSO content, we could observe a constant behavior for both **ABAB-1** and **A_3B-1** compounds, indicating that a stable situation is reached. In the case of **A_4-1**, a sudden decrease of the *Q*-band, as well as a broadening and rising of a band at shorter wavelength compatible with the formation of aggregates, are observed starting at 80:20 DMSO/water ratios. In the case

of emission studies, we can discern that the fluorescence of **A_3B-1** and **A_4-1** shows a sharp decrease in intensity when the water proportion increases, until a total cancellation of fluorescence at 70:30 DMSO/water ratio. On the other hand, **ABAB-1** shows a similar behavior than that observed in the absorption spectrum, that is, is a huge decrease of the emission after the addition of 30% water. A magnification of this spectrum shows that,since this moment, a residual fluorescence signal remains with the same intensity, which means that an equilibriumsituation has been reached with the presence of non-aggregated species in the medium.

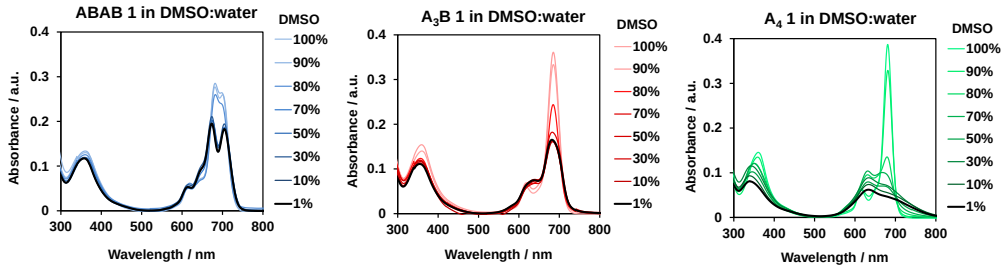

*Figure 3. 4. UV-vis spectra of **ABAB-1**, **A_3B-1** and **A_4-1** in different DMSO/water ratios.*

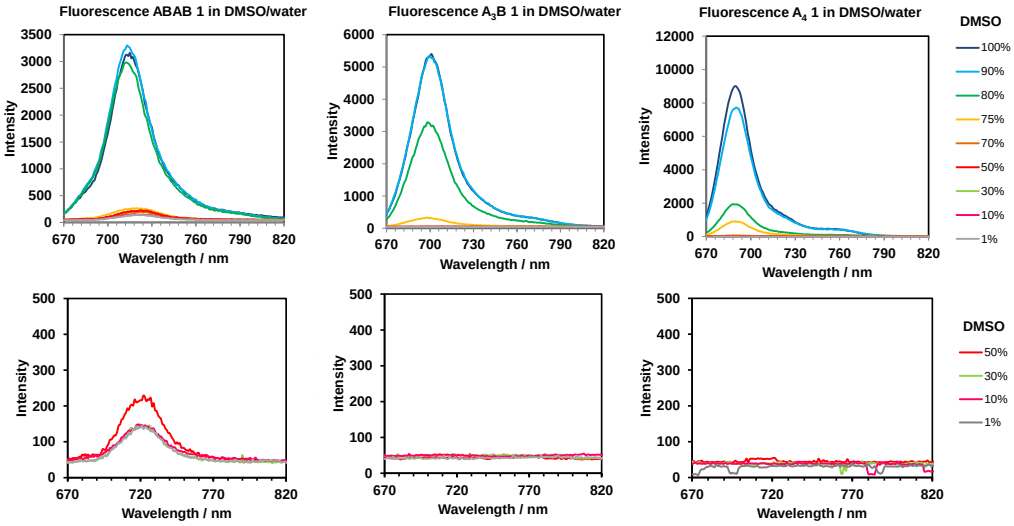

*Figure 3. 5. Fluorescence spectra of **ABAB-1**, **A_3B-1** and **A_4-1** in different DMSO/water ratios.*

d) Determination of the log Po/w

For a preliminar evaluation of the relative lipophilicity of **ABAB-1**, **A_3B-1** and **A_4-1**, and their affinity for cell membranes, n-octanol/PBS partition coefficients were determined

using the shake-flask method (see Figure 3. 6), which does not require standard compounds and is based on the direct determination of equilibrium partition concentrations of a compound in a biphasic system.

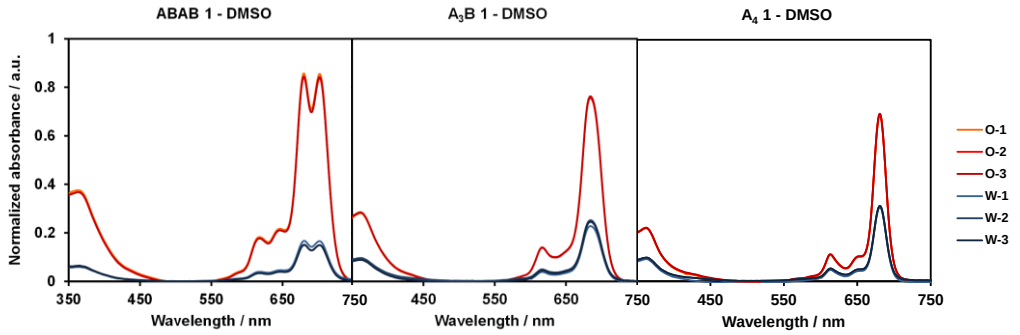

*Figure 3. 6. UV-vis spectra of the octanol (O) and water (W) phases (three consecutive experiments) in n-octanol/water partition experiments with **ABAB-1**, **A$_3$B-1** and **A$_4$-1**.*

Although the three compounds have a common structural Pc core, they exhibited different amphiphilic character. **ABAB-1** renders a higher octanol/water partition coefficient than **A$_3$B-1** and **A$_4$-1**, (see Figure 3. 7) thus indicating that the relative order of lipophilicity nature. In fact, the log $P_{O/W}$ values suggest that **ABAB-1** and **A$_3$B-1** are mostly hydrophobic and have very high affinity for membranes. On the other hand, **A$_4$-1** is more amphiphilic, and its presence in the aqueous phase is more abundant, which is concordant which its higher solubility in this medium.

Zn(II)Pc	$logP_{W/O}$
ABAB-1	0.74
A$_3$B-1	0.50
A$_4$-1	0.35

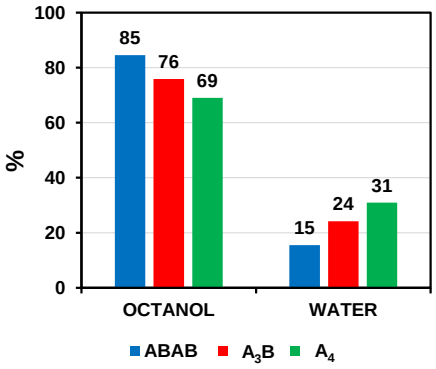

*Figure 3. 7. n-octanol/water partition experiments with **ABAB-1, A$_3$B-1** and **A$_4$-1.***

e) Biological studies

Biological experiments with HeLa (cervical adenocarcinoma cells) and SCC-13 (skin squamous carcinoma cells) strains have been performed using **ABAB-1**, **A_3B-1** and **A_4-1** as PS, in order to evaluate the potential of our designed PS

i. *Cytotoxicity studies*

Phototoxicity of some Zn(II)Pcs has already been tested against cervical and skin squamous carcinoma cells in *in vitro* experiments. However, due to the aggregation problems they present, it is necessary to transport them through complex conjugates.[15–17] Herein, we have studied the activity of **ABAB-1**, **A_3B-1** and **A_4-1** Zn(II)Pcs as independent molecular entities upon red light irradiation by the 3-(4,5-dimethylthiazol-2-yl)-2,5-diphenyltetrazolium bromide (MTT) assay in SCC-13 and HeLa cell lines. For this purpose, we first evaluated the inherent toxicity of two different concentrations of the three Zn(II)Pcs ($1\cdot10^{-6}$ and $1\cdot10^{-7}$ M) in cells, after 5 h of incubation in presence of PS in the dark. Separately, we have evaluated the possible damage caused by irradiation, treating the cells with the highest red light dose used in this work (9 J/cm^2), in the absence of the PS. The results shown in Table 3. 2 indicate that neither the presence of the Zn(II)Pc at these concentrations, nor the administration of red light, induced significant cytotoxic effects in the cell lines studied, and survival rates above 95% were obtained.

Table 3. 2. Toxicity effects in SCC-13 and HeLa cells induced by red light, in the absence of any Pcs, and by incubation with either of the Zn(II)Pcs 1 in the dark. Cell toxicity was evaluated by the MTT assay, 24 h after treatment.

Compound	Concentration [M]	Surviving fraction (% ± SD)[1]	
		SCC-13	HeLa
No Zn(II)Pc – Control dark		101 ± 2.4	100 ± 1.1
No Zn(II)Pc – Control light (9 J/cm^2)		100 ± 1.7	99 ± 2.3
ABAB-1	$1\cdot10^{-6}$	98 ± 5.4	101 ± 5.5
	$1\cdot10^{-7}$	102 ± 3.1	95 ± 2.8
A_3B-1	$1\cdot10^{-6}$	97 ± 6.3	97 ± 3.5
	$1\cdot10^{-7}$	99 ± 5.5	99 ± 3.6
A_4-1	$1\cdot10^{-6}$	99 ± 4.5	97 ± 5.5
	$1\cdot10^{-7}$	98 ± 5.0	98 ± 2.8

[1] Data are expressed as mean values obtained from three independent experiments ± standard deviation (SD).

Then, we evaluated the photodynamic activity of **ABAB-1**, **A_3B-1** and **A_4-1** toward SCC-13 and HeLa cells upon irradiation. For the photodynamic treatments, we used two different concentrations (i.e. $1 \cdot 10^{-6}$ and $1 \cdot 10^{-7}$ M) and, after 5 h of incubation, cells were exposed to different red light doses (3, 6 and 9 J/cm^2).

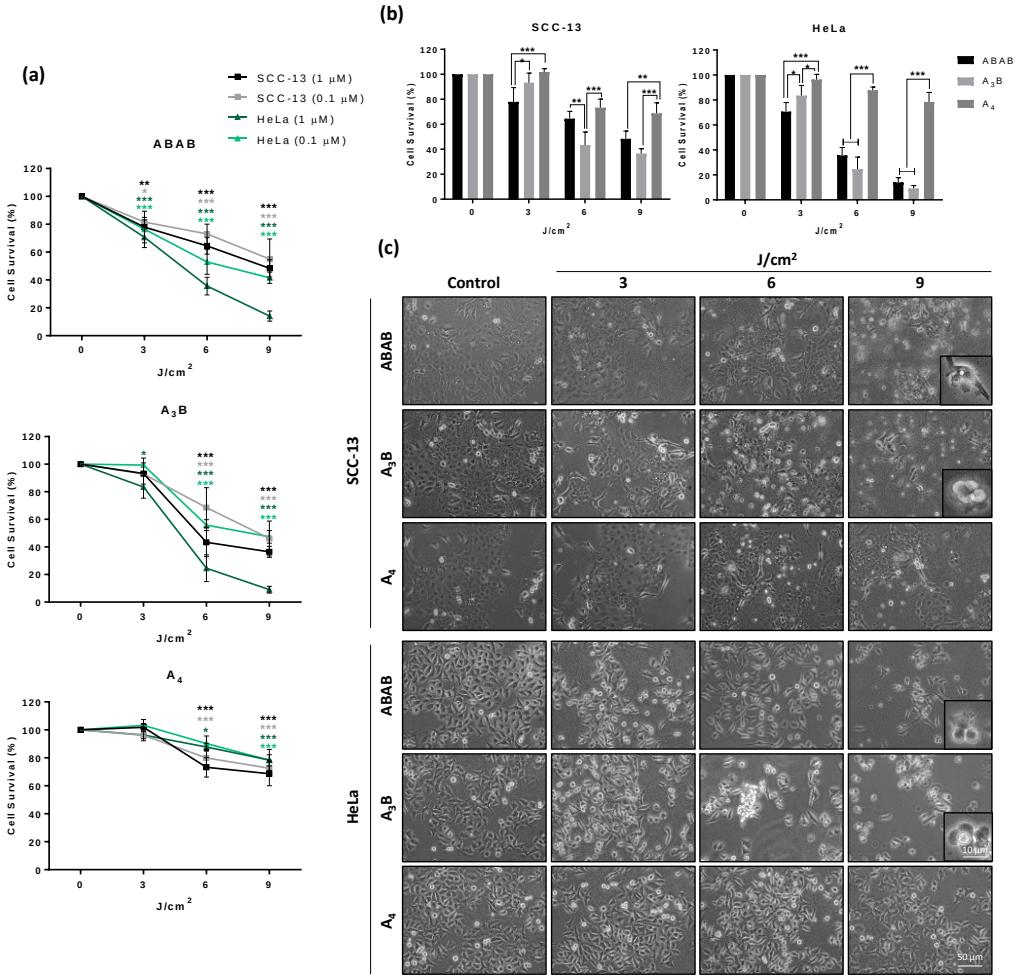

*Figure 3. 8. (a) Phototoxicity induced by **ABAB-1**, **A_3B-1** and **A_4-1** in SCC-13 and HeLa cells, which were incubated with concentrations of $1 \cdot 10^{-6}$ or $1 \cdot 10^{-7}$ M for 5 h and then irradiated with red light at variable doses. The response was dependent on both the concentration of Pcs and the light dose. (b) Comparison of the photoeffect ($1 \cdot 10^{-6}$ M) between the three Pcs in SCC-13 and HeLa cells with different light doses. The cell survival were evaluated by the MTT test 24 h after treatments. Each value corresponds to the mean obtained from three independent experiments ± SD. (* $p < 0.05$; ** $p<0.01$; *** $p < 0.001$). (c) Morphological changes observed in SCC-13 and HeLa cells 24 h after photodynamic treatment with the three Pcs ($1 \cdot 10^{-6}$ M, 5 h incubation followed by different red light doses).*

In Figure 3. 8a, we could observe a concentration-dependent response for the three compounds, since for higher concentration ($1 \cdot 10^{-6}$ M) cells are more sensitive to PDT. In addition, a drastic decrease in cell survival was revealed upon increasing the light dose in both cells lines. In order to compare the relative efficiency of each member of the series, Figure 3. 8b shows the results for both cell lines at the higher concentration ($1 \cdot 10^{-6}$ M) for the three compounds. **ABAB-1** was the most efficient at low red light dose, but the results for **ABAB-1** and **A_3B-1** were similar when using 6 or 9 J/cm^2 irradiations. Notably, the measured cell survival values are actually comparable with those of monomeric Si(IV)Pc-PEG species reported by Uslan et al., which present IC_{50} values for HeLa cells of 0.28 μM.[9] On the other hand, **A_4-1** was always less efficient in comparison with the other Zn(II)Pcs, leading to only 20% of cell death in both cell lines with the highest light dose (i.e. 9 J/cm^2) (Figure 3. 8a). Importantly, the trend found for cell survival values is parallel to the relative efficiency of the three Pcs dyes as $^1O_2$ generators (Table 3. 1). Cell morphology of the treated cells was also analyzed 24 h after PDT using phase contrast microscopy (Figure 3. 8c), revealing cytoplasmic retraction, with a rounded aspect similar to that of cells in apoptosis, in both cell lines treated with **ABAB-1** and **A_3B-1** at higher light doses.[18] Interestingly, these images are well correlated with the results obtained from cell viability assays.

ii. *Localization study*

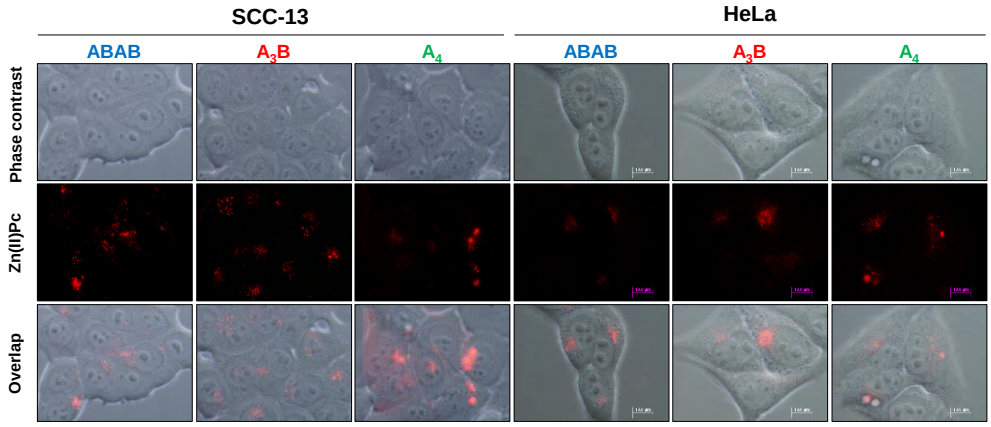

Figure 3. 9. Cellular localization of ABAB-1, A_3B-1 and A_4-1 (red) in SCC-13 and HeLa cells when they are observed with a fluorescence microscopy (irradiated with green light at 545 nm) and without other cell dye. They appear with a vesicular morphology inside cells.

To localize the Zn(II)Pcs in the treated cells, they were irradiated with green light (545 nm) with a BP545 filter. In Figure 3. 9 we can see that **ABAB-1**, **A_3B-1** and **A_4-1** are located inside the cells. They appear with a vesicular morphology and they are probably

localized in lysosomes or endosomes, which suggest that they are internalized through an endocytic pathway.

Unfortunately, the fluorescence of these Zn(II)Pcs is too weak to be appreciated if specific probes for each organelle are used, which fluorescence mask the emission of the Zn(II)Pcs. For the sake of comparison, we are including in Figure 3. 10 images of subcellular localization of organelles for SCC-13 and HeLa cells after incubation with known fluorescent probes. To analyze the intracellular localization of organielles, SCC-13 and HeLa cells were grown on coverslips and, incubated with known fluorescent probes for lysosomes (LysoTracker Green DND-26, Invitrogen), mitochondria (MitoTracker Green FM, Invitrogen), or Golgi apparatus (NBD, C6-ceramide (*N*-[6-[(7-nitro-2-1,3-benzoxadiazol-4-yl)amino]hexanoyl]-*D*-erythro-sphingosine, Invitrogen)) at the concentrations indicated by the suppliers. Then, cells were briefly washed in PBS, mounted on slides with a drop of PBS and immediately observed under the fluorescence microscope.

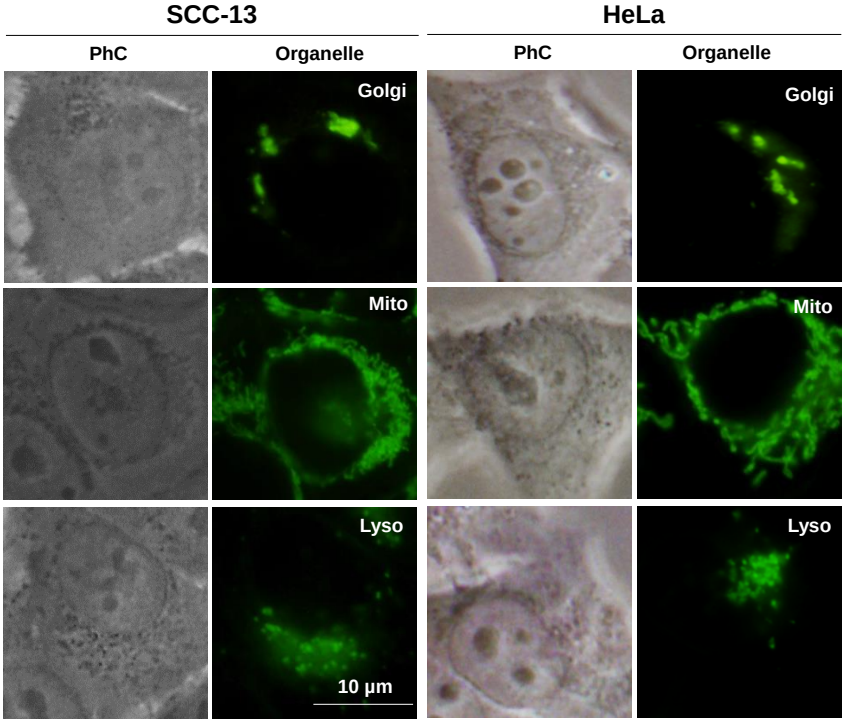

Figure 3. 10. Subcellular localization of organelles of SCC-13 and HeLa cells after incubation with known fluorescent probes. Phase contrast (PhC). Green fluorescence is from Golgi apparatus (Golgi), mitochondrial (Mito) and lysosomes (Lyso). A blue (450–490 nm) exciting lamp was used for organelles probes. Scale bar 10 µm

3.4. Conclusions

Three amphiphilic polyethyleneglycol-functionalized Zn(II)Pcs, namely **ABAB-1**, **A_3B-1** and **A_4-1** have been synthesized in the search of new PS for PDT applications. **ABAB-1**, **A_3B-1** are both obtained in a crossed- condensation reaction of two differently substituted phthalonitriles, combining bulky fluorinated substituents in the **B** isoindoles, which have previously proved effective in suppressing aggregation and increasing the $^1O_2$ generation efficiency, and hydrophilic triethyleneglycol substituents in **A** isoindoles to impart water-solubility. On the other hand, **A_4-1** is an octa(triethyleneglycol) Pc which has been prepared to experimentally demonstrate that the presence of the bulky fluorinated substituents is fundamental to achieve good photosensitization abilities. In fact, photophisycal and aggregation studies have determined that **ABAB-1** is the compound that more efficiently generates $^1O_2$ (Φ_Δ trend is **ABAB-1>A_3B-1>A_4-1)** and is less prone to aggregate in water media. Finally, *in vitro* assays have been carried out in order to determine the toxicity for tumor cells for the three Zn(II)Pcs. It has been proved that none of these Pcs are toxic for tumor cells in darkness, but when the tissue is irradiated in the presence of the PS fatality turns out. Moreover, consistently with the $^1O_2$ generation studies, the impact is higher in the case of **ABAB-1** and **A_3B-1**, than **A_4-1**. These findings make Zn(II)Pcs with bulky bis(trifluoromethyl)phenyl groups, particularly those with an ABAB pattern candidates of choice as PS.

3.5. Experimental section

a) Materials and methods

i. *Determination of the log Po/w*

Initially, equal volumes of *n*-octanol and water were mixed vigorously for 3 days at 25°C to promote solvent saturation in both phases. Each sample of Zn(II)Pc **1** was then added from stock solutions in DMSO to 2 mL of the mixture (%DMSO < 1%, [Zn(II)Pc] = 10^{-5} M) and stirred for 30 min; next, they were incubated 1 h at room temperature. After separation, 10 µL of *n*-octanol phase and 10 µL of PBS phase were taken and diluted by DMSO to 1.01 mL. The UV–vis spectra of both phases were recorded, and the partition coefficient was calculated based on the absorbance values at *Q*-band maxima (702 nm for **ABAB-1**, 685 nm for **A_3B-1** and 681 nm for **A_4-1**). The results are the average of three independent measurements.

$$logP_{OW} = log\left(\frac{A(DMSO)_O \cdot V_W}{A(DMSO)_W \cdot V_O}\right)$$

ii. *Biological assays*

Cell Culture:

HeLa (cervical adenocarcinoma cells) and SCC-13 (skin squamous carcinoma cells) cancer cell lines were used for cell cultures. They were grown using DMEM (Dulbecco's Modified Eagle's medium) culture media, supplemented with 10% Foetal Bovine Serum (FBS) and 1% antibiotics (G penicillin, 100 U/mL, and streptomycin, 100 µg/mL), purchased from Fisher. They were incubated in HERACell incubator (Heraus) at 37ºC with 5% CO_2 concentration and 95% relativity humidity.

Photodynamic treatment:

Solutions of **ABAB-1**, **A_3B-1** and **A_4-1** were prepared in concentrations of $1 \cdot 10^{-6}$ and $1 \cdot 10^{-7}$ M and added to cell cultures in well plates P24 with DMEM (supplemented with antibiotics but without FBS). The cells were incubated with each Pcs for 5 h in darkness, immediately were irradiated with different red light doses (3, 6 and 9 J/cm^2). Light source was constituted by a rectangular matrix with 384 LED (light emitting diodes), (WP7143 SURC, Kingbright) with an emission peak of 637 nm and a bandwidth of ± 17 nm. The fluence rate used was 12.7 mW/cm^2. After irradiation, cell culture was replaced by fresh media supplemented with antibiotics and FBS, and cells were incubated 24 h until their evaluation.

Cell viability:

Cell survival was determined after photodynamic treatment, both darkness plates and irradiated plates, through MTT assays. This, is a colorimetric technique based on mitochondrial enzymes capacity of alive cells to reduce the water-soluble compound 3-(4,5-dimethylthiazol-2-yl)-2,5-diphenyltetrazolium bromide (MTT) to formazan, an insoluble compound which has a purple colour. After 24 h of incubation, MTT was added to well plates in a final concentration of 100 µg/mL, for 3 h at 37 °C. Then, DMSO (Panreac) was added in order to solve formazan and optical density was measured in SpectraFluor plate reader (Tecan), with a wavelength of 542 nm.

Optical Microscopy and statistical analysis:

Microscopic observations were carried out using an Olympus BX61 epifluorescence microscope equipped with green filter (exciting filter BP510-550). Photographs were obtained with the digital camera Olympus CCD DP70 and processed using the Adobe Photoshop CS5 extended version 12.0 software (Adobe Systems Inc., San Jose, CA, USA). Data are expressed as the mean value of at least three experiments ± standard deviations (SD). The statistical significance was determined using analysis of variance (ANOVA) followed by Bonferroni's test, and $p < 0.05$ was considered statistically significant.

Subcellular localization:

In order to determine intracellular localization of Zn(II)Pcs, cells were grown in coverslips in P12 well plates and they were incubated with the PS in a concentration of 10^{-6} M for 18 h at 37 °C. After incubation, cells were washed with PBS and were observed with fluorescence microscopy.

b) Synthesis

Compounds 3,3'',5,5''-tetrakis(trifluoromethyl)-[1,1':4',1''-terphenyl]-2',3'-dicarbonitrile (**B**)[19], 4,5-bis(4-hidroxiphenoxy)phthalonitrile (**A-2**)[12], 2-(2-(2-methoxyethoxy)ethoxy)ethyl *p*-toluenesulfonate (**TEG-Ts**)[14]**,** have been prepared according to published procedures.

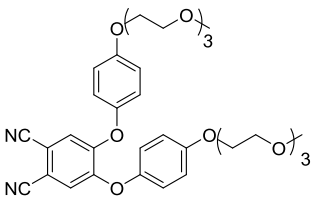

4,5-bis-(4-(2-(2-(2-methoxyethoxy)ethoxy)ethoxy) phenoxy)phthalonitrile (A-1): In a two neck round bottom flask, **A-2** (150 mg, 0.44 mmol), and **TEG-Ts** (291 mg, 0.91 mmol) were solved in dry DMF (6 mL) and heated to 50 °C. Then, anhydrous K_2CO_3 (199 mg, 1.44 mmol) was added in several portions. Reaction was kept at this temperature under argon atmosphere for three days. After cooling the reaction mixture was diluted with 100 mL of water and extracted with EtOAc (3x50 mL). The collected organic phase was washed with water (3x50 mL), brine (50 mL) and dried with $MgSO_4$. The solvent was filtered and evaporated under reduced pressure. Then, product was purified by column chromatography on SiO_2 with EtOAc as eluent, resulting in 275 mg (98% yield) of a brown oil. ^{1}H NMR (300 MHz, $CDCl_3$): δ 3.38 (s, 6H, TEG-CH_3), 3.53-3.62 (m, 4H, TEG-CH_2), 3.63-3.83 (m, 12H, TEG-CH_2), 3.85-3.95 (m, 4H, TEG-CH_2), 4.12-4.23 (m, 4H, TEG-CH_2), 6.96-7.13 (m, 10H, CHAr). ^{13}C NMR (75 MHz, $CDCl_3$): δ 59.2 , 68.2, 69.8, 70.7, 70.8, 71.0, 72.1, 109.9, 115.3, 116.5, 120.7, 121.6, 147.4, 152.6, 157.0. IR (ATR) v^{-1} (cm^{-1}): 2875, 2229, 1499, 1292, 1246, 1206, 1105. HR-MS (ESI+, +TOF, Ionizing phase: MeOH+NaI) for $C_{34}H_{40}N_2O_{10}$: *m/z* 659.2568 $[M+Na]^+$, (calculated: 659.2575).

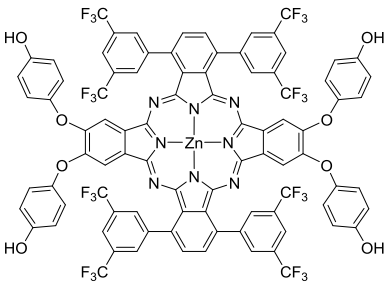

Zn(II)Pc ABAB-2: Phthalonitrile **B** (1 eq), phthalonitrile **A-4** (1 eq) and anhydrous $Zn(AcO)_2$ (1 eq) were placed in a 5 mL high pressure resistant flask equipped with a magnetic stirrer, and then 2.7 mL ([**B**]=0.1 M) of dry o-DCB/DMF 2:1 were added. The mixture was heated to 150-160ºC overnight under an argon atmosphere. After cooling the solvent was removed under vacuum. The product was purified by column chromatography on SiO_2 (dioxane/heptane in gradient from 1:1 to

2:1) where the first fraction to elute containing the desired ABAB-ZnPc **4**. The product was further purified by an additional column chromatography on Bio-Beads using $CHCl_3$ as eluent. After evaporation of the solvent, a blue solid was obtained, which were recrystallized from DCM/heptane. Yield: 17%. ^{1}H-NMR (300 MHz, DMSO-d_6) δ (ppm): 6.84 (d, J = 8.72Hz, 8H, O-Ph-O); 6.98 (d, J = 8.72Hz, 8H, O-Ph-O); 7.72 (s, 4H, CHAr); 8.03 (s, 4H, CHAr); 8.23 (s, 4H, CHAr); 8.77 (s, 8H, CHAr); 9.33 (s, 4H, OH). ^{13}C-NMR (75 MHz, DMSO-d_6): 116.1, 118.7, 125.2, 129.8, 130.3, 131.1, 132.1, 133.6, 134.6, 136.0, 136.9, 142.3, 147.1, 149.7, 150.8, 152.1, 153.6; IR (ATR) v^{-1} (cm^{-1}): 3392 (O-H st), 2924 (ar, C-H st), 1505, 1411, 1378 (pyrrole ring), 1277 (C-O-C st as), 1196 (C-F st), 1181 (O-H δ ip), 1134 (C-F st); HR-MS (MALDI, matrix: DCTB) for $C_{88}H_{40}F_{24}N_8O_8Zn$: m/z 1856.1870 (calculated: 1856.1872).

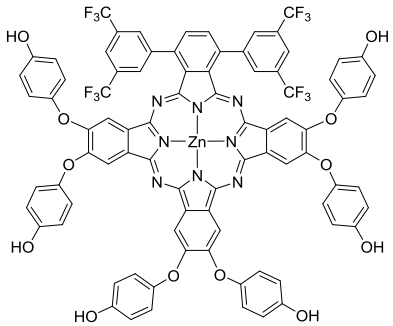

Zn(II)Pc A$_3$B-2: Phthalonitrile **B** (150 mg, 0.27 mmol), phthalonitrile **A-2** (93 mg, 0.27 mmol) and anhydrous $Zn(AcO)_2$ (50 mg, 0.27 mmol) were placed in a 5 mL high pressure resistant flask equipped with a magnetic stirrer, and then 2.7 mL ([**B**] = 0.1 M) of dry *o*-DCB/DMF (2:1) were added. The mixture was heated to 150-160 °C overnight under an argon atmosphere. After cooling the solvent was removed under vacuum. The product was purified by column chromatography on SiO_2 (dioxane/heptane in gradient from 1:1 to 2:1) where the second fraction to elute containing the desired product **A$_3$B-2**. The product was further purified by an additional column chromatography on Bio-Beads using $CHCl_3$ as eluent. After evaporation of the solvent blue solid was obtained, which were recrystallized from DCM/heptane. Yield: 16 mg (7%). ^{1}H NMR (300 MHz, DMSO-d_6): δ 6.71-7.21 (m, 24H, O-Ph-O), 7.76 (s, 2H, CHAr), 8.04 (s, 2H, CHAr), 8.21 (s, 2H, CHAr), 8.63 (s, 4H, CHAr), 8.78 (s, 4H, CHAr), 9.28-9.56 (br s, 6H, OH). ^{13}C NMR (75 MHz, THF-d_8): δ 116.1, 116.4, 116.5, 118.8, 120.1, 120.9, 121.7, 125.3, 129.4, 129.8, 130.2, 131.1, 131.7, 133.4, 133.6, 134.4, 135.8, 142.5, 148.9, 149.0, 149.7, 150.1, 150.7, 150.8, 151.2, 151.2, 151.3, 153.1, 153.2, 153.5, 153.6, 153.9, 154.6, 154.9. IR (ATR) v^{-1} (cm^{-1}): 3416, 2954, 2883, 1723, 1507, 1449, 1362, 1279, 1196, 1182, 1133, 1034. MS (MALDI, matrix DCTB + PEGNa 1500) for $C_{84}H_{44}F_{12}N_8O_{12}Zn$: *m/z* 1648.2177 $[M]^+$, (calculated: 1648.2173).

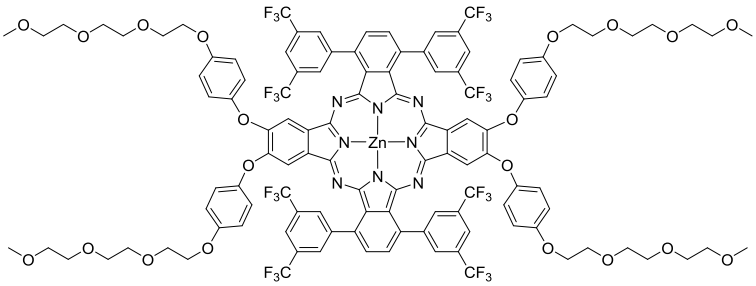

Zn(II)Pc ABAB-1: Method a: Phthalonitrile **B** (150 mg, 0.27 mmol), and **A-1** (172 mg, 0.27 mmol) and anhydrous $Zn(AcO)_2$ (50 mg, 0.27 mmol) were placed in a 5 mL high pressure resistant flask equipped with a magnetic stirrer, and then 2.7 mL ([**B**] = 0.1 M) of dry *o*-DCB/DMF 2:1 were added. The mixture was heated to 150-160 °C overnight under an argon atmosphere. After cooling the solvent was removed under vacuum. Then, the product was purified by column chromatography on SiO_2 (heptane/dioxane 1:1 as eluent) where the first green fraction to elute contained the desired product. It was further purified by an additional column chromatography on Bio-Beads using $CHCl_3$ as eluent. After evaporation of the solvent a blue solid was obtained, which was recrystallized from DCM/heptane. Yield: 33 mg (10%). **Method b: ABAB-2** (10 mg, 0.0054 mmol) and **TEG-Ts** (34 mg, 0.11 mmol) were solved in dry DMF (7 mL) and heated to 50 °C. Then, anhydrous K_2CO_3 was added (7 mg, 0.048 mmol) and the reaction was kept under this temperature and argon atmosphere overnight. The reaction was monitored by TLC (heptane/dioxane) and extra anhydrous K_2CO_3 additions could be needed until complete the conversion. After cooling the solvent was evaporated under reduced pressure. Then, the product was purified by column chromatography on SiO_2 (heptane/dioxane 1:1 as eluent). It was further purified by an additional column chromatography on Bio-Beads using $CHCl_3$ as eluent. After evaporation of the solvent a blue solid was obtained, which was washed with heptane. Yield: 2 mg (15%). ^{1}H NMR (500 MHz, $CDCl_3$): δ 3.05 (s, 12H, TEG-CH_3), 3.29 (m, 8H, TEG-CH_2), 3.37 (m, 8H, TEG-CH_2), 3.43 (m, 8H, TEG-CH_2), 3.54 (m, 8H, TEG-CH_2), 3.60 (m, 8H, TEG-CH_2), 3.89 (m, 8H, TEG-CH_2) 6.76 (d, 8H, J = 9.01 Hz, O-Ph-O), 6.98 (d, 8H, J = 9.01 Hz, O-Ph-O), 7.77 (s, 4H, CHAr), 7.85 (s, 4H, CHAr), 7.97 (s, 4H, CHAr), 8.52 (s, 8H, CHAr). ^{13}C NMR (125 MHz, $CDCl_3$): δ 58.8, 67.6, 69.7, 70.2, 70.4, 70.7, 71.8, 114.5, 115.5, 118.7, 121.5, 123.6 (q, J = 271.6 Hz, CF_3); 131.2, 131.5, 134.8, 135.3, 136.8, 142.6, 151.1, 151.9, 152.4, 153.4, 154.6. IR (ATR) v^{-1} (cm^{-1}): 2916, 2874, 1501, 1410, 1377, 1275, 1198, 1178, 1127, 1104, 896. HR-MS (MALDI, matrix: DCTB + PPGNa 2000) for $C_{116}H_{96}F_{24}N_8O_{20}Zn$: *m/z* 2440.5741 $[M]^+$, (calculated: 2440.5644).

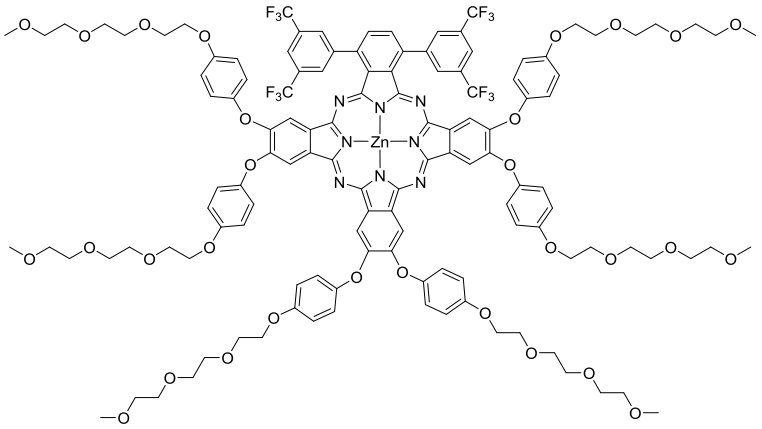

Zn(II)Pc A_3B-1: Method a: Phthalonitrile **B** (150 mg, 0.27 mmol), and **A-1** (172 mg, 0.27 mmol) and anhydrous $Zn(AcO)_2$ (50 mg, 0.27 mmol) were placed in a 5 mL high pressure resistant flask equipped with a magnetic stirrer, and then 2.7 mL ([**B**]=0.1 M) of dry *o*-DCB/DMF 2:1 were added. The mixture was heated to 150-160 °C overnight under an argon atmosphere. After cooling the solvent was removed under vacuum. Then, the product was purified by column chromatography on SiO_2 (heptane/dioxane in gradient) where the second green fraction to elute contained the desired product. It was further purified by an additional column chromatography on Bio-Beads using $CHCl_3$ as eluent. After evaporation of the solvent a blue solid was obtained, which was recrystallized from DCM/heptane. Yield: 27 mg (8%). **Method b: A_3B-2** (10 mg, 0.0061 mmol) and excess of **TEG-Ts** (39 mg, 0.12 mmol) were solved in dry DMF (7 mL) and heated to 50 °C. Then, K_2CO_3 (7.5 mg, 0.054 mmol) was added, and the reaction was kept under this temperature and argon atmosphere overnight. The reaction was monitored by TLC (heptane/dioxane) and extra anhydrous K_2CO_3 additions could be needed until complete the conversion. After cooling the solvent was evaporated under reduced pressure. Then, the product was purified by column chromatography on SiO_2 (heptane/dioxane in gradient). It was further purified by an additional column chromatography on Bio-Beads using $CHCl_3$ as eluent. After evaporation of the solvent a blue solid was obtained, which was recrystallized from EtOAc/heptane. Yield: 2 mg (13%). ^{1}H NMR (300 MHz, THF-d_8): δ 3.27 (br s, 18H, TEG-CH_3); 3.45 (br s, 12H, TEG-CH_2), 3.52-3.75 (m, 36H, TEG-CH_2); 3.85 (br s, 12H, TEG-CH_2); 4.16 (br s, 12H, TEG-CH_2); 6.93-7.18 (m, 24H, O-Ph-O); 7.98 (br s, 2H, CHAr); 8.10 (br s, 4H, CHAr); 8.74 (s, 4H, CHAr); 8.84 (s, 2H, CHAr); 8.87 (s, 2H, CHAr). ^{13}C NMR (75 MHz, THF-d_8): δ 59.0, 69.0, 70.8, 71.5, 71.7, 71.8, 74.6, 116.0, 116.2, 116.6, 116.8, 119.1, 119.6, 120.3, 120.4, 122.2, 123.8, 131.7, 132.0, 132.2, 133.2, 135.6, 135.8, 135.9, 136.0, 136.1, 136.6, 137.5, 138.3, 152.3, 153.4, 156.0, 156.5. IR (ATR) v^{-1} (cm^{-1}): 2870, 1501, 1450, 1404, 1276, 1198, 1127, 1093, 1029, 890, 800. HR-MS (MALDI, matrix: DCTB + PPGNa 2000) for $C_{126}H_{128}F_{12}N_8O_{30}Zn$: *m/z* 2524.7894 $[M]^+$, (calculated: 2524.7831).

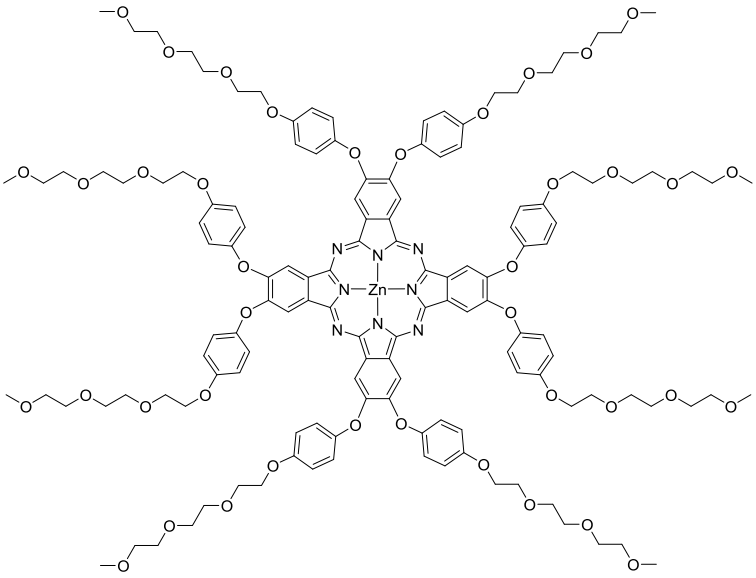

Zn(II)Pc A_4-1: A mixture of **A-1** (90 mg, 0.14 mmol) and $Zn(OAc)_2$ (9.7 mg, 0.053 mmol) was placed in a 5 mL high pressure resistant flask equipped with a magnetic stirrer, and then 1.4 mL of pentanol and 0.1 mL of DBU were added. Then mixture was heated to 150 °C under argon atmosphere for 1h. After cooling the solvent was removed under vacuum. The product was purified by column chromatography on SiO_2 (EtOAc/MeOH in gradient from 100:0 to 0:100). After evaporate the solvent under reduced pressure, the product was washed with DCM/heptane and a green solid was obtained. Yield: 9.7 mg (11%). ^{1}H NMR (500 MHz, DMSO-d_6): δ 3.22 (s, 24H, TEG-CH_3); 3.43 (t, 16H, J = 5.05 Hz, TEG-CH_2); 3.54 (t,16H, J = 5.05 Hz, TEG-CH_2); 3.58 (t, 16H, J = 4.94 Hz, TEG-CH_2); 3.65 (t, 16H, J = 4.94 Hz, TEG-CH_2); 3.82 (br t, 16H, TEG-CH_2); 4.14 (br t, 16H, TEG-CH_2); 7.04 (d, 16H, J = 8.70 Hz, O-Ph-O); 7.31 (d, 16H, J = 8.70 Hz, O-Ph-O); 8.40 (br s, 3H, CHAr-Pc(core)). ^{13}C NMR (125 MHz, DMSO-d_6): δ 58.0, 67.6, 69.1, 69.6, 69.9, 70.0, 71.3, 112.3, 115.7, 119.8, 133.2, 149.8, 150.4, 154.9. IR (ATR) v^{-1} (cm^{-1}): 3016, 2933, 1502, 1450, 1425, 1400, 1284, 1200, 1130, 936. HR-MS (MALDI, matrix DCTB + PPGNa 2000 + PPGNa 2700) for $C_{136}H_{160}N_8O_{40}Zn$: *m/z* 2608.9966 $[M]^+$, (calculated: 2609.0018).

3.6. References

(1) van Vlerken, L. E.; Vyas, T. K.; Amiji, M. M. Poly(Ethylene Glycol)-Modified Nanocarriers for Tumor-Targeted and Intracellular Delivery. *Pharm. Res.* **2007**, *24* (8), 1405–1414.

(2) Liu, J.-Y.; Jiang, X.-J.; Fong, W.-P.; Ng, D. K. P. Highly Photocytotoxic 1,4-Dipegylated Zinc (II) Phthalocyanines. Effects of the Chain Length on the in Vitro Photodynamic Activities. *Org. Biomol. Chem.* **2008**, *6* (24), 4560–4566.

(3) Kroon, J. M.; B. M. Koehorst, R.; van Dijk, M.; Sanders, G. M.; J. R. Sudhölter, E. Self-Assembling Properties of Non-Ionic Tetraphenylporphyrins and Discotic Phthalocyanines Carrying Oligo(Ethylene Oxide) Alkyl or Alkoxy Units. *J. Mater. Chem.* **1997**, *7* (4), 615–624.

(4) Tuncel, S.; Dumoulin, F.; Gailer, J.; Sooriyaarachchi, M.; Atilla, D.; Durmuş, M.; Bouchu, D.; Savoie, H.; Boyle, R. W.; Ahsen, V. A Set of Highly Water-Soluble Tetraethyleneglycol-Substituted Zn(II) Phthalocyanines: Synthesis, Photochemical and Photophysical Properties, Interaction with Plasma Proteins and in Vitro Phototoxicity. *Dalt. Trans.* **2011**, *40* (16), 4067–4079.

(5) Uslan, C.; Köksoy, B.; Durmuş, M.; Durmuş İşleyen, N.; Öztürk, Y.; Çakar, Z. P.; Hepuzer Gürsel, Y.; Sesalan, B. S. The Synthesis and Investigation of Photochemical, Photophysical and Biological Properties of New Lutetium, Indium, and Zinc Phthalocyanines Substituted with PEGME-2000 Blocks. *J. Biol. Inorg. Chem.* **2019**, *24* (2), 191–210.

(6) Foley, S.; Jones, G.; Liuzzi, R.; J. McGarvey, D.; H. Perry, M.; George Truscott, T. The Synthesis and Photophysical Properties of Polyether Substituted Phthalocyanines of Potential Use in Photodynamic Therapy. *J. Chem. Soc. Perkin Trans. 2* **1997**, No. 9, 1725–1730.

(7) Bandera, Y.; Burdette, M. K.; Shetzline, J. A.; Jenkins, R.; Creager, S. E.; Foulger, S. H. Synthesis of Water Soluble Axially Disubstituted Silicon (IV) Phthalocyanines with Alkyne & Azide Functionality. *Dye. Pigment.* **2016**, *125*, 72–79.

(8) Huang, J.-D.; Wang, S.; Lo, P.-C.; Fong, W.-P.; Ko, W.-H.; Ng, D. K. P. Halogenated Silicon (IV) Phthalocyanines with Axial Poly(Ethylene Glycol) Chains. Synthesis, Spectroscopic Properties, Complexation with Bovine Serum Albumin and in Vitro Photodynamic Activities. *New J. Chem.* **2004**, *28* (3), 348–354.

(9) Uslan, C.; İşleyen, N. D.; Öztürk, Y.; Yıldız, B. T.; Çakar, Z. P.; Göksel, M.; Durmuş, M.; Gürsel, Y. H.; Sesalan, B. Ş. A Novel of PEG-Conjugated Phthalocyanine and Evaluation of Its Photocytotoxicity and Antibacterial Properties for Photodynamic Therapy. *J. Porphyr. Phthalocyanines* **2018**, *22* (01n03), 10–24.

(10) Jin, Y.; Zhang, X.; Zhang, B.; Kang, H.; Du, L.; Li, M. Nanostructures of an Amphiphilic Zinc Phthalocyanine Polymer Conjugate for Photodynamic Therapy of Psoriasis. *Colloids Surfaces B Biointerfaces* **2015**, *128*, 405–409.

(11) Revuelta-Maza, M. A.; Nonell, S.; de la Torre, G.; Torres, T. Boosting the Singlet Oxygen Photosensitization Abilities of Zn(II) Phthalocyanines through Functionalization with Bulky Fluorinated Substituents. *Org. Biomol. Chem.* **2019**, *17* (32), 7448–7454.

(12) Li, M.; Khoshdel, E.; Haddleton, D. M. Synthesis of Water Soluble PEGylated (Copper) Phthalocyanines via Mitsunobu Reaction and Cu(I)-Catalysed Azide–

Alkyne Cycloaddition (CuAAC) "Click" Chemistry. *Polym. Chem.* **2013**, *4* (16), 4405–4411.

(13) Revuelta-Maza, M. Á.; González-Jiménez, P.; Hally, C.; Agut, M.; Nonell, S.; Torre, G. de la; Torres, T. Fluorine-Substituted Tetracationic ABAB-Phthalocyanines for Efficient Photodynamic Inactivation of Gram+ and Gram- Bacteria. *Eur. J. Med. Chem.* Submited.

(14) Ajiro, H.; Takahashi, Y.; Akashi, M. Thermosensitive Biodegradable Homopolymer of Trimethylene Carbonate Derivative at Body Temperature. *Macromolecules* **2012**, *45* (6), 2668–2674.

(15) Garcia, A. M.; de Alwis Weerasekera, H.; Pitre, S. P.; McNeill, B.; Lissi, E.; Edwards, A. M.; Alarcon, E. I. Photodynamic Performance of Zinc Phthalocyanine in HeLa Cells: A Comparison between DPCC Liposomes and BSA as Delivery Systems. *J. Photochem. Photobiol. B Biol.* **2016**, *163*, 385–390.

(16) Young, J.; Yee, M.; Kim, H.; Cheung, J.; Chino, T.; Düzgüneş, N.; Konopka, K. Phototoxicity of Liposomal Zn- and Al-Phthalocyanine against Cervical and Oral Squamous Cell Carcinoma Cells in Vitro. *Med. Sci. Monit. Basic Res.* **2016**, *22*, 156–164.

(17) Li, L.; Luo, Z.; Chen, Z.; Chen, J.; Zhou, S.; Xu, P.; Hu, P.; Wang, J.; Chen, N.; Huang, J.; et al. Enhanced Photodynamic Efficacy of Zinc Phthalocyanine by Conjugating to Heptalysine. *Bioconjug. Chem.* **2012**, *23* (11), 2168–2172.

(18) Rello, S.; Stockert, J. C.; Moreno, V.; Gámez, A.; Pacheco, M.; Juarranz, A.; Cañete, M.; Villanueva, A. Morphological Criteria to Distinguish Cell Death Induced by Apoptotic and Necrotic Treatments. *Apoptosis* **2005**, *10* (1), 201–208.

(19) Fazio, E.; Jaramillo-García, J.; de La Torre, G.; Torres, T. Efficient Synthesis of ABAB Functionalized Phthalocyanines. *Org. Lett.* **2014**, *16* (18), 4706–4709.

Chapter 4 – Fluorine-substituted tetracationic ABAB-Pcs for efficient photodynamic inactivation of Gram-positive and Gram-negative bacteria

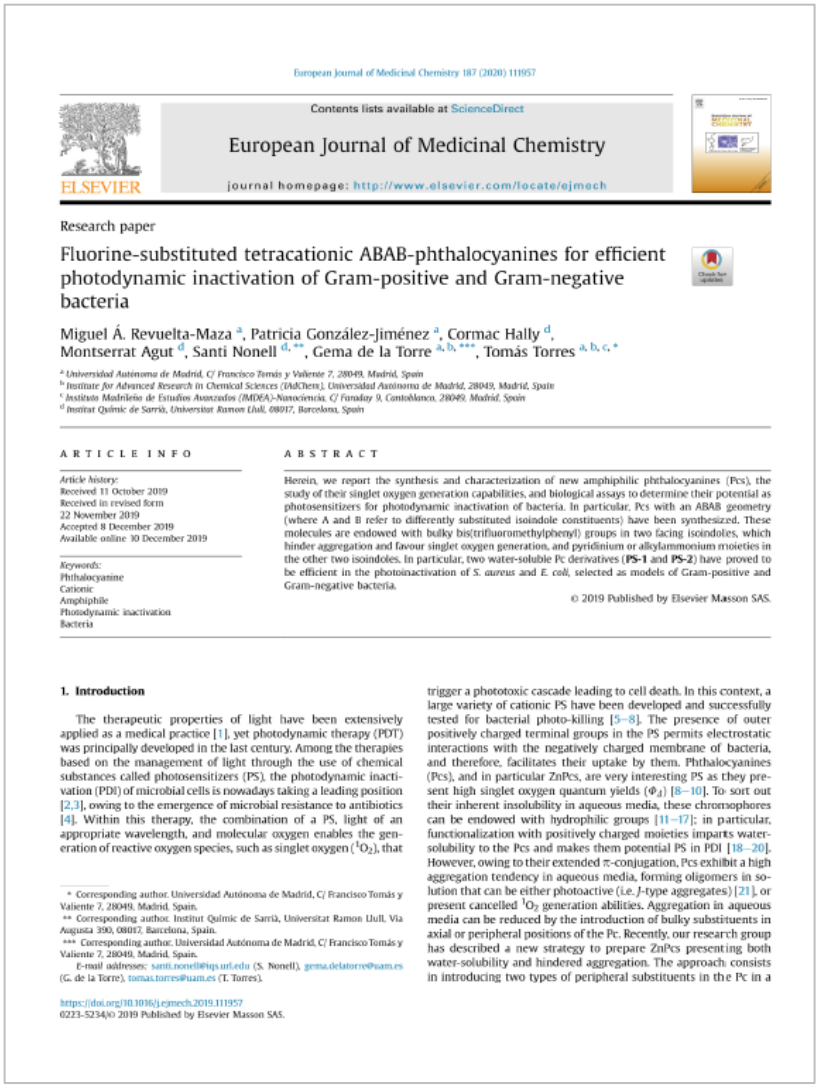

European Journal of Medicinal Chemistry 187 (2020) 111957

Contents lists available at ScienceDirect

European Journal of Medicinal Chemistry

journal homepage: http://www.elsevier.com/locate/ejmech

Research paper

Fluorine-substituted tetracationic ABAB-phthalocyanines for efficient photodynamic inactivation of Gram-positive and Gram-negative bacteria

Miguel Á. Revuelta-Maza [a], Patricia González-Jiménez [a], Cormac Hally [d], Montserrat Agut [d], Santi Nonell [d, **], Gema de la Torre [a, b, ***], Tomás Torres [a, b, c, *]

[a] Universidad Autónoma de Madrid, C/ Francisco Tomás y Valiente 7, 28049, Madrid, Spain
[b] Institute for Advanced Research in Chemical Sciences (IAdChem), Universidad Autónoma de Madrid, 28049, Madrid, Spain
[c] Instituto Madrileño de Estudios Avanzados (IMDEA)-Nanociencia, C/ Faraday 9, Cantoblanco, 28049, Madrid, Spain
[d] Institut Químic de Sarrià, Universitat Ramon Llull, 08017, Barcelona, Spain

ARTICLE INFO

Article history:
Received 11 October 2019
Received in revised form
22 November 2019
Accepted 8 December 2019
Available online 30 December 2019

Keywords:
Phthalocyanine
Cationic
Amphiphile
Photodynamic inactivation
Bacteria

ABSTRACT

Herein, we report the synthesis and characterization of new amphiphilic phthalocyanines (Pcs), the study of their singlet oxygen generation capabilities, and biological assays to determine their potential as photosensitizers for photodynamic inactivation of bacteria. In particular, Pcs with an ABAB geometry (where A and B refer to differently substituted isoindole constituents) have been synthesized. These molecules are endowed with bulky bis(trifluoromethylphenyl) groups in two facing isoindoles, which hinder aggregation and favour singlet oxygen generation, and pyridinium or alkylammonium moieties in the other two isoindoles. In particular, two water-soluble Pc derivatives (**PS-1** and **PS-2**) have proved to be efficient in the photoinactivation of *S. aureus* and *E. coli*, selected as models of Gram-positive and Gram-negative bacteria.

1. Introduction

The therapeutic properties of light have been extensively applied as a medical practice [1], yet photodynamic therapy (PDT) was principally developed in the last century. Among the therapies based on the management of light through the use of chemical substances called photosensitizers (PS), the photodynamic inactivation (PDI) of microbial cells is nowadays taking a leading position [2,3], owing to the emergence of microbial resistance to antibiotics [4]. Within this therapy, the combination of a PS, light of an appropriate wavelength, and molecular oxygen enables the generation of reactive oxygen species, such as singlet oxygen ($^1O_2$), that trigger a phototoxic cascade leading to cell death. In this context, a large variety of cationic PS have been developed and successfully tested for bacterial photo-killing [5–8]. The presence of outer positively charged terminal groups in the PS permits electrostatic interactions with the negatively charged membrane of bacteria, and therefore, facilitates their uptake by them. Phthalocyanines (Pcs), and in particular ZnPcs, are very interesting PS as they present high singlet oxygen quantum yields (Φ_Δ) [8–10]. To sort out their inherent insolubility in aqueous media, these chromophores can be endowed with hydrophilic groups [11–17]; in particular, functionalization with positively charged moieties imparts water-solubility to the Pcs and makes them potential PS in PDI [18–20]. However, owing to their extended π-conjugation, Pcs exhibit a high aggregation tendency in aqueous media, forming oligomers in solution that can be either photoactive (i.e., *J*-type aggregates) [21], or present cancelled $^1O_2$ generation abilities. Aggregation in aqueous media can be reduced by the introduction of bulky substituents in axial or peripheral positions of the Pc. Recently, our research group has described a new strategy to prepare ZnPcs presenting both water-solubility and hindered aggregation. The approach consists in introducing two types of peripheral substituents in the Pc in a

* Corresponding author. Universidad Autónoma de Madrid, C/ Francisco Tomás y Valiente 7, 28049, Madrid, Spain.
** Corresponding author. Institut Químic de Sarrià, Universitat Ramon Llull, Via Augusta 390, 08017, Barcelona, Spain.
*** Corresponding author. Universidad Autónoma de Madrid, C/ Francisco Tomás y Valiente 7, 28049, Madrid, Spain.
E-mail addresses: santi.nonell@iqs.url.edu (S. Nonell), gema.delatorre@uam.es (G. de la Torre), tomas.torres@uam.es (T. Torres).

https://doi.org/10.1016/j.ejmech.2019.111957
0223-5234/© 2019 Published by Elsevier Masson SAS.

4.1. Citation and contribution

Miguel. Á. Revuelta-Maza, P. González-Jiménez, C. Hally, M. Agut, S. Nonell, G. de la Torre, T. Torres, Fluorine-substituted tetracationic ABAB-phthalocyanines for efficient photodynamic inactivation of Gram-positive and Gram-negative bacteria, *European Journal of Medicinal Chemistry* **2020**, doi: https://doi.org/10.1016/j.ejmech.2019.111957.

Contribution: Revuelta-Maza, M. A.: Synthesis and characterization (together with P. G.-J.), aggregation studies, photophysical and microbiolgy experiments (together with C. H.). Preparation of the manuscript.

Funding and supervision: Agut, M.; Nonell, S.; de la Torre, G. and Torres T. This work has been supported by MINECO, Spain (CTQ2017-85393-P and CTQ2016-78454-C2-1-R).

Abstract:

Herein, we report the synthesis and characterization of new amphiphilic phthalocyanines (Pcs), the study of their singlet oxygen generation capabilities, and biological assays to determine their potential as photosensitizers for photodynamic inactivation of bacteria. In particular, Pcs with an ABAB geometry (where A and B refer to differently substituted isoindole constituents) have been synthesized. These molecules are endowed with bulky bis(trifluoromethylphenyl) groups in two facing isoindoles, which hinder aggregation and favour singlet oxygen generation, and pyridinium or alkylammonium moieties in the other two isoindoles. In particular, two water-soluble Pc derivatives (**PS-1** and **PS-2**) have proved to be efficient in the photoinactivation of S. aureus and E. coli, selected as models of Gram-positive and Gram-negative bacteria.

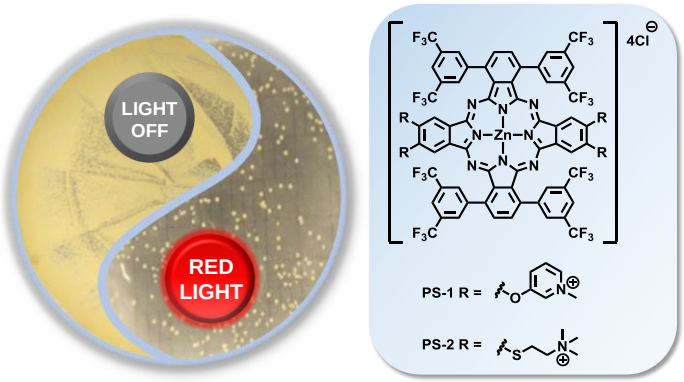

4.2. Introduction and Objectives

Among the therapies based on the management of light, the photodynamic inactivation (PDI) of microbial cells is nowadays taking a leading position,[1,2] owing to the emergence of microbial resistance to antibiotics.[3] In this context, a large variety of cationic PS have been developed and successfully tested for bacterial photo-killing.[4–7] The presence of outer positively charged terminal groups in the PS permits electrostatic interactions with the negatively charged membrane of bacteria, and therefore, facilitates their uptake by them.

Zn(II)Pcs are very interesting PS as they present high singlet oxygen quantum yields.[7–9] To sort out their inherent insolubility in aqueous media, these chromophores can be endowed with hydrophilic groups;[10–16] in particular, functionalization with positively charged moieties imparts water-solubility to the Pcs and makes them potential PS in PDI.[17–19] However, as we have seen in previous chapters, owing to their extended π-conjugation, Pcs exhibit a high aggregation tendency in aqueous media, forming oligomers in solution that can be either photoactive (i.e. *J*-type aggregates),[20] or present cancelled $^1O_2$ generation abilities.

Herein, we apply our succesful design to prepare Zn(II)Pcs presenting water-solubility, hindered aggregation, and potential use as PS for PDI. The approach consists again in introducing two types of peripheral substituents in the Pc in a crosswise, ABAB architecture that has proved to produce high Φ_Δ.[21–24] Therefore, the target molecules will hold two facing isoindoles endowed with bulky bis(trifluoromethylphenyl) moieties that avoid the aggregation in solution, and other two endowed with hydrophilic cationic-terminated substituents in the A isoindole that provide these ABAB Zn(II)Pcs with solubility in aqueous media. *In vitro* assays with two selected Zn(II)Pcs (**PS-1** and **PS-2**) have been performed to examine their toxicity in different strains of Gram-positive and Gram-negative bacteria.

4.3. Results and discussion

a) Synthesis

Two different functionalization approaches have been undertaken to perform the preparation of amphiphilic tetracationic ABAB Zn(II)Pcs, namely the functionalization with either pyridines or tertiary amines, which could be quaternized in a final step (Scheme 4. 1). The aim is to compare the effect of the nature of the positively charged groups and/or the bridge between the positive charge and the aromatic core on their activity as PS. The synthesis of phthalonitrile **B** was carried out following the methodology described in our group.[21]

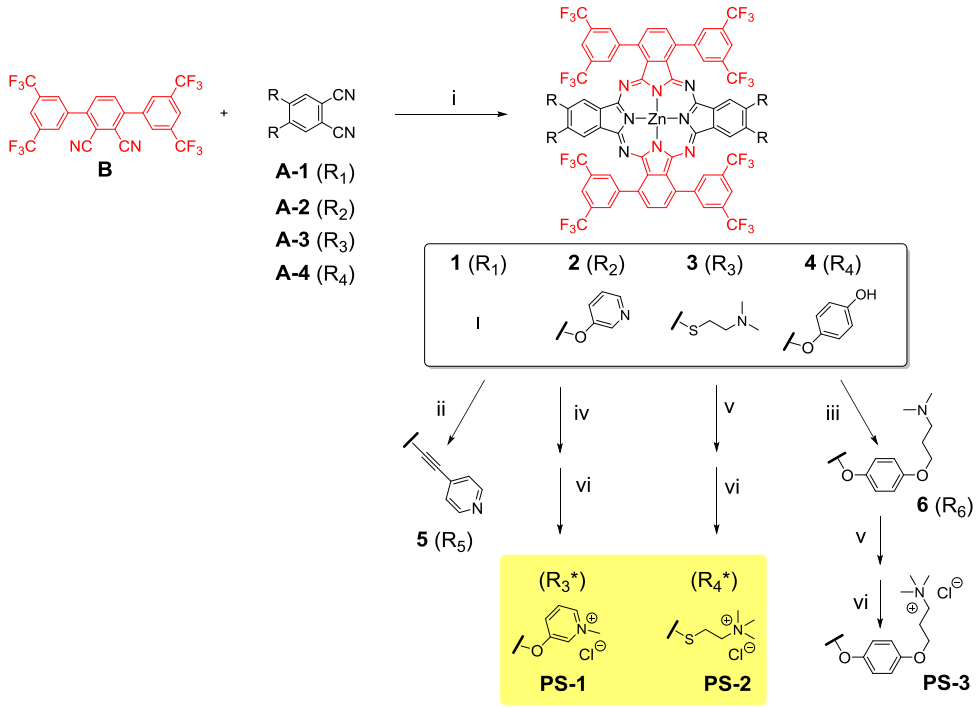

Scheme 4. 1. Synthesis of pyridil or alkylamino-substituted Zn(II)Pcs and their respective pyridinium and ammonium salts. i) $Zn(OAc)_2$, o-DCB/DMF (2:1), 150 ºC, overnight; ii) 4-ethynylpyridine, $PdCl_2(PPh_3)_2$, CuI, diisopropylamine, 70 ºC, overnight; iii) 3-(dimethylamino)propyl methyl carbonate, CH_3CN, 180 ºC, MW, 90 min; iv) MeI, DMF, 4h; v) MeI, EtOH, reflux, overnight; vi) Dowex® (1x8 200-400), MiliQ water, DMSO.

The preparation of Zn(II)Pcs functionalized with pyridine units was undertaken by two different synthetic approaches. First, we prepared the already described Zn(II)Pc **1**[21] and subjected it to a four-fold Sonogashira coupling with 4-ethynylpyridine, yielding **5**. Although the product was isolated and fully characterized, the low yield of this reaction (11%), preceded by the 10% yield of the mixed cyclotetramerization between **A-1** and **B**, which makes and overall yield of 1%, made us discard this route as an operative method to obtain pyridine functionalized PS for *in vitro* assays. Therefore, we prepared **2**, resulting from the straightforward cross-condensation between bulky phthalonitrile **B** and **A-2,** which had been previously synthesized following reported procedures.[25] (Scheme 4. 1). Although the cross-condensation yield was low (8%), **2** was easily purified, and the pyridyl moieties could be quaternized by reaction with MeI. In a last step, the molecules were exposed to Dowex® resin in order to exchange the initial counterions for chloride anions, rendering a compound that was partially soluble in water, from now coded as **PS-1** for the photophysical characterization and further *in vitro* experiments.

Moving to the preparation of ABAB Zn(II)Pcs functionalized with alkyl ammonium moieties, we intended to explore the preparation of a series of compounds with different separation between the aromatic core and the positive charges. The first tailored ABAB Zn(II)Pc derivative was compound **3**, in which the tertiary amines were separated from the Zn(II)Pc core by a $(CH_2)_2$-S- bridge. Since alkyl thioether chains can be easily introduced in the starting phthalonitriles by aromatic nucleophilic substitution over 4,5-dichlorophthalonitrile,[26] phthalonitrile **A-3** was synthesized and reacted with phthalonitrile **B** under the typical conditions applied for the preparation of ABAB Zn(II)Pc derivatives. Worth mentioning, the reaction proceeded in 20% yield, proving this conversion as one of the most efficient cross-condensation reactions performed between bulky phthalonitrile **B** and another differently substituted phthalonitrile performed to date. **3** was then methylated with MeI in dry EtOH, in 36% yield. It is noteworthy that, after this transformation, the solubility of the resulting product changed drastically, becoming soluble only in polar solvents such as DMSO or DMF. In a last step, the product was exposed to Dowex® resin for ionic exchange, thus yielding a compound soluble in water. From now this product will be coded as **PS-2** for the photophysical characterization and *in vitro* tests.

Our second approach towards an alkyl-ammonium functionalized Zn(II)Pc was to increase the distance between the Zn(II)Pc and the positive charge by preparing compound **4**, (Scheme 4. 1) previously decribed in Chapter 3, which was consecutively subjected to a four-fold *O*-alkylation to introduce *N*-dimethylamino-*N*-propyl residues. In particular, we performed the *O*-alkylation by heating at 180 ºC a mixture of **4** and excess of 3-(dimethylamino)propyl methyl carbonate[27] in acetonitrile. The formation of **6** was efficient, namely, 11% yield starting from the mixture of **A-4** and **B** phthalonitriles. **6** was then subjected to a methylation reaction, and further exposed to Dowex® resin to exchange the initial iodides for chloride anions. Unfortunately, this compound, coded as **PS-3** in Scheme 4. 1, proved unstable in solution, undergoing Hoffman-type eliminations of the alkylammonium moieties that lead to molecules with terminal double bonds in the peripheral alkyl chains, as detected by mass spectrometry. This chemical instability made us discard **PS-3** for *in vitro* assays. Figure 4. 1 shows the ^{1}H-NMR spectra of **PS-1** and **PS-2**. In both cases, the signals are well resolved due to their non-aggregated state in DMSO-d_6 solutions. The reduced number of signals derives from the high molecular symmetry these compounds possess (i.e. D_{2h}). In the case of **PS-1**, the spectrum presents four singlets for the aromatic protons of the isoindole units and the CF_3-substituted phenyl rings, a group of signals corresponding to the *ortho* substituted pyridines (two doublets, a doublet of doublets and one singlet), and one singlet for the methyl groups. In the case of **PS-2**, the distinctive signals of this product (i.e. the two triplets for the methylenes) appear overlapped with the DMSO signal, but the singlet corresponding to the methyl groups of the tertiary amines could be clearly observed. Moreover, HR-MS characterization confirmed the structure of the compound.

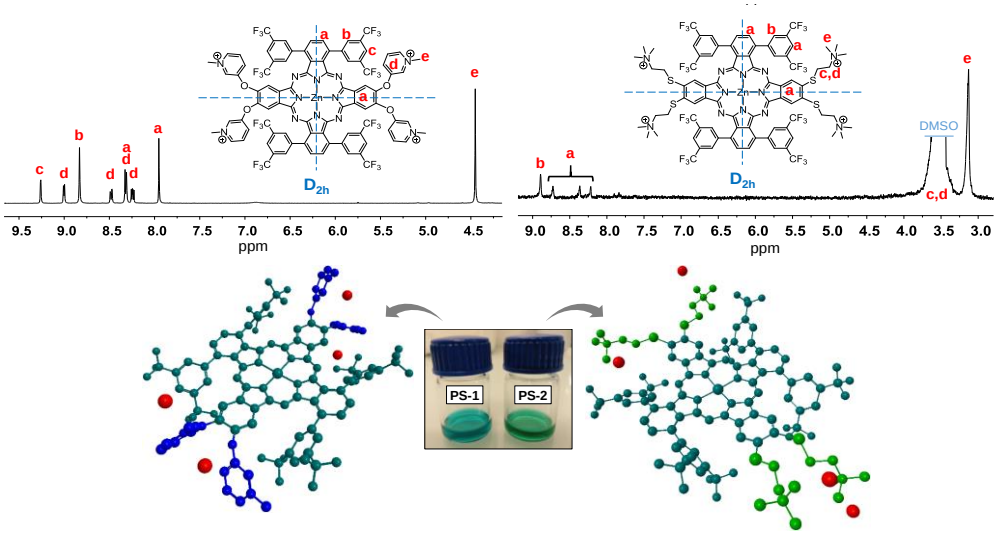

*Figure 4. 1. ^{1}H-NMR in DMSO-d_6 of **PS-1** (up); and **PS-2** (down). And structural models for **PS-1** (left) and **PS-2** (right), which were realized with the SCIGRESS (FJ 2.8.1 EU 3.3.1) software, and a geometry optimization through MM2. Hydrophilic region are highlighted in blue (**PS-1**) and green (**PS-2**) with chloride counterions in red.*

b) Photophysical studies

Table 4. 1 presents a summary of the photophysical properties of **PS-1** and **PS-2** in methanol, including molar absorption coefficients (ε), wavelength, lifetime (τ_S) and quantum yield (Φ_F) of fluorescence emission, and singlet oxygen quantum yield (Φ_Δ). The absorption spectra of **PS-1** and **PS-2** (see Figure 4. 2 for the UV-vis spectra in MeOH) show symmetric, non-split *Q*-bands, which is not usual for MPcs with D_{2h} symmetry. The tioeher-derivatized Pc (**PS-2**) shows a *Q*-band more shifted to the red than the ether-derivatized one (**PS-1**), and with a higher absorption coefficient. Indeed, the absorption spectra of these compounds in MeOH do not show any evidence of aggregation. Absorption spectra were registered in a range of concentrations (between 8.7 x 10^{-7} M and 4.1 x 10^{-6} M for **PS-1**, and 1.6 x 10^{-6} M and 4.9 x 10^{-6} M for **PS-2**) (Figure 4. 2). For the verification of the Lambert-Beer law, an analysis of linear regression between the intensity of the *Q*-band and the concentration was performed, with R^2 values of ~0.999.

*Table 4. 1. Photophysical properties of **PS-1** and **PS-2** in MeOH.*

Sample	*Solvent*	*log ε (λ)*: max*	*λ_f / nm*	*ϕ_f*	*τ_S / ns*	*ϕ_Δ*
PS-1	MeOH	4.59 (350), 5.13 (678)*	683	0.13	2.7	0.49
PS-2	MeOH	4.74 (359), 5.20 (694)*	699	0.11	2.4	0.35

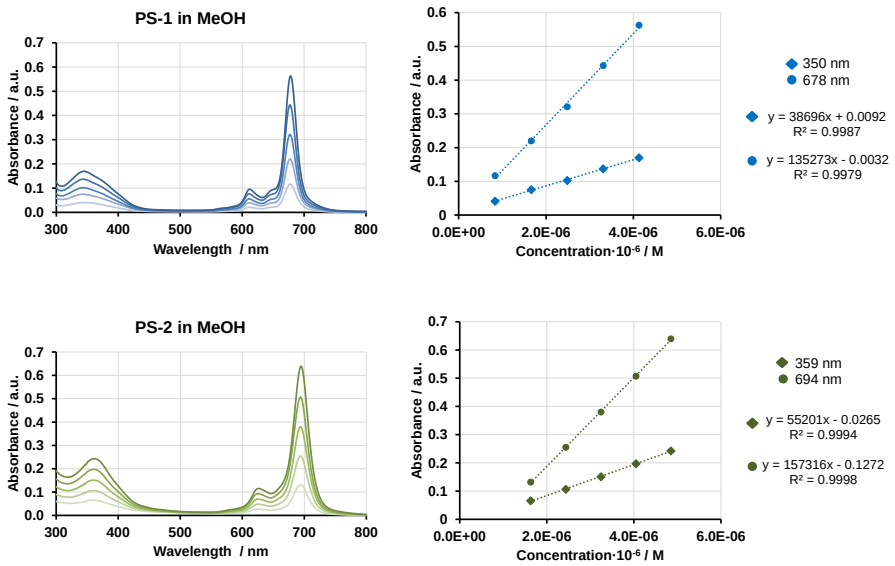

*Figure 4. 2. UV-vis spectra of **PS-1** and **PS-2** in MeOH at different concentrations (between $8.7 \cdot 10^{-7}$ M and $4.1 \cdot 10^{-6}$ M for **PS-1** and $1.6 \cdot 10^{-6}$ M and $4.9 \cdot 10^{-6}$ M for **PS-2**); and linear regression between maxima intensity and concentration.*

Fluorescence studies (Table 4. 1 and Figure 4. 3) were also performed in MeOH, and are in line with absorption assays; the monoexponential fluorescence decay kinetics confirm that **PS-1** and **PS-2** are in monomeric form in solution.

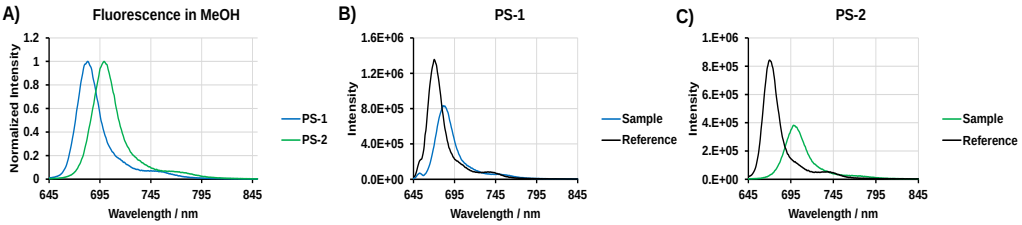

*Figure 4. 3. a) Normalized fluorescence spectra of **PS-1** and **PS-2** in MeOH. b) and c) comparative fluorescence of **PS-1** and **PS-2** in MeOH versus Zn(II)Pc in 1-propanol as reference for the determination of Φ_f.*

Also, the quantification of the Φ_Δ was performed for these compounds, by direct observation of the $^1O_2$ phosphorescence at 1275 nm after excitation at 355 nm. The values of Φ_f and τ_S are similar for the two compounds, however **PS-2** shows a lower Φ_Δ than **PS-1**. These results point to an enhanced internal conversion in **PS-2**, which is consistent with the higher flexibility of its structure. Comparing the photophysical parameters of **PS-1** with those of a neutral Zn(II)Pc described previously with a similar

functionalization (i.e. 4-methoxyphenoxy moieties)[24] (Chapter 1), τ_S of **PS-1** is 50% longer, its Φ_f has almost doubled and its Φ_Δ has decreased by 42%, which indicate a decrease in the intersystem-crossing rate constant, probably due to the presence of the positive charges. Still, the values are adequate for phototherapeutic applications. Importantly, we tried to perform measurements of $^1O_2$ generation in water, but only residual signals were detected, which can be rationalized by the formation of aggregates, which is not fully hindered for these PS in aqueous media (see below).

c) Aggregation studies and determination of the log $P_{O/W}$

In addition to the photophysical and photochemical characterization, some aggregation studies are also needed to evaluate the possible application of our ABAB Zn(II)Pcs as potential PS. Due to the hydrophobic nature of the Pc ring, these chromophores have tendency to form aggregates in solution to minimize the solvation energy, particularly in the case of polar solvents as water. Aggregation is a complex process that depends on the van der Waals interaction, π–π stacking, concentration and the environment characteristics. Although a certain organization of the PS in vesicles or micelles can facilitate their transport through the blood system, it is important that once the PS are delivered to the target cell they stay as non-aggregated species, at least to some extent, leading to a more efficient $^1O_2$ generation after light excitation. For that reason, aggregation studies in aqueous media are fundamental for the former evaluation of the potential PS. These studies are usually performed by means of UV-vis studies. As mentioned above, **PS-2** is soluble in pure water, but not **PS-1**, although it happens to be soluble upon addition from a stock of a polar organic solvent solution, such as MeOH or DMSO, to water. In fact, **PS-1** remained soluble until a 99:1 water/organic solvent ratio was reached. Therefore, we performed aggregation studies by progressively adding water to MeOH solutions of **PS-1** and **PS-2**, keeping the concentration constant (Figure 4. 4). Upon the addition of water, the two compounds showed a similar behaviour that is a decrease in the intensity of the *Q*-band and a slight red shift and broadening. While **PS-2** proved only slightly aggregated in MeOH/water 99:1 solution, a much more pronounced aggregation was observed for **PS-1,** due to the larger hydrophobic nature of the pyridine rings compared to the alkyl amines of **PS-2**.

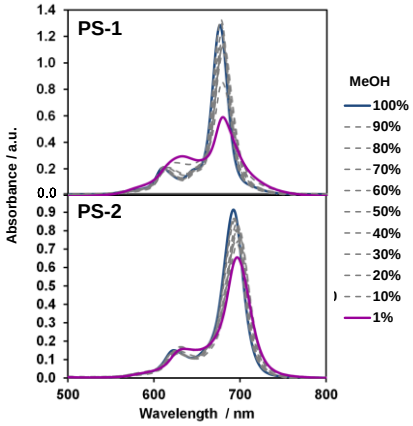

*Figure 4. 4. Aggregation tendency upon increasing water percentage over **PS-1** and **PS-2** solutions in MeOH at constant concentration of the PS in the range: 6-9·10^{-6} M.*

In order to compare the aggregation behaviour of both PS in physiologically relevant medium, that is phosphate buffered saline (PBS), concentration-dependent UV-vis studies were performed (Figure 4. 5). The solutions were prepared starting from stock solutions in DMSO, following the same protocol than will be further used for dosing the PS to bacteria.

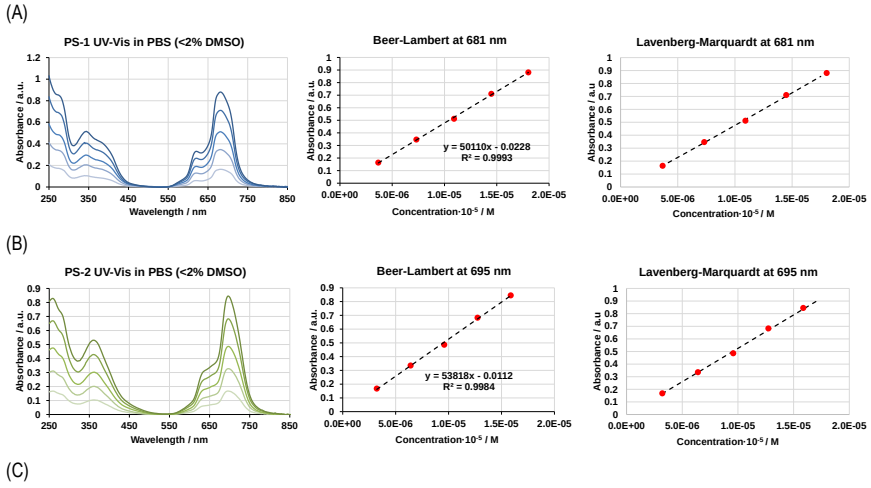

$$A(\lambda) = \varepsilon_M(\lambda) \cdot l \cdot C_T \qquad (1)$$

$$A(\lambda) = \frac{\varepsilon_D(\lambda)}{2} \cdot C_T + \left[\varepsilon_M(\lambda) - \frac{\varepsilon_D(\lambda)}{2}\right] \cdot \frac{\sqrt{1+8KC_T}-1}{4K} \qquad (2)$$

*Figure 4. 5. Aggregation study in PBS (from stock solution in DMSO <2%), for **PS-1** (A) (concentration range 3.7·10^{-6} to 1.8·10^{-5} M) and **PS-2** (B) (concentration range 3.2·10^{-6} to 1.6·10^{-5} M), and (C) Beer Lambert (1) and Lavenberg-Marquardt (2) equations for data fitting.*

Although the recorded spectra resemble those typical of non-aggregated Pcs, the relative intensity of the *Q*-band for **PS-1** (at 681 nm), and for **PS-2** (at 695 nm) with respect to their respective shoulder at 650 nm is very different from that of molecularly dissolved Pcs. Moreover, while a Beer-Lambert plot is apparently linear, the slope yields values of log (ε / $cm^{-1}\cdot M^{-1}$) = 4.7 for both PS, which are one order of magnitude lower than in methanol. Also the intercept is negative for both PS, which suggests a curve with upward-deviation from linearity. Indeed, a much better fit can be obtained by using the monomer-dimer equilibrium model equation,[28] indicating that the dimer absorbs more than two monomers. Data reduction yields the absorption coefficients for the monomer and the dimer, and the equilibrium constant for dimerization (K) (Table 4. 2). Formation of aggregates is consistent with the almost complete inhibition of $^1O_2$ production in water.

*Table 4. 2. Photophysical properties and log $P_{O/W}$ of **PS-1** and **PS-2** in PBS.*

Sample	$\varepsilon(m^*)^{[a]}$ / $M^{-1}\cdot cm^{-1}$	$\varepsilon(m^*)^{[b]}$ / $M^{-1}\cdot cm^{-1}$	$\varepsilon(d^{**})^{[b]}$ / $M^{-1}\cdot cm^{-1}$	K	log $P_{O/W}$
PS-1	50110	24181	106290	$1.1\cdot10^6$	2.33
PS-2	53818	48422	107351	$7.5\cdot10^5$	0.73

* m: monomer; ** d: dimer; [a] Beer Lambert; [b] Lavenberg-Marquardt;

Photodynamic efficiency depends also on lipophilicity, which has been recognized as a factor that can determine cellular uptake, and consequently, the phototoxicity of PS.[29,30] As mentioned in the previous Chapter, the affinity of a compound for cell membranes may be numerically represented by its membrane-water partition coefficient, that is, the membrane-water concentration ratio. As this value is usually difficult to measure, the $P_{O/W}$ is a useful quantitative parameter for evaluating the lipophilic/hydrophilic balance, and has been extensively utilized to predict the relative tendency of drugs to interact or incorporate in biological membranes.[31–33] To evaluate the affinity of **PS-1** and **PS-2** for cell membranes, and the relative lipophilicity of the compounds, the *n*-octanol/PBS partition coefficient for each Pc was determined using the shake-flask method, as explained in Experimental section – materials and methods.

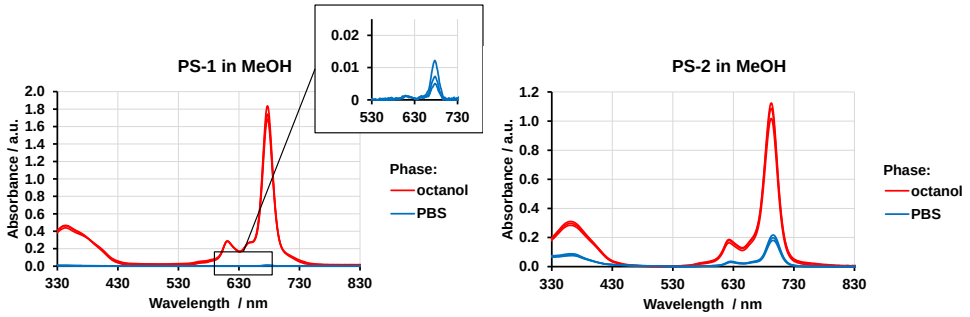

*Figure 4. 6. UV-vis of aliquots from n-octanol/PBS phases **PS-1** and **PS-2** diluted in MeOH.*

Although both compounds have a common structural core, they exhibited different amphiphilic character. **PS-1** renders a higher octanol/water partition coefficient than **PS-2**, (see Table 4. 2) indicating that the former has a more lipophilic nature. In fact, the Pc concentration reached for **PS-1** in n-octanol was approximately 200 times higher than in PBS, while the **PS-2** concentration was only 5-6 times higher in *n*-octanol than in PBS. Therefore, the *log* $P_{O/W}$ values suggest that **PS-1** is mostly hydrophobic and have very high affinity for membranes. Nevertheless, **PS-2** is more amphiphilic and its presence in the aqueous phase is bigger, which is concomitant which its higher solubility in this medium.

d) Photodynamic inactivation studies

The photodynamic studies were performed testing **PS-1** and **PS-2** in *S. aureus* and *E. coli* bacteria, chosen as models for Gram-positive and Gram-negative bacteria, respectively (Figure 4. 7). The inactivation studies present a typical light- and concentration-dependent profile. **PS-1** and **PS-2** were able to induce 99,9% (3 log decrease in colony-forming units, CFUs) of *S. aureus* inactivation at 0.1 and 0.5 μM, respectively, using a red light fluence of 33 $J \cdot cm^{-2}$. This observation indicates that the Zn(II)Pcs must be in monomeric, i.e., photochemically active form, which in turn indicates that they are bound to the bacterial cell wall, where they de-aggregate.[34] Reducing the light fluence to 11 $J \cdot cm^{-2}$ only resulted in a cell survival increase of 1 log CFU. Full inactivation (7 log CFUs) could be achieved at 10 μM for both **PS-1** and **PS-2**, even though 4-logs can be attributed to dark cytotoxicity at such high concentration. Regarding *E. coli,* larger concentrations were required to induce a comparable cell death. Up to 50 μM of either photosensitizer was needed to completely inactivate the bacterial strain, whilst 10 μM and 33 $J \cdot cm^{-2}$ were enough to achieve a disinfection (99.9%) status. In this case, no dark toxicity could be observed even at the highest concentration, which likely indicates that the compounds are not taken up by the bacteria but stick to the outer membrane.[35] This confirms that Gram-negative bacteria are harder to photo-inactivate by PDT than Gram-positive ones, an observation that has been thoroughly described in the literature.[36] The reason behind this difference is found in the composition of the bacterial wall. Importantly, there are no dramatic differences in activity between **PS-1** and **PS-2** against the microbial strains tested, indicating a minor effect of the nature of the cationic moieties, as observed previously by Ruiz-González and co-workers for two related porphycene macrocycles.[37] Compared to other symmetrically-substituted cationic Pcs, the bulky bis(trifluoromethylphenyl) groups attached to **PS-1** and **PS-2** provide them with much stronger photo-antimicrobial activity. Indeed, related Pcs lacking these groups achieved only a modest 1-2 log CFUs cell death, owing to their strong aggregation.[38,39] This issue has now been solved by constructing asymmetric compounds with large steric hindrance that alleviate the aggregation problems.

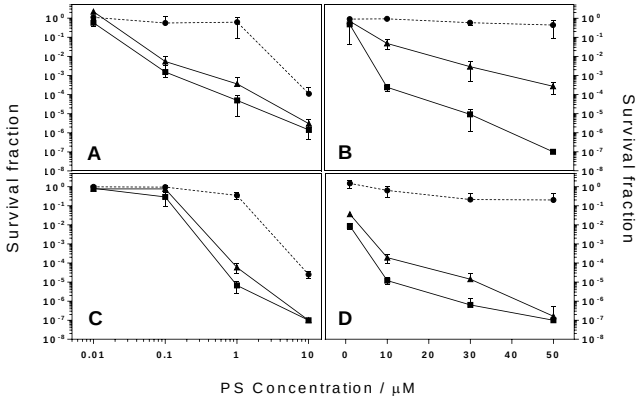

*Figure 4. 7. Survival curves of S. aureus (A, C) and E. coli (B, D) with **PS-1** (A, B) and **PS-2** (C, D) after PDI treatment. Circles, triangles and squares represent 0 (dark toxicity), 11 and 33 J·cm^{-2}, respectively.*

4.4. Conclusions

Two different cationic ABAB-ZnPcs (**PS-1** and **PS-2**) have been synthesized as PS for PDI. The peculiar functionalization of these Pcs with facing bulky substituents that provide the molecules with hampered aggregation and lipophilicity, and facing hydrophilic pyridinum (**PS-1**) or alkylammonium (**PS-2**) moieties that impart water-solubility, makes these molecules suitable candidates for the inactivation of bacteria. In order to probe the validity of the design, photophysical evaluation of their $^1O_2$ generation capabilities, as well as aggregation assays, have been carried out with **PS-1** and **PS-2**. Non-aggregated MeOH solutions of both PS efficiently generate $^1O_2$, but only residual signals were detected in water, which can be rationalized by a certain degree of aggregation. In fact, UV-vis experiments in aqueous media indicate that both PS form aggregates at some extent. Nevertheless, *in vitro* photodynamic assays carried out over *E. coli* and *S. aureus* show that they are photochemically active, inducing bacteria inactivation under red light irradiation, which in turn indicates that they are bound to the bacterial cell wall, where they de-aggregate. It has been proved that **PS-1** and **PS-2** are not toxic for bacteria in darkness in the selected range of concentrations, but when the colonies are irradiated a high fatality turns out. In this regard, there is a minor effect of the nature of the cationic moieties on the activity of these PS. Nevertheless, an important conclusion is that these cationic PS have proved much stronger activity than other related cationic Pcs as a result of the rational design that has rendered improved oxygen generation abilities,[24] well-balanced lipophilicity/hydrophilicity and diminished aggregation issues.

4.5. Experimental section

a) Materials and methods

i. *Determination of the log $P_{O/W}$*

Initially, equal volumes of *n*-octanol and PBS (pH = 7.2–7.6 at 25 °C) were mixed vigorously for 3 days at 25°C to promote solvent saturation in both phases. Each sample (**PS-1** and **PS-2**) was then added to 2 mL of the mixture and stirred for 30 min; next, they were incubated 1 h at room temperature. After separation, 100 µL of *n*-octanol phase and 100 µL of PBS phase were taken and diluted by MeOH to 1.1 mL. The UV–vis spectra of both phases were recorded, and the partition coefficient was calculated based on the absorbance values at *Q*-band maxima (677 nm for **PS-1** and 693 nm for **PS-2**). The results are the average of three independent measurements.

$$logP_{OW} = log\left(\frac{A(MeOH)_O \cdot V_W}{A(MeOH)_W \cdot V_O}\right)$$

ii. *Microbial strains, culture conditions and photodynamic inactivation studies*

The microorganisms studied were *Staphylococcus aureus* (ATCC® 29213) as a Gram-positive model and *Escherichia coli* (ATCC® 25922) as Gram-negative bacteria. Bacterial cells were grown overnight in an orbital shaker at 37 °C in tryptic soy broth (TSB) medium. An aliquot was then suspended in fresh TSB and set to grow in exponential phase at 37 °C to achieve approximately 10^8 colony forming units (CFU,·mL^{-1}). They were later centrifuged (5000 rpm, 10 min) and re-suspended in PBS (pH = 7.4). Solutions of PS-1 and PS-2 in DMSO were added to the cells keeping the DMSO content below 1% in PBS and the cells were then incubated in the dark for 30 minutes. Two independent experiments were done for each photoinactivation treatment, which in turn was carried out in duplicate. The average and SD values were calculated. Cells were then irradiated from the top in 96-well plates by means of a Red 670 Device (Red Man Light, United Kingdom; 660 ± 10 nm; 70 mW·cm^{-2}). The fluence of the lamp was regularly monitored with a power meter to ensure the light dose delivered. Controlling the cell irradiation without PS was also performed in order to exclude any inactivation due to light or heating effects, along with the evaluation of the toxicity of **PS-1** and **PS-2** in the dark. After illumination, the samples were serially diluted and streaked on agar plates and incubated in the dark for 18 h at 37 °C.

b) Synthesis

Compounds 3,3'',5,5''-tetrakis(trifluoromethyl)-[1,1':4',1''-terphenyl]-2',3'-dicarbonitrile (**B**),[21] 4,5-diiodophthalonitrile (**A-1**),[40] 4,5-bis(pyridin-3-yloxy)phthalonitrile (**A-2**),[25] 4,5-bis(4-hidroxiphenoxy)phthalonitrile (**A-3**),[41] 4,5-bis[(2-(dimethylamino)ethyl)thio]phthalonitrile (**A-4**),[26] ZnPc **1**,[21] 4-ethinylpyridine,[42] 3-(dimethylamino)propyl methyl carbonate (**8**),[43] and ZnPc **4** (**Chapter 3**) were prepared according to previously reported procedures.

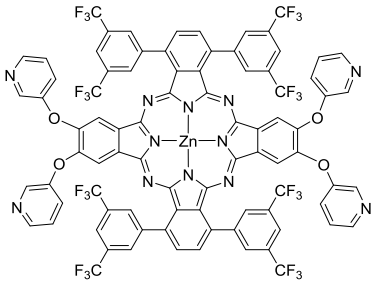

ZnPc 2: Phthalonitrile **B** (1 eq), phthalonitrile **A-2** (1 eq) and anhydrous $Zn(OAc)_2$ (1 eq) were placed in a 5 mL high pressure resistant flask equipped with a magnetic stirrer, and then 2.7 mL ([**B**]=0.1 M) of dry o-DCB/DMF 2:1 were added. The mixture was heated to 150-160ºC overnight under an argon atmosphere. After cooling the solvent was removed under vacuum. The product was purified by column chromatography on SiO_2 (heptane/EtOAc 1:3 with 1% pyridine) where the second blue-green fraction to elute containing the desired product **2**. A second batch of the product that was strongly retained can be eluted from the column using THF:pyridine (7:1). After evaporation of the solvent a blue-green solid was obtained, which was precipitated from MeOH with water. Yield: 18.8 mg, (8%). ^{1}H-NMR (300 MHz, THF-d_8): δ 8.75 (s, 8H, Ar), 8.41 (dd, J = 11.15 Hz, J = 2.76 Hz, 8H, Ar-py), 8.23 (s, 4H, Ar), 8.10 (s, 4H, Ar), 8.03 (s, 4H, Ar), 7.46-7.31 (m, 8H, Ar-py); ^{13}C-NMR (125 MHz, DMSO-d_6): 120.1, 123.4, 124.5, 124.7, 130.5, 131.2, 134.8, 136.1, 139.7, 142.4, 144.1, 144.8, 147.9, 148.7, 149.8, 151.7, 152.5, 153.7; IR(ATR) v^{-1} (cm^{-1}): 2920, 2851, 1592, 1458, 1377, 1275, 1132. HR-MS (MALDI, matrix DCTB + PMMANa 2100 + NaI) for $C_{84}H_{36}F_{24}N_{12}O_4Zn$: m/z 1796.1857 [$M^+$] (calculated: 1796.1885).

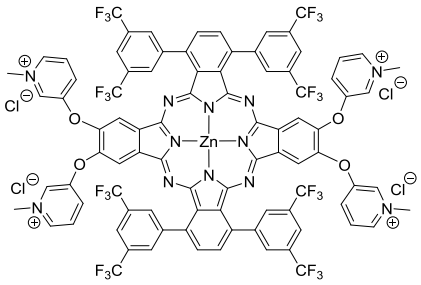

PS-1: **2** (10 mg, $5.56 \cdot 10^{-3}$ mmol) was placed in a 10 mL round bottom flask equipped with a magnetic stirrer and 1 mL of dry DMF (dried over 4Å molecular sieves) were added. Then, an excess of MeI (150 µL) was added and the mixture was stirred at room temperature for 4h under argon atmosphere. Then 10 mL of diethylether were added and the product was collected by filtration and washed several times with diethylether as a blue solid. Yield: 8.0 mg (61%). 250 mg of Dowex® (1x8 200-400) were suspended in 10 mL of MiliQ water, the product was previously dissolved in 0.2 mL of DMSO was added and stirred for 2 h. Then, the mixture was filtered, washed with diethylether, and evaporated under vacuum. ^{1}H-NMR (500 MHz, DMSO-d_6): δ 9.26 (s, 4H, Ar), 9.00 (d, J^1 = 6.00 Hz, 4H, Ar-py), 8.83 (s, 8H, Ar),

8.48 (d, J^2 = 8.87 Hz, 4H, Ar-py), 8.33 (s, 4H, Ar), 8.31 (s, 4H, Ar-py), 8.24 (dd, J^2 = 8.87 Hz, J^1 = 6.00 Hz, 4H, Ar-py), 7.95 (s, 4H, Ar), 4.45 (s, 12H, Me); IR (ATR) v^{-1} (cm^{-1}): 3016, 2931, 1584, 1498, 1409, 1276, 1171, 1125. HR-MS (ESI Positive TOF_MS-100-3500.m) for $C_{88}H_{48}F_{24}N_{12}O_4Zn$: m/z 630.4153 $[MCl]^{3+}$ (calculated: 630.4167); 963.1093 $[MCl_2]^{2+}$ (calculated: 963.1098).

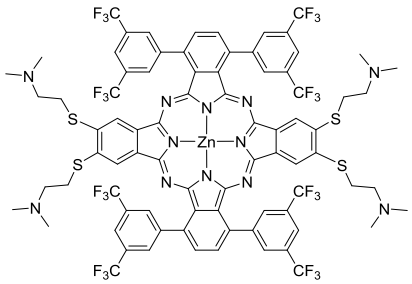

ZnPc 3: Phthalonitrile **B** (1 eq), phthalonitrile **A-3** (1 eq) and anhydrous $Zn(AcO)_2$ (1 eq) were placed in a 5 mL high pressure resistant flask equipped with a magnetic stirrer, and then 2.7 mL ([**B**]=0.1 M) of dry o-DCB/DMF 2:1 were added. The mixture was heated to 150-160ºC overnight under an argon atmosphere. After cooling the solvent was removed under vacuum. The product was purified by column chromatography on Bio-Beads using $CHCl_3$ as eluent. After evaporation of the solvent a blue solid was obtained, which was washed with heptane. Yield: 50 mg, (20%). ^{1}H-NMR (300 MHz, THF-d_8) δ (ppm): 2.35 (s, 24H, NMe_2); 2.81 (t, J = 7.09 Hz, 8H, CH_2); 3.23 (t, J = 7.09 Hz, 8H, CH_2); 8.12 (s, 4H, Ar); 8.24 (s, 4H, Ar); 8.58 (s, 4H, Ar); 8.84 (s, 8H, Ar). ^{13}C-NMR (75 MHz, THF-d_8): 33.4 (CH_2), 45.6 (NMe_2), 58.7 (CH_2), 122.4, 122.8 (brs, C*CF_3), 125.0 (q, J = 272.42 Hz, CF_3), 132.1, 132.4, 132.8, 136.4, 136.9, 137.9, 142.0, 144.3, 153.4, 154.4 (C=N). IR (ATR) v^{-1} (cm^{-1}): 2930 (ar, C-H st), 1729, 1668, 1380 (pyrrole ring), 1279, 1179 (C-F st), 1134 (C-F st). HR-MS (MALDI, matrix: DCTB+PMMA 2100+NaI) for $C_{80}H_{60}F_{24}N_{12}S_4Zn$: m/z 1837.2917 $[M+H]^+$ (calculated: 1837.2928).

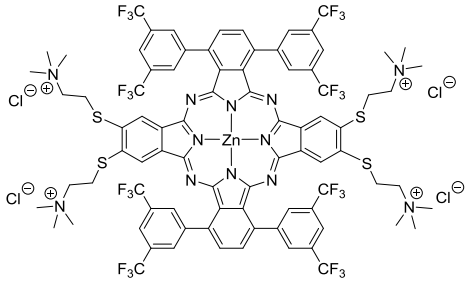

PS-2: **3** (1 eq) was placed in a 5 mL high pressure resistant flask equipped with a magnetic stirrer and 0.9 mL of dry ethanol (EtOH) (dried over 4Å molecular sieves) were added. Then, an excess of IMe (20 eq) was added and the mixture was refluxed overnight. After cooling the solvent was removed under vacuum. The residue was washed with $CHCl_3$, heptane, diethylether and $CHCl_3$ again, and a green solid was obtained. Yield: 13 mg (36%). 250 mg of Dowex® (1x8 200-400) were suspended in 10 mL of MiliQ water, the product was dissolved in 0.2 mL of DMSO was added and stirred for 2h. Then, the mixture was filtered, washed with diethylether, and evaporated under vacuum. ^{1}H-NMR (300 MHz, DMSO-d_6) δ (ppm): 3.13 (s, 36H, NMe_3); 8.22 (s, 4H, CHAr); 8.36 (s, 4H, CHAr); 8.73 (s, 4H, CHAr); 8.89 (s, 8H, CHAr); CH_2 signals are overlapped by the solvent. IR (ATR) v^{-1} (cm^{-1}): 2929 (ar, C-H st), 1682, 1482, 1388 (pyrrole ring), 1278, 1179 (C-F st), 1132 (C-F st). HR-MS (ESI Positive TOF_MS-50-3000.m) for $C_{84}H_{72}F_{24}N_{12}S_4Zn$: m/z 474.0942 $[M]^{4+}$ (calculated: 474.0943); 643.7829 $[MCl]^{3+}$ (calculated: 643.7822); 983.1589 $[MCl_2]^{2+}$ (calculated: 983.1580).

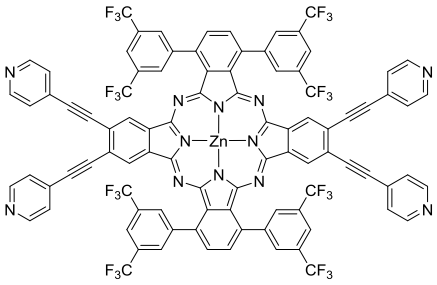

ZnPc 5: **1** (15 mg, 1 eq), **7** (6.67 eq.), $PdCl_2(PPh_3)_2$ (0.040 eq.) and CuI (0.040 eq.), were dissolved in 1 mL of dry diisopropylamine (distilled with CaH_2 and collected over 4Å activated molecular sieves) and stirred at 70 °C overnight under argon atmosphere. The mixture was diluted with chloroform (20 mL) and washed with water (3x20 mL), dried over $MgSO_4$, filtrated and evaporated under vacuum. The product was purified by column in Bio-Beads using chloroform as eluent, and then by column chromatography on SiO_2 (EtOAc/pyridine 99:1 and then THF/pyridine) being the product the last eluted fraction. After evaporation the green solid was washed with heptane. Yield: 1.5 mg (11%). ^{1}H-NMR (300 MHz, THF-d_8) δ (ppm): 7.67 (d, J = 5.76 Hz, 8H, py), 8.34 (s, 4H, Ar), 8.45 (s, 4H, Ar), 8.63 (s, 4H, Ar), 8.72 (d, J = 5.76 Hz, 8H, py), 8.85 (s, 8H, Ar). ^{13}C-NMR The low amount obtained due to the low yield prevented obtaining the spectrum IR (ATR) v^{-1} (cm^{-1}): 2959, 2927, 2359, 1591, 1377, 1275, 1165, 1132. HR-MS (MALDI (ULTRAFLEX III) DCTB + PEGNa 2000) for $C_{92}H_{36}F_{24}N_{12}Zn$: m/z 1828.2112 $[M]^+$ (calculated: 1828.2089).

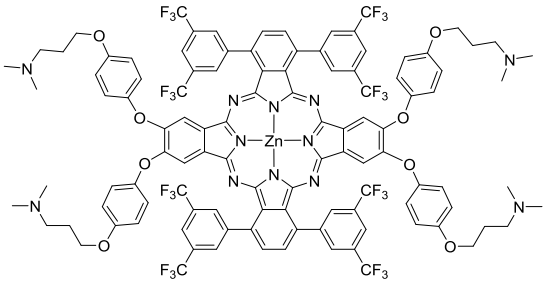

ZnPc 6: **4** (15 mg, 0.008 mmol) and **8** (15.6 mg, 0.09 mmol) were placed in a 5 mL high pressure resistant flask equipped with a magnetic stirrer and 0.85 mL of dry acetonitrile were added. Solution was heated for 90 minutes at 180 ºC under MW irradiation. After cooling, the mixture was transferred into a flask and the solvent evaporated to dryness. Finally, product was poured onto heptane and the resulting green precipitate was filtered off and dried over vacuum. Yield: 11 mg (62%). ^{1}H-NMR (500 MHz, DMSO-d_6) δ (ppm): 1.91 (t, J = 6.52 Hz, 8H, CH_2), 2.19 (s, 24H, CH_3), 2.45 (m, 8H, CH_2), 4.03 (t, J = 6.45 H, 8H, CH_2), 7.02 (d, J = 8.34 Hz, 8H, Ar), 7.06 (d, J = 8.34 Hz, 8H, Ar), 7.75 (s, 4H, Ar), 7.97 (s, 4H, Ar), 8.23 (s, 4H, Ar), 8.77 (s, 8H, Ar). ^{13}C-NMR (125 MHz, DMSO-d_6): 26.9, 45.1, 55.8, 66.3, 115.5, 115.7, 116.1, 118.5, 122.4, 129.9, 130.2, 131.2, 132.1, 134.6, 136.0, 152.2. IR (ATR) v^{-1} (cm^{-1}): 2948 (Ar, C-H st), 1711, 1593 (pyrrole ring), 1500, 1276, 1199 (C-F st), 1132 (C-F st). MS (MALDI, matrix: DCTB) for $C_{108}H_{84}F_{24}N_{12}O_8Zn$: m/z [M] + $[M+H]^+$ mixture 2196.5 (calculated: 2196.5), 2151.4 (calculated: 2151.5) [M-($HNMe_2$)], 2106.3 (calculated: 2016.4) [M-2($HNMe_2$)]. Due to the large number of ions in the region of the molecular ion it is not possible to measure the exact mass reliably by possible interference with the internal standard.

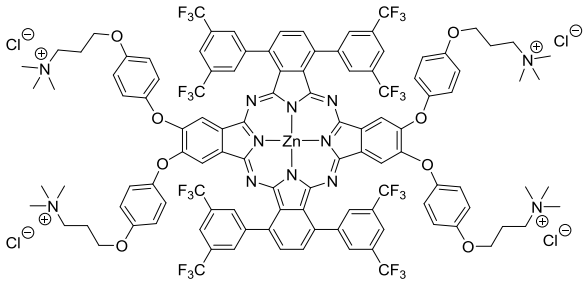

PS-3: ZnPc **6** (1 eq.) was placed in a 5 mL high pressure resistant flask equipped with a magnetic stirrer and 0.9 mL of dry ethanol (EtOH) (dried over 4Å molecular sieves) were added. Then, an excess of MeI (20 eq.) was added and the mixture was refluxed overnight. After cooling the solvent was removed under vacuum. The residue was washed with EtOAc and heptane and it was filtered off to obtain a green solid. Yield: 2 mg (19%).250 mg of Dowex® (1x8 200-400) were suspended in 10 mL of MiliQ water, the product was previously dissolved in 0.2 mL of DMSO was added and stirred for 2h. Then, the mixture was filtered, washed with diethylether, and evaporated under vacuum. ^{1}H-NMR (500 MHz, DMSO-d_6) δ (ppm): 2.25 (br s, 8H, CH_2), 3.14 (s, 36H, CH_3), 3.54 (m, 8H, CH_2), 4.10 (br s, 8H, CH_2), 6.85-7.17 (m, 16H, Ar), 7.76 (s, 4H, Ar), 7.98 (s, 4H, Ar), 8.24 (s, 4H, Ar), 8.77 (s, 8H, Ar). IR (ATR) v^{-1} (cm^{-1}): 2929 (ar, C-H st), 1616 (pyrrole ring), 1501, 1277, 1196 (C-F st), 1133 (C-F st). HR-MS (ESI Positive TOF_MS-100-3500.m) for $C_{112}H_{96}F_{24}N_{12}O_8Zn$: m/z 763.8681 $[MCl]^{3+}$ (calculated: 763.8685); 1163.2876 $[MCl_2]^{2+}$ (calculated: 1163.2874).

c) Photophysical studies

i. *Fluorescence spectra:*

The samples were excited at: **PS-1** 667 nm (MeOH), and **PS-2** 684 nm (MeOH).

ii. *Fluorescence Quantum Yields:*

The samples were excited at: **PS-1** 651.5 nm (MeOH), and **PS-2** 634 nm (MeOH).

4.6. References

(1) Szeimies, R. M.; Karrer, S.; Abels, C.; Landthaler, M.; Elmets, C. A. Photodynamic Therapy in Dermatology. *Dermatological Phototherapy and Photodiagnostic Methods* **2009**, No. 5, 241–280.

(2) Vera, D. M. A.; Haynes, M. H.; Ball, A. R.; Dai, T.; Astrakas, C.; Kelso, M. J.; Hamblin, M. R.; Tegos, G. P. Strategies to Potentiate Antimicrobial Photoinactivation by Overcoming Resistant Phenotypes. *Photochem. Photobiol.* **2012**, *88* (3), 499–511.

(3) Wainwright, M. Photodynamic Antimicrobial Chemotherapy (PACT). *J. Antimicrob. Chemother.* **1998**, *42* (1), 13–28.

(4) Alves, E.; Faustino, M. A. F.; Neves, M. G. P. M. S.; Cunha, Â.; Nadais, H.; Almeida, A. Potential Applications of Porphyrins in Photodynamic Inactivation beyond the Medical Scope. *J. Photochem. Photobiol. C Photochem. Rev.* **2015**, *22*, 34–57.

(5) Yin, R.; Agrawal, T.; Khan, U.; Gupta, G. K.; Rai, V.; Huang, Y.-Y.; Hamblin, M. R. Antimicrobial Photodynamic Inactivation in Nanomedicine: Small Light Strides against Bad Bugs. *Nanomedicine (Lond).* **2015**, *10* (15), 2379–2404.

(6) Habermeyer, B.; Guilard, R. Some Activities of PorphyChem Illustrated by the Applications of Porphyrinoids in PDT, PIT and PDI. *Photochem. Photobiol. Sci.* **2018**, *17* (11), 1675–1690.

(7) Mesquita, M. Q.; Dias, C. J.; Neves, M. G. P. M. S.; Almeida, A.; Faustino, M. A. F. Revisiting Current Photoactive Materials for Antimicrobial Photodynamic Therapy. *Molecules* **2018**, *23* (10), 1–47.

(8) Almeida-Marrero, V.; van de Winckel, E.; Anaya-Plaza, E.; Torres, T.; de la Escosura, A. Porphyrinoid Biohybrid Materials as an Emerging Toolbox for Biomedical Light Management. *Chem. Soc. Rev.* **2018**, *47* (19), 7369–7400.

(9) Li, X.; Zheng, B.-D.; Peng, X.-H.; Li, S.-Z.; Ying, J.-W.; Zhao, Y.; Huang, J.-D.; Yoon, J. Phthalocyanines as Medicinal Photosensitizers: Developments in the Last Five Years. *Coord. Chem. Rev.* **2019**, *379*, 147–160.

(10) Li, Y.; Wang, J.; Zhang, X.; Guo, W.; Li, F.; Yu, M.; Kong, X.; Wu, W.; Hong, Z. Highly Water-Soluble and Tumor-Targeted Photosensitizers for Photodynamic Therapy. *Org. Biomol. Chem.* **2015**, *13* (28), 7681–7694.

(11) Koç, V.; Topal, S. Z.; Aydın Tekdaş, D.; Ateş, Ö. D.; Önal, E.; Dumoulin, F.; Gürek, A. G.; Ahsen, V. Assessment of the Relevance of GaPc Substituted with Azido-Polyethylene Glycol Chains for Photodynamic Therapy. Design, Synthetic Strategy, Fluorescence, Singlet Oxygen Generation, and PH-Dependent Spectroscopic Behaviour. *New J. Chem.* **2017**, *41* (18), 10027–10036.

(12) Lourenço, L. M. O.; Sousa, A.; Gomes, M. C.; Faustino, M. A. F.; Almeida, A.; Silva, A. M. S.; Neves, M. G. P. M. S.; Cavaleiro, J. A. S.; Cunha, Â.; Tomé, J. P. C. Inverted Methoxypyridinium Phthalocyanines for PDI of Pathogenic Bacteria. *Photochem. Photobiol. Sci.* **2015**, *14* (10), 1853–1863.

(13) van de Winckel, E.; David, B.; Simoni, M. M.; González-Delgado, J. A.; de la Escosura, A.; Cunha, Â.; Torres, T. Octacationic and Axially Di-Substituted Silicon (IV) Phthalocyanines for Photodynamic Inactivation of Bacteria. *Dye. Pigment.* **2017**, *145*, 239–245.

(14) Lourenço, L. M. O.; Rocha, D. M. G. C.; Ramos, C. I. V; Gomes, M. C.; Almeida, A.; Faustino, M. A. F.; Almeida Paz, F. A.; Neves, M. G. P. M. S.; Cunha, Â.; Tomé,

J. P. C. Photoinactivation of Planktonic and Biofilm Forms of Escherichia Coli through the Action of Cationic Zinc(II) Phthalocyanines. *ChemPhotoChem* **2019**, *3* (5), 251–260.

(15) İşci, Ü.; Beyreis, M.; Tortik, N.; Topal, S. Z.; Glueck, M.; Ahsen, V.; Dumoulin, F.; Kiesslich, T.; Plaetzer, K. Methylsulfonyl Zn Phthalocyanine: A Polyvalent and Powerful Hydrophobic Photosensitizer with a Wide Spectrum of Photodynamic Applications. *Photodiagnosis Photodyn. Ther.* **2016**, *13*, 40–47.

(16) Spesia, M. B.; Rovera, M.; Durantini, E. N. Photodynamic Inactivation of Escherichia Coli and Streptococcus Mitis by Cationic Zinc(II) Phthalocyanines in Media with Blood Derivatives. *Eur. J. Med. Chem.* **2010**, *45* (6), 2198–2205.

(17) Ullah, A.; Zhang, Y.; Iqbal, Z.; Zhang, Y.; Wang, D.; Chen, J.; Hu, P.; Chen, Z.; Huang, M. Household Light Source for Potent Photo-Dynamic Antimicrobial Effect and Wound Healing in an Infective Animal Model. *Biomed. Opt. Express* **2018**, *9* (3), 1006–1019.

(18) Zhao, Y.; Ying, J.-W.; Sun, Q.; Ke, M.-R.; Zheng, B.-Y.; Huang, J.-D. A Novel Silicon(IV) Phthalocyanine-Oligopeptide Conjugate as a Highly Efficient Photosensitizer for Photodynamic Antimicrobial Therapy. *Dye. Pigment.* **2020**, *172*, 107834.

(19) Sindelo, A.; Kobayashi, N.; Kimura, M.; Nyokong, T. Physicochemical and Photodynamic Antimicrobial Chemotherapy Activity of Morpholine-Substituted Phthalocyanines: Effect of Point of Substitution and Central Metal. *J. Photochem. Photobiol. A Chem.* **2019**, *374*, 58–67.

(20) Zhang, X. F.; Xi, Q.; Zhao, J. Fluorescent and Triplet State Photoactive J-Type Phthalocyanine Nano Assemblies: Controlled Formation and Photosensitizing Properties. *J. Mater. Chem.* **2010**, *20* (32), 6726–6733.

(21) Fazio, E.; Jaramillo-García, J.; de La Torre, G.; Torres, T. Efficient Synthesis of ABAB Functionalized Phthalocyanines. *Org. Lett.* **2014**, *16*, 4706–4709.

(22) Fazio, E.; Jaramillo-García, J.; Medel, M.; Urbani, M.; Grätzel, M.; Nazeerudin, M. K.; de la Torre, G.; Torres, T. ABAB Phthalocyanines: Scaffolds for Building Unprecedented Donor–π–Acceptor Chromophores. *ChemistryOpen* **2017**, *6* (1), 121–127.

(23) Revuelta-Maza, M. A.; Hally, C.; Nonell, S.; de la Torre, G.; Torres, T. Crosswise Phthalocyanines with Collinear Functionalization: New Paradigmatic Derivatives for Efficient Singlet Oxygen Photosensitization. *Chempluschem* **2019**, *84* (6), 673–679.

(24) Revuelta-Maza, M. A.; Nonell, S.; de la Torre, G.; Torres, T. Boosting the Singlet Oxygen Photosensitization Abilities of Zn(II) Phthalocyanines through Functionalization with Bulky Fluorinated Substituents. *Org. Biomol. Chem.* **2019**, *17* (32), 7448–7454.

(25) Li, H.; Jensen, T. J.; Fronczek, F. R.; Vicente, M. G. H. Syntheses and Properties of a Series of Cationic Water-Soluble Phthalocyanines. *J. Med. Chem.* **2008**, *51* (3), 502–511.

(26) Duan, W.; Lo, P. C.; Duan, L.; Fong, W. P.; Ng, D. K. P. Preparation and in Vitro Photodynamic Activity of Amphiphilic Zinc(II) Phthalocyanines Substituted with 2-(Dimethylamino)Ethylthio Moieties and Their N-Alkylated Derivatives. *Bioorganic Med. Chem.* **2010**, *18* (7), 2672–2677.

(27) Campbell, L. J.; Borges, L. F.; Heldrich, F. J. Microwave Accelerated Preparation of Aryl 2-(N,N-Diethylamino)Ethyl Ethers. *Bioorganic Med. Chem. Lett.* **1994**, *4*

(21), 2627–2630.

(28) Abós, P.; Artigas, C.; Bertolotti, S.; Braslavsky, S. E.; Fors, P.; Lang, K.; Nonell, S.; Rodríguez, F. J.; Sesé, M. L.; Trull, F. R. Polymer Bound Pyrrole Compounds, IX. Photophysical and Singlet Molecular Oxygen Photosensitizing Properties of Mesoporphyrin IX Covalently Bound to a Low Molecular Weight Polyethylene Glycol. *J. Photochem. Photobiol. B Biol.* **1997**, *41* (1), 53–59.

(29) Ezzeddine, R.; Al-Banaw, A.; Tovmasyan, A.; Craik, J. D.; Batinic-Haberle, I.; Benov, L. T. Effect of Molecular Characteristics on Cellular Uptake, Subcellular Localization, and Phototoxicity of Zn(II) N-Alkylpyridylporphyrins. *J. Biol. Chem.* **2013**, *288* (51), 36579–36588.

(30) Bacellar, I. O. L.; Pavani, C.; Sales, E. M.; Itri, R.; Wainwright, M.; Baptista, M. S. Membrane Damage Efficiency of Phenothiazinium Photosensitizers. *Photochem. Photobiol.* **2014**, *90* (4), 801–813.

(31) Engelmann, F. M.; Rocha, S. V. O.; Toma, H. E.; Araki, K.; Baptista, M. S. Determination of N-Octanol/Water Partition and Membrane Binding of Cationic Porphyrins. *Int. J. Pharm.* **2007**, *329* (1), 12–18.

(32) Alonso, L.; Sampaio, R. N.; Souza, T. F. M.; Silva, R. C.; Neto, N. M. B.; Ribeiro, A. O.; Alonso, A.; Gonçalves, P. J. Photodynamic Evaluation of Tetracarboxy-Phthalocyanines in Model Systems. *J. Photochem. Photobiol. B Biol.* **2016**, *161*, 100–107.

(33) Lei, W.; Xie, J.; Hou, Y.; Jiang, G.; Zhang, H.; Wang, P.; Wang, X.; Zhang, B. Mitochondria-Targeting Properties and Photodynamic Activities of Porphyrin Derivatives Bearing Cationic Pendant. *J. Photochem. Photobiol. B Biol.* **2010**, *98* (2), 167–171.

(34) Ragàs, X.; He, X.; Agut, M.; Roxo-Rosa, M.; Gonsalves, R. A.; Serra, C. A.; Nonell, S. Singlet Oxygen in Antimicrobial Photodynamic Therapy: Photosensitizer-Dependent Production and Decay in E. Coli. *Molecules*. 2013, pp 2712–2725.

(35) Ragàs, X.; Agut, M.; Nonell, S. Singlet Oxygen in Escherichia Coli: New Insights for Antimicrobial Photodynamic Therapy. *Free Radic. Biol. Med.* **2010**, *49* (5), 770–776.

(36) Hamblin, R. Y. and M. R. Antimicrobial Photosensitizers: Drug Discovery Under the Spotlight. *Current Medicinal Chemistry*. 2015, pp 2159–2185.

(37) Ruiz-González, R.; Agut, M.; Reddi, E.; Nonell, S. A Comparative Study on Two Cationic Porphycenes: Photophysical and Antimicrobial Photoinactivation Evaluation. *International Journal of Molecular Sciences*. 2015, pp 27072–27086.

(38) Pereira, J. B.; Carvalho, E. F. A.; Faustino, M. A. F.; Fernandes, R.; Neves, M. G. P. M. S.; Cavaleiro, J. A. S.; Gomes, N. C. M.; Cunha, Â.; Almeida, A.; Tomé, J. P. C. Phthalocyanine Thio-Pyridinium Derivatives as Antibacterial Photosensitizers†. *Photochem. Photobiol.* **2012**, *88* (3), 537–547.

(39) Anaya-Plaza, E.; van de Winckel, E.; Mikkilä, J.; Malho, J.-M.; Ikkala, O.; Gulías, O.; Bresolí-Obach, R.; Agut, M.; Nonell, S.; Torres, T.; et al. Photoantimicrobial Biohybrids by Supramolecular Immobilization of Cationic Phthalocyanines onto Cellulose Nanocrystals. *Chem. – A Eur. J.* **2017**, *23* (18), 4320–4326.

(40) Terekhov, D. S.; Nolan, K. J. M.; McArthur, C. R.; Leznoff, C. C. Synthesis of 2,3,9,10,16,17,23,24-Octaalkynylphthalocyanines and the Effects of Concentration and Temperature on Their 1H NMR Spectra. *J. Org. Chem.* **1996**, *61* (9), 3034–3040.

(41) Li, M.; Khoshdel, E.; Haddleton, D. M. Synthesis of Water Soluble PEGylated

(Copper) Phthalocyanines via Mitsunobu Reaction and Cu(I)-Catalysed Azide–Alkyne Cycloaddition (CuAAC) "Click" Chemistry. *Polym. Chem.* **2013**, *4* (16), 4405–4411.

(42) Bonakdarzadeh, P.; Topić, F.; Kalenius, E.; Bhowmik, S.; Sato, S.; Groessl, M.; Knochenmuss, R.; Rissanen, K. DOSY NMR, X-Ray Structural and Ion-Mobility Mass Spectrometric Studies on Electron-Deficient and Electron-Rich M6L4 Coordination Cages. *Inorg. Chem.* **2015**, *54* (12), 6055–6061.

(43) Aricò, F.; Evaristo, S.; Tundo, P. Chemical Behavior and Reaction Kinetics of Sulfur and Nitrogen Half-Mustard and Iprit Carbonate Analogues. *ACS Sustain. Chem. Eng.* **2013**, *1* (10), 1319–1325.

- PART 2 -

AABB

PHTHALOCYANINES

Chapter 5 – Synthesis and aggregation studies of functional binaphthyl-bridged chiral phthalocyanines

OL | Organic Letters

Cite This: Org. Lett. 2019, 21, 8183−8186

Letter

pubs.acs.org/OrgLett

Synthesis and Aggregation Studies of Functional Binaphthyl-Bridged Chiral Phthalocyanines

Miguel Á. Revuelta-Maza,[†] Tomás Torres,*[,†,‡,§] and Gema de la Torre*[,†,‡]

[†]Universidad Autónoma de Madrid, c/Francisco Tomás y Valiente 7, 28049 Madrid, Spain

[‡]Institute for Advanced Research in Chemical Sciences (IAdChem), Universidad Autónoma de Madrid, 28049 Madrid, Spain

[§]Instituto Madrileño de Estudios Avanzados (IMDEA)-Nanociencia, c/Faraday 9, Cantoblanco, 28049 Madrid, Spain

Supporting Information

ABSTRACT: We describe the preparation of a battery of chiral Zn(II) phthalocyanines with an AABB substitution pattern through cross-condensation of different chiral, binaphthyloxy-linked bisphthalonitriles and (non)-functionalized single phthalonitriles. All the compounds are endowed with reactive groups (halogen and/or ethynyl moieties) that will allow us to prepare customized amphiphilic phthalocyanines. Preliminary self-assembly studies in solution have been performed by UV−vis and circular dichroism experiments.

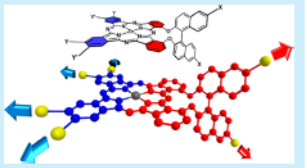

Because of their excellent optical and electronic properties, phthalocyanines (Pcs) are appealing functional chromophores with applications in different fields that span from materials science to nanomedicine.[1] In particular, helical supramolecular architectures fabricated from optically active Pc compounds have attracted widespread attention in relation with their potential applications in chiral sensing, catalysis, and chiroptical devices.[2−4] Among the different strategies to induce chirality in Pcs,[5−7] the introduction of optically active binaphthyl conformers as substituents deserves special mention. Binaphthyl-containing Pcs were formerly described by Kobayashi and co-workers,[8] who demonstrated that the optical purity of the binaphthyloxy-phthalonitrile precursor was preserved under the harsh conditions of the Pc core formation. From then on, several Pcs and related compounds endowed with optically pure binaphtyl cores have been prepared,[9−13] some of them (i.e., symmetrically substituted derivatives) showing self-assembly abilities that lead to chiral supramolecular structures.[14−17]

Within this family of compounds, particularly interesting are the low-symmetry, optically active "adjacent" type Pcs with C_{2v} symmetry (Scheme 1), which can be envisioned as central cores for the development of amphiphilic Pcs after proper functionalization at the different positions of the macrocycle. This type of compounds was previously synthesized by mixed condensation between a (non)functionalized phthalonitrile (B) and a geometrically constrained binaphthyloxy-bridged bisphthalonitrile (AA). This approach substantially reduced the number of possible Pcs formed in the statistical cross-condensation from six to three, namely AAAA, AABB, and BBBB Pcs. Several groups have reported a number of optically active AABB Pcs and related derivatives functionalized with solubilizing alkyl or alkoxy moieties at the B isoindoles,[18−22] but there are no reports on the synthesis and characterization of chiral C_{2v}-type AABB Pcs with an amphiphilic character imparted by the proper substitution at either the binaphthyl rings or the A isoindoles, or at both sites.[22] Self-assembling amphiphile systems, specially π-conjugated[23] and chromophoric[24] building blocks, is an efficient route to construct a large variety of useful nanostructures.[25] Therefore, a customized functionalization of optically active AABB Pcs could convert them in amphiphiles prone to self-assemble in a chiral fashion through an interplay of π−π interactions and solvent-induced effects.

In recent years, we have reported several examples of "oppositely" substituted-Pcs (ABAB, D_{2h} type),[26] which have been successfully employed either for building unprecedented donor-π-acceptor chromophores for photovoltaic cells[27] or as potential photosensitizers for photodynamic therapy when appropriately functionalized with hydrophilic groups.[28] Now, we are focusing our attention on the synthesis of binaphthyl-containing AABB Pcs as platforms for the preparation of differently functionalized C_{2v} systems provided with amphiphilic character and self-assembly abilities that can give rise to outstanding chiral nanostructures. To this aim, we have explored the preparation of a battery of optically active, low symmetrical AABB Pcs (1−6, Scheme 1) from AA bisphthalonitriles (7a−d) and (non)functionalized single phthalonitriles (8a−d). The final goal is to prepare AABB

Received: August 2, 2019
Published: September 26, 2019

DOI: 10.1021/acs.orglett.9b02718
Org. Lett. 2019, 21, 8183−8186

5.1. Citation and contribution

Revuelta-Maza, M.Á.; Torres, T.; Torre, G. de la Synthesis and Aggregation Studies of Functional Binaphthyl-Bridged Chiral Phthalocyanines. *Org. Lett.* **2019**, *21*, 8183–8186.

Contribution: Revuelta-Maza, M.A.: Synthesis, characterization, and aggregation studies. Preparation of the manuscript.

Funding and supervision: de la Torre, G.; Torres, T. This work has been supported by MINECO (CTQ2017-85393-P) and ERA-NET/MINECO EuroNanoMed2017-191/PCIN-2017-042.

Abstract:

We describe the preparation of a battery of chiral Zn(II) phthalocyanines with an AABB substitution pattern through cross-condensation of different chiral, binaphthyloxy-linked bisphthalonitriles and (non)- functionalized single phthalonitriles. All the compounds are endowed with reactive groups (halogen and/or ethynyl moieties) that will allow us to prepare customized amphiphilic phthalocyanines. Preliminary self-assembly studies in solution have been performed by UV−vis and circular dichroism experiments.

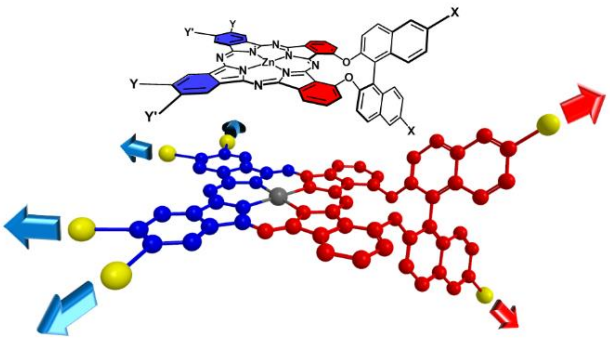

5.2. Introduction and Objectives

Helical supramolecular architectures fabricated from optically active Pc compounds have attracted widespread attention in relation with their potential applications in chiral sensing, catalysis, and chiroptical devices.[1–3] Among the different strategies to induce chirality in Pcs,[2–6] the introduction of optically active binaphthyl conformers as substituents deserves special mention. Binaphthyl-containing Pcs were formerly described by Kobayashi and co-workers,[7] who demonstrated that the optical purity of the binaphthyloxy-phthalonitrile precursor was preserved under the harsh conditions of the Pc core formation. From then on, several Pcs and related compounds endowed with optically pure binaphtyl cores have been prepared,[8–12] some of them (i.e. symmetrically substituted derivatives) showing self-assembly abilities that lead to chiral supramolecular structures.[13–16]

Within this family of compounds, particularly interesting are the low-symmetry, optically active 'adjacent' type Pcs with C_{2v} symmetry (Figure 5.1) which can be envisioned as central cores for the development of amphiphilic Pcs after proper functionalization at the different positions of the macrocycle. This type of compounds were previously synthesized by mixed condensation between a (non-)functionalized phthalonitrile (B) and a geometrically-constrained binaphthyloxy-bridged bisphthalonitrile (AA). This approach substantially reduced the number of possible Pcs formed in the statistical cross-condensation from six to three, namely AAAA, AABB and BBBB Pcs. Several groups have reported a number of optically active AABB Pcs and related derivatives functionalized with solubilizing akyl or alkoxy moieties at the B isoindoles,[17–21] but there are no reports on the synthesis and characterization of chiral C_{2v}-type AABB Pcs with an amphiphilic character imparted by the proper substitution at either the binaphthyl rings or the A isoindoles, or at both sites. However, non-chiral Zn(II)Pcs but with an amphiphilic character and C_{2v} geometry have been described by B. Ongarora et al.[22] Self-assembling amphiphile systems, specially π-conjugated[23,24] and chromophoric[25,26] building blocks, is an efficient route to construct a large variety of useful nanostructures.[27–29] Therefore, a customized functionalization of optically active AABB Pcs could convert them in amphiphiles prone to self-assemble in a chiral fashion through an interplay of π-π interactions and solvent-induced effects.

In recent years, as shown in **Part 1** of this thesis (**Background** and **Chapters 1 to 4**), we have reported several examples of 'oppositely' substituted-Pcs (ABAB, D_{2h} type),[30] that have been successfully employed either for building unprecedented donor-π-acceptor chromophores for photovoltaic cells,[31,32] or as potential PS for photodynamic therapy when appropriately functionalized with hydrophilic groups.[33,34] Next, we are focusing our attention on the synthesis of binaphthyl-containing AABB Pcs (Figure 5. 1) as platforms for the preparation of differently functionalized C_{2v} systems provided with

amphiphilic character and self-assembly abilities that can give rise to outstanding chiral nanostructures.

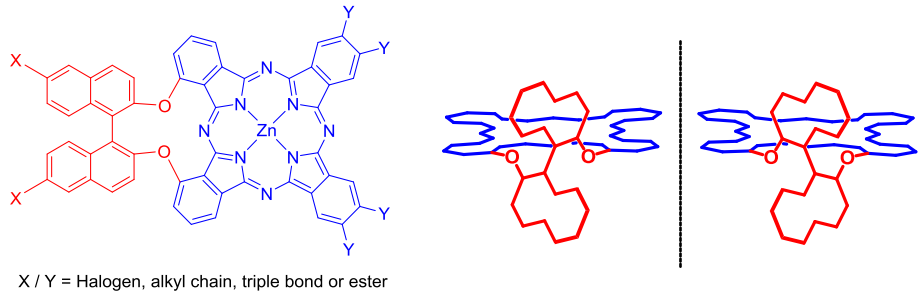

Figure 5. 1. Binaphthyl-containing AABB Zn(II)Pcs as platforms for the preparation of differently functionalized C_{2v} systems.

To this aim, we have explored the preparation of a battery of optically active, low symmetrical AABB Pcs (**1-6**, Scheme 5. 2, see below) from AA bisphthalonitriles (**7a-d,** Scheme 5. 1 see below) and (non-)functionalized single phthalonitriles (**8a-d**). The final goal is to prepare AABB Pcs in reasonable yields, and containing reactive groups (halogen, and ethynyl moieties) that can give rise to further chemical transformations directed towards the introduction of hydrophilic residues. On the other hand, in order to enhance the solubility and enlarge the hydrophobic part of the final Pc, some of the AA and B precursors have been decorated with alkyl chains. In such a way, the prepared Pc building blocks can give rise to a variety of customized compounds with amphiphilic features that will allow us to modulate their properties in terms of solubility, supramolecular organization, and plausible biological applications.

5.3. Results and discussion

a) Synthesis

Key AA-bisphthalonitriles **7a-d** were prepared from the chiral (R)-1,1'-bi-2-naphthol (BINOL), (see Scheme 5. 1). The synthesis of **7a** [17,35] and **7b**[13,36,37] had been previously described. (R)-**7a** can be obtained via a single step high yielding reaction from commercially available 3-nitrophthalonitrile and (S)- or (R)-BINOL. In order to enhance its solubility and the hydrophobic character of the final Pc, this BINOL can be decorated with two alkyl chains attached to the binaphthyl linker. (R)-**7b** was prepared trough nucleophilic aromatic substitution reaction using 3-nitrophthalonitrile and (R)-2,2'-dihydroxy-6,6'-dioctyl-1,1'-binaphthyl (**12**), which was obtained after a protection step, Grignard reaction, and deprotection of (R)-**9**. In the case of **7c**, we have also prepared the (S)-enantiomer in order to check if the chirality of the binapthyl unit is preserved

under the conditions that we apply for the preparation of Pcs. Therefore, **7c** was prepared through a double *ipso*-substitution of 3-nitrophthalonitrile with either (S)- or (R)-6,6'-dibromo-1,1'-bi-2-naphthol **9** (Scheme 5. 1), which were previously obtained by bromination of the corresponding enantiomer of BINOL.[36] Finally, (R)-**9** was subjected to Sonogashira coupling with ^{t}BuMe$_2$Si-acetylene,[38] yielding a BINOL derivative functionalized with protected ethynyl moieties (**10**) that led to the latter bisphthalonitrile **7d** (Scheme 5. 1). For the novel **7c** and **7d** COSY and ^{1}H NMR spectra are respectively showed in Figure 5. 2 and Figure 5. 3.

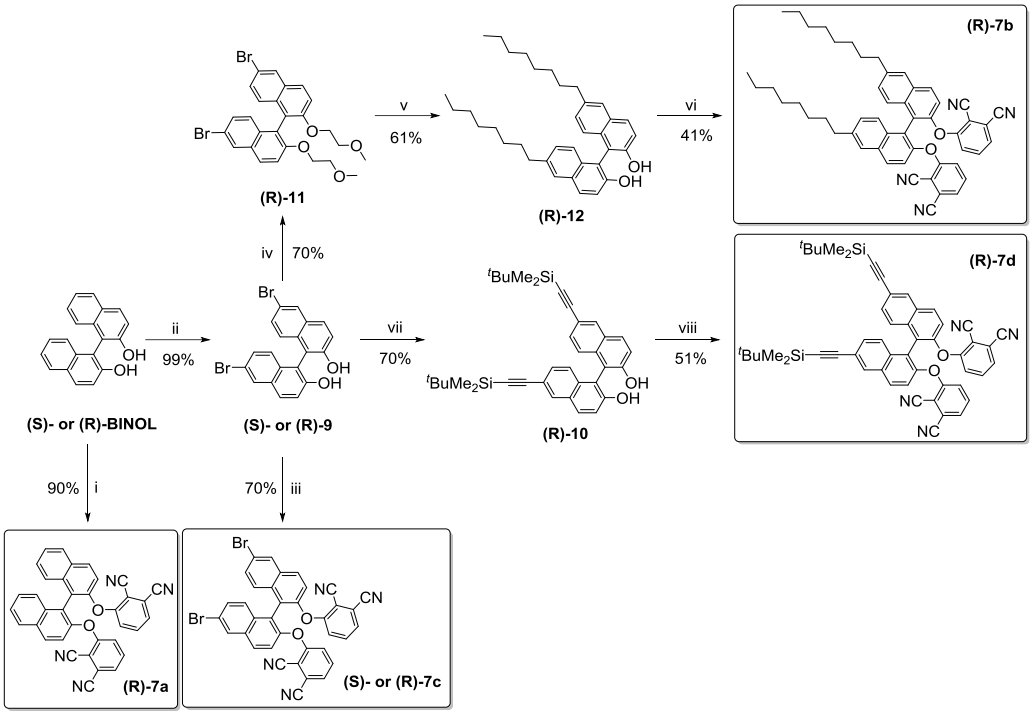

*Scheme 5. 1. i) Synthesis of optically active (R)- or (S)- **AA** phthalonitriles (**7 a-d**). i) 3-nitrophthalonitrile, K_2CO_3, DMF, r.t., 72h; ii) Br_2, DCM, -78°C to r.t., 3.5h; iii) 3-nitrophthalonitrile, K_2CO_3, DMSO, r.t., 5h; iv) NaH, CH_3OCH_2Cl, THF, 0°C to r.t., 12h; v) (1) (dppp)$NiCl_2$, 1-$C_8H_{17}MgBr$, Et_2O, r.t. to reflux, 40h, (2) HCl, $CHCl_3$/MeOH, r.t., 10h; vi) 3-nitrophthalonitrile, K_2CO_3, DMSO, r.t., 72h; vii) ^{t}BuMe$_2$Si-acetylene, $PdCl_2(PPh_3)_2$, CuI, Et_3N, 60°C, 4h; viii) 3-nitrophthalonitrile, K_2CO_3, DMSO, r.t., 48h.*

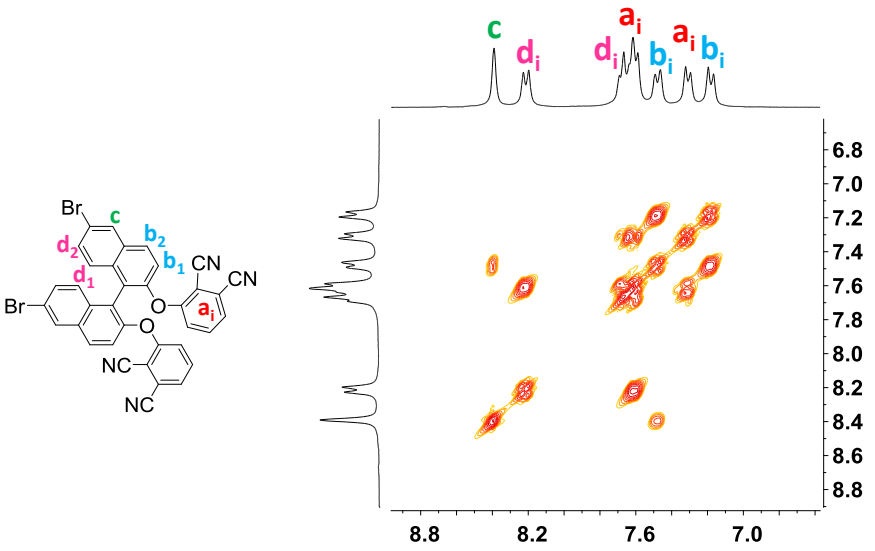

*Figure 5. 2. COSY of **7c** in DMSO-d_6*

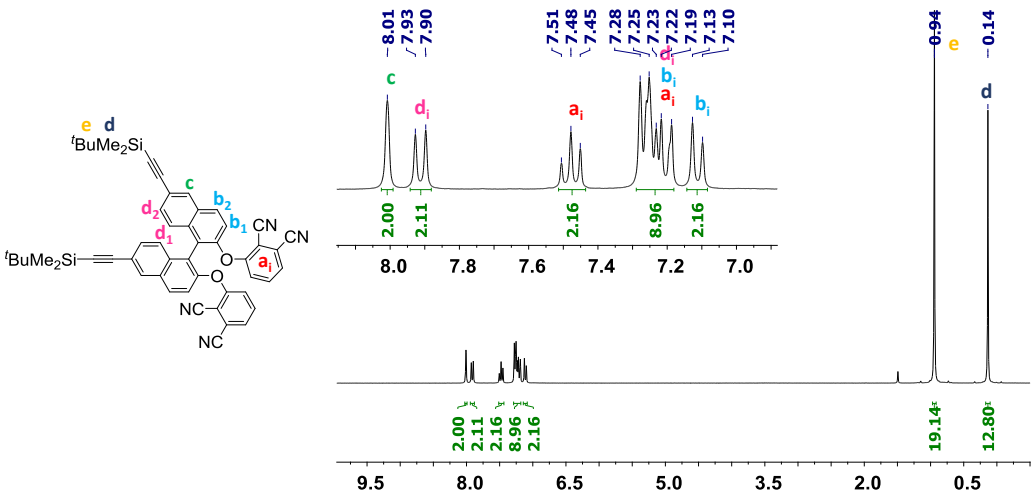

*Figure 5. 3. ^{1}H-NMR of **7d** in $CDCl_3$.*

With the bisphthalonitriles **7a-d** in hand, we proceeded to carry out the mixed condensation with single phthalonitriles, **8a-d** (Scheme 5. 2), which are either commercially available or prepared following reported procedures (see Experimental section). The cross condensation was performed by heating a 1:2 mixture of the corresponding AA-bisphthalonitriles and the single phthlonitriles B, respectively, in the presence of $Zn(OAc)_2$ in *o*-DCB/DMF 2:1 at 160°C. In these conditions, the target AABB derivatives **1-6** were formed, together with the corresponding symmetrical $(B)_4$ and $(AA)_2$

Zn(II)Pcs. It is worth mentioning that in the previous reports on binaphthyl AABB Pcs, AA phthalonitriles had to be converted into their more reactive isoindoline forms, and then reacted with another 1,3-diiminoisoindoline derivative, followed by a metalation step.[17,20,21] In our case, using the above mentioned conditions, we could skip the activation of both precursors and the subsequent metalation, and still obtaining our Zn(II)Pcs **1-6** in similar, or even higher yields, than those previously reported.

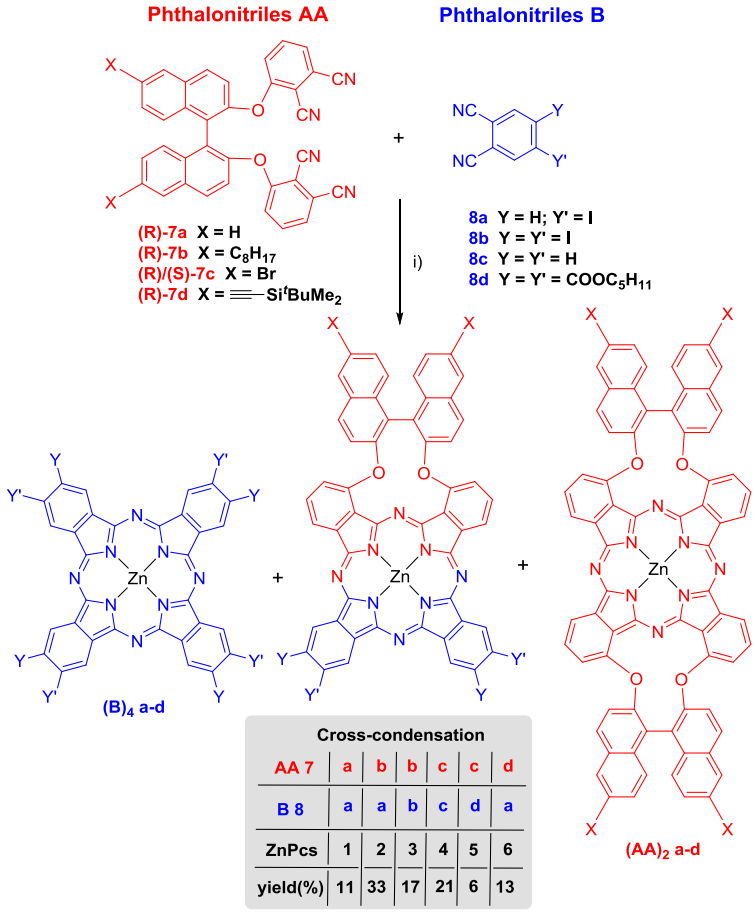

Scheme 5. 2. Synthesis of AABB Zn(II)Pcs. (i): o-DCB:DMF, 2:1, $Zn(OAc)_2$ 150-160°C, overnight.

From all the possible combinations of bisphthalonitriles **7a-d** and phthalonitriles **8a-d**, we selected those in which: i) halogens are installed in only one of the components, AA or B (i.e. Zn(II)Pcs **1** and **4**), which would permit further coupling reactions with, for instance, hydrophilic moieties; ii) one of the components is endowed with hydrophobic alkyl chains and the other holds halogen atom(s), (i.e. Zn(II)Pcs **2**, **3** and **5**); and iii) the ethynyl-containing bisphthalonitrile **7d** is reacted with halogen-containing phthalonitriles, affording the possibility of orthogonal functionalization of both components through

cross-coupling methodologies. First, cross condensation between non-functionalized bisphthalonitrile **7a** and iodo-containing phthalonitriles **8a** and **8b** was tackled. Isolation of the target AABB Zn(II)Pc **1** proved difficult, but it was finally obtained in 11% yield. However, the condensation of **7a** with **8b** gave rise to mixtures from which the target AABB compound could not be isolated. Bisphthalonitrile **7b**, functionalized with two octyl chains, reacted successfully with both iodo-containing phthalonitriles **8a** and **8b,** leading to Zn(II)Pcs **2** and **3** in 17% and 33% yields, respectively, which can be considered from moderate to good considering the statistical nature of the process. However the opposite approach that implies the reaction of the hydrophobic phthalonitrile **8d** with the bromo-containing bisphthalonitrile **7c** led to the corresponding AABB Zn(II)Pc **5** in the lowest yield of the series (6%). **7c** was also reacted with the non-functionalized phthalonitrile **8c** to give Zn(II)Pc **4** in 21% yield. Finally, ethynyl-containing bisphthalonitrile **7d** was reacted with **8a** and **8b**, but only Zn(II)Pc **6** endowed with two iodine atoms could be obtained in moderate 13% yield. Attending to their interesting functionalization pattern, which can also lead to interesting nanostructures upon appropriate derivatization, the symmetrical tetrabromo- (**$(AA)_2$-c**) and tetraethynyl- (**$(AA)_2$-d**) Zn(II)Pcs were isolated from the reaction mixtures, and properly characterized (see the Experimental Section).

^{1}H NMR spectra of Zn(II)Pcs **1**-**6** were registered in coordinative solvents such as THF-d_8 or DMSO-d_6 to avoid aggregation, but, in most of the cases, heating at 50ºC (in THF) or 90ºC (in DMSO) was also necessary to further break the aggregation that most of the compounds show at NMR concentrations (i.e. 10^{-3} M). In Figure 5. 4, the well-resolved spectrum of AABB Zn(II)Pc **5** is compared with those of its **B_4** and **$(AA)_2$** counterparts.

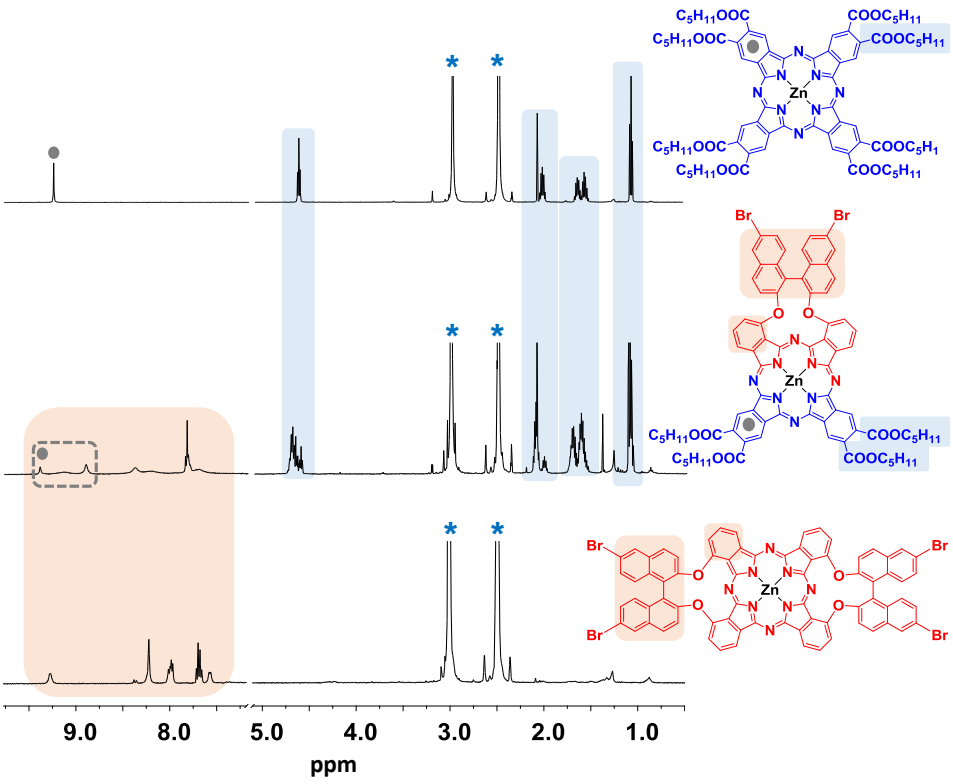

*Figure 5. 4. ^{1}H NMR of **B_4-d**, Zn(II)Pc **5** and **$(AA)_2$-c** in DMSO-d_6 (*) at 90°C. For full assignation, see the Experimental Section.*

b) Aggregation studies

To confirm the optical stability of the binaphthyl unit under the reaction conditions, and therefore, the optical purity of the final Zn(II)Pcs, we have recorded the circular dichroism (CD) spectra in THF of Zn(II)Pcs **4** prepared from the two different enantiomers of **7c** (Figure 5. 5A). The presence of the optically active binaphthyl moieties induces the appearance of CD signals in both the Soret and *Q*-band regions,[8] although the latter is much less intense than the Soret contribution. The spectra recorded with identical concentrations of the (R) and (S) enantiomers show transitions that are mirror images, thus confirming that racemization do not occur during the formation of the Pc. Figure 5. 5B shows how CD signal is cancelled by mixing R and S enantiomers of Zn(II)Pc **4** in different ratios.

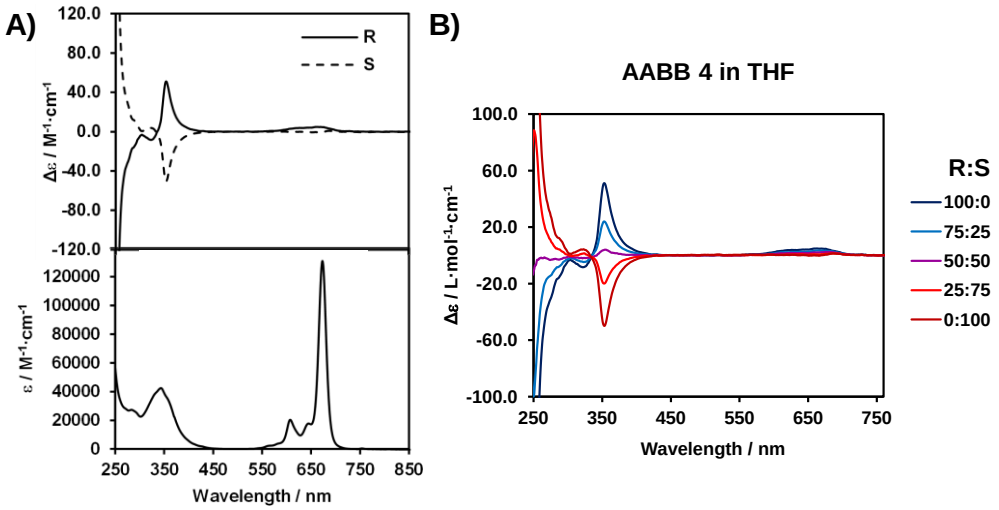

*Figure 5. 5. (A) CD of Zn(II)Pcs (S)-**4** and (R)-**4** (top) together with the electronic absorption spectrum in THF (bottom); (B) (S)-**4** and (R)-**4** mixed together in different ratios in THF.*

Importantly, as observed in similar, previously reported, (R)-binapthyloxy-bridged AABB Pcs,[17] and for Zn(II)Pc **4** (Figure 5. 5), the spectra of the rest of Zn(II)Pcs **1-6** in THF solution, where they are molecularly dissolved, show also mainly positive CD envelopes corresponding to the main Soret and *Q*-bands. Following with the optical characterization of Zn(II)Pcs **1-6**, we registered their absorption in different solvents. For all the compounds, UV-vis spectra in THF at concentration *ca*. 10^{-6} M showed a single, narrow *Q*-band typical for metallic monomeric Pcs, which is also compatible with their C_{2v} symmetry (see Figure 5. 6B, blue line). Turning to toluene solutions, Zn(II)Pcs **1**, **4** and **5** do not aggregate either in this solvent, but the compounds holding alkyl chains or alkylsilyl-protected ethynyl moieties at the binaphthyl unit (**2**, **3**, **6**) show evidences of aggregation in their spectra (see Figure 5. 6B, red line), probably as a consequence of their most pronounced amphiphilic character imparted by the presence of hydrocarbon chains and the polarization of the aromatic core induced by the halogen atoms. For the three derivatives we recorded the absorption spectra in a more non-polar solvent, namely methylcyclohexane (MCH), discerning broad blue-shifted bands compatible with the formation of *H*-aggregates (see Figure 5. 6B, green line).

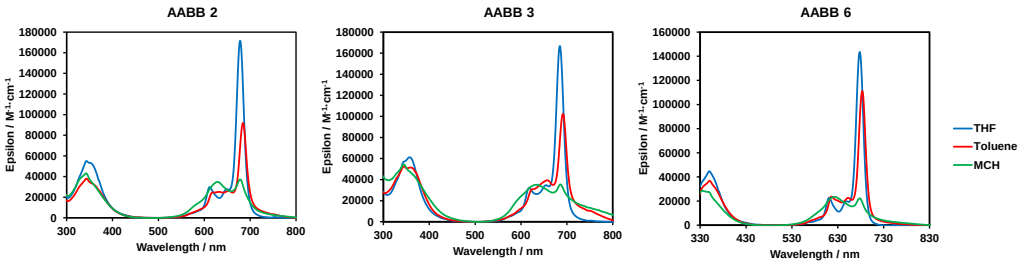

*Figure 5. 6. UV-vis spectra for AABB Zn(II)Pcs **2**, **3** and **6** in three solvents.*

As Zn(II)Pcs **2**, **3** and **6** show more evidences of aggregation more exhaustive experiments were performed. CD spectra were also recorded for Zn(II)Pcs **2**, **3** and **6** in the same three solvents as shown in Figure 5. 7.

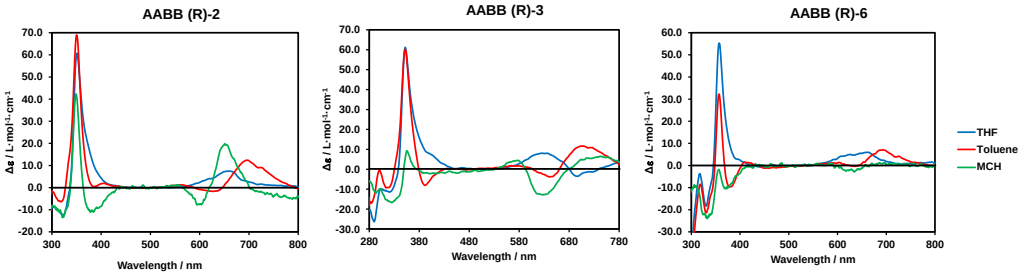

*Figure 5. 7. CD spectra for AABB Zn(II)Pcs **2**, **3** and **6** in three solvents.*

To check the stability of the aggregates formed in non-coordinative solvents, we heated the toluene and MCH solutions of Zn(II)Pc **2**, **3** and **6** up to 353K (Figure 5. 8 top and Figure 5. 9 top). In toluene, the absorption spectrum of the monomeric species was recovered, but for MCH the monomer/aggregate band ratio remained similar.

Similarly, addition of THF to the solutions of Zn(II)Pcs in toluene at room temperature led to the recovery of the monomeric species (with only 1% of THF), but in MCH, disaggregation was not achieved even at 10% of THF (Figure 5. 8 down and Figure 5. 9 down).

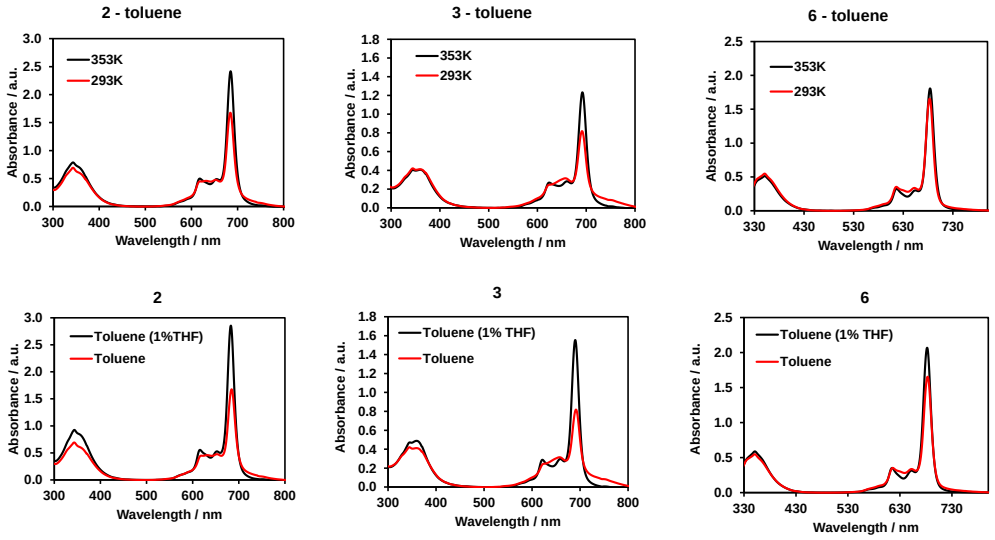

*Figure 5. 8. Temperature changes or upon THF adition to toluene solutions of Zn(II)Pcs **2, 3** and **6** at concentration ~5·10^{-6} and 2·10^{-5} M.*

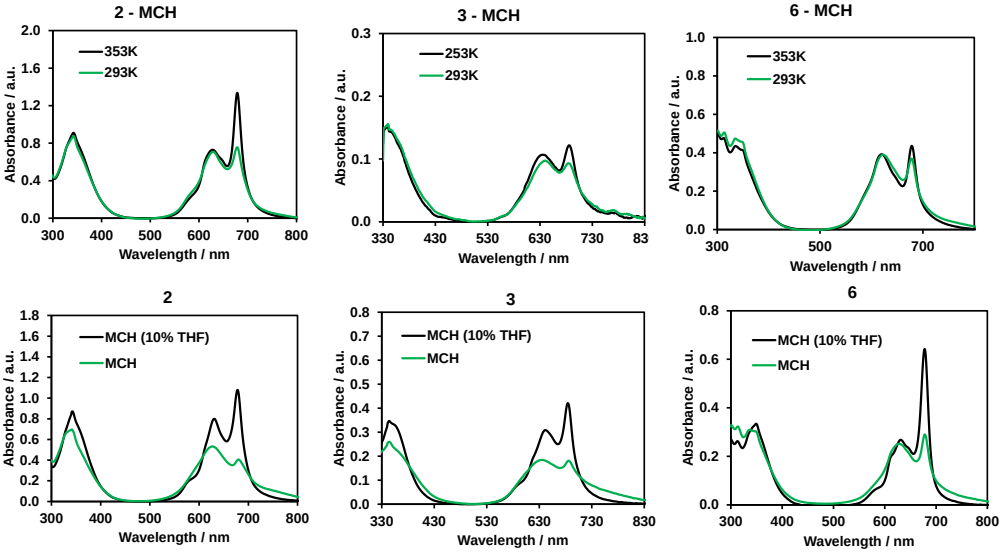

*Figure 5. 9. Temperature changes or upon THF adition to MCH solutions of Zn(II)Pcs **2, 3** and **6** at concentration ~5·10^{-6} and 2·10^{-5} M.*

In MCH **2** seems to be harder disaggregated than **3** with temperature, and harder disaggregated than **6** upon addition of THF. These two facts, together with the wider band in the UV-vis spectrum, and a more pronounced negative sign in MCH CD spectrum

for Zn(II)Pc **3** (Figure 5. 7), suggest that this compound forms more stable aggregates, which could be rationalized on the basis of: i) it largest polarization, due to the presence of four iodine atoms (instead of the two installed in **2** and **6**); and/or ii) a better organization of the Pcs in the assembly, as Zn(II)Pc **3** is composed of a single regioisomer, while **2** and **6** are, indeed**,** a mixture of three positional isomers (see Figure 5. 10).

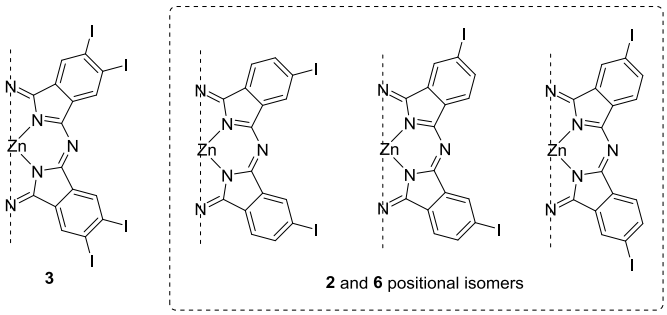

*Figure 5. 10. Zn(II)Pc **3** single regioisomer, versus **2** and **6** as a mixture of three positional isomers.*

Turning to CD experiments for Zn(II)Pc **3**, and comparing the spectra in THF with those in toluene and MCH (Figure 5. 7), we can observe a change in the dichroic behavior of the monomeric species and the aggregates. In THF, a weak Cotton effect was observed in the *Q*-band transition, with a negative and a positive sign at 696 and 627 nm, respectively, and a very strong positive signal at 352 nm for the *B*-band transition. In toluene, a change of sign for the CD signals in the *Q*-band region is observed (i.e. positive signal at 743 nm and negative at 637 nm), together with the raising of a new small positive signal at 565 nm, while the *B*-band region remains similar. The spectrum recorded in MCH exhibits similar signals than in toluene for the *Q* band transitions, whereas the intensity of the signal at 352 nm decreases.

Temperature dependence experiments for Zn(II)Pc were reproduced at higher concentration ($\sim 10^{-4}$ M) in order to favour the aggregates formation. Accordingly to the UV-vis experiments, heating the toluene solution at 353K (Figure 5. 11) leads to a disassembly of the aggregate (please compare the spectrum at 353K in toluene in Figure 5. 11A and the spectrum in THF in Figure 5. 6), but in the case of MCH solutions, the CD signals remain similar and only an increase in intensity is observed. This behavior matches with that observed in the UV-vis experiments, both indicating that robust H-aggregates of Zn(II)Pc **3** are formed in MCH.

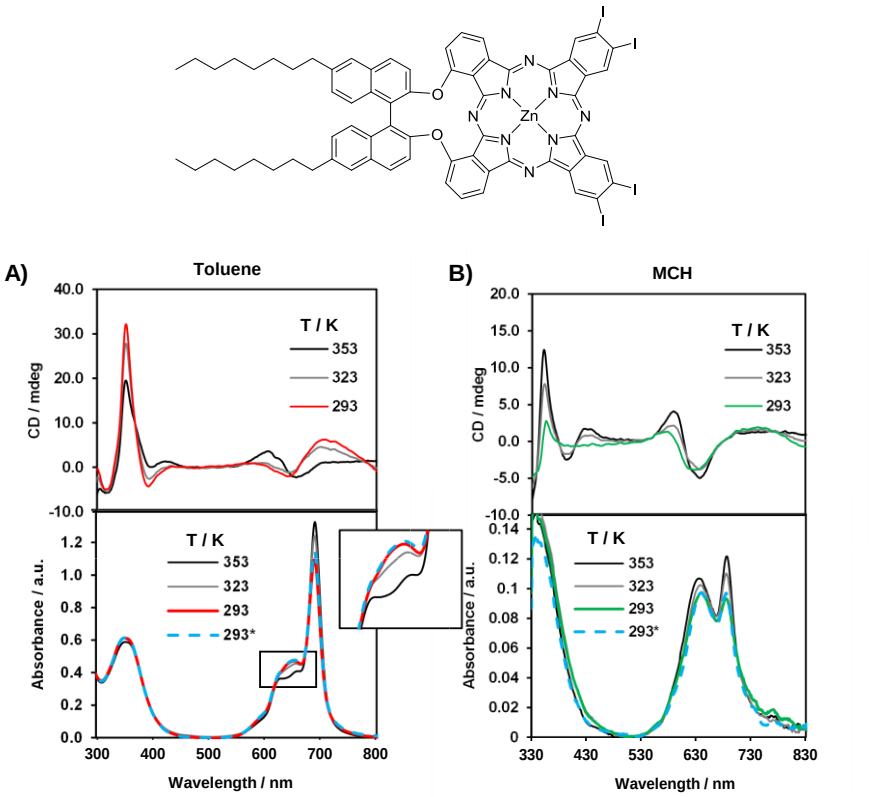

*Figure 5. 11. CD and absorption spectra for Zn(II)Pc **3**: temperature dependence of the CD signals (top) and the absorption bands (bottom) in toluene (A) and MCH (B). Concentration: ~ 10^{-4} M. *: Spectra recorded after cooling down from 353K.*

Finally, we tried to complete the disaggregation completely upon addition of THF but even at 40 % THF signs of aggregation were observed (Figure 5. 12).

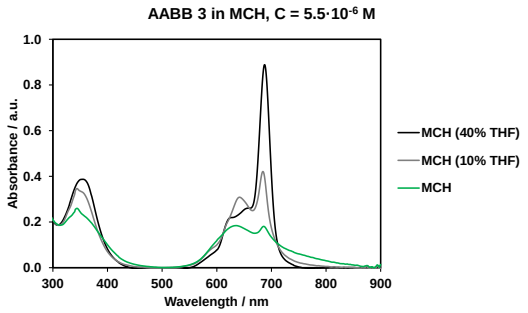

*Figure 5. 12. AABB Zn(II)Pc **3** disaggregation with THF in MCH.*

5.4. Conclusions

As a conclusion, we have improved the previously reported synthetic methodology towards binaphthyl-functionalized AABB Zn(II)Pcs, and successfully prepared a battery of chiral derivatives endowed with halogen or ethynyl moieties that can be further transformed to obtain a variety of customized compounds with amphiphilic features. Some of the Zn(II)Pcs show aggregation behavior in nonpolar solvents and, in particular, Zn(II)Pc **3** with a well-defined C_{2v} geometry, forms robust, chiral nanostructures in solution. This feature, together with its functionalization with both alkyl chains and iodine atoms, turn this derivative into a model synthon for further preparation of amphiphilic Zn(II)Pcs able to self-assemble in polar media.

5.5. Experimental section

Chemicals were purchased from commercial suppliers and used without further purification unless stated otherwise. Compounds **7a**,[17,35] **7b**,[13,37] **8a**,[39] **8b**,[40] **8d**,[41] **9**,[36] and **10**[38] have been prepared according to published procedures.

i. *Synthesis of phthalonitriles:*

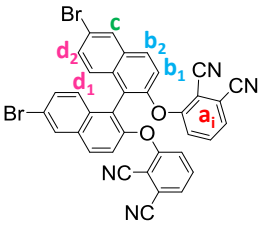

Synthesis of 7c: To a solution of 3-nitrophthalonitrile (0.858 g, 4.95 mmol) and (R)- or (S)-6,6'-dibromo-BINOL **9** (1 g, 2.25 mmol) in dry DMSO (10 mL) at room temperature, potassium carbonate (1.15 g, 8.33 mmol) was added in several portions. The mixture was stirred at room temperature under an argon atmosphere for 5h. The reaction mixture was poured into ice water (100 mL), filtered and the solid was washed with water (250 mL) and dried. The product was recrystallized in EtOAc, giving the product as a yellowish solid. Yield: 1.10 g (70%). ^{1}H-NMR (300 MHz, DMSO-d_6): δ 7.18 (d, J = 9.04 Hz, 2H, HAr-b_i), 7.30 (d, J = 8.50 Hz, 2H, HAr-a_i), 7.48 (d, J = 9.04 Hz, 2H, HAr-b_i), 7.62 (m, 4H, HAr-a_i), 7.67 (m, 2H, HAr-d_i), 8.22 (d, J = 8.90 Hz, 2H, HAr-d_i), 8.39 (s, 2H, HAr-c). ^{13}C-NMR (75 MHz, DMSO-d_6): δ 104.6, 112.6, 115.3, 115.6, 119.4, 121.0, 121.6, 121.9, 127.4, 128.2, 130.3, 130.5, 130.8, 131.5, 132.3, 135.7, 150.0, 158.8. **IR(ATR)** v^{-1} (cm^{-1}):3074, 2227 (C≡N st), 1568, 1491, 1449, 1350, 1319, 1258, 801. **HR-MS** for $C_{36}H_{16}Br_2N_4O_2$: APCI Positive (ULTRAFLEX II), apci + fia hplc1100 t = 300.m; MeOH as ionizing phase; $[M+H]^+$ 726.9975 (calculated), 726.9995 (experimental); $[M+H+MeOH]^+$ is also observed. $[\alpha]_D^{20}$ = +71.6° (c = 0.4, CH_2Cl_2) for (R)-**8c**; and $[\alpha]_D^{20}$ = -78.7° (c = 0.4, CH_2Cl_2) for (S)-**8c**. **m.p.** = 280-282°C.

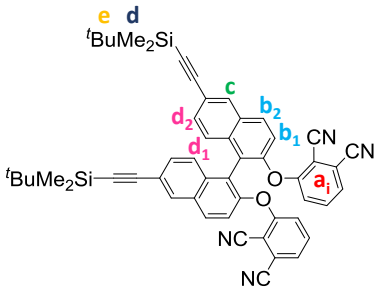

Synthesis of 7d: To a solution of 3-nitrophthalonitrile (154 mg, 0.888 mmol) and (R)-BINOL derivative **10** (200 mg, 0.355 mmol) in dry DMSO (5 mL) at room temperature, potassium carbonate (245 mg, 1.78 mmol) was added in several portions. The mixture was stirred at room temperature under an argon atmosphere for 48h. The reaction mixture was poured into ice water (100 mL), and the aqueous layer was extracted with ethyl acetate. After being dried with anhydrous $MgSO_4$, the organic layer was evaporated, and the residue was purified by silica gel chromatography (heptane:EtOAc, 3:1), giving the product as a withe solid. Yield: 147 mg (51%). **^{1}H-NMR** (300 MHz, $CDCl_3$): δ 0.14 (s, 12H, Me-d), 0.94 (s, 18H, ^{t}Bu-e), 7.12 (d, J = 8.75 Hz, 2H, HAr-b_i), 7.19-7.28 (m, 8H, HAr-a_i,b_i,d_i), 7.48 (t, J = 8.32 Hz, 2H, HAr-a_i), 7.91 (d, J = 9.01 Hz, 2H, HAr-d_i), 8.01 (s, 2H, HAr-c). **^{13}C-NMR** (75 MHz, $CDCl_3$): δ -4.5, 16.9, 26.3, 77.2, 105.2, 105.9, 109.1, 112.3, 115.0, 117.1, 120.0, 121.4, 121.6, 122.6, 125.5, 127.5, 130.6, 131.1, 131.4, 132.5, 133.0, 134.9, 150.3, 159.8. **IR(ATR)** v^{-1} (cm^{-1}):3073, 2951, 2928, 2855, 2232 (C≡N st), 2150 (C≡C st), 1574, 1458, 1347, 1268, 1208, 823. **HR-MS** for $C_{52}H_{46}N_4O_2Si_2$: FAB EI+, Matrix: m-NBA, HR FB+; $[M+H]^+$ 815,32375 (calculated), 815.3237 (experimental); $[M+H-^tBu]^+$ is also observed. $[\alpha]_D^{20}$ = +63.8° (c = 0.3, CH_2Cl_2) for (R)-**7d**. **m.p.** = 278-280°C.

ii. *General procedure for the synthesis of Zn(II)Pcs **1-6**:*

Bishthalonitrile **AA 7** (1 eq.), phthalonitrile **B 8** (2 eq.) and anhydrous $Zn(AcO)_2$ (1.5-2 eq.) were placed in a 5 mL high pressure resistant flask equipped with a magnetic stirrer, and then dry *o*-dichlorobenzene/DMF (dried over 4Å molecular sieves) 2:1 were added, for [**AA 7**]=0.05 M. The mixture was heated to 150-160°C overnight under argon atmosphere. After cooling, the solvent was removed under vacuum. The mixture of products was then purified as follows.

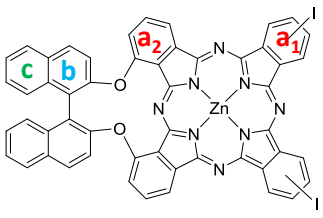

Synthesis of Zn(II)Pc 1: Following the general procedure: **7a** (63.6 mg, 0.118 mmol), **8a** (60 mg, 0.236 mmol) and $Zn(OAc)_2$ (43.3 mg, 0.236 mmol). Solid was initially washed with heptane and purified by column chromatography on SiO_2 (THF/heptane from 1:2 to 1:1). The first compound to elute was **B_4-a**, unequivocally confirmed by MALDI-TOF mass spectrometry, sequentially followed by the target **AABB 1** and **A_4-a** which show similar R_f. To achieve full separation after common silica gel column chromatography, an additional column chromatography on Bio-Beads using THF as eluent was necessary. Elution sequence was monitored by semipreparative chiral HPLC (see Figure 5. 13). Unfortunately HPLC separation is not

good enough, preventing the semipreparative application of this technique. After evaporation of the solvent, a blue solid was obtained, which was washed with MeOH. Yield: 14.1 mg, (11%). **^{1}H-NMR** (500 MHz, DMSO-d_6): δ 7.50, 7.62, 7.84, 7.94, 7.97, 8.18, 8.28 (m, 12H, HAr-b,c); 8.35, 8.43, 8.66, 8.77, 8.91, 8.97, 8.99, 9.13, 9.29, 9.45 (m, 12H, HAr-a_i). **IR(ATR)** v^{-1} (cm^{-1}): 2960, 2923, 2853, 1260, 1089, 1021, 804. **HR-MS** for $C_{52}H_{24}I_2N_8O_2Zn$: MALDI (ULTRAFLEX III); DCTB + PPGNa 1000; 1109.9398 (calculated), 1109.9385 (experimental). **UV-vis** (THF) log(ε/$M^{-1}cm^{-1}$) (λ): 4.8 (343 nm); 4.5 (612 nm); 5.3 (678 nm). **Fluorescence:** $\lambda_{maximum}$ = 690 nm; $\lambda_{excitation}$ = 668 nm.

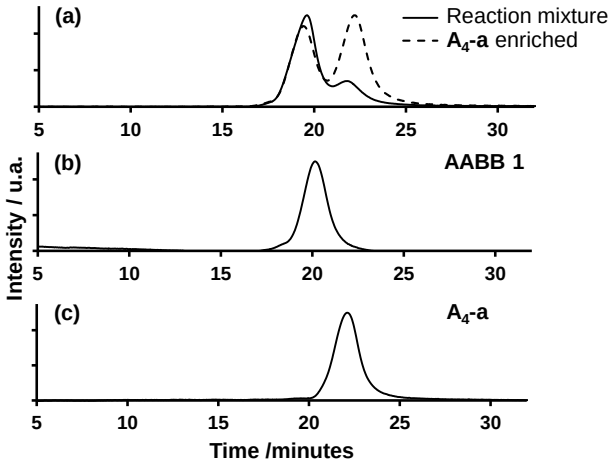

*Figure 5. 13. HPLC chromatograms of: (a) **AABB 1** + **A_4-1a** reaction mixture (continuous line) and reaction mixture enriched with **A_4-1a** (dashed line); (b) pure **AABB 1**; and (c) pure **A_4-1a**. Semipreparative chiral column chromatography for HPLC: Chiralpack IC 10mmϕ x 250mL, particle size 5 µm, Part No. 83335, Daicel Corporation. Conditions: flow 1mL/min, chloroform:THF (99:1), T=25°C, detection by UV-vis at 350 nm and 676 nm; injection volume 15 µL from a solution of the **AABB 1** and **$(AA)_2$-a** mixture ~1 mg/mL.*

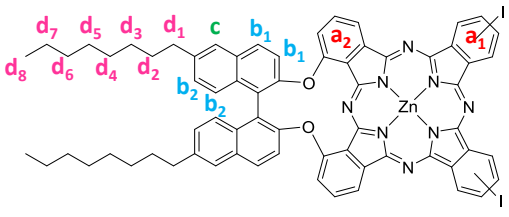

Synthesis of Zn(II)Pc 2: Following the general procedure: **7b** (60 mg, 0.079 mmol), **8a** (40 mg, 0.157 mmol) and $Zn(OAc)_2$ (21.6 mg, 0.1180 mmol). Solid was initially washed with heptane and purified by column chromatography on SiO_2 (dioxane/heptane, 1:4). Symmetrical phthalocyanine **$(AA)_2$-b** was eluted in the first fraction, followed by Zn(II)Pc **2**, and finally **B_4-a**. The fraction containing Zn(II)Pc **2** was further purified by an additional column chromatography on Bio-Beads using THF as eluent. After evaporation of the solvent, a blue solid was obtained, which was washed with MeOH. Yield: 35 mg, (33%). **^{1}H-NMR** (500 MHz, THF-d_8, 363K): δ 0.84 (m, 6H, CH_3-d_8); 1.29 (m, 12H, CH_2-$d_{5\text{-}7}$); 1.40 (m, 4H, CH_2-d_4); 1.47 (m, 4H, CH_2-d_3); 1.83 (m, 4H, CH_2-d_2); 2.88 (m, 4H, CH_2-d_1); 7.46, 7.54, 7.61, 7.71, 7.80, 7.90, 7.99, 8.01, 8.06

(m, 16H, HAr-a_i,b_i,c); 8.25, 8.39, 8.52, 8.69, 8.82, 8.91, 9.00, 9.11 (m, 6H, HAr-a_i). **IR(ATR)** ν^{-1} (cm^{-1}): 2961, 2922, 2853, 1259, 1088, 1017, 798. **HR-MS** for $C_{68}H_{56}I_2N_8O_2Zn$: MALDI (ULTRAFLEX III); DCTB + PEGNa 1500; 1334.1902 (calculated), 1334.1877 (experimental). **UV-vis** (THF) log(ε/$M^{-1}cm^{-1}$) (λ): 4.7 (343 nm); 4.5 (612 nm); 5.2 (678 nm). **Fluorescence:** $\lambda_{maximum}$ = 690 nm; $\lambda_{excitation}$ = 668 nm.

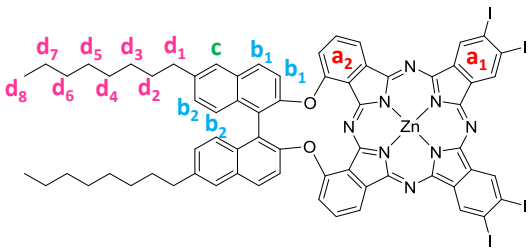

Synthesis of Zn(II)Pc 3: Following the general procedure: **7b** (52 mg, 0.068 mmol), **8b** (52 mg, 0.136 mmol) and $Zn(OAc)_2$ (19 mg, 0.102 mmol). Solid was initially washed with heptane and purified by column chromatography on SiO_2 (dioxane/heptane, 1:2). **$(AA)_2$-b** was eluted in the first fraction, followed by Zn(II)Pc **3**, and finally **B_4-b**. The fraction containing **Zn(II)Pc 3** was further purified by an additional column chromatography on Bio-Beads using THF as eluent. After evaporation of the solvent, a blue solid was obtained, which was washed with MeOH. Yield: 18 mg, (17%). **^{1}H-NMR** (500 MHz, THF-d_8, 363K): δ 0.83 (m, 6H, CH_3-d_8); 1.28 (m, 12H, CH_2-$d_{5,6,7}$); 1.41 (m, 4H, CH_2-d_4); 1.47 (m, 4H, CH_2-d_3); 1.82 (m, 4H, CH_2-d_2); 2.87 (m, 4H, CH_2-d_1); 7.33, 7.50, 7.69, 7.80, 7.95, 8.15 (m, 16H, HAr-a_i,b_i,c); 9.14, 9.36 (m, 4H, HAr-a_i). **IR(ATR)** ν^{-1} (cm^{-1}): 2951, 2919, 2850, 1578, 1475, 1386, 1332, 1259, 1087, 1019, 800. **HR-MS** for $C_{68}H_{54}I_4N_8O_2Zn$: MALDI (ULTRAFLEX III); DCTB + PPGNa 1000 + PPGNa 2000; 1585.9834 (calculated), 1585.9808 (experimental). **UV-vis** (THF) log(ε/$M^{-1}cm^{-1}$) (λ): 4.8 (357 nm); 4.5 (618 nm); 5.2 (685 nm). **Fluorescence:** $\lambda_{maximum}$ = 694 nm; $\lambda_{excitation}$ = 680 nm.

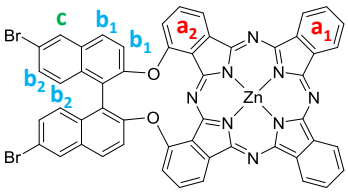

Synthesis of Zn(II)Pc 4: Following the general procedure: **7c** (100 mg, 0.144 mmol), **8c** (36.8 mg, 0.287 mmol) and $Zn(OAc)_2$ (39.5 mg, 0.215 mmol). Solid was initially washed with MeOH and filtered in a silica gel plug with THF. After evaporation of the solvent, the product was purified by column chromatography on Bio-Beads using THF as eluent, monitored by TLC (heptane:THF, 3:1, 1% pyridine), being the second eluted fraction. After evaporation of the solvent, a blue solid was obtained, which was washed with MeOH. Yield: 30 mg, (21%). **^{1}H-NMR** (500 MHz, DMSO-d_6, 363K): δ 7.65 (d, J = 9.96 Hz, 2H, HAr-a_i); 7.71 (d, J = 9.41 Hz, 2H, HAr-b_i); 7.75 (d, J = 9.41 Hz, 2H, HAr-b_i); 7.98 (d, J = 9.68 Hz, 2H, HAr-b_i); 8.04 (d, J = 9.68 Hz, 2H, HAr-b_i); 8.14 (m, 4H, HAr-a_i); 8.24 (m, 2H, HAr-a_i); 8.25 (s, 2H, HAr-c); 9.19 (m, 2H, HAr-a_i); 9.26 (m, 4H, HAr-e). **IR(ATR)** ν^{-1} (cm^{-1}): 2917, 2850, 1575, 1484, 1332, 1270, 1260, 1121, 1090. **HR-MS** for $C_{52}H_{24}Br_2N_8O_2Zn$: MALDI (ULTRAFLEX III); DCTB + PPGNa 1000; 1013.9675 (calculated); 1013.9681 (experimental). **UV-vis** (THF) log(ε/$M^{-1}cm^{-1}$) (λ): 4.6

(343 nm); 4.3 (607 nm); 5.1 (673 nm). **Fluorescence:** $\lambda_{maximum}$ = 684 nm; $\lambda_{excitation}$ = 663 nm.

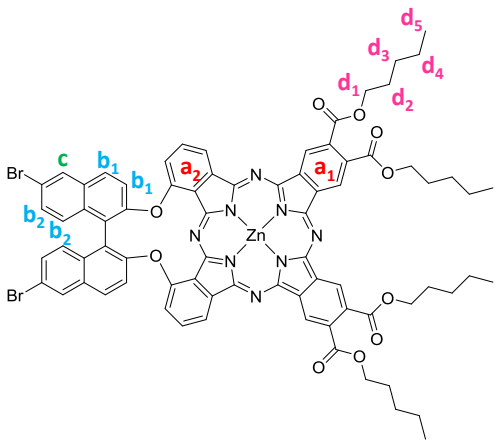

Synthesis of Zn(II)Pc 5: Following the general procedure: **7c** (100 mg, 0.144 mmol), **8d** (102 mg, 0.287 mmol) and $Zn(OAc)_2$ (39.5 mg, 0.215 mmol). The mixture was purified by column chromatography on SiO_2 (THF/heptane 2:1) containing the first fraction a mixture of **B_4-d** and Zn(II)Pc **5**, and the second fraction **$(AA)_2$-c**. The first fraction was purified by column chromatography on SiO_2 (THF/heptane 1:1 with pyridine 1%) being the first fraction **B_4-d** (10 mg, yield: 9%) and the second fraction the desired Zn(II)Pc **5**. After evaporation of the solvent, a blue solid was obtained, which was washed with MeOH. Yield: 12 mg, (6%). **^{1}H-NMR** (500 MHz, DMSO-d_6, 363K): δ 1.09 (m, 12H, CH_3-d_5); 1.60 (m, 8H, CH_2-d_4); 1.71 (m, 8H, CH_2-d_3); 2.10 (m, 8H, CH_2-d_2); 4.70 (m, 8H, CH_2-d_1); 7.73 (m, 2H, HAr-a_i); 7.84 (m, 6H, HAr-b_i); 8.23 (m, 2H, HAr-a_i); 8.39 (m, 2H, HAr-b_i); 8.91 (m, 4H, HAr-a_i,c); 9.16 (m, 2H, HAr-a_i); 9.40 (m, 2H, HAr-a_i). **IR(ATR)** v^{-1} (cm^{-1}): 2956, 1724, 1577, 1485, 1322, 1269, 1090. **HR-MS** for $C_{76}H_{64}Br_2N_8O_{10}Zn$: MALDI (ULTRAFLEX III); DCTB + PEGNa 1500; 1470.2398 (calculated), 1470.2386 (experimental). **UV-vis** (THF) $\log(\varepsilon/M^{-1}cm^{-1})$ (λ):4.8 (346 nm); 4.5 (614 nm); 5.3 (681 nm). **Fluorescence:** $\lambda_{maximum}$ = 698 nm; $\lambda_{excitation}$ = 670 nm.

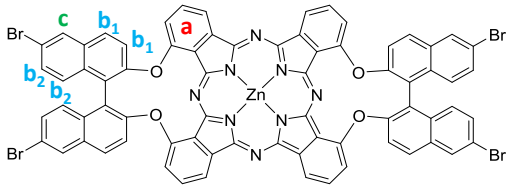

Synthesis of $(AA)_2$-c: This product was obtained in the synthesis of Zn(II)Pc **5** as secondary product in the second fraction of the first column chromatography on silica gel. After evaporation of the solvent, the product was purified by column chromatography on Bio-Beads using toluene as eluent. After evaporation of the solvent, a blue solid was obtained, which was washed with MeOH. Yield: 14 mg, (13%). **^{1}H-NMR** (500 MHz, DMSO-d_6, 363K): δ 7.57 (m, 4H, HAr-a); 7.68, 7.60 (m, 8H; HAr-b_i); 7.98, 8.01 (m, 8H, HAr-b_i); 8.22 (m, 8H, HAr-a,c); 9.27 (m, 4H,HAr-a). **IR(ATR)** v^{-1} (cm^{-1}): 1577, 1483, 1330, 1267, 1260, 1198, 1103. **HR-MS** for $C_{72}H_{32}Br_4N_8O_4Zn$: MALDI (ULTRAFLEX III); DCTB + PPGNa 1000 + PPGNa 2000; 1451.8566 (calculated); 1451.8511 (experimental). **UV-vis** (THF) $\log(\varepsilon/M^{-1}cm^{-1})$ (λ): 4.5 (345 nm); 4.2 (613 nm); 5.0 (684 nm). **Fluorescence:** $\lambda_{maximum}$ = 693 nm; $\lambda_{excitation}$ = 674 nm.

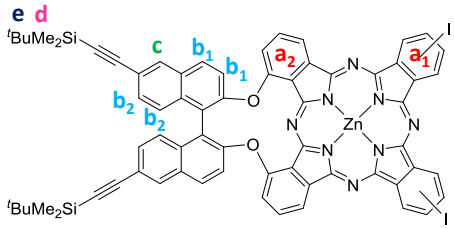

Synthesis of Zn(II)Pc 6: Following the general procedure: **7d** (45 mg, 0.055 mmol), **8a** (28 mg, 0.110 mmol) and $Zn(OAc)_2$ (11.1 mg, 0.061 mmol). Solid was purified by column chromatography on SiO_2 (THF/heptane from 1:4 to 1:2). The first eluted fraction contains a mixture of **$(AA)_2$-d** and Zn(II)Pc **6**, followed by a second fraction with **B_4-a**. First fraction was further purified by two additional column chromatography on Bio-Beads using THF as eluent. First eluted fraction contains **$(AA)_2$-d** (traces), and **AABB 6** is in the second fraction. After evaporation of the solvent, a blue solid was obtained, which was washed with MeOH. Yield: 10.3 mg, (13%). **^{1}H-NMR** (500 MHz, THF-d_8, 323K): δ 0.22 (m, 12H, Me-d); 1.05 (m, 18H, ^{t}Bu-e); 7.67 (m, 2H, HAr-b_i); 7.77-7.85 (m, 4H, HAr-a_i,b_i); 7.95-8.02 (m, 4H, HAr-b_i); 8.08-8.30 (m, 6H, HAr-a_i,c); 8.45-8.53 (m, 2H, HAr-a_i); 8.65, 7.72, 8.78 (m, 2H, HAr-a_i); 8.95, 9.06, 9.15 (m, 2H, HAr-a_i). **IR(ATR)** ν^{-1} (cm^{-1}): 2923, 2853, 2147, 1730, 1576, 1470, 1337, 1254, 1088, 827. **HR-MS** for $C_{68}H_{52}I_2N_8O_2Si_2Zn$: MALDI (ULTRAFLEX III); DCTB + PEGNa 1500; 1386.1127 (calculated), 1386.1101 (experimental). **UV-vis** (THF) log(ε/$M^{-1}cm^{-1}$) (λ): 4.6 (350 nm); 4.4 (611 nm); 5.2 (678 nm). **Fluorescence:** $\lambda_{maximum}$ = 688 nm; $\lambda_{excitation}$ = 668 nm.

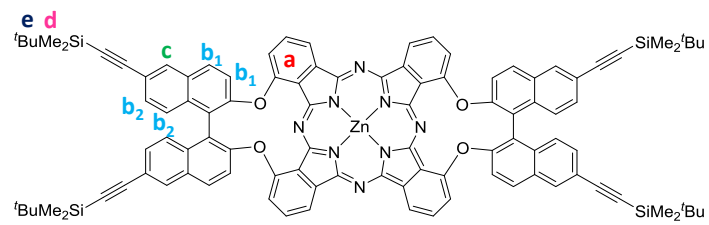

Synthesis of $(AA)_2$-d: As **$(AA)_2$-d** was obtained in the synthesis of Zn(II)Pc **6** with very low yield, it was prepared independently by mixing **7d** (75 mg, 0.092 mmol) and $Zn(OAc)_2$ (13 mg, 0.069 mmol) in dry *o*-dichlorobencene:DMF (2:1), for [**8d**]= 0.05 M at 160°C overnight. Solid was purified by column chromatography on SiO_2 (dioxane/heptane, 1:1). The mixture was further purified by two additional column chromatography on Bio-Beads using first toluene and then THF as eluents. After evaporation of the solvent, a blue solid was obtained, which was washed with MeOH. Yield: 5.2 mg, (7%). **^{1}H-NMR** (500 MHz, THF-d_8, 298K): δ 0.19 (m, 24H, Me-d); 1.01 (m, 36H, ^{t}Bu-e); 8.06 (m, 8H, HAr-b_i); 7.82 (m, 8H, HAr-b_i); 7.92, 8.04, 8.21 (m, 4H, HAr-a,c); 9.36 (m, 4H, HAr-a). **IR(ATR)** ν^{-1} (cm^{-1}): 2953, 2147, 1710, 1574, 1470, 1358, 1250, 1219, 1087, 825. **HR-MS** for $C_{104}H_{92}N_8O_4Si_4Zn$: MALDI (ULTRAFLEX III); DCTB + PEGNa 1500; 1692.5605 (calculated), 1692.5578 (experimental). **UV-vis** (THF) log(ε/$M^{-1}cm^{-1}$) (λ):4.7 (299 nm); 4.7 (349 nm); 4.4 (614 nm); 5.2 (684 nm). **Fluorescence:** $\lambda_{maximum}$ = 694 nm; $\lambda_{excitation}$ = 680 nm.

5.6. References

(1) Kobayashi, N. Optically Active Phthalocyanines. *Coord. Chem. Rev.* **2001**, *219–221*, 99–123.

(2) Jiang, Y.; Liu, C.; Wang, X.; Wang, T.; Jiang, J. Fluorescent Phthalocyanine Assembly Distinguishes Chiral Isomers of Different Types of Amino Acids and Sugars. *Langmuir* **2017**, *33* (29), 7239–7247.

(3) Thordarson, P.; Nolte, R. J. M.; Rowan, A. E. *Porphyrin Handbook*; ; Kadish, K. M., Smith, K. M., Guilard, R., Ed.; Academic Press, 2003.

(4) Engelkamp, H.; Middelbeek, S.; Nolte, R. J. M. Self-Assembly of Disk-Shaped Molecules to Coiled-Coil Aggregates with Tunable Helicity. *Science (80-.).* **1999**, *284* (5415), 785–788.

(5) Rai, R.; Saxena, A.; Ohira, A.; Fujiki, M. Programmed Hyperhelical Supramolecular Assembly of Nickel Phthalocyanine Bearing Enantiopure 1-(p-Tolyl)Ethylaminocarbonyl Groups. *Langmuir* **2005**, *21* (9), 3957–3962.

(6) García-Iglesias, M.; Torres, T.; González-Rodríguez, D. Well-Defined, Persistent, Chiral Phthalocyanine Nanoclusters via G-Quadruplex Assembly. *Chem. Commun.* **2016**, *52* (60), 9446–9449.

(7) Kobayashi, N.; Kobayashi, Y.; Osa, T. Optically Active Phthalocyanines and Their Circular Dichroism. *J. Am. Chem. Soc.* **1993**, *115*, 10994–10995.

(8) Kobayashi, N.; Higashi, R.; Titeca, B. C.; Lamote, F.; Ceulemans, A. Substituent-Induced Circular Dichroism in Phthalocyanines. *J. Am. Chem. Soc.* **1999**, *121* (51), 12018–12028.

(9) Liu, H.; Liu, Y.; Liu, M.; Chen, C.; Xi, F. Synthesis and Properties of Optically Active 6,6′-Didodecyl-1,1′-Binaphthyl-Phthalocyanine Linked through Crown Ether Units. *Tetrahedron Lett.* **2001**, *42* (40), 7083–7086.

(10) Zhao, L.; Wang, K.; Furuyama, T.; Jiang, J.; Kobayashi, N. Synthesis and Spectroscopic Properties of Chiral Binaphthyl-Linked Subphthalocyanines. *Chem. Commun.* **2014**, *50* (57), 7663–7665.

(11) Zhou, H.; Wang, K.; Qi, D.; Jiang, J. Chiral Bis(Phthalocyaninato) Yttrium Double-Decker Complexes. Synthesis, Structure, Spectroscopy, and Electrochemistry. *Dalt. Trans.* **2014**, *43* (4), 1699–1705.

(12) Zhao, L.; Wang, K.; Shang, H.; Jiang, J. Novel Chiral ABBB-Type Unsymmetrical Phthalocyanine. Ring-Expansion Synthesis, Spectroscopic, and Electrochemical Properties. *Dye. Pigment.* **2015**, *120*, 52–56.

(13) Lv, W.; Zhang, X.; Lu, J.; Zhang, Y.; Li, X.; Jiang, J. Synthesis and Hollow-Sphere Nanostructures of Optically Active Metal-Free Phthalocyanine. *Eur. J. Inorg. Chem.* **2008**, *27*, 4255–4261.

(14) Wu, L.; Wang, Q.; Lu, J.; Bian, Y.; Jiang, J.; Zhang, X. Helical Nanostructures Self-Assembled from Optically Active Phthalocyanine Derivatives Bearing Four Optically Active Binaphthyl Moieties: Effect of Metal-Ligand Coordination on the Morphology, Dimension, and Helical Pitch of Self-Assembled Nanostructures. *Langmuir* **2010**, *26* (10), 7489–7497.

(15) Wang, K.; Qi, D.; Wang, H.; Cao, W.; Li, W.; Jiang, J. A Chiral Phthalocyanine Dimer with Well-Defined Supramolecular Symmetry Based on π–π Interactions. *Chem. – A Eur. J.* **2012**, *18* (50), 15948–15952.

(16) Zhang, C.; Jing, L.; Lin, S.; Hao, Z.; Tian, J.; Zhang, X.; Zhu, P. Helical Self-

Assembly of Optically Active Phthalocyanine Derivatives: Effect of Zn·O Coordination Bond on Morphology and Handedness of Nanostructures. *ChemPhysChem* **2013**, *14* (16), 3827–3833.

(17) Kobayashi, N. Optically Active ' Adjacent ' Type Non-Centrosymmetrically Substituted Phthalocyanines in High Yields in a Mixed Condensation Using Bisphthaloni- Conditions) and a Second Phthalonitrile , and Characterized. *Chem. Commun.* **1998**, *2*, 487–488.

(18) Kobayashi, N.; Miwa, H.; Isago, H.; Tomura, T. An Adjacent Dibenzotetraazaporphyrin: A Structural Intermediate between Tetraazaporphyrin and Phthalocyanine. *Inorg. Chem.* **1999**, *38* (3), 479–485.

(19) Kobayashi, N.; Miwa, H.; Nemykin, V. N. Adjacent versus Opposite Type Di-Aromatic Ring-Fused Phthalocyanine Derivatives: Synthesis, Spectroscopy, Electrochemistry, and Molecular Orbital Calculations. *J. Am. Chem. Soc.* **2002**, *124* (27), 8007–8020.

(20) Seotsanyana-Mokhosi, I.; Nyokong, T. Synthesis and Photochemical Studies of Substituted Adjacent Binaphthalophthalocyanines. *J. Porphyr. Phthalocyanines* **2004**, *8* (10), 1214–1221.

(21) Seotsanyana-Mokhosi, I.; Chen, J. Y.; Nyokong, T. Synthesis, Photophysicochemical Studies of Adjacently Tetrasubstituted Binaphthalo-Phthalocyanines. *J. Porphyr. Phthalocyanines* **2005**, *9* (5), 316–325.

(22) Ongarora, B. G.; Hu, X.; Li, H.; Fronczek, F. R.; Vicente, M. G. H. Syntheses and Properties of Trimethylaminophenoxy-Substituted Zn(Ii)-Phthalocyanines. *Medchemcomm* **2012**, *3* (2), 179–194.

(23) Hill, J. P.; Jin, W.; Kosaka, A.; Fukushima, T.; Ichihara, H.; Shimomura, T.; Ito, K.; Hashizume, T.; Ishii, N.; Aida, T. Self-Assembled Hexa-Peri-Hexabenzocoronene Graphitic Nanotube. *Science (80-.).* **2004**, *304* (5676), 1481–1483.

(24) Jin, W.; Yamamoto, Y.; Fukushima, T.; Ishii, N.; Kim, J.; Kato, K.; Takata, M.; Aida, T. Systematic Studies on Structural Parameters for Nanotubular Assembly of Hexa-Peri-Hexabenzocoronenes. *J. Am. Chem. Soc.* **2008**, *130* (29), 9434–9440.

(25) Chen, Z.; Liu, Y.; Wagner, W.; Stepanenko, V.; Ren, X.; Ogi, S.; Würthner, F. Near-IR Absorbing J-Aggregate of an Amphiphilic BF 2 -Azadipyrromethene Dye by Kinetic Cooperative Self-Assembly. *Angew. Chemie - Int. Ed.* **2017**, *56* (21), 5729–5733.

(26) Würthner, F.; Saha-Möller, C. R.; Fimmel, B.; Ogi, S.; Leowanawat, P.; Schmidt, D. Perylene Bisimide Dye Assemblies as Archetype Functional Supramolecular Materials. *Chem. Rev.* **2016**, *116* (3), 962–1052.

(27) Barclay, T. G.; Constantopoulos, K.; Matisons, J. Nanotubes Self-Assembled from Amphiphilic Molecules via Helical Intermediates. *Chem. Rev.* **2014**, *114* (20), 10217–10291.

(28) Wang, C.; Wang, Z.; Zhang, X. Amphiphilic Building Blocks for Self-Assembly: From Amphiphiles to Supra-Amphiphiles. *Acc. Chem. Res.* **2012**, *45* (4), 608–618.

(29) Ramanathan, M.; Shrestha, L. K.; Mori, T.; Ji, Q.; Hill, J. P.; Ariga, K. Amphiphile Nanoarchitectonics: From Basic Physical Chemistry to Advanced Applications. *Phys. Chem. Chem. Phys.* **2013**, *15* (26), 10580–10611.

(30) Fazio, E.; Jaramillo-García, J.; de La Torre, G.; Torres, T. Efficient Synthesis of

ABAB Functionalized Phthalocyanines. *Org. Lett.* **2014**, *16* (18), 4706–4709.

(31) Fazio, E.; Nazeerudin, M. K.; de la Torre, G.; Medel, M.; Grätzel, M.; Jaramillo-García, J.; Urbani, M.; Torres, T. ABAB Phthalocyanines: Scaffolds for Building Unprecedented Donor-π-Acceptor Chromophores. *ChemistryOpen* **2016**, *6* (1), 121–127.

(32) Fazio, E.; Winterfeld, K. A.; López-Pérez, A.; Torres, T.; Guldi, D. M.; de la Torre, G. Synergy of Light Harvesting and Energy Transfer as Well as Short-Range Charge Shift Reactions in Multicomponent Conjugates. *Nanoscale* **2018**, *10* (47), 22400–22408.

(33) Revuelta-Maza, M. A.; Hally, C.; Nonell, S.; de la Torre, G.; Torres, T. Crosswise Phthalocyanines with Collinear Functionalization: New Paradigmatic Derivatives for Efficient Singlet Oxygen Photosensitization. *Chempluschem* **2019**, *84* (6), 673–679.

(34) Revuelta-Maza, M. A.; Nonell, S.; de la Torre, G.; Torres, T. Boosting the Singlet Oxygen Photosensitization Abilities of Zn(II) Phthalocyanines through Functionalization with Bulky Fluorinated Substituents. *Org. Biomol. Chem.* **2019**, *17* (32), 7448–7454.

(35) Leznoff, C. C.; Marcuccio, S. M.; Greenberg, S.; Lever, A. B. P.; Tomer, K. B. Metallophthalocyanine Dimers Incorporating Five-Atom Covalent Bridges. *Can. J. Chem.* **1985**, *63* (3), 623–631.

(36) Sogah, G. D. Y.; Cram, D. J. Host-Guest Complexation. 14. Host Covalently Bound to Polystyrene Resin for Chromatographic Resolution of Enantiomers of Amino Acid and Ester Salts. *J. Am. Chem. Soc.* **1979**, *101* (11), 3035–3042.

(37) Hu, Q.-S.; Zheng, X.-F.; Pu, L. The First Optically Active and Sterically Regular Poly(1,1`-Bi-2-Naphthol)s: Precursors to a New Generation of Polymeric Catalysts. *J. Org. Chem.* **1996**, *61* (16), 5200–5201.

(38) Sasai, H.; Tokunaga, T.; Watanabe, S.; Suzuki, T.; Itoh, N.; Shibasaki, M. Efficient Diastereoselective and Enantioselective Nitroaldol Reactions from Prochiral Starting Materials: Utilization of La-Li-6,6′-Disubstituted BINOL Complexes as Asymmetric Catalysts. *J. Org. Chem.* **1995**, *60* (23), 7388–7389.

(39) Marcuccio, S. M.; Svirskaya, P. I.; Greenberg, S.; Lever, A. B. P.; Leznoff, C. C.; Tomer, K. B. Binuclear Phthalocyanines Covalently Linked through Two- and Four-Atom Bridges. *Can. J. Chem.* **1985**, *63* (11), 3057–3069.

(40) Terekhov, D. S.; Nolan, K. J. M.; McArthur, C. R.; Leznoff, C. C. Synthesis of 2,3,9,10,16,17,23,24-Octaalkynylphthalocyanines and the Effects of Concentration and Temperature on Their 1H NMR Spectra. *J. Org. Chem.* **1996**, *61* (9), 3034–3040.

(41) Tylleman, B.; Gómez-Aspe, R.; Gbabode, G.; Geerts, Y. H.; Sergeyev, S. Ester-Functionalized Phthalonitriles and Zinc Phthalocyanines via Palladium-Catalyzed Cyanation of 4,5-Dichlorophthalates. *Tetrahedron* **2008**, *64* (19), 4155–4161.

Chapter 6 – Binaphthyl-bridged tetracationic AABB-phthalocyanines: Self-assembled amphiphiles for efficient antimicrobial photodynamic therapy.

6.1. Citation and contribution

Miguel Á. Revuelta-Maza, Elena de las Heras, Montserrat Agut, Santi Nonell, Gema de la Torre and Tomás Torres. Binaphthyl-bridged tetracationic AABB-phthalocyanines: Self-assembled amphiphiles for efficient antimicrobial photodynamic therapy. Submited to *Chemical Communications*.

Contribution: Revuelta-Maza, M. A.: Synthesis and characterization, aggregation studies, photophysical and microbiolgy experiments (together with E. de las Heras). Preparation of the manuscript.

Funding and supervision: Agut, M.; Nonell, S.; de la Torre, G.; Torres, T.

Abstract:

Herein, we report the synthesis and characterization of two new amphiphilic phthalocyanines (Pcs) (**PS-1** and **PS-2**), the study of their photophysical properties, and biological assays to determine their antimicrobial potential. In particular, we describe the preparation of chiral Zn(II)Pcs with an AABB geometry (where A and B refer to differently substituted isoindole constituents) through cross-condensation of different chiral binaphthyloxy-linked bisphthalonitriles, which determine the drug hydrophobicity, and cationic methyl pyridinium moieties in the other two isoindoles to embody hydrophilicity. The main difference between the two PS is the presence or not, of *n*-octyl chains at the binaphthyl core (**PS-2** and **PS-1**, respectively), which determines the degree of hydrophobia but does not influence the photophysical properties. Both compounds have the ability to self-assemble into micelles in water media, and have proved efficient in the photoinactivation of *S. aureus* and *E. coli*, selected as models of Gram-positive and Gram-negative bacteria. The micelle size average and dark toxicity are determined by the substitution at the binaphthyl core, being the non-substituted **PS-1** more effective in killing both types of strains.

6.2. Introduction and Objectives

Amphiphilic drugs are among the most promising compounds to be used as PS for photodynamic therapy. This intrinsic feature facilitates both aqueous media circulation[1] and traversing of the cellular membranes,[2] since amphiphilic molecules are easily localized both at hydrophobic-hydrophilic interfaces.[3] Regarding to photodynamic inactivation of bacteria as a non-antibiotic option for the treatment of infectious diseases, several examples of amphiphilic drugs application have been reported in recent years. Specifically, Gram-positive bacteria have been shown to be highly susceptible to PDI, however the inactivation of Gram-negative bacteria has been more challenging due to the impermeability properties of the outer membrane.[4] Porphyrinoid second generation PS are among the most used within this area, that turned into third generation PS when their self-assembly capabilities in aqueous media facilitates their transport and incorporate new specific functions.

Regarding to porphyrinoid dyes as PS, as we have explained in the Introduction-PDT section, charged functions can be attached to the macrocycles to render solubility in aqueous media. Cationic dyes can be obtained by quaternization of aliphatic or aromatic nitrogen atoms in their substituents. For instance, pyridine-based substituents are a common structural motif to prepare water soluble PS.[5] This heterocycle provides a lone nitrogen pair not conjugated within the aromatic ring, susceptible of quaternization.

It has been shown that the molecular charge of the PS is an important factor in the antibacterial activity, being positively charged PS, namely cationic Pors and Pcs, generally more efficient than neutral or anionic dyes.[6] For Pors, it is extensively proved that the number of charges and their distribution in the PS core have an important role on PDI efficiency and determine if the PS permeates through the membrane of the cells or not.[7–13] Por with three or four positive charges are highly efficient against bacteria, and those bearing cationic groups in adjacent *meso* positions seem to be significantly more efficient than those with the cationic groups located in opposite *meso* positions.[14] However much less effort has been done with Pcs in this matter, although some works have been reported. For instance, The linkage of pyridines has be achieved through a ether or thioether bond, with hydroxy- or mercapto- pyridines,[15] and Pcs symmetrically substituted at the peripheral positions with methylpyridinium units have proved promising PS for PDI.[16,17] Regarding to the A_2B_2 Pc substitution, there is one example of a cationic AABB Pc studied as PS. Vicente and coworkers studied the photophysical properties and *in vitro* biological behavior in human carcinoma HEp2 cells of an AABB trimethylaminophenoxy-substituted Zn(II)Pc with a biphenyl unit linker between adjacent isoindole units (see Introduction-PDT section).[18]

Herein, we report the synthesis of two new PS based on AABB Zn(II)Pcs, (see Scheme 6. 1) in order to study their activity against Gram-positive and Gram-negative bacteria. These compounds are highly oriented amphiphiles that are expected to self-assemble in water as previous reports for A_3B amphiphilic cationic Zn(II)Pcs.[19,20]

6.3. Results and Discussion

a) Synthesis

Key bisphthalonitriles **(R)-7a-C5** and **(R)-7b-C5**, previously showed in **Chapter 5**, were prepared from the chiral (R)- 1,1'-bi-2-naphthol (**(R)-BINOL**). The synthesis of the target Zn(II)Pcs was carried out by cross- condensation between two equivalents of 5-bis(pyridin-3-yloxy)phthalonitrile (**B-py**),[15] and one equivalent of the corresponding bisphthalonitriles **(R)-7a-C5** or **(R)-7b-C5** for **AABB-py-1** or **AABB-py-2** respectively, by heating in *o*-DCB/DMF (2:1) at 160°C overnight (Scheme 6. 1). In both reactions, the targeted AABB Zn(II)Pcs were formed together with the corresponding $(AA)_2$ derivatives (Figure 6. 1), constituted by four isoindole units liked by two binaphthyl units, which have been already described in **Chapter 5**. On the other hand, B_4 Zn(II)Pc with eight pyridyloxy units was not isolated in any of the reactions. Targeted compounds were easily isolated by chromatographic means, in 13% yield for **AABB-py-1** and 10% for **AABB-py-2**.

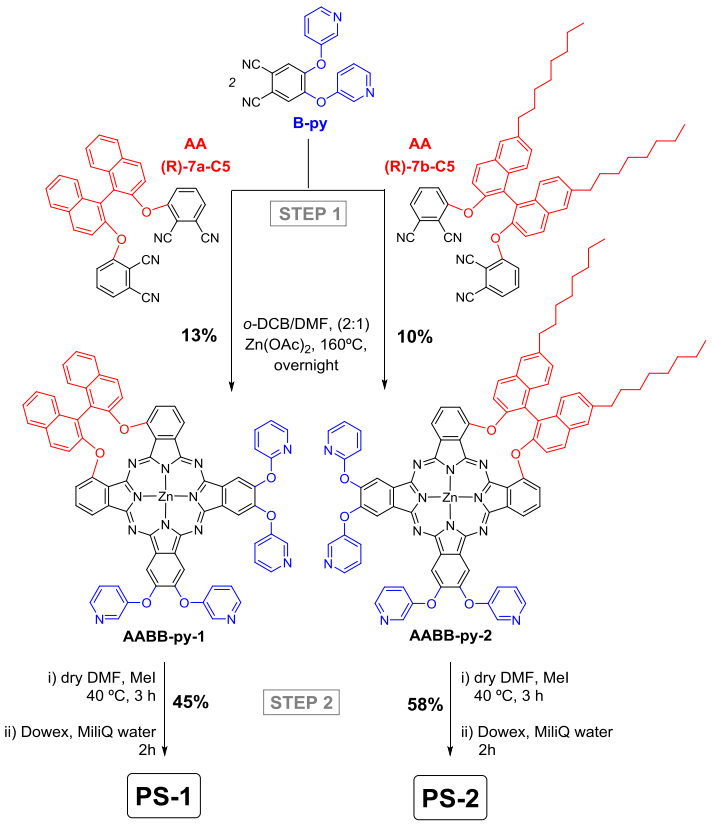

*Scheme 6. 1. Synthesis of Zn(II)Pcs **AABB-py-1** and **AABB-py-2** from phthalonitriles **(R)-7a-C5, (R)-7a-C5** and **B-py** as starting materials. **PS-1** and **PS-2** full structure is detailed in Figure 6. 3.*

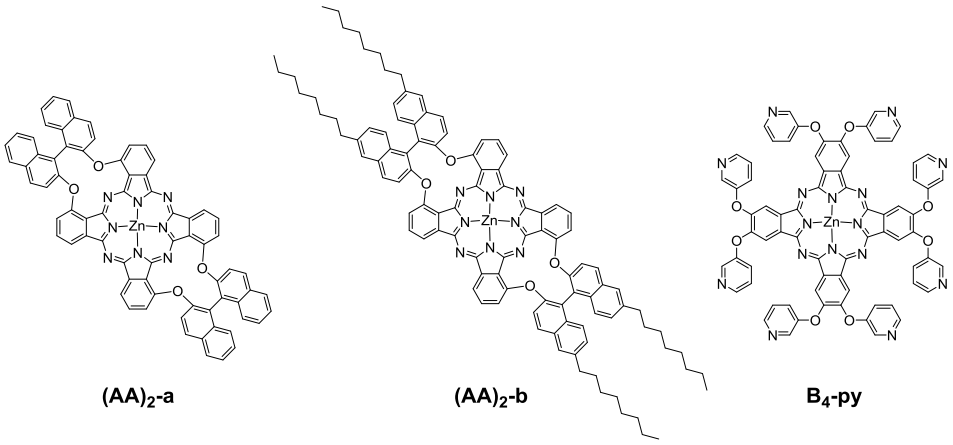

*Figure 6. 1. Zn(II)Pcs structures of expected subproducts in the synthesis of **AABB-py-1** and **2**.*

The synthesized Zn(II)Pcs have in common good solubility features in typical organic solvents. ^{1}H NMR spectra of Zn(II)Pcs **AABB-py-1** and **AABB-py-2** were registered in DMSO-d_6 as coordinative solvent to avoid aggregation problems. However, even upon heating al 363 K the compounds remain in a highly aggregated state in solution, which makes difficult their full characterization at this stage of the PS synthetic process (Figure 6. 2). For this reason, we proceeded with the methylation step (Scheme 6. 1) by reaction with MeI in DMF. After a counterion exchange (iodine was substituted by chlorine atoms), **PS-1** and **PS-2** were isolated in 45 and 58 % yield respectively.

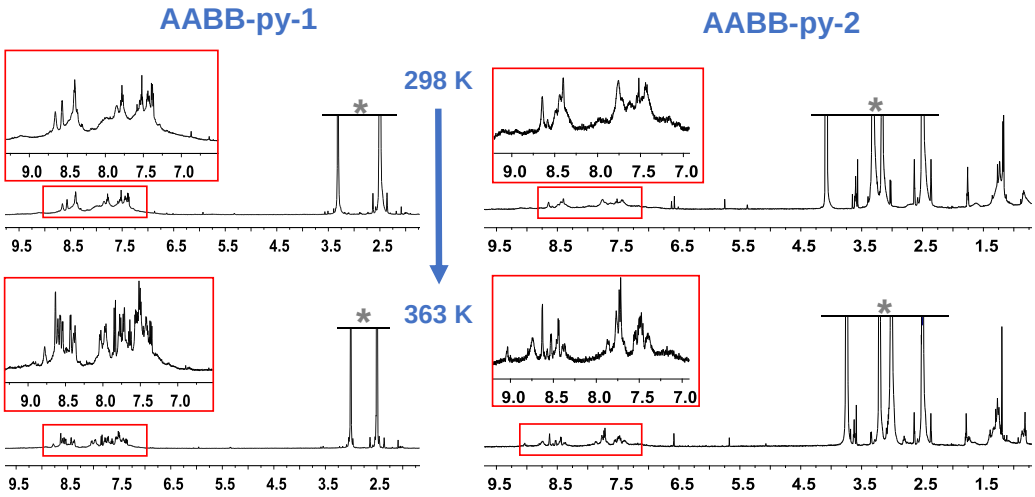

*Figure 6. 2. ^{1}H-NMR of **AABB-py-1** and **AABB-py-2** in DMSO-d_6 at 298 K and 363 K. Broadening of the signals in the aromatic region (see highlighted areas) indicates aggregation phenomena which makes difficult the peaks assignation. Signal at 1.2 ppm for **AABB-py-2** indicate the presence of alkyl chains. *: residual solvent peaks.*

As repulsion between positive charges avoids aggregation phenomena in organic solvents, **PS-1** and **PS-2** could be easily characterized by ^{1}H-NMR in DMSO-d_6. The spectra for both PS at room temperature is shown in Figure 6. 3 and Figure 6. 4. The lack of aggregation exhibited by the two PS results in extremely well-resolved ^{1}H-NMR spectra, which is infrequent for this type of Zn(II)Pcs. In the magnification of the aromatic region of the ^{1}H-NMR spectra of **PS-1** and **PS-2** shown in Figure 6. 3 and Figure 6. 4, we can distinguish two singlets for the pyridyloxy-substituted isoindole protons, a set of four signals for pyridyloxy substituents, two doublets and a triplet for the binaphthyl-functionalized isoindoles, and two doublets for the protons of the inner BINOL ring. Finally, the signals of the outer BINOL aromatic ring constitute the main difference between **PS-1** and **PS-2**. The presence of alkyl chains in **PS-2** simplifies the pattern to two

doublets and a singlet, instead of a set of four correlated signals (two doublets and two triples) for **PS-1**.

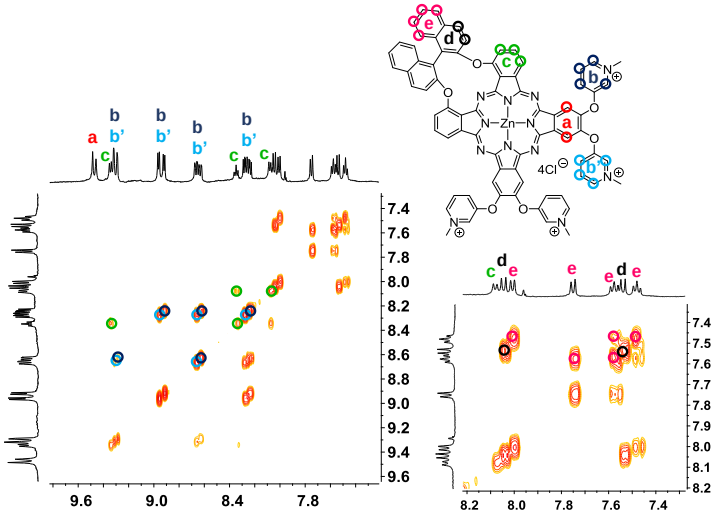

*Figure 6. 3. COSY (500 MHz, DMSO-d_6) of **PS-1**.*

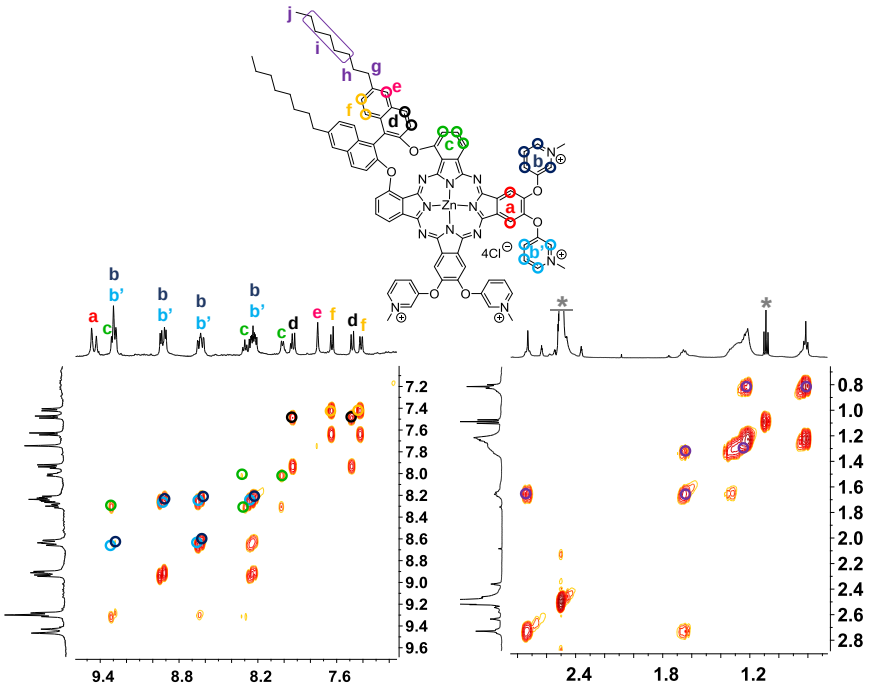

*Figure 6. 4. COSY (500 MHz, DMSO-d_6) of **PS-2**.*

b) Photophysical studies

First, UV-vis absorption spectra were recorded in *N,N*-dimethylacetamide (DMA), a solvent that is able to coordinate the Zn(II) metal center, hampering the aggregation of Zn(II)Pcs independently of the substitution pattern. Ground-state absorption experiments were performed for both **PS-1** and **PS-2**, showing the typical *Q*-band, accompanied by vibrational absorptions, and the *B*-band transition. The lack of aggregation was proven by the absorption studies performed at a range of concentrations (Figure 6. 5). For the verification of the Lambert-Beer law, an analysis of linear regression between the intensity of the *Q*-band and the concentration of the PS was performed, showing R^2 values close to 1. The presence of alkyl chains does not affect the molar extinction coefficient of both PS, showing $\log\varepsilon$ = 5.2.

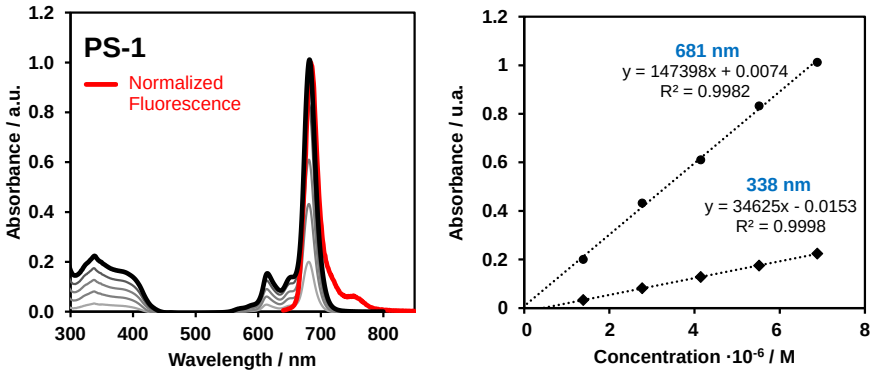

*Figure 6. 5. Concentration-dependent UV-vis experiment for **PS-1** in DMA (~1·10⁻⁶ - 7·10⁻⁶ M) and normalized fluorescence in red.*

Fluorescent experiments are in line with absorption assays, with both compounds presenting again the same spectroscopical features. Difference between absorption and fluorescence maxima is very small, which minimizes Stokes shift (Figure 6. 5). On the other hand, fluorescence quantum yield (ϕ_F) is slightly larger for **PS-2**, which is convergent with a lower triplet excited state lifetime (τ_T). Quantification of the ϕ_Δ was done by direct observation of the $^1O_2$ phosphorescence at 1275 nm after excitation at 355 nm in DMA solutions, giving the same value for both **PS-1** and **PS-2** (ϕ_Δ = 0.57). Also, time-resolved fluorescence (TRF) decays pointed out in the same direction, showing singlet excited-state lifetime of 2.4 ns for both compounds. These observations support that the substitution with alkyl chains have a minor impact in the photosensitization abilities of these Zn(II)Pcs. All these parameters are summarized in Table 6. 1.

Table 6. 1. Photophysical properties of PS-1 and PS-2 in N,N-dimethylacetamide (DMA) solutions.

ZnPc	logε (λ)	λ_f / nm	ϕ_f	τ_S / ns	τ_T / μs[a]	ϕ_Δ
PS-1	4.5 (338), 5.2 (681)[b]	684	0.23	2.4	0.53	0.57
PS-2	4.6 (343), 5.2 (681)[b]	683	0.18	2.4	0.78	0.57

[a] In air-saturated solutions. [b] Q-band maximum.

c) Aggregation experiments

The large hydrophobic part in both **PS-1** and **PS-2** make these compounds insoluble in pure water. However, when injected in water from stock concentrated solutions in DMSO, the two PS remain dissolved. In this way, we registered the CD and UV-vis spectra of both PS in concentrations of ~$1 \cdot 10^{-5}$ M. First, in DMSO (black lines in **¡Error! No se encuentra el origen de la referencia.**) we could appreciate similar Soret and *Q*-bands to those observed in the DMA spectra. Second, we registered the spectra in MiliQ water solutions, after injection from a stock solution in DMSO and incubation overnight by standing at room temperature (red lines in **¡Error! No se encuentra el origen de la referencia.**). In this case, we observed a broadening in the *Q*-band with a red shift, and the rising of a new band at 642 nm for **PS-1**, and at 638 nm for **PS-2**, which is typical of *H*-type aggregates. Decreasing of the intensity of the *Q*-band of the monomer is more notorious for **PS-1** than for **PS-2**. We can rationalize the formation of aggregates in water solution by the determinant role of the solvophobic forces versus the ionic repulsion between pyridinium moieties. Moreover, the asymmetrical distribution of substituents in the Pc core permits that, even if the hydrophobic cores stack, the cationic pyridinium moieties can accommodate to minimize repulsion.

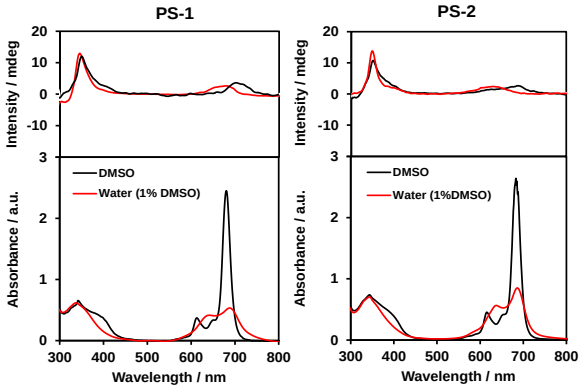

*Figure 6. 6. CD of **PS-1** and **PS-2** in DMSO and water (1% DMSO) (top), together with the corresponding electronic absorption spectra (bottom).*

The presence of the chiral (R)-binaphthol unit has allowed us to study the self-assembly behavior of these molecules in solution by CD spectroscopy. No significant differences are observed between both PS. In DMSO the UV-vis Soret and *Q*-bands have the correspondent signal in the CD spectrum with positive sign and low intensity. In aqueous solutions, we could observe a blue shift from 690 nm to 670 nm or 640 nm for **PS-1** and **PS-2** respectively, related in both cases with the formation aggregates with a different chiral environment around the Zn(II)Pc core.

Next step was to assess the effect of concentration in the formation of self-assembled structures. Concentration dependent experiments were performed over **PS-1** and **PS-2** solutions in PBS from stock solutions in DMSO, so that % DMSO was <1% in a range of concentrations approximately from $0.5 \cdot 10^{-6}$ M to $3.5 \cdot 10^{-5}$ M, (see Figure 6. 7 and Figure 6. 8). In both cases absorbance versus concentration showed linearity with R^2 values close to 1, indicating that no variations in the aggregation state are taking place in this range of concentrations. Moreover, temperature dependence experiments by heating at 40 °C and 80 °C are shown. For both PS no significative changes are observed, which also point to the stability of the aggregates. Turning to fluorescence experiments performed in the same concentration range, although the emission is considerably quenched, a remanent signal was detected, that is more intense in the case of **PS-1**.

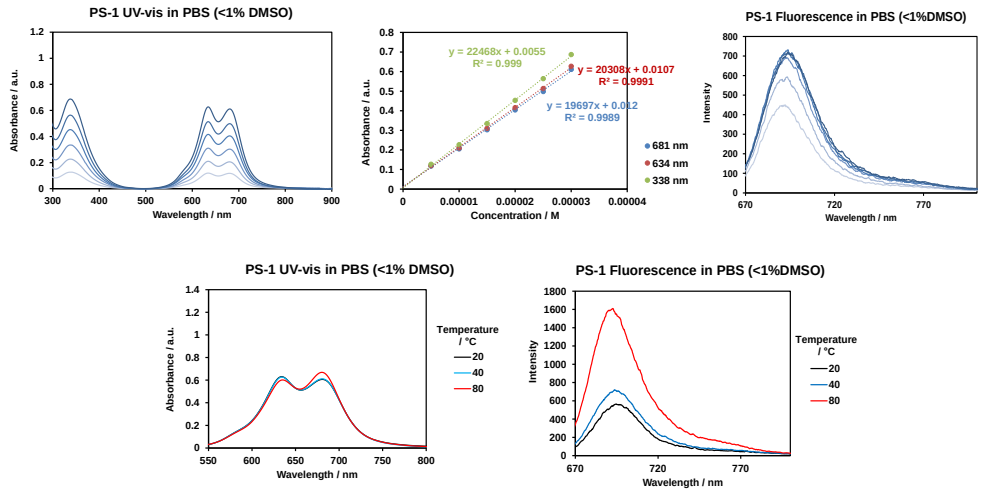

*Figure 6. 7. Concentration and temperature dependent experiments for **PS-1**.*

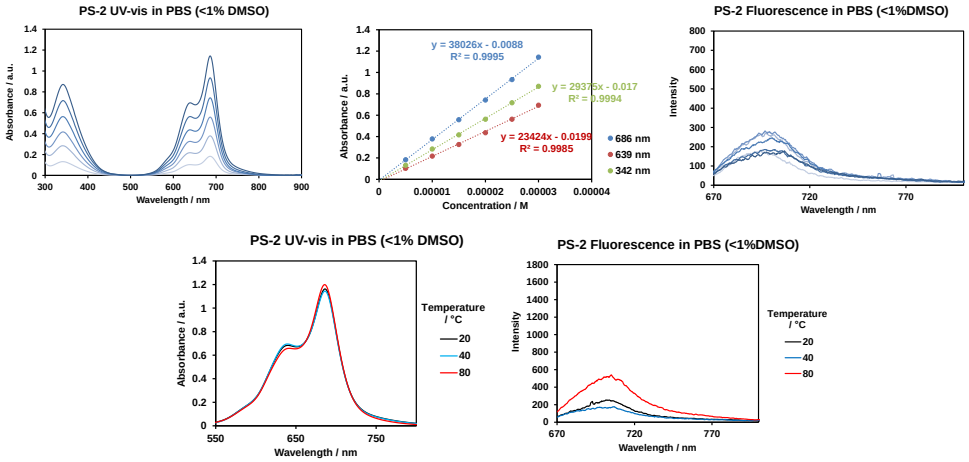

*Figure 6. 8. Concentration and temperature dependent experiments for **PS-2**.*

To obtain information about the morphology of the aggregates in water, the same MiliQ water solutions (C = $2 \cdot 10^{-5}$ M, 1%DMSO) were observed by transmission electronic microscopy (TEM) after deposition over specific grids. Both **PS-1** and **PS-2** self-assemble into spherical vesicles. The presence of alkyl chains modulate the size. **PS-1** forms vesicles with an average size of 20-42 nm, while **PS-2** vesicles are between 12-20 nm (see Figure 6. 9). Unfortunately, experimental corroboration of the nanoparticle size could not be obtained from DLS experiments since the sizes of the vesicles are out of the detection range of the equipment.

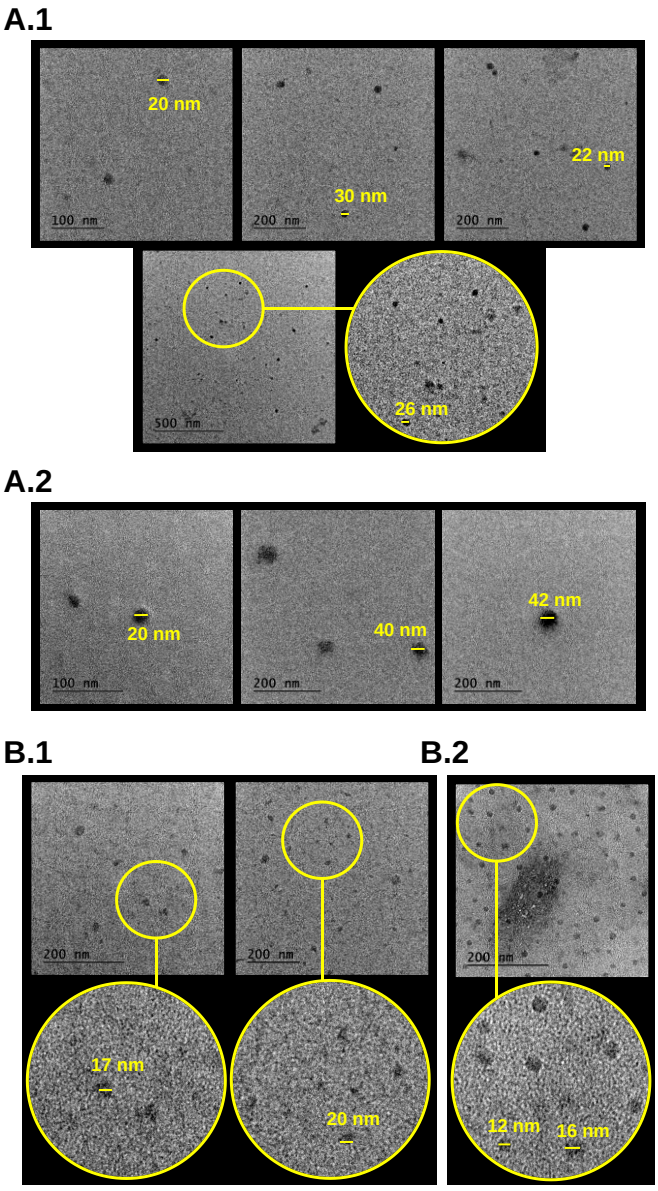

*Figure 6. 9. TEM images of: A) **PS-1** and B) **PS-2**, prepared over Formvar/Carbon 200 Mesh, Copper FCF200-CU grilles (1), or after glow discharge treatment (2).*

d) Determination of the log Po/w

For a quick evaluation of the relative lipophilicity of **PS-1** and **PS-2**, and their affinity for cell membranes, *n*-octanol/PBS partition coefficients were determined using the shake-flask method, (Figure 6. 10 and Materials and methods section).

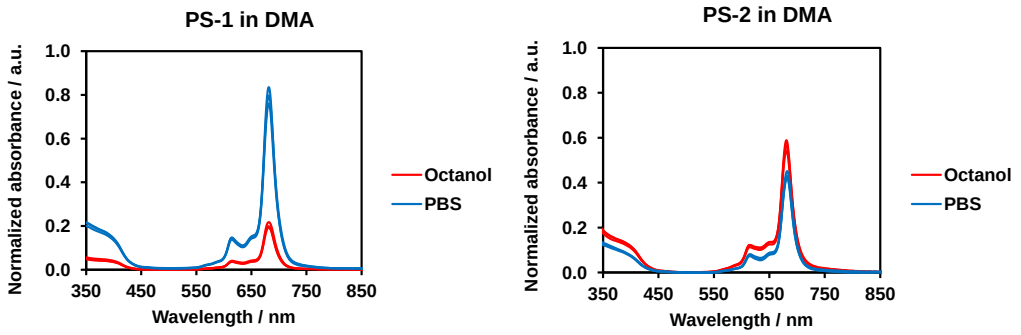

*Figure 6. 10. UV-vis of aliquots from n-octanol/PBS phases **PS-1** and **PS-2** diluted in DMA.*

The affinity of each compound for cell membranes is numerically represented by its membrane-water partition coefficient, that is, the membrane-water concentration ratio as the *n*-octanol/PBS partition coefficient ($P_{O/W}$).[21–23] Although both compounds have a common structural core, they exhibited very different amphiphilic character. **PS-2** (log $P_{O/W}$ = 0.12) renders a higher octanol/PBS partition coefficient than **PS-1** (log $P_{O/W}$ = -0.59) indicating that the former has a more lipophilic nature. The Pc ratio reached for **PS-1** in n-octanol/PBS was approximately 20:80, while the **PS-2** ratio was 57:43. At a first glance, the very different behavior of the two compounds is somehow surprising. Although **PS-2** is clearly more lipophilic due to the presence of octyl chains over binapthol linkers, one would not expect that **PS-1** showed such a large negative value of log $P_{O/W,}$ considering that the compound is not even soluble in pure water. However, this result can be rationalized considering the formation of vesicles after injection of the PS from stock solutions in DMSO, and g that **PS-1** forms larger vesicles, with a larger cationic surface than **PS-2**.

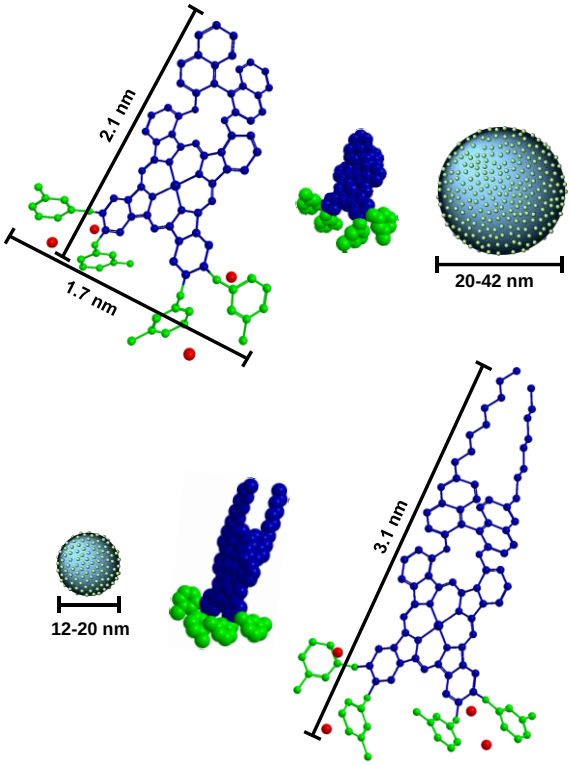

Figure 6. 11. Structure models designed with SCIGRESS (FJ 2.8.1 EU 3.3.1) geometry optimization MM2 with molecular amphiphilic character representation: hydrophobic area (blue), hydrophilic area (green), counterions (red). And schematic representation of PS self-assembled micelles.

e) Biological studies

The photoinactivation studies were performed testing **PS-1** and **PS-2** in S. aureus and E. coli bacteria, chosen as models for Gram-positive and Gram-negative bacteria, respectively (Figure 6. 12). The inactivation studies present a typical light- and concentration-dependent profile. Light fluence to 11 J·cm^{-2} only resulted in a cell survival increase of 1 log CFU for both PS. However, **PS-1** and **PS-2** were able to induce 99,9% (3 log decrease in colony-forming units, CFUs) of S. aureus inactivation at 0.1 μM, increasing the red light fluence to 33 J·cm^{-2}. This observation indicates that the ZnPcs must be in monomeric, i.e., photochemically active, form, which in turn indicates that they are bound to the bacterial cell wall, where they de-aggregate.[24] Full inactivation (7 log CFUs) could be achieved at 2 μM for **PS-1**, or 4 μM for **PS-2**. By other hand, full inactivation (8 log CFUs) can be attributed to dark cytotoxicity at high concentration (10 μM) for **PS-1**, while PS-2 seems to be slightly less toxic with 3 log decrease in colony-forming units. Regarding E. coli, surprisingly no larger concentrations were required to induce a

comparable cell death. 1 μM for **PS-1**, or 10 μM for **PS-2**, together with 33 J·cm^{-2} light dose were enough to achieve a disinfection (99.9%) status. In this case, no dark toxicity could be observed even at the highest concentration, which likely indicates that the compounds are not taken up by the bacteria but stick to the outer membrane.[25] Importantly, **PS-1** seems more toxic than **PS-2** against the microbial strains tested, indicating a clear effect of the alkyl chains presence over the binaphtol linker. Compared to other symmetrically-substituted cationic Pcs, the inherent oriented amphiphilic character of **PS-1** and **PS-2** provide them with much stronger photo-antimicrobial activity. Indeed, related Pcs lacking these groups achieved only a modest 1-2-log CFUs cell death, owing to their strong aggregation.[26,27] Only sorted out for S. aureus strains by our ABAB Zn(II)Pcs recently reported, (Chapter 4) but now remarkably improved against E. coli.

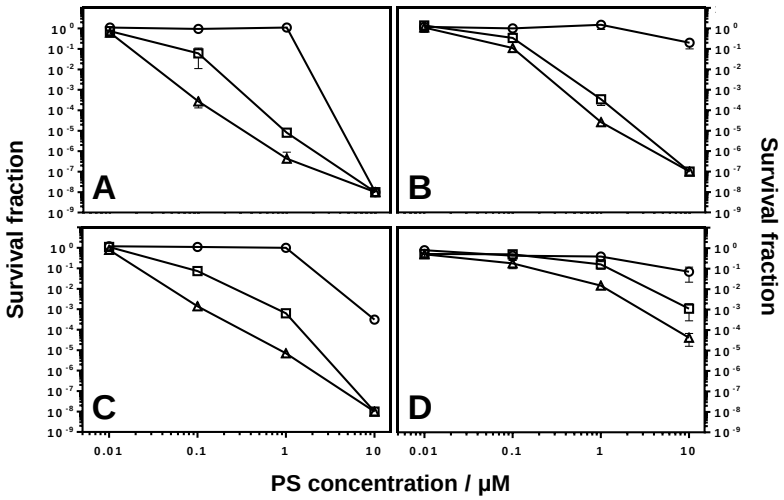

*Figure 6. 12. Survival curves of S. aureus (A, C) and E. coli (B, D) with **PS-1** (A, B) and **PS-2** (C, D) after PDI treatment. Circles, triangles and squares represent 0 (dark toxicity), 11 and 33 J·cm-2, respectively.*

6.4. Conclusions

Both **PS-1** and **PS-2** were efficient in the photoinactivation of Gram-positive and Gram-negative bacteria. The difference in the degree of hydrophobia did not generate major changes in the inactivation of S aureus, showing **PS-1** greater toxicity in darkness for high concentrations. In the case of E. coli, **PS-1** was better than **PS-2**. Specifically, the presence of alkyl chains determines the type of aggregates in aqueous solution. It seems that a larger particle size facilitates interaction with the bacteria wall and produces greater toxicity upon irradiation.

6.5. Experimental section

a) Materials and methods

i. *Determination of the log $P_{O/W}$*

Initially, equal volumes of n-octanol and PBS (pH = 7.2–7.6 at 25 °C) were mixed vigorously for 3 days at 25°C to promote solvent saturation in both phases. Each sample (**PS-1** and **PS-2**) was then added from concentrated stock solutions ($1 \cdot 10^{-3}$ M) to 2 mL of the mixture and stirred for 30 min; next, they were incubated 1 h at room temperature. After separation, 100 µL of n-octanol phase and 100 µL of PBS phase were taken and diluted by DMA to 1.1 mL with a concentration of approximately $1 \cdot 10^{-5}$ M. The UV–vis spectra of both phases were recorded, and the partition coefficient was calculated based on the absorbance values at *Q*-band maxima (681 nm for both **PS-1** and **PS-2**). The results are the average of three independent measurements.

$$logP_{OW} = log\left(\frac{A(MeOH)_O \cdot V_W}{A(MeOH)_W \cdot V_O}\right)$$

ii. *Microbial strains, culture conditions and photodynamic inactivation studies*

The microorganisms studied were Staphylococcus aureus (ATCC® 29213) as a Gram-positive model and Escherichia coli (ATCC® 25922) as Gram-negative bacteria. Bacterial cells were grown overnight in an orbital shaker at 37 °C in tryptic soy broth (TSB) medium. An aliquot was then suspended in fresh TSB and set to grow in exponential phase at 37 °C to achieve approximately 108 colony forming units (CFU,·mL^{-1}). They were later centrifuged (5000 rpm, 10 min) and re-suspended in PBS (pH = 7.4). The cells were incubated with the drug, delivered in DMSO, in the dark for 30 minutes. Two independent experiments were done for each photoinactivation treatment, which in turn was carried out in duplicate. The average and SD values were calculated. Cells were then irradiated from the top in 96-well plates by means of a Red 670 Device (Red Man Light, United Kingdom; 660 ± 10 nm; 70 mW·cm^{-2}). The fluence of the lamp was regularly monitored with a power meter to ensure the light dose delivered. Controlling the cell irradiation without PS was also performed in order to exclude any inactivation due to light or heating effects, along with the evaluation of the toxicity of **PS-1** and **PS-2** in the dark. After illumination, the samples were serially diluted and streaked on agar plates and incubated in the dark for 18 h at 37 °C.

b) Synthesis

4,5-Bis(pyridin-3-yloxy)phthalonitrile (**B-py**), (R)- or (S)-2,2'-Bis(2,3-dicyanophenyl)-1,1'-binaphthalene (**(R)-7a-C5**), and (R)- or (S)-2,2'-Bis(2,3-dicyanophenyl)-6,6'-dioctyl-1,1'-binaphthalene (**(R)-7b-C5**), have been prepared according to published procedures. Given the structural complexity of **PS-1** and **PS-2** tertiary and quaternary carbons were hardly detected by ^{13}C-NMR. However, primary and secondary carbons, where the structural difference between both PS lies, are detailed. These signals were obtained by HSQC experiments as shown in Figure 6. 13.

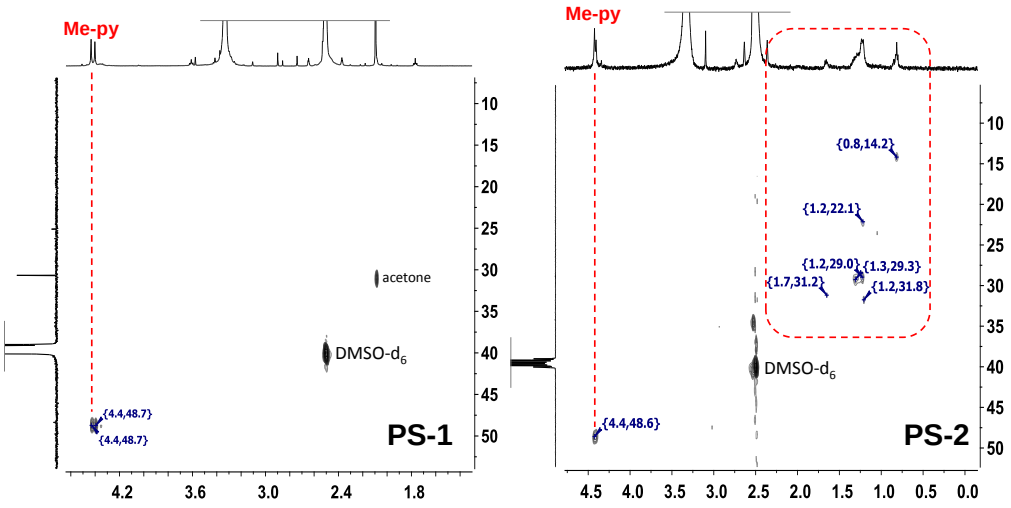

*Figure 6. 13. HSQC comparison for primary and secondary carbons for **PS-1** and **PS-2** in DMSO-d_6.*

iii. *Synthesis of PS-1:*

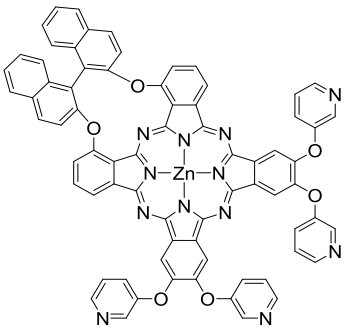

Step 1 - Synthesis of AABB-py-1: B (85 mg, 0.27 mmol), phthalonitrile **AA-1** (73 mg, 0.14 mmol) and anhydrous $Zn(AcO)_2$ (50 mg, 0.27 mmol) were placed in a 5 mL high pressure resistant flask equipped with a magnetic stirrer, and then 2.7 mL ([**AA-1**]=0.05 M) of dry *o*-DCB/DMF (dried over 4Å molecular sieves) 2:1 were added. The mixture was heated to 160°C overnight under argon atmosphere. After cooling, the solvent was removed under vacuum. The mixture of products was purified by column chromatography on SiO_2, (in gradient from dioxane to dioxane/MeOH 9:1). Zn(II)Pc **$(AA)_2$-1** eluted first

followed by the desired product **AABB-1**. After evaporation of the solvent, a blue-green solid was obtained, which was washed with heptane and MeOH. Yield: 22 mg, (13%). HR-MS (MALDI ULTRAFLEX III, matrix DCTB + PPGNa 1000): *m/z* 1230.2326 (calculated for $C_{72}H_{38}N_{12}O_6Zn$: 1230.2323).

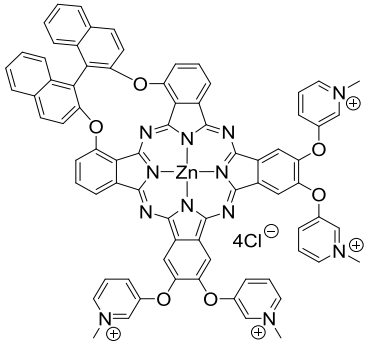

Step 2 – Methylation and counteranion exchange: AABB-py-1 (10 mg, $8.1 \cdot 10^{-3}$ mmol) was placed in a 10 mL round bottom flask equipped with a magnetic stirrer and 1 mL of dry DMF (dried over 4Å molecular sieves) were added. Then, an excess of MeI (150 µL) was added and the mixture was stirred at 40°C for 3h under argon atmosphere. After evaporation of the solvent, with the necessary safety precautions given the toxicity of IMe, the product (with iodine as counterion) was washed several times with diethylether, and isolated as a green solid. 250 mg of Dowex® (1x8 200-400) were suspended in 10 mL of MiliQ water, the product was previously dissolved in 0.2 mL of DMSO was added and stirred for 2 h. Then, the mixture was filtered, washed with diethylether, and evaporated under vacuum. Yield: 5.2 mg (45%). ^{1}H-NMR (500 MHz, DMSO-d_6): δ 4.39 (s, 6H, Me-py), 4.42 (s, 6H, Me-py), 7.47 (td, *J* = 7.48 Hz, *J* = 0.91 Hz, 2H, H_e), 7.53 (d, *J* = 9.21 Hz, 2H, H_d), 7.57 (td, *J* = 8.10 Hz, *J* = 1.07 Hz, 2H, H_e), 7.74 (d, *J* = 8.40 Hz, 2H, H_e), 8.00 (d, *J* = 8.16 Hz, 2H, H_e), 8.04 (d, *J* = 9.21 Hz, 2H, H_d), 8.07 (d, *J* = 7.67 Hz, 2H, H_c), 8.21-8.30 (m, 8H, $H_{b/b'}$), 8.34 (t, *J* = 7.57 Hz, 2H, H_c), 8.62 (dd, *J* = 8.86 Hz, *J* = 2.28 Hz, 4H, $H_{b/b'}$), 8.66 (dd, *J* = 8.84 Hz, *J* = 2.27 Hz, 4H, $H_{b/b'}$), 8.91 (d, *J* = 6.01 Hz, 4H, $H_{b/b'}$), 8.96 (d, *J* = 6.02 Hz, 4H, $H_{b/b'}$), 9.28 (s, 4H, $H_{b/b'}$), 9.31 (s, 4H, $H_{b/b'}$), 9.34 (d, *J* = 7.46 Hz, 2H, H_c), 9.45 (s, 2H, H_a), 9.48 (s, 2H, H_a); ^{13}C-NMR (125 MHz, DMSO-d_6): δ 48.7 (Me-py); IR (ATR) v^{-1} (cm^{-1}): 3346, 3055, 1623, 1581, 1503, 1085. HR-MS ((ESI Positive TOF_MS-100-3500.m, MAXIS II): Exact mass calculated for $[C_{76}H_{50}ClN_{12}O_6Zn]^{3+}$: 1325.2940, *m/z*: 441.7648; experimental: 441.7642. Exact mass calculated for $[C_{76}H_{50}Cl_2N_{12}O_6Zn]^{2+}$: 1360.2634, *m/z*: 680.1317; experimental: 680.1317.

iv. *Synthesis of PS-2:*

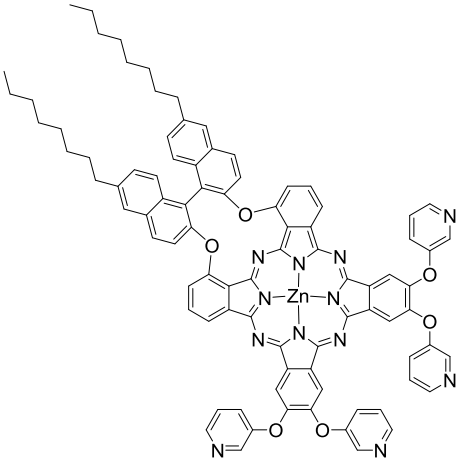

Step 1 - Synthesis of AABB-py-2: B (77 mg, 0.29 mmol), phthalonitrile **AA-2** (94 mg, 0.14 mmol) and anhydrous $Zn(AcO)_2$ (45 mg, 0.29 mmol) were placed in a 5 mL high pressure resistant flask equipped with a magnetic stirrer, and then 2.5 mL ([**AA-2**]=0.05 M) of dry *o*-DCB/DMF (dried over 4Å molecular sieves) 2:1 were added. The mixture was heated to 160°C overnight under argon atmosphere. After cooling, the solvent was removed under vacuum. The mixture of products was purified by column chromatography on SiO_2, (first using heptane/dioxane 1:1 as eluent and then in gradient from dioxane to dioxane/MeOH 9:1). Zn(II)Pc **$(AA)_2$-1** with other subproducts eluted first followed by the desired product **AABB-2**. After evaporation of the solvent, a blue-green solid was obtained, which was washed with MeOH. Yield: 20 mg, (10%). HR-MS (MALDI ULTRAFLEX III, matrix DCTB + PEGNa 1500): *m/z* 1454.4820 (calculated for $C_{88}H_{70}N_{12}O_6Zn$: 1454.4827).

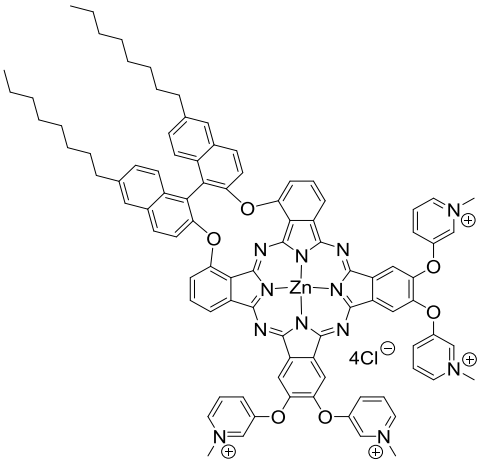

Step 2 – Methylation and counteranion exchange: AABB-py-2 (10 mg, $6.9 \cdot 10^{-3}$ mmol) was placed in a 10 mL round bottom flask equipped with a magnetic stirrer and 1 mL of dry DMF (dried over 4Å molecular sieves) were added. Then, an excess of MeI (150 µL) was added and the mixture was stirred at 40°C for 4h under argon atmosphere. After evaporation of the solvent, with the necessary safety precautions given the toxicity of IMe, the product (with iodine as counterion) was washed several times with diethylether, and isolated as a green solid. 250 mg of Dowex® (1x8 200-400) were suspended in 10 mL of MiliQ water, the product was previously dissolved in 0.2 mL of DMSO was added and stirred for 2 h. Then, the mixture was filtered, washed with diethylether, and evaporated under vacuum. Yield: 6.6 mg (58%). ^{1}H-NMR (500 MHz, DMSO-d_6): δ 0.77-0.85 (m, 6H, H_j), 1.16-1.32 (m, 20H, H_i), 1.62-1.70 (m, 4H, H_h), 2.72-2.75 (m, 4H, H_g), 4.39 (s, 6H, Me-py), 4.41 (s, 6H, Me-py), 7.42 (d, *J* = 8.87 Hz, 2H, H_f), 7.48 (d, *J* = 9.05 Hz, 2H, H_d), 7.64 (d, *J* =

8.87 Hz, 2H, H_f), 7.74 (s, 2H, H_e), 7.93 (d, *J* = 9.05 Hz, 2H, H_d), 8.02 (d, *J* = 7.32 Hz, 2H, H_c), 8.20-8.27 (m, 4H, $H_{b/b'}$), 8.30 (t, *J* = 7.40 Hz, 2H, H_c), 8.62 (dd, *J* = 8.98 Hz, *J* = 2.01 Hz, 2H, $H_{b/b'}$), 8.65 (dd, *J* = 9.11 Hz, *J* = 2.18 Hz, 2H, $H_{b/b'}$), 8.90 (d, *J* = 5.92 Hz, 2H, $H_{b/b'}$), 8.94 (d, *J* = 6.24 Hz, 2H, $H_{b/b'}$), 9.28 (s, 2H, $H_{b/b'}$), 9.30 (s, 2H, $H_{b/b'}$), 9.31 (d, *J* = 7.49 Hz, 2H, H_c), 9.43 (s, 2H, H_a), 9.47 (s, 2H, H_a); ^{13}C-NMR (125 MHz, DMSO-d_6): δ 14.2 (CH_2), 22.1 (CH_2), 29.0 (CH_2), 29.3 (CH_2), 31.2 (CH_2), 31.8 (CH_2), 48.6 (Me-py); IR (ATR) v^{-1} (cm^{-1}): 3347, 3034, 2920, 2851, 1723, 1582, 1465, 1270, 1086. HR-MS ((ESI Positive TOF_MS-100-3500.m, MAXIS II): Exact mass calculated for $[C_{92}H_{82}ClN_{12}O_6Zn]^{3+}$: 1549.5444, *m/z*: 516.5148; experimental: 516.5147. Exact mass calculated for $[C_{92}H_{82}Cl_2N_{12}O_6Zn]^{2+}$: 1584.5138, *m/z*: 792.2569; experimental: 792.2573.

c) Photophysical studies

i. *Fluorescence spectra:*

The samples were excited at: **PS-1** 670 nm (DMA), and **PS-2** 671 nm (DMA).

ii. *Fluorescence Quantum Yields:*

The samples were excited at: **PS-1** 639 nm (DMA), and **PS-2** 632 nm (DMA).

6.6. References

(1) Sun, T.; Zhang, Y. S.; Pang, B.; Hyun, D. C.; Yang, M.; Xia, Y. Engineered Nanoparticles for Drug Delivery in Cancer Therapy. *Angew. Chemie Int. Ed.* **2014**, *53* (46), 12320–12364.

(2) Minnock, A.; Vernon, D. I.; Schofield, J.; Griffiths, J.; Parish, J. H.; Brown, S. B. Mechanism of Uptake of a Cationic Water-Soluble Pyridinium Zinc Phthalocyanine across the Outer Membrane of Escherichia Coli. *Antimicrob. Agents Chemother.* **2000**, *44* (3), 522–527.

(3) *Amphiphiles at Interfaces*; Texter, J., Ed.; Progress in Colloid & Polymer Science; Steinkopff: Darmstadt, 1997; Vol. 103.

(4) Galstyan, A.; Dobrindt, U. Breaching the Wall: Morphological Control of Efficacy of Phthalocyanine-Based Photoantimicrobials. *J. Mater. Chem. B* **2018**, *6* (28), 4630–4637.

(5) Alenezi, K.; Tovmasyan, A.; Batinic-Haberle, I.; Benov, L. T. Optimizing Zn Porphyrin-Based Photosensitizers for Efficient Antibacterial Photodynamic Therapy. *Photodiagnosis Photodyn. Ther.* **2017**, *17*, 154–159.

(6) Jori, G.; Camerin, M.; Soncin, M.; Guidolin, L.; Coppellotti, O. Chapter 1 Antimicrobial Photodynamic Therapy: Basic Principles. In *Photodynamic Inactivation of Microbial Pathogens: Medical and Environmental Applications*; The Royal Society of Chemistry, 2011; Vol. 11, pp 1–18.

(7) Alves, E.; Costa, L.; Carvalho, C. M. B.; Tomé, J. P. C.; Faustino, M. A.; Neves, M. G.; Tomé, A. C.; Cavaleiro, J. A. S.; Cunha, Â.; Almeida, A. Charge Effect on the Photoinactivation of Gram-Negative and Gram-Positive Bacteria by Cationic Meso-Substituted Porphyrins. *BMC Microbiol.* **2009**, *9* (1), 70.

(8) Lazzeri, D.; Rovera, M.; Pascual, L.; Durantini, E. N. Photodynamic Studies and Photoinactivation of Escherichia Coli Using Meso-Substituted Cationic Porphyrin Derivatives with Asymmetric Charge Distribution¶. *Photochem. Photobiol.* **2004**, *80* (2), 286–293.

(9) Spesia, M. B.; Lazzeri, D.; Pascual, L.; Rovera, M.; Durantini, E. N. Photoinactivation of Escherichia Coli Using Porphyrin Derivatives with Different Number of Cationic Charges. *FEMS Immunol. Med. Microbiol.* **2005**, *44* (3), 289–295.

(10) Caminos, D. A.; Spesia, M. B.; Durantini, E. N. Photodynamic Inactivation of Escherichia Coli by Novel Meso-Substituted Porphyrins by 4-(3-N,N,N-Trimethylammoniumpropoxy)Phenyl and 4-(Trifluoromethyl)Phenyl Groups. *Photochem. Photobiol. Sci.* **2006**, *5* (1), 56–65.

(11) Costa, L.; Alves, E.; Carvalho, C. M. B.; Tomé, J. P. C.; Faustino, M. A. F.; Neves, M. G. P. M. S.; Tomé, A. C.; Cavaleiro, J. A. S.; Cunha, Â.; Almeida, A. Sewage Bacteriophage Photoinactivation by Cationic Porphyrins: A Study of Charge Effect. *Photochem. Photobiol. Sci.* **2008**, *7* (4), 415–422.

(12) Simões, C.; Gomes, M. C.; Neves, M. G. P. M. S.; Cunha, Â.; Tomé, J. P. C.; Tomé, A. C.; Cavaleiro, J. A. S.; Almeida, A.; Faustino, M. A. F. Photodynamic Inactivation of Escherichia Coli with Cationic Meso-Tetraarylporphyrins – The Charge Number and Charge Distribution Effects. *Catal. Today* **2016**, *266*, 197–204.

(13) Hurst, A. N.; Scarbrough, B.; Saleh, R.; Hovey, J.; Ari, F.; Goyal, S.; Chi, R. J.; Troutman, J. M.; Vivero-Escoto, J. L. Influence of Cationic Meso-Substituted

Porphyrins on the Antimicrobial Photodynamic Efficacy and Cell Membrane Interaction in Escherichia Coli. *Int. J. Mol. Sci.* **2019**, *20* (1), 134.

(14) Kessel, D.; Luguya, R.; Vicente, M. G. H. Localization and Photodynamic Efficacy of Two Cationic Porphyrins Varying in Charge Distribution¶. *Photochem. Photobiol.* **2003**, *78* (5), 431–435.

(15) Li, H.; Jensen, T. J.; Fronczek, F. R.; Vicente, M. G. H. Syntheses and Properties of a Series of Cationic Water-Soluble Phthalocyanines. *J. Med. Chem.* **2008**, *51* (3), 502–511.

(16) van de Winckel, E.; David, B.; Simoni, M. M.; González-Delgado, J. A.; de la Escosura, A.; Cunha, Â.; Torres, T. Octacationic and Axially Di-Substituted Silicon (IV) Phthalocyanines for Photodynamic Inactivation of Bacteria. *Dye. Pigment.* **2017**, *145*, 239–245.

(17) Lourenço, L. M. O.; Sousa, A.; Gomes, M. C.; Faustino, M. A. F.; Almeida, A.; Silva, A. M. S.; Neves, M. G. P. M. S.; Cavaleiro, J. A. S.; Cunha, Â.; Tomé, J. P. C. Inverted Methoxypyridinium Phthalocyanines for PDI of Pathogenic Bacteria. *Photochem. Photobiol. Sci.* **2015**, *14* (10), 1853–1863.

(18) Ongarora, B. G.; Hu, X.; Li, H.; Fronczek, F. R.; Vicente, M. G. H. Syntheses and Properties of Trimethylaminophenoxy-Substituted Zn(Ii)-Phthalocyanines. *Medchemcomm* **2012**, *3* (2), 179–194.

(19) Li, X.; Yu, S.; Lee, Y.; Guo, T.; Kwon, N.; Lee, D.; Yeom, S. C.; Cho, Y.; Kim, G.; Huang, J. D.; et al. In Vivo Albumin Traps Photosensitizer Monomers from Self-Assembled Phthalocyanine Nanovesicles: A Facile and Switchable Theranostic Approach. *J. Am. Chem. Soc.* **2019**, *141* (3), 1366–1372.

(20) Li, X.; Lee, D.; Huang, J. D.; Yoon, J. Phthalocyanine-Assembled Nanodots as Photosensitizers for Highly Efficient Type I Photoreactions in Photodynamic Therapy. *Angew. Chemie - Int. Ed.* **2018**, *57* (31), 9885–9890.

(21) Engelmann, F. M.; Rocha, S. V. O.; Toma, H. E.; Araki, K.; Baptista, M. S. Determination of N-Octanol/Water Partition and Membrane Binding of Cationic Porphyrins. *Int. J. Pharm.* **2007**, *329* (1), 12–18.

(22) Alonso, L.; Sampaio, R. N.; Souza, T. F. M.; Silva, R. C.; Neto, N. M. B.; Ribeiro, A. O.; Alonso, A.; Gonçalves, P. J. Photodynamic Evaluation of Tetracarboxy-Phthalocyanines in Model Systems. *J. Photochem. Photobiol. B Biol.* **2016**, *161*, 100–107.

(23) Lei, W.; Xie, J.; Hou, Y.; Jiang, G.; Zhang, H.; Wang, P.; Wang, X.; Zhang, B. Mitochondria-Targeting Properties and Photodynamic Activities of Porphyrin Derivatives Bearing Cationic Pendant. *J. Photochem. Photobiol. B Biol.* **2010**, *98* (2), 167–171.

(24) Ragàs, X.; He, X.; Agut, M.; Roxo-Rosa, M.; Gonsalves, R. A.; Serra, C. A.; Nonell, S. Singlet Oxygen in Antimicrobial Photodynamic Therapy: Photosensitizer-Dependent Production and Decay in E. Coli. *Molecules*. 2013, pp 2712–2725.

(25) Ragàs, X.; Agut, M.; Nonell, S. Singlet Oxygen in Escherichia Coli: New Insights for Antimicrobial Photodynamic Therapy. *Free Radic. Biol. Med.* **2010**, *49* (5), 770–776.

(26) Anaya-Plaza, E.; van de Winckel, E.; Mikkilä, J.; Malho, J.-M.; Ikkala, O.; Gulías, O.; Bresolí-Obach, R.; Agut, M.; Nonell, S.; Torres, T.; et al. Photoantimicrobial Biohybrids by Supramolecular Immobilization of Cationic Phthalocyanines onto Cellulose Nanocrystals. *Chem. – A Eur. J.* **2017**, *23* (18), 4320–4326.

(27) Terekhov, D. S.; Nolan, K. J. M.; McArthur, C. R.; Leznoff, C. C. Synthesis of

2,3,9,10,16,17,23,24-Octaalkynylphthalocyanines and the Effects of Concentration and Temperature on Their 1H NMR Spectra. *J. Org. Chem.* **1996**, *61* (9), 3034–3040.

Chapter 7 – Amphiphilic PEG-functionalized binaphthyl-bridged chiral phthalocyanines: Synthesis and aggregation studies

7.1. Citation and contribution

Miguel Á. Revuelta-Maza, Nicolás M. Casellas, Miguel García-Iglesias, Gema de la Torre and Tomás Torres. Manuscript in preparation.

Contribution: Revuelta-Maza, M.A.: Synthesis, characterization, and agreggation studies. Casellas, N. M.: synthesis of compound **L-PEG**.

Funding and supervision: García-Iglesias, M.; de la Torre, G.; Torres, T.

Abstract:

We describe the preparation of amphiphilic chiral, binaphthyloxy-bridged Zn(II) phthalocyanines with an AABB substitution pattern, containing hydrophilic tetraethylene glycol chains. Self-assembly studies in aqueous solution have been performed by UV-vis, fluorescence and circular dichroism experiments in order to elucidate the aggregation processes. The data collected together with images of transmission electron microscopy confirms the formation of aggregates with micellar typology.

7.2. Introduction and Objectives

Amphiphiles self-assembly has attracted researches attention for decades due to their extensive applications in material science and drug delivery. This unique properties have been widely used to mimic biological systems, while their integrated actions allow the performance of highly specific cellular functions, as cellular recognition, creating an extensive field of study in bionanotechnology. The combination of amphiphile natural organization with the advanced concept of supramolecular self-assembly, leads to the development of more complex, hierarchical nanostructures into a wide variety of structures including micelles, vesicles, nanotubes, nanofibers, and lamellae.[1–3] The control of the growth and shape of these supramolecular nanostructures in water, constitutes one of the main challenges within this research area,[4] together with the full understanding of the mechanism this molecules face the process. Tradicionally, temperature- and concentration-dependent UV/Vis and fluorescence spectroscopic studies in water are conducted to explore the self-assembly process of the dyes, as well as circular dichroism in the case of chiral centers containing dyes.[5–7]

Within the extended dye family, as natural Por derivatives possess many interesting functions in biological systems, self-assembly has become one of the popular methods to construct porphyrin/protein-mimicking materials with bioactive functions,[8] and numerous examples of self-organized Por in water are known.[9–11] However, much less works have been published about Pcs self-assembly in water.[12–14] In **Chapter 5** the synthesis of a new family of binaphthyl-containing AABB Pcs was intended for their use as platforms for the preparation of differently functionalized C_{2v} systems, over which induce amphiphilic character and self-assembly abilities, that can give rise to outstanding chiral nanostructures. Herein, we plan to use this methodology to synthesize AABB Zn(II)Pc using phthalonitriles with already contain the hydrophilic substituents, or take advantage of **Chapter 5** compounds to incorporate a new substitution pattern that turns them into amphiphilic molecules. Specifically, the main goal is to obtain AABB Zn(II)Pc amphiphiles incorporating polyethylene glycol chains programmed to self-assemble in aqueous media and, therefore, aggregation studies and evaluation of their photosensitizing abilities will be carried out. While the Zn(II)Pc hydrophobic block can be tailored to interact with lipophilic components of cell membranes, as well as to encapsulate other drugs, the hydrophilic block formed by poly(ethylene glycol) chains, assures the requested biocompatibility and the desired "stealth" characteristic that minimize unwanted interactions with cellular components.[1] Thus, as we have explained in the **PDT-Introduction Section**, PEG chains lead to a prolonged blood circulating lifetime, allows for the minimization of non-specific uptake and favors the enhanced permeability and retention (EPR) effect, which result in an elevated concentration of the drug at the tumor site.[15,16] Finally, as topology of hydrophobic moieties can affect the stability of self-assembled micelles,[17] one of the main objectives of the current **Chapter 7** is to determine the influence of the BINOL motive in the generated nanostructures.

The synthesis of PEG-containing AABB Zn(II)Pcs **PEG-1** and **PEG-2** was accomplished following two different approaches, namely, the straightforward condensation of phthalonitrile **A-1-C3** prepared in **Chapter 3 (C3)** with the binaphthyloxy-bridged bisphthalonitrile **(R)-7a-C5** from **Chapter 5 (C5)** (Scheme 7. 1a), and the functionalization of the dibromo-AABB Zn(II)Pc synthon **4-C5** with the triply PEGylated derivative of 5-ethynylbenzene-1,2,3-triol (**L-PEG**) (Scheme 7. 1b). Both the convergent and the divergent routes could yield amphiphilic Zn(II)Pcs comprising hydrophobic aromatic cores and hydrophilic PEGylated substituents, either at the isoindol untis in the former case, or at the binaphthyloxy unit in the latter.

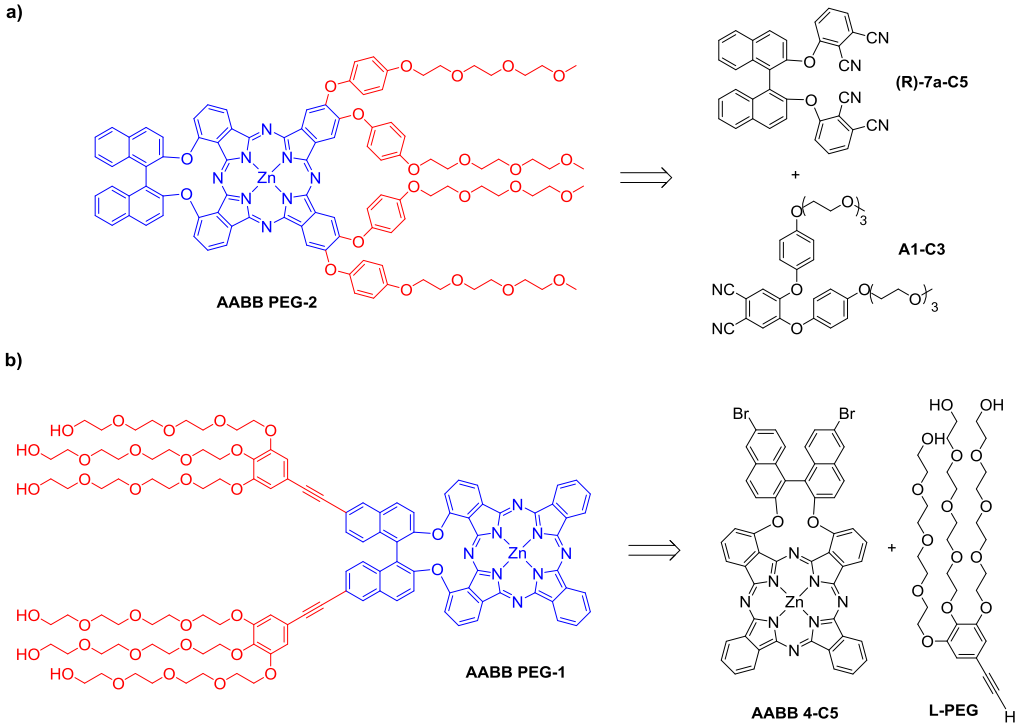

*Scheme 7. 1. Retrosynthesis scheme of AABB **PEG-1** and **2**.*

7.3. Results and discussion

a) Synthesis

The synthesis of compound AABB **PEG-2** was tried via direct cross-condensation between the corresponding phthalonitriles **A-1-C3** and **(R)-7a-C5** in *o*-DCB:DMF (2:1) with $Zn(OAc)_2$ at 160 °C overnight. Sadly, no blue products of phthalonitrile cyclotramerization were formed and no AABB Zn(II)Pc were detected. On the other hand,

the synthesis of Zn(II)Pc **PEG-1** was carried out through Pd-catalized Sonogashira cross-coupling between AABB Zn(II)Pc synthon **4-C5** with the triply PEGylated derivative of 5-ethynylbenzene-1,2,3-triol (**L-PEG**), (Scheme 7. 2 and Figure 7. 1).

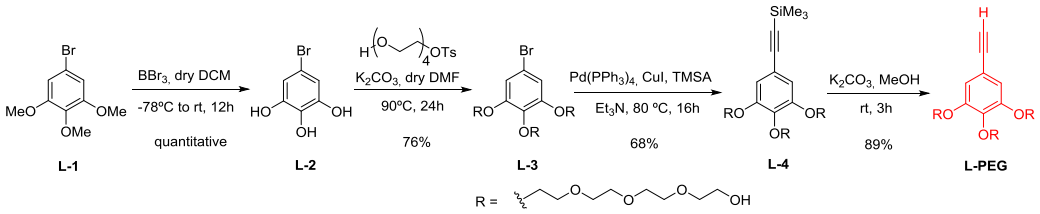

*Scheme 7. 2. Synthesis of **L-PEG** from comertially available **L-1**.*

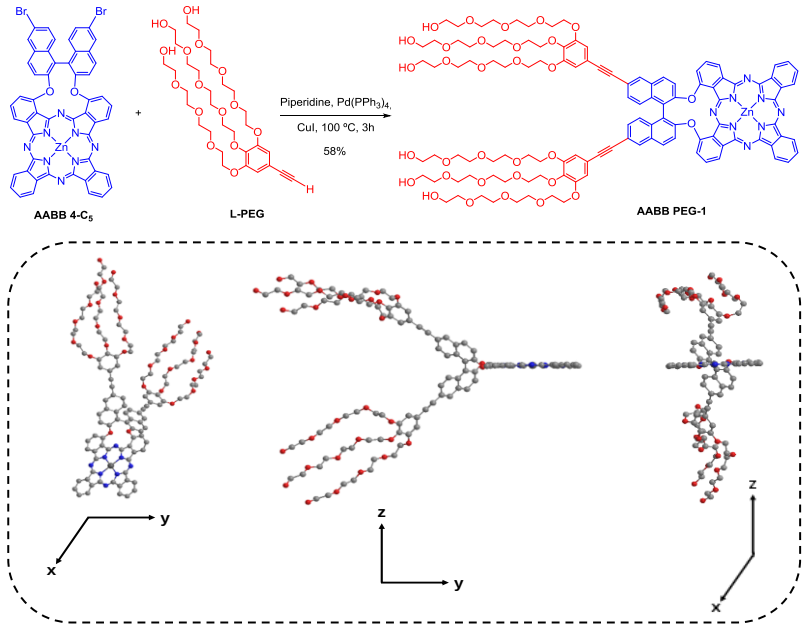

*Figure 7. 1. Synthesis of AABB Zn(II)Pc **PEG-2**. Hydrophilic region is highlighted in red, while hydrophobic region is highlighted in blue. And structural model (three views) realized with the SCIGRESS (FJ 2.8.1 EU 3.3.1) software, and a geometry optimization through MM2.*

One of the advantages of this route is that the PEG chains are attached at the Pc once the AABB compound is synthesized and isolated, facilitating the purification of the target compound, since the presence of PEG chains usually make difficult the separation by column chromathography.

L-PEG was prepared trought in a four step process as depicted in Scheme 7. 2 starting from commercially available 1-Bromo-3,4,5-trimethoxybenzene (**L-1**). Ome groups were removed with BBr_3 and bromine was substituted by TMSA *via* palladium catalized

Sonogashira cross-coupling. Triple bond deprotection in basic conditions gave L-PEG in 89% yield (46% overal yield). Reaction between (R- or S-)**AABB-4-C5** and **L-PEG** was performed with $Pd(PPh_4)_3$ and CuI, by heating up to 50-60 °C in different solvent ratio. First, we tried in a mixture of dry THF:Et_3N (3:1), however, low solubility of **L-PEG** in THF hindered the process. In a simililar way THF:Et_3N (1:1) did not result in the expected product. Finally the reaction was tried in freeshly destiled piperidine, and by heating at 100 °C it was completed after 3h with 58% yield. Figure 7. 2 shows AABB Zn(II)Pc **PEG-1** ^{1}H-NMR and COSY in DMSO heating at 323K to avoid aggregation and maximized resolution. COSY shows correlation between PEG chains but only a weak response was obtained for the aromatic region.

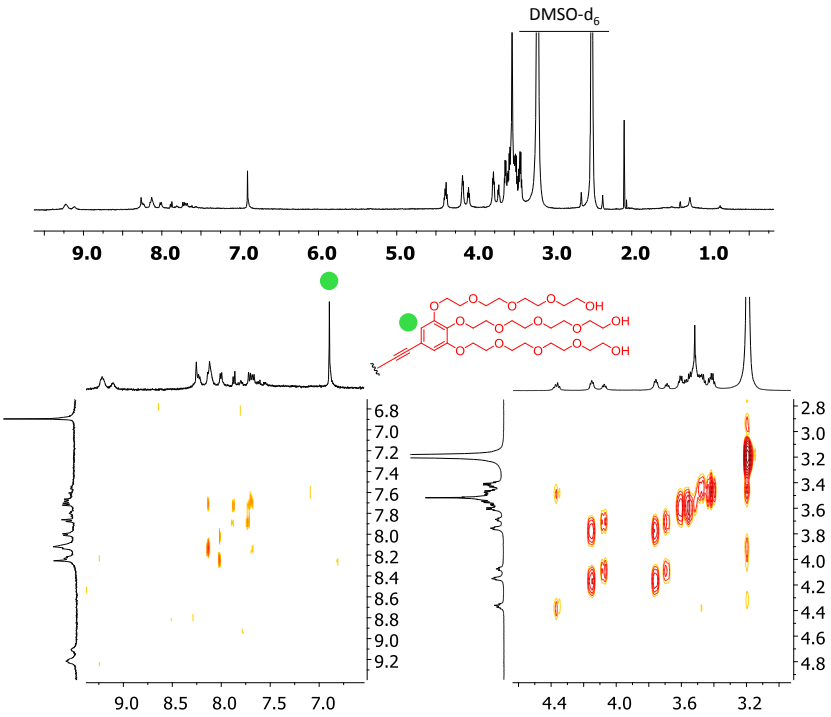

*Figure 7. 2. ^{1}H-NMR and COSY for AABB Zn(II)Pc **PEG-1** in DMSO at 323K. Green spot shows the more characteristic aromatic proton signal dor this compound.*

b) Aggregation studies

First, ground-state absorption experiments were performed for AABB Zn(II)Pc **PEG-1** in polar coordinating solvents, that is DMF and DMSO, showing in both solvents the typical *Q*-band and *B*-band transitions for non-aggregated species.[18] Also, when the UV-vis experiments were performed in chloroform, typical features of molecularly dissolved species were observed. To confirm the lack of aggregation in the three solvents,

absorption spectra were registered in a range of concentrations (approximately between 0.5-5.0·x 10^{-6}) (Figure 7. 3). For the verification of the Lambert-Beer law, an analysis of linear regression between the intensity of the *Q*-band and the concentration was performed, with R^2 values of ~0.999.

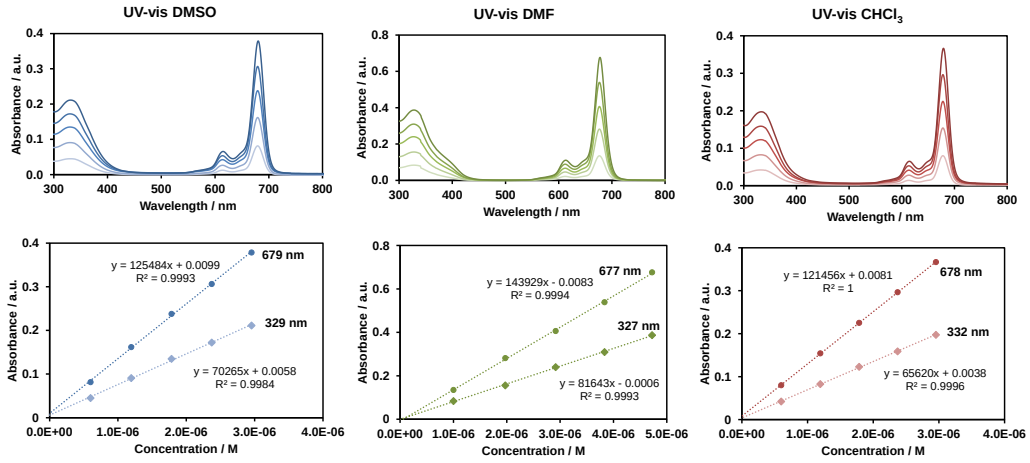

*Figure 7. 3. UV-vis spectra of AABB **PEG-1** in three different solvents.*

In spite of the large hydrophilic tail of Zn(II)Pc **PEG-1**, it proved insoluble in pure water. However, it remained soluble in this medium upon addition from stock solutions of **PEG-1** in DMSO and DMF, even at a 1:99 DMSO(DMF)/water ratio. For that reason, we studied the aggregation behaviour of **PEG-1** in water media following the spectrocopic features of the compound through the addition of water over DMSO and DMF solutions. Importantly, through all successive additions of mili-Q water, the concentration of the resulting solution remained constant.

Thus, starting from a 5·10^{-5} M solution of **PEG-1** in DMSO, a decreasing of the Q-band was observed together with the rising of a new band at lower wavelength, compatible with the formation of *H*-aggregates, when going from 100% to 60% DMSO From this ratio onwards, the spectra did not suffer major changes, but small overall decrease in intensity and broadening of the absorption (see Figure 7. 4a). Similar experiments were recorded with a more concentrated solution, that is 1·10^{-4} M, with similar results (see Figure 7. 4b).

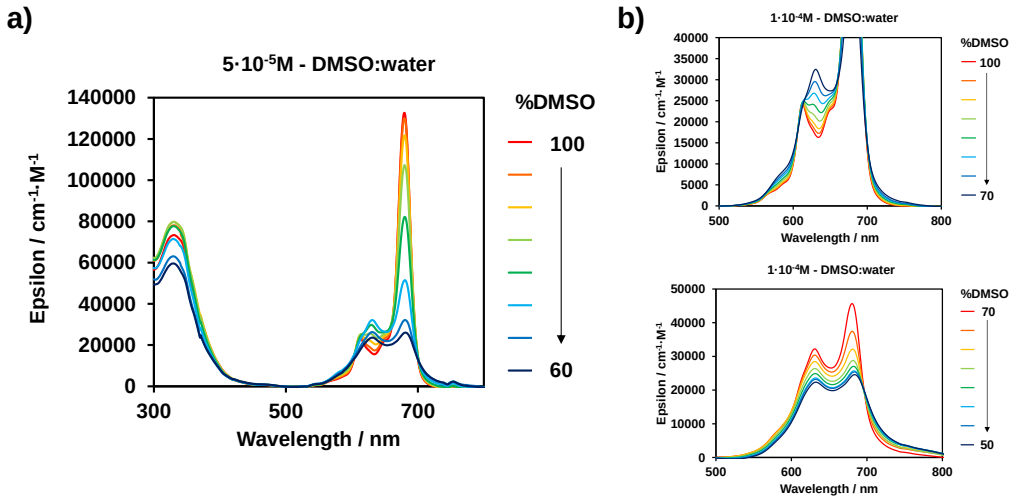

*Figure 7. 4. AABB Zn(II)Pc **PEG-1** absorption in DMSO:water mili-Q mixtures at a) 1·10^{-5} M, b) 1·10^{-4} M.*

We perfomed a temperature dependent experiment with a 5·10^{-5} M solution of **PEG-1** at 70:30 DMSO/water ratio in order to estimate the stabily of the aggregate. First we heated the solution to 318 K and then it was slowly cooled to 298 K (a), heated again until 338 K and cooled to 298 K (b), and finally heated to 348 K and cooled to 298 K (c). As we can observe in Figure 7. 5, the heating cycles produced a certain degree of deaggregation but, after cooling down to room temperature, the aggregation status was recovered in all cases.

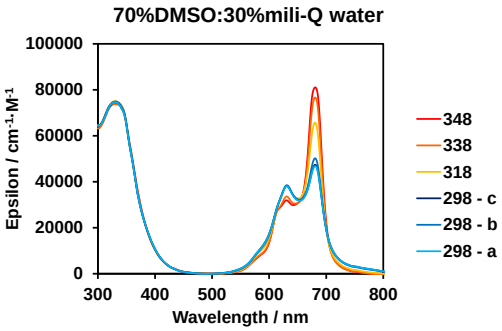

*Figure 7. 5. Temperature dependent UV-vis experiment over AABB Zn(II)Pc **PEG-1**.*

On the other hand, similar experiments were performed with DMF. In this case, the new blue-shifted band did not appear progressively, but suddenly at a 40% water content. From this ratio onwards, the latter maximum remains constant while the intensity of the

monomer band decreases until a stable situation is reached at *ca*. 60% water. Similar results were observed starting from a more diluted DMF solution, i.e. $5 \cdot 10^{-6}$ M, although the water ratio necessary to trigger the changes in the spectrum was slightly larger (Figure 7. 7, left).

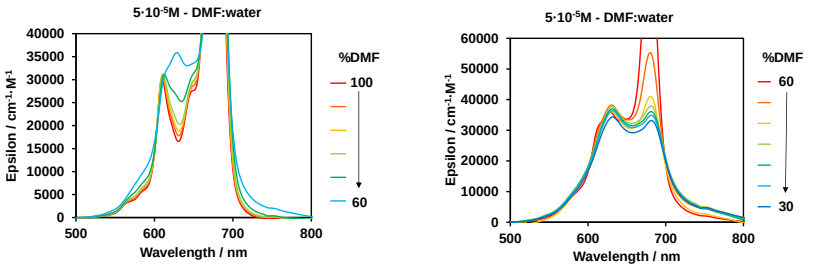

*Figure 7. 6. AABB Zn(II)Pc **PEG-1** absorption in DMF:water mili-Q mixtures.*

Temperature experiments were also performed over $5 \cdot 10^{-6}$ M solutions of **1.** again the influence of the temperature in a diluted situation where the aggregation can be, in principle, more easily disrupted. Spectra were registered spectra in different DMF:water ratios with 10% variations at 25 °C and 65 °C (Figure 7. 7). Importantly, experiments could not be performed at higher temperatures because precipitation of the compound takes place at the lower critical solution temperature (LCST) around 70 °C induced by the PEG chains. This commonly would produce a PEG phase separation from water, but the Pc core presence results in the precipitation of the system.[19] The analysis of the spectra indicates that between 100% and 60% DMF, the influence of the temperature is very low. From 60% to 40%, differences can be found in the relative intensity of the monomeric *Q*-band. Eventually, from 40% to 1% DMF the aggregate seems to be stable regardless the temperature applied.

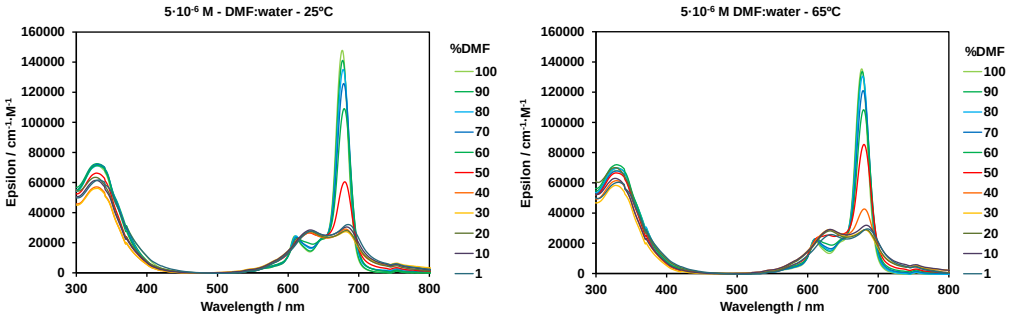

*Figure 7. 7. UV-vis changes in DMF:water for AABB Zn(II)Pc **PEG-1** at 25 and 65 °C.*

Next, we moved to CD spectroscopy as a tool to study the aggregation and its influence on the chirality of the nanostructures formed in solution. CD spectra in DMSO 100% and water (1% DMSO) of AABB Zn(II)Pc **PEG-1** were first recorded for both R and S enantiomers at $3 \cdot 10^{-5}$ M concentration. Both *Q*-band and *B*-band absorptions have their corresponding signal in the CD spectra, which intensity increases notably with the formation of the aggregate. As expected, the spectra of the enantiomers are mirror images. The following experiments were performed only with the R enantiomer.

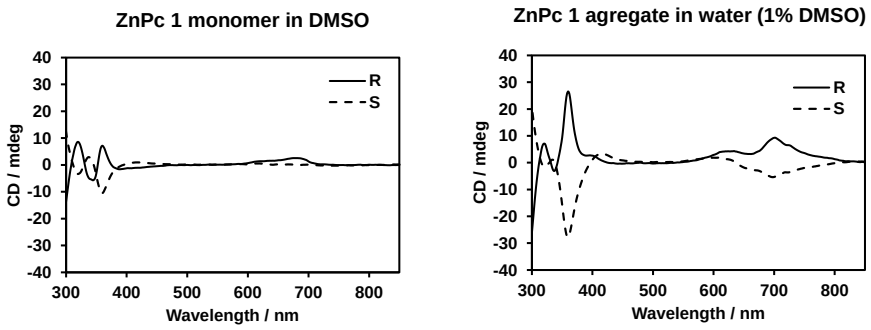

*Figure 7. 8. CD in DMSO and water (1% DMSO) of AABB Zn(II)Pc **PEG-1** for both enantiomers R and S.*

In Figure 7. 9a, the spectra of the monomer in DMSO and DMF and the respective aggregates in water/DMSO(DMF) 99:1 are superimposed. Apparently, the changes in the CD spectrum for the aggregate are more pronounced in DMF than in DMSO. When we performed temperature-dependent CD spectra over both 99% water solutions, we observed that, as previously inferred from absorption experiments, once the aggregate is formed, it does not break upon increasing the temperature (Figure 7. 9b).

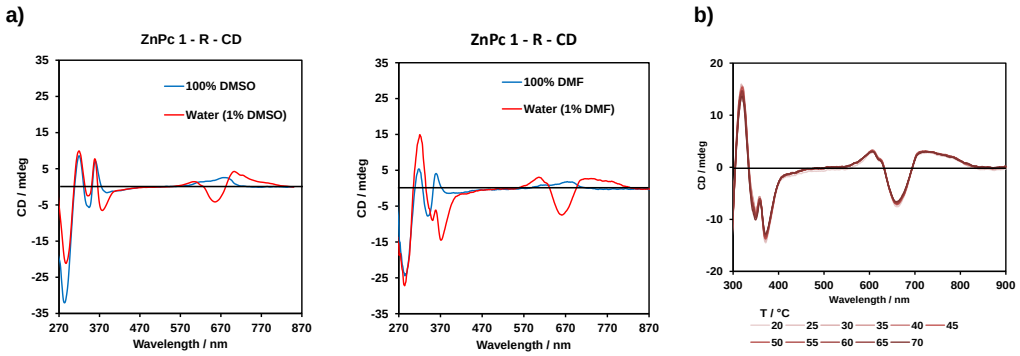

*Figure 7. 9. a) CD of Zn(II)Pc **PEG-1** in DMSO and DMF for the monomer and its aggregate in water (1% organic solvent). b) CD variation with temperature in water (1% DMF) at $3 \cdot 10^{-5}$ M.*

Next, in order to find out the main self-assembly pathway, we performed careful UV-vis, fluorescence and CD assays. We selected DMF as starting solvent since previous experiments seemed to indicate that the aggregation process was easier to control. $3 \cdot 10^{-5}$ M concentration was selected to observe the spectral changes upon slow addition of water over DMF solutions. The UV-vis titration experiments showed two isosbestic points at 603 and 698 nm (Figure 7. 10), which is concordant with the presence of two species in equilibrium (i.e. monomeric form of Zn(II)Pc **PEG-1** and its corresponding aggregate). As in former UV-vis experiments we observed that the aggregation process was stabilized from *ca.* 50% to 1% DMF.

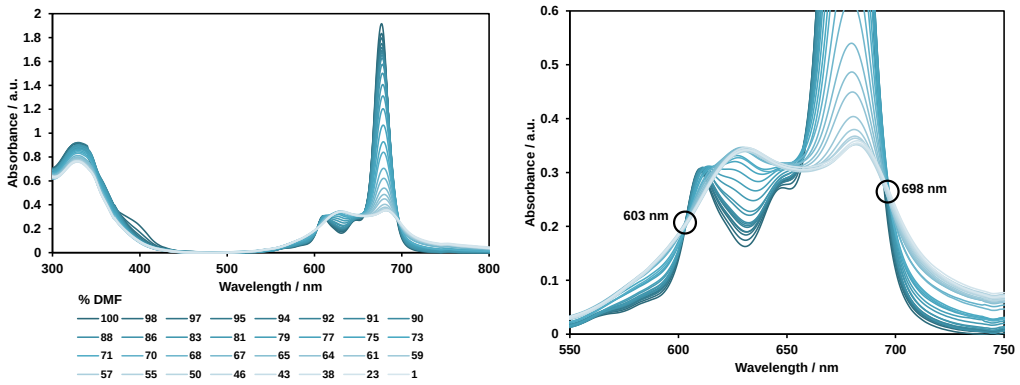

*Figure 7. 10. UV-vis changes for **PEG-1** from 100% DMF to 1%DMF (in water) at $1 \cdot 10^{-4}$ M.*

In CD, signals corresponding to monomeric species are observed until *ca*. 60% DMF, and, at that point changes start to be remarkable. In fluorescence, from 100% to 60% DMF an increase in the intensity is registered, probably due to the solvation of the PEG chains by water molecules, and then the quenching starts until the complete cancellation of the signal. For each experiment variation of the intensity of the maximum of the corresponding band was registered and represented versus % DMF: (A) UV-vis at 680 nm, (B) CD at 660 nm (C) fluorescence at 704 nm. For the UV-vis experiments, an isodesmic profile is observed, as otherwise expected for π-π conjugated systems. In CD titrations the changes due to self-assembly are less notorious since the signal of the monomer is intense and persists. Finally, fluorescence is affected, as mentioned above by other factors that mask the self-assembly. Therefore, we selected the UV-vis experiments to fit the values to a polymerization mechanism and extract the thermodynamic parameters. To meet this goal, we reproduced the UV-vis study using different concentrations, as showed in Figure 7. 12.

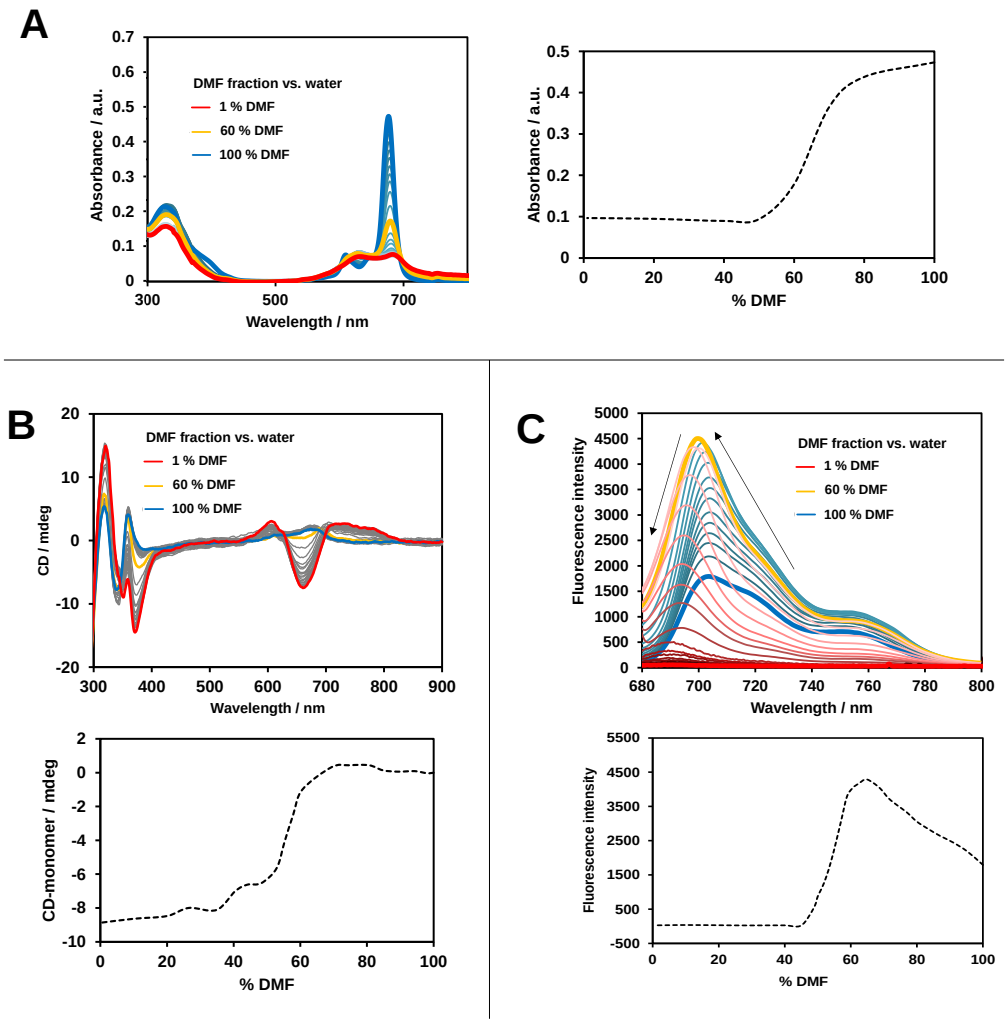

Figure 7. 11. Spectra variation from DMF 100% (blue) to mili-Q water (1% DMF) (red), with 60% DMF-40%water highlighted in yelow for (A) UV-vis (B) CD and (C) fluorescence. For each experiment variation of the signal was registered and represented versus %DMF for a especific wavelength: (A) UV-vis at 680 nm, (B) CD at 660 nm (C) fluorescence at 704 nm.

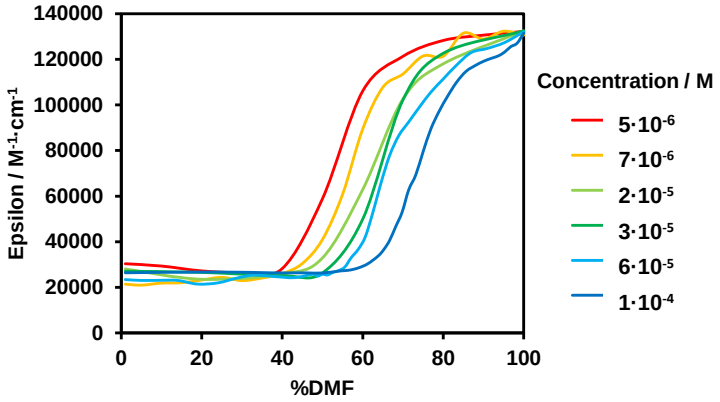

Figure 7. 12. UV-vis variation at 680 nm versus %DMF at different concentrations.

Transmission Electron Microscopy revealed the morphology of the aggregates. First we prepared $1 \cdot 10^{-4}$ M solutions of Zn(II)Pc 1 in miliQ water from a stock solution in DMF. The copper grids were in contact with the solution and the aggregates seeded by dropcastting. With freshly prepared solutions a homogenous distribution of spherical micellar-type aggregates was observed, with an average size of 30 nm as shown in Figure 7. 13.

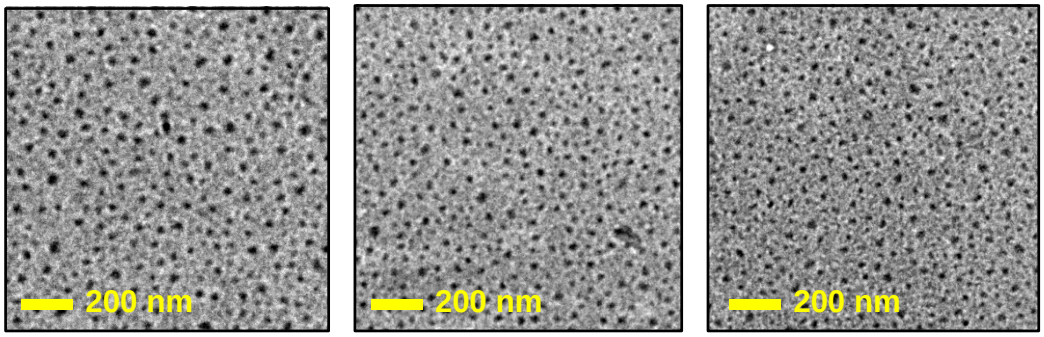

*Figure 7. 13. TEM images of Zn(II)Pc **PEG-1** from miliQ water solutions (1% DMF) at $1 \cdot 10^{-4}$ M.*

When the solution was incubated overnight and seeded in the grill after 24 hours at room temperature we observed an uncontrolled growing of the nanoparticles with the corresponding increasing of the size. This process was homogeneous in some regions as showed in Figure 7. 14 with size distributions around 80 nm.

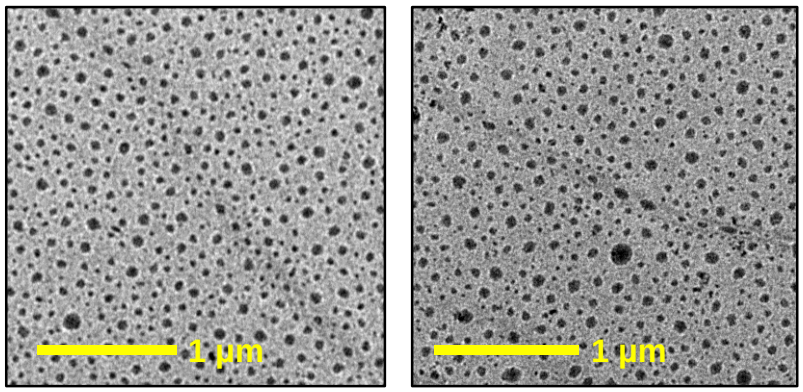

*Figure 7. 14. TEM images of Zn(II)Pc **PEG-1** from miliQ water solutions (1% DMF) at $1 \cdot 10^{-4}$ M incubated 24 hours.*

However, an exhaustive analysis of the grills in this last situation revealed regions with inhomogeneous size distribution with a mixture of different sizes until 900 nm.

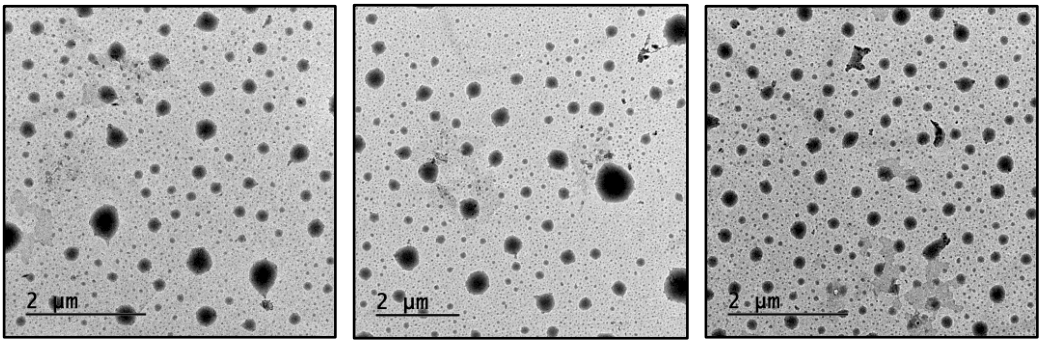

*Figure 7. 15. TEM images of Zn(II)Pc **PEG-1** from miliQ water solutions (1% DMF) at $1 \cdot 10^{-4}$ M incubated 24 hours that show an inhomogeneus size distriution.*

A closer look to this giant micelles shows that they are composed by the combination of lower size nanoparticles.

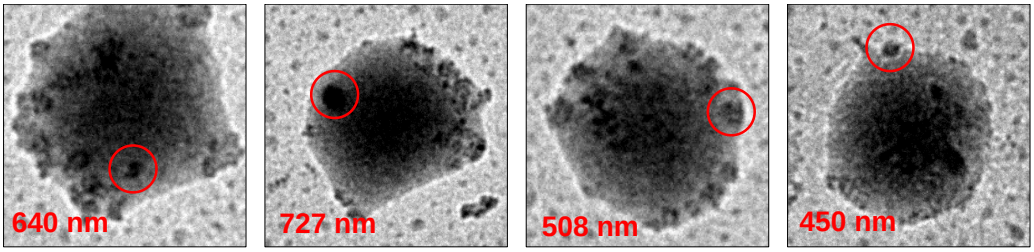

Figure 7. 16. Nanoparticles composed by combined aggregates.

These observations would be compatible with the mechanism recently proposed by Kenneth D. Singer et al. (see Figure 7. 17) by which afer an isodesmic formation of micelles, they can polymerize growing in larger nanosystems.[10]

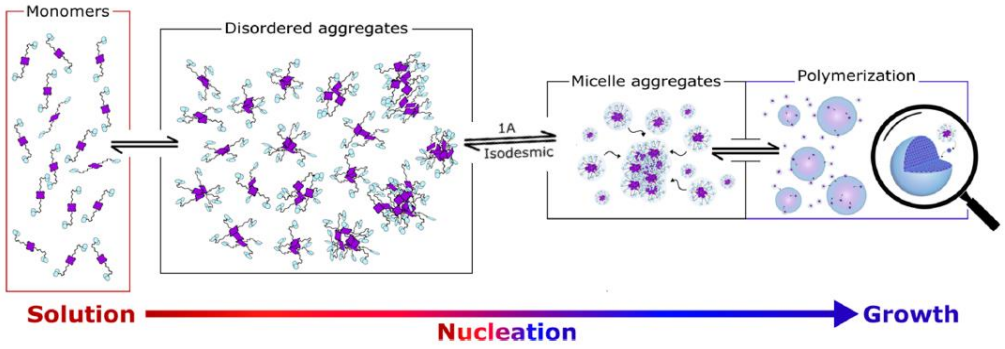

Figure 7. 17. Cartoon of a possible self-assembly pathway that occurs from the molecularly dissolved to the fully assembled state.[10]

With the aim of obtaining a more controlled distribution of sizes after an overnight incubation, we repeated the experiments using $1 \cdot 10^{-5}$ M and $1 \cdot 10^{-6}$ M solutions. In the latter case, the images did not show any nanostructure over the grills. For $1 \cdot 10^{-5}$ M solutions the size distribution was the same than for $1 \cdot 10^{-4}$ M. The only difference was the population, as the number of nanoparticles was lower (Figure 7. 18). In this way we can propose that the concentration does not determine the final size but the nucleation kinetics.

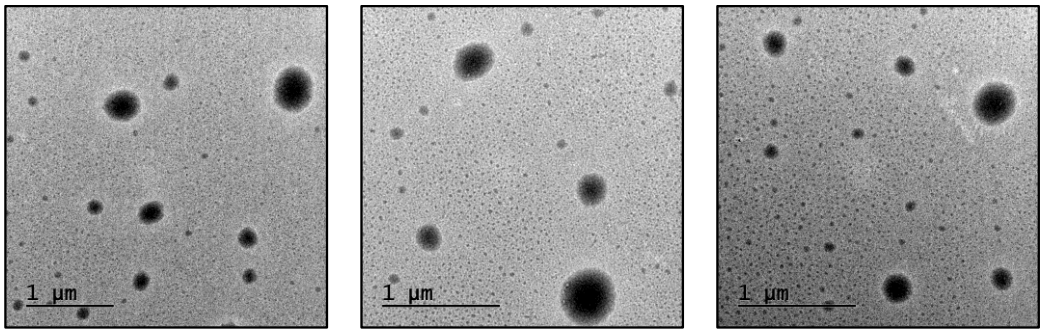

*Figure 7. 18. TEM images of Zn(II)Pc **PEG-1** from miliQ water solutions (1% DMF) at $1 \cdot 10^{-5}$ M incubated 24 hours that show an inhomogeneus size distriution.*

Finally, DLS experiments were performed in order to confirm this size distribution in solution for $1 \cdot 10^{-4}$ M (see Figure 7. 19) confirming the large size distribution with maxima at 94 nm and 660 nm.

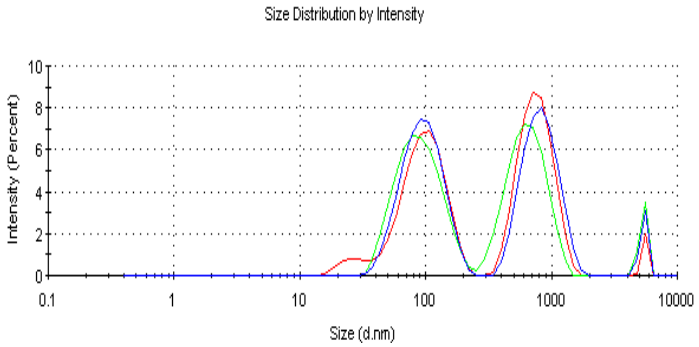

*Figure 7. 19. DLS of Zn(II)Pc **PEG-1** in miliQ water (1% DMF). Concentration*

7.4. Conclusions

AABB Zn(II)Pc **4-C5** is a useful synthon for the construction of an amphiphilic system after replacing the bromine atoms by a hydrophilic fragment (**L-PEG**). Zn(II)Pc **PEG-1** as a high oriented amphiphile, is able to self-assemble in water from stock solutions in organic solvents in supramolecular micelles. This process can be followed via UV-vis, fluorescence and CD spectroscopies. Self-assembled nanostructures shows a wide size distribution but population seems to be homogeneous for freshly prepared solutions. Micelles were observed by TEM microscopy. Facing the final PDT application, the formation of supramolecular micelles can be of interest to facilitate the transport of the PS in aqueous biological media in order to reach the therapeutic target. Further biological assays with this molecules are envisioned.

7.5. Experimental section

1-Bromo-3,4,5-trihydroxybenzene (**L-2**),[20] and tetraethylene glycol *p*-toluenesulfonate[21] were prepared following previously reported procedures. **A-1-C3**, **(R)-7a-C5** and **4-C5** are described in Chapters 3 and 5.

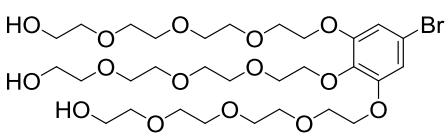

Synthesis of L-3: 1-Bromo-3,4,5-trihydroxybenzene (1, 0.15 g, 0.73 mmol), tetraethylene glycol *p*-toluenesulfonate (1.22 g, 3.50 mmol), and powder K_2CO_3 (0.60 g, 4.35 mmol) were mixed together in dry DMF (8 mL). The mixture was heated at 90 °C under argon atmosphere for 24 hours. After cooling the mixture was poured into water and extracted with DCM, washed with brine and dried over anhydrous $NaSO_4$. Solvent was removed under vacuum and the residue was purified by column chromatography on silica gel using a $CHCl_3$:MeOH (95:5 v/v) affording **L-3** (0.41 g, 0.56 mmol) as a brownish oil

in 76% yield. ^{1}H-NMR (300 MHz, $CDCl_3$): δ 6.72 (s, 2H, Ar) 4.12 (m, 6H, CH_2-OAr), 3.84-3.56 (m, 42H, ethylene glycol chains). ^{13}C-NMR (101 MHz, $CDCl_3$): δ 153.4, 137.9, 115.8, 111.5, 77.2, 72.7, 72.7, 70.9, 70.8, 70.8, 70.7, 70.6, 70.6, 70.5, 70.4, 69.7, 69.2, 61.8. FT-IR (ATR) v (cm^{-1}): 3399 (O-H st), 2868, 1743, 1640, 1585, 1491, 1451, 1420, 1349, 1240, 1095, 940, 834. HR-MS (ESI+; MeOH+NaI): *m/z* calculated for $C_{30}H_{53}O_{15}Br$: 757.2446 (100) $[M+Na]^+$; found 757.2448 (100) $[M+Na]^+$, 752.2868 (17) $[M+NH_4]^+$, 771.2107 (5) $[M+K]^+$.

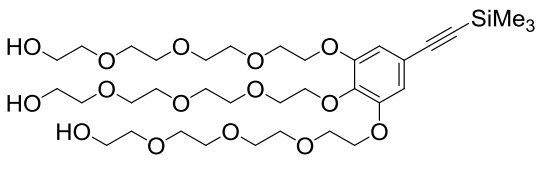

Synthesis of L-4: Compound **L-3** (0.25 g, 0.34 mmol), $Pd(PPh_3)_4$ (12.0 mg, 0.01 mmol), CuI (4.0 mg, 0.02 mmol) were mixed together in dry Et_3N (4 mL) and degassed by three freeze-pump-thaw cycles. Trimethylsilylacetylene (TMSA) (0.50 g, 5.10 mmol) was added and the mixture was heated at 80 °C under argon atmosphere for 16 hours. The solvent was removed under vacuum and the residue was purified by column chromatography on silica gel using a mixture of $CHCl_3$:MeOH (90:10 v/v) yielding **L-4** (0.17 g, 0.23 mmol) in 68% yield. ^{1}H-NMR (300 MHz, $CDCl_3$): δ 6.70 (s, 2H, Ar) 4.16 (m, 6H, CH_2-OAr), 3.87-3.57 (m, 42H, ethylene glycol chains) 2.20 (br, 3H, OH), 0.23 (s, 9H, TMSA) ^{13}C-NMR (101 MHz, $CDCl_3$): δ 152.3, 139.4, 118.0, 105.0, 93.2 (C≡C), 77.2, 73.0, 72.7, 72.7, 72.6, 72.6, 70.8, 70.8, 70.7, 70.7, 70.7, 70.6, 70.5, 70.4, 70.1, 69.7, 69.7, 68.9, 61.6, 0.0. FT-IR (ATR) v (cm^{-1}): 3429 (O-H st), 2870, 1743, 1571, 1496, 1453, 1420, 1329, 1243, 1104, 943, 886, 839. HR-MS (ESI^+; MeOH+NaI): *m/z* calculated for $C_{35}H_{62}O_{15}Si$: 773.3720 (100) $[M+Na]^+$; found 773.3750 $[M+Na]^+$.

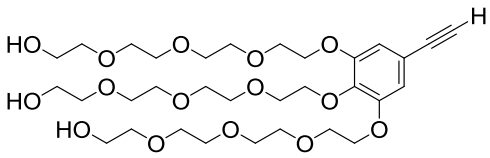

Synthesis of L-PEG: Compound **L-4** (0.17 g, 0.23 mmol) was dissolved in MeOH (3 mL) and K_2CO_3 was added (0.09 g, 0.65 mmol). The mixture was stirred at room temperature for 3 hours and filtrated trough celite. The solvent was removed under vacuum and the residue was purified by column chromatography in silica gel using $CHCl_3$:MeOH (90:10 v/v) as eluent yielding **L-PEG** (0.14 g, 0.21 mmol) as a brown oil in 89% yield. ^{1}H-NMR (300 MHz, $CDCl_3$): δ 6.66 (s, 2H, Ar) 4.09 (m, 6H, CH_2-OAr), 3.87-3.59 (m, 42H, ethylene glycol chains), 3.00 (s, 1H, C≡CH). ^{13}C-NMR (101 MHz, $CDCl_3$): δ 152.1, 138.3, 117.4, 111.0, 83.2 (C≡C), 77.2, 72.8, 72.5, 72.4, 72.3, 70.4, 70.3, 70.2, 70.0, 70.0, 69.9, 69.9, 69.5, 69.1, 68.2, 61.3, 61.1, 60.9. FT-IR (ATR) v (cm^{-1}): 3396 (O-H st), 3224 (≡C-H st) 2919, 2871, 2094 (C≡C st) 1695, 1574, 1496, 1101, 941, 885, 838. HR-MS (ESI^+; MeOH+NaI): *m/z* calculated for $C_{35}H_{54}O_{15}$: 717.3094 (100) $[M+K]^+$, 701.3355 (49) $[M+Na]^+$; found 717.3100 (100) $[M+K]^+$, 701.3370 (49) $[M+Na]^+$.

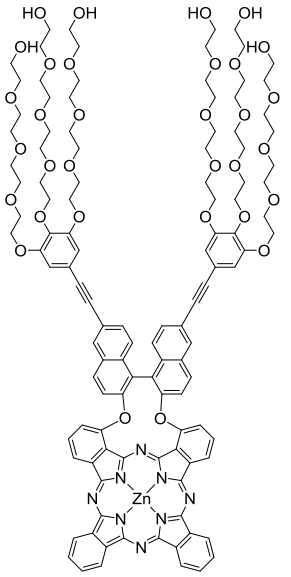

Synthesis of AABB Zn(II)Pc PEG-1: AABB Zn(II)Pc **4-C5** (10 mg, 0.0099 mmol), **L-PEG** (15 mg, 0.022 mmol), $Pd(PPh_3)_4$ (5% mol) and CuI (10% mol), were dissolved in dry piperidine (3 mL) and stirred 3 hours at 100 °C under argon atmosphere. The disappearance of the product was monitored by TLC in heptane:THF (3:4), and mono and disubstituted products were distinguished in $CHCl_3$:MeOH (5:1). After evaporation of the solvent, the product was purified by column chromatography in Bio-Beads using THF as eluent, and then by column chromatography on Sephadex in MeOH. After evaporation the blue solid was washed with acetonitrile. Yield: 13 mg (58%). ^{1}H-NMR (500 MHz, 323 K, DMSO-d_8): δ 3.37-3.45, 3.45-3.63, 3.66-3.71, 3.73-3.79, 4.05-4.10, 4.12-4.18 and 4.34-4.40 (m, 102H, PEG chains); 6.90 (s, 4H, HAr-L-PEG); 6.68 (d, *J* = 8.90 Hz, HAr); 7.71 (d, *J* = 9.40 Hz, HAr); 7.87 (d, *J* = 8.90 Hz, HAr); 8.00 (d, *J* = 7.51 Hz, HAr); 8.07-8.16 (m, 6H, HAr); 8.19-8.24 (m, 2H, HAr); 8.25 (s, 2H, HAr); 9.06-9.15 (m, 2H, HAr); 9.15-9.26 (m, 4H, HAr) . ^{13}C-NMR The aggregation tendency prevented obtaining a good resolved spectrum IR (ATR) v^{-1} (cm^{-1}): 3359 (O-H st), 2921, 2870, 2360, 1466, 1333, 1258, 1011. HR-MS (MALDI (ULTRAFLEX III) DCTB + PEGMeNa 2000) for $C_{116}H_{130}N_8NaO_{32}Zn$: *m/z* 2233.7975 $[M+Na]^+$ (calculated: 2233.7975).

7.6. References

(1) Lombardo, D.; Kiselev, M. A.; Magazù, S.; Calandra, P. Amphiphiles Self-Assembly: Basic Concepts and Future Perspectives of Supramolecular Approaches. *Adv. Condens. Matter Phys.* **2015**, *2015*.

(2) Wang, Y.; Wang, L.; Li, B.; Cheng, Y.; Zhou, D.; Chen, X.; Jing, X.; Huang, Y. Compact Vesicles Self-Assembled from Binary Graft Copolymers with High Hydrophilic Fraction for Potential Drug/Protein Delivery. *ACS Macro Lett.* **2017**, *6* (11), 1186–1190.

(3) Wei, W.; Bai, F.; Fan, H. Surfactant-Assisted Cooperative Self-Assembly of Nanoparticles into Active Nanostructures. *iScience* **2019**, *11*, 272–293.

(4) Besenius, P.; Portale, G.; Bomans, P. H. H.; Janssen, H. M.; Palmans, A. R. A.; Meijer, E. W. Controlling the Growth and Shape of Chiral Supramolecular Polymers in Water. *Proc. Natl. Acad. Sci. U. S. A.* **2010**, *107* (42), 17888–17893.

(5) Yang, L.; Fan, G.; Ren, X.; Zhao, L.; Wang, J.; Chen, Z. Aqueous Self-Assembly of a Charged BODIPY Amphiphile via Nucleation-Growth Mechanism. *Phys. Chem. Chem. Phys.* **2015**, *17* (14), 9167–9172.

(6) Zhao, D.; Moore, J. S. Nucleation-Elongation: A Mechanism for Cooperative Supramolecular Polymerization. *Org. Biomol. Chem.* **2003**, *1* (20), 3471–3491.

(7) Sorrenti, A.; Leira-Iglesias, J.; Markvoort, A. J.; De Greef, T. F. A.; Hermans, T. M. Non-Equilibrium Supramolecular Polymerization. *Chem. Soc. Rev.* **2017**, *46* (18), 5476–5490.

(8) Zhao, L.; Qu, R.; Li, A.; Ma, R.; Shi, L. Cooperative Self-Assembly of Porphyrins with Polymers Possessing Bioactive Functions. *Chem. Commun.* **2016**, *52* (93), 13543–13555.

(9) Li, J.; An, Y.; Chen, X.; Xiong, D.; Li, Y.; Huang, N.; Shi, L. Chiral Polymeric Micelles from Electrostatic Assembly between Achiral Porphyrins and Block Copolymers. *Macromol. Rapid Commun.* **2008**, *29* (3), 214–218.

(10) Peters, K. C.; Mekala, S.; Gross, R. A.; Singer, K. D. Cooperative Self-Assembly of Helical Exciton-Coupled Biosurfactant-Functionalized Porphyrin Chromophores. *ACS Appl. Bio Mater.* **2019**, *2* (4), 1703–1713.

(11) Wei, W.; Sun, J.; Fan, H. Cooperative Self-Assembly of Porphyrins and Derivatives. *MRS Bull.* **2019**, *44* (3), 183–188.

(12) Li, X.; Yu, S.; Lee, Y.; Guo, T.; Kwon, N.; Lee, D.; Yeom, S. C.; Cho, Y.; Kim, G.; Huang, J.-D.; et al. In Vivo Albumin Traps Photosensitizer Monomers from Self-Assembled Phthalocyanine Nanovesicles: A Facile and Switchable Theranostic Approach. *J. Am. Chem. Soc.* **2019**, *141* (3), 1366–1372.

(13) Li, X.; Lee, D.; Huang, J. D.; Yoon, J. Phthalocyanine-Assembled Nanodots as Photosensitizers for Highly Efficient Type I Photoreactions in Photodynamic Therapy. *Angew. Chemie - Int. Ed.* **2018**, *57* (31), 9885–9890.

(14) Guldi, D. M.; Gouloumis, A.; Vázquez, P.; Torres, T.; Georgakilas, V.; Prato, M. Nanoscale Organization of a Phthalocyanine−Fullerene System: Remarkable Stabilization of Charges in Photoactive 1-D Nanotubules. *J. Am. Chem. Soc.* **2005**, *127* (16), 5811–5813.

(15) van Vlerken, L. E.; Vyas, T. K.; Amiji, M. M. Poly(Ethylene Glycol)-Modified Nanocarriers for Tumor-Targeted and Intracellular Delivery. *Pharm. Res.* **2007**, *24* (8), 1405–1414.

(16) Liu, J.-Y.; Jiang, X.-J.; Fong, W.-P.; Ng, D. K. P. Highly Photocytotoxic 1,4-Dipegylated Zinc (II) Phthalocyanines. Effects of the Chain Length on the in Vitro Photodynamic Activities. *Org. Biomol. Chem.* **2008**, *6* (24), 4560–4566.

(17) Dong, X.; Guo, X.; Liu, G.; Fan, A.; Wang, Z.; Zhao, Y. When Self-Assembly Meets Topology: An Enhanced Micelle Stability. *Chem. Commun.* **2017**, *53* (27), 3822–3825.

(18) Günsel, A.; Güzel, E.; Bilgiçli, A. T.; Atmaca, G. Y.; Erdoğmuş, A.; Yarasir, M. N. Synthesis and Investigation of Photophysicochemical Properties of Novel Ketone-Substituted Gallium (III) and Indium (III) Phthalocyanines with High Singlet Oxygen Yield for Photodynamic Therapy. *J. Lumin.* **2017**, *192*, 888–892.

(19) Saeki, S.; Kuwahara, N.; Nakata, M.; Kaneko, M. Phase Separation of Poly(Ethylene Glycol)-Water-Salt Systems. *Polymer (Guildf).* **1977**, *18* (10), 1027–1031.

(20) Yasuda, T.; Shimizu, T.; Liu, F.; Ungar, G.; Kato, T. Electro-Functional Octupolar π-Conjugated Columnar Liquid Crystals. *J. Am. Chem. Soc.* **2011**, *133* (34), 13437–13444.

(21) Perlin, P.; Gharakhanian, E. G.; Deming, T. J. Homoallylglycine Residues Are Superior Precursors to Orthogonally Modified Thioether Containing Polypeptides. *Chem. Commun.* **2018**, *54* (48), 6196–6199.

GENERAL METHODS

1. Synthesis and characterization

a) Reagents and solvents

Chemical reagents were purchased from Merck-Sigma Aldrich, Alfa Aesar, Acros Organics, TCI or Fluorochem, as main commercial suppliers, and were used without further purification unless it is indicated. Solvents were purchased from Carlo Erba Reagents, and anhydrous solvents were dried with 4Å molecular sieves (Panreac). All reactions were performed in standard glasswares, except for the cyclotetramerization reactions that were carried out in high pressure sealed tubes.

b) Chromatography

The monitoring of the reactions has been carried out by thin layer chromatography (TLC), employing aluminum sheets coated with silica gel type 60 F254 (0.2 mm thick, E. Merck). Purification and separation of the synthesized products was performed by column chromatography, using silica gel (230–400 mesh, 0.040-0.063 mm, Merck). Eluents and relative proportions of the solvents are indicated for each particular case. Size exclusion (SEC) / Gel permeation chromatography (GPC), was performed using Bio-Beads S-X1 (200–400 mesh, Bio-Rad), or using Sephadex®–G25 beads as the stationary phase. Eluents are indicated in the experimental sections.

c) Microwave activated reactions

Microwave activated reactions were performed in a Biotage Initiator+ 4.1.2 equipment, all reactions were performed in capped glass vials (Biotage Microwave vials 2–5 mL) under argon atmosphere.

d) Infrared spectra

Infrared (IR) spectra were recorded on an Agilent Technologies Cry 630 FTIR spectrophotometer, employing in all cases solid samples (diamond ATR).

e) Mass Spectrometry

Mass Spectrometry (MS) and High Resolution Mass Spectrometry (HRMS) spectra were recorded employing: Electronic Impact (EI) or Fast Atom Bombardment (FAB-MS) using a Waters VG-AutoSpec spectrometer; Electrospray Ionization (ESI Positive TOF_MS) mass spectra using an API Q-Star Pulsar i from Sciex; Matrix Assisted Laser

Desorption/Ionization-Time of Flight (MALDI-TOF) using a Bruker Ultraflex III TOF/TOF spectrometer, with a nitrogen laser operating at 337 nm, or with a NdYAG laser operating at 335 nm; or Atmospheric pressure chemical ionization (APCI) using a Bruker MAXIS II with a high resolution Q-TOF analyzer and MeOH as ionizing phase. The different matrixes employed are indicated for each spectrum. Mass spectrometry data are expressed in *m/z* units. All MS experiments were carried out at the Servicio Interdepartmental de Investigación (SIdI) of the Universidad Autónoma de Madrid.

f) Nuclear magnetic resonance spectra

^{1}H NMR and ^{13}C NMR were recorded on Bruker AC-300 (300 MHz), Bruker DPX 400 MHz, or Bruker XRD-500 (500 MHz) instruments. Deuterated solvents employed are indicated in each spectrum.

g) Aggregation studies

Aggregation studies were performed using aqueous miliQ-water (purified on an EMD Milipore Mili-Q Integral Water Purification System), phosphate-buffered saline solution (PBS, pH = 7.2–7.6 at 25 °C), and organic spectroscopy grade solvents.

h) UV-vis spectroscopy

UV-vis spectra were recorded on a JASCO-V660 UV-vis spectrophotometer using spectroscopic grade solvents and 10x10mm quartz cuvettes with a Jasco Peltier ETCS-761 temperature controller incorporated.

i) Fluorescence

Fluorescence spectra were recorded with a JACSO FP-8600 spectrophotometer using spectroscopic grade solvents and quartz cuvettes (1cm) with a Jasco Peltier ETCS-761 temperature controller incorporated.

j) Circular Dichroism

Circular dichroism (CD) spectra were recorded on a Jasco J-815 CD-spectrometer including a Jasco Peltier ETCT-762 temperature controller using spectroscopic grade solvents and quartz cuvettes (1cm).

k) Dynamic Light Scattering (DLS)

DLS measurements were performed in a Malvern Zetasizer Nanoseries Nano-ZS.

2. Photophysical studies

a) UV-Vis spectroscopy

All spectroscopic measurements were carried out in 1 cm quartz cuvettes (Hellma, Germany) in air-saturated solutions, at room temperature using spectroscopic grade solvents. Absorption spectra were recorded using a double beam UV-Vis-NIR Varian Cary 6000i spectrophotometer (Varian, Palo Alto, CA, USA). Absorption coefficients were derived from the slopes of Lambert-Beer plots.

b) Fluorescence spectra

Emission spectra were recorded using a Spex Fluoromax-4 spectrofluorometer (Horiba Jobin-Yvon, Edison, NJ, USA).

c) Fluorescence quantum yield

Fluorescent quantum yields (Φ_F) were determined by comparing the integrated fluorescent intensity of optically matched solutions between studied compounds and Zn(II)Pc in 1-propanol (Φ_F = 0.20 ± 0.03). The original literature value for this solvent (Φ_F = 0.45)[1] was reassessed as it resulted in the sum of fluorescence and singlet oxygen quantum yields exceeding 1. To this end, Zn(II)Pc in DMSO (Φ_F = 0.20)[2] and Zn(II)Pc in toluene (Φ_F = 0.35)[3] were used as references. Fluorescence intensity was corrected using the refractive index of the solvents used (eq. 1).

$$\Phi_F = \frac{Area_{Sample} \cdot n^2_{Sample}}{Area_{Reference} \cdot n^2_{Reference}} \qquad (1)$$

d) Singlet Oxygen Quantum Yields – Direct Method

Singlet oxygen generation was studied by time-resolved near-infrared phosphorescence by means of a customised setup.[4,5] Briefly, a pulsed Nd:YAG laser (FTSS355-Q, Crystal Laser, Berlin, Germany) working at 1 kHz repetition rate (for THF and toluene) or 10 kHz (DMSO) at 355 nm (third harmonic, 0.5 µJ per pulse) was used to excite the sample. A 1064-nm rugate notch filter (Edmund Optics) and an uncoated SKG-5 filter (CVI Laser Corporation) were placed in the laser path to remove any residual NIR emission. The light emitted by the sample was filtered with a 1100-nm long-pass filter (Edmund Optics) and later by a narrow bandpass filter at 1275 nm (BK-1270-70-B, bk Interferenzoptik). A thermoelectric-cooled NIR-sensitive photomultiplier tube assembly (H9170-45, Hamamatsu Photonics, Hamamatsu, Japan) was used as detector. Photon counting was

achieved with a multichannel scaler (NanoHarp 250, PicoQuant, Berlin, Germany). The time dependence of the $^1O_2$ phosphorescence with the signal intensity $S(t)$ is described by Equation 2, in which τ_T and τ_Δ are the lifetimes of the photosensitizer triplet state and of $^1O_2$ respectively, and $S(0)$ is a pre-exponential parameter proportional to Φ_Δ.

$$S(t) = S(0) \times \frac{\tau_\Delta}{\tau_\Delta - \tau_T} \times \left(e^{-t/\tau_\Delta} - e^{-t/\tau_T}\right) \quad (2)$$

Curve fitting was performed with the Graphpad Prism version 7.00 for Windows,(GraphPad Software, La Jolla California USA, www.graphpad.com). Φ_Δ was determined by comparing the $S(0)$ values of optically matched solutions of the drug and the reference phenalenone (PN), (in toluene and THF Φ_Δ = 0.99 and 0.96 respectively),[6,7] or Zn(II)Pc, (in DMSO Φ_Δ = 0.67);[8] as described by Equation 3.

$$\Phi_{\Delta,\text{sample}} = \Phi_{\Delta,\text{ref}} \times \frac{S(0)_{Sample}}{S(0)_{ref}} \quad (3)$$

e) Singlet Oxygen Quantum Yields – Relative Method

Φ_Δ were measured in DMSO following the well-known relative method based on the photoinduced decomposition of the chemical scavenger 1,3-diphenylisobenzofuran (DPBF) which reacts readily with $^1O_2$ after excitation with visible light filtered below 530 nm ($hv_{>530}$).[9] Non-substituted Zn(II)Pc was used as reference compound (Φ_Δ(DMSO) = 0.67) and the procedure was as follows: 2 mL of a stock solution of DPBF (with an absorption of ca. 1) in DMSO was transferred into a 10x10 mm quartz optical cell and bubbled with $^3O_2$ for 1 min. A concentrated stock solution of the PS in the same solvent was then added, in a defined amount to reach a final *Q*-band absorbance value of about 0.1 a.u. The solution was stirred and irradiated for defined time intervals, using a halogen lamp (300 W). The duration of these intervals are tuned in each experiment, in order to get a decrease in DPBF absorption of about 3-4%. Incident light was filtered through a water filter (6 cm) and an additional filter to remove light under 530 nm (Newport filter FSQ-OG530). In addition, neutral density filters (FBS-ND03 and FB-ND10) were used as appropriate. The decrease of DPBF absorbance with irradiation time was monitored at 414 nm and Φ_Δ was calculated through the following equation:

$$\phi_\Delta^S = \phi_\Delta^R \frac{k^S I_{aT}^R}{k^R I_{aT}^S} \quad (4)$$

R, S: reference and sample respectively. ***k:*** is the slope of a plot of $ln(A_0/A_t)$ versus irradiation time *t*. ***A_0, A_t:*** absorbance of scavenger at the monitoring wavelength before and after irradiation time *t*, respectively. ***I_{aT}:*** total amount of light absorbed by the dye. It is calculated as the sum of intensities of the absorbed light I_a from wavelength 530 up to 850 nm.

I_a at given wavelength is calculated using Beer's law:

$$I_a = I_0(1 - e^{-2.3A}) \qquad (5)$$

***I_0*:** transmittance of the filter at a given wavelength. ***A*:** absorbance of the dye at this wavelength.

All experiments were performed three times and the obtained data represent mean values of those three experiments. The concentration of the scavenger (DPBF) was monitored spectroscopically at 414 nm in function of the irradiation time of the photosensitizer, from which the values of Φ_Δ could be determined. Importantly, the decrease of the absorption of DPBF was completely linear (R^2=0.99) and at the same time no change in the absorption of the phthalocyanines could be observed throughout the measurement indicating its stability.

f) Time-resolved fluorescence (TRF)

Time-resolved fluorescence decays were measured using a Fluotime 200 time-correlated fluorescence lifetime spectrophotometer (PicoQuant, Berlin, Germany), equipped with a red sensitive photomultiplier. Excitation was achieved by means of a 654 nm picosecond laser working at 10 MHz repetition rate. The counting frequency was always below 1%. Fluorescence lifetimes were analyzed using PicoQuant FluoFit 4.0 data analysis software.

3. References

(1) Gradyushko, A. T.; Sevchenko, A. N.; Solovyov, K. N.; Tsvirko, M. P. Energetics of Photophysical Processes in Chlorophyll-like Molecules. *Photochem. Photobiol.* **1970**, *11* (6), 387–400.

(2) Ogunsipe, A.; Maree, D.; Nyokong, T. Solvent Effects on the Photochemical and Fluorescence Properties of Zinc Phthalocyanine Derivatives. *J. Mol. Struct.* **2003**, *650* (1), 131–140.

(3) Bishop, S. M.; Beeby, A.; Parker, A. W.; Foley, M. S. C.; Phillips, D. The Preparation and Photophysical Measurements of Perdeutero Zinc Phthalocyanine. *J. Photochem. Photobiol. A Chem.* **1995**, *90* (1), 39–44.

(4) Nonell, S.; Braslavsky, S. E. [4] Time-Resolved Singlet Oxygen Detection. In *Methods in Enzymology*; Academic Press, 2000; Vol. 319, pp 37–49.

(5) Jiménez-Banzo, A.; Ragàs, X.; Kapusta, P.; Nonell, S. Time-Resolved Methods in Biophysics. 7. Photon Counting vs. Analog Time-Resolved Singlet Oxygen Phosphorescence Detection. *Photochem. Photobiol. Sci.* **2008**, *7* (9), 1003–1010.

(6) Martí, C.; Jürgens, O.; Cuenca, O.; Casals, M.; Nonell, S. Aromatic Ketones as Standards for Singlet Molecular Oxygen O2(1Δg) Photosensitization. Time-Resolved Photoacoustic and near-IR Emission Studies. *J. Photochem. Photobiol. A Chem.* **1996**, *97* (1), 11–18.

(7) Schmidt, R.; Tanielian, C.; Dunsbach, R.; Wolff, C. Phenalenone, a Universal Reference Compound for the Determination of Quantum Yields of Singlet Oxygen O2(1Δg) Sensitization. *J. Photochem. Photobiol. A Chem.* **1994**, *79* (1), 11–17.

(8) Kuznetsova, N. A.; Gretsova, N. S.; Kalmykova, E. A.; Makarova, E. A.; Dashkevich, S. N.; Negrimovsky, V. M.; Lukyanets, E. A. Structure-Photochemical Properties Relationship for Porphyrins and Related Compounds. *Zh. Obs. Khim* **2000**, *70*, 140–148.

(9) Makhseed, S.; Tuhl, A.; Samuel, J.; Zimcik, P.; Al-Awadi, N.; Novakova, V. New Highly Soluble Phenoxy-Substituted Phthalocyanine and Azaphthalocyanine Derivatives: Synthesis, Photochemical and Photophysical Studies and Atypical Aggregation Behavior. *Dye. Pigment.* **2012**, *95* (2), 351–357.

CONCLUSIONES

Las ftalocianinas con un patrón de sustitución A_2B_2 han demostrado ser fotosensibilizadores eficientes para terapia fotodinámica. Hemos aprovechado sus geometrías altamente orientadas, tanto en el caso de la versión ABAB como AABB, para preparar fotosensibilizadores anfifílicos, los cuales pueden considerarse como nuevos arquetipos en ámbito de los fotosensibilizadores porfirinoides. A su vez hemos mejorado los protocolos sintéticos, obteniendo mejores rendimientos y con procedimientos más simples que los previamente reportados.

En la Parte 1 de esta tesis doctoral:

El estudio de varias ABAB Zn(II)Pcs con un patrón de sustitución variable, es decir, nodificando en número de unidades isoindol B que contienen sustituyentes trifluorometilfenilo (i.e. ABAB, A_3B y A_4), y con diferente funcionalización en la unidad isoindolica A, nos ha permitido elucidar el rol determinate de los sustituyentes fluorados voluminosos en cuanto a su influencia en las propiedades fotofísicas y la capacidad de generar $^1O_2$ en este tipo de compuestos. La sustitución ABAB provoca en las Zn(II)Pcs propiedades de absorción particulares con bandas muy desplazadas hacia el rojo, evita fenómenos de agregación independientemente del tipo de disolvente empleado, y además da lugar a rendimientos cuánticos de producción de $^1O_2$ muy elevados. Estas características, las cuales no son son fáciles de conseguir en Zn(II)Pcs, son fundamentales para su aplicación como PS en PDT. Por otra parte, se ha introducido una amplia variedad de grupos funcionales en las unidades isoindol A, lo cual sin embargo, parece tener un impacto muy leve en las propiedades fotofísicas de las Zn(II)Pcs estudiadas, que vienen determinadas por los sustituyentes fluorados.

Además, manteniendo nuestro diseño, hemos preparado ABAB Zn(II)Pcs anfifílicas tanto con cadenas de polietilenglicosl como con grupo cargados positivamente, los cuales se han utilizado ampliamente en la literatura como sustituyentes para dotar de solubilidad en medio acuoso, y especificidad hacia lineas celulares cancerosas o cultivos bacterianos respectivamente. El principal objetivo es testear *in vitro* el potencial de este nuevo tipo de PS basados en Zn(II)Pcs. En el caso de ABAB Zn(II)Pc fincionalizadas con polietilenglicol han demostrado no ser tóxicas para las células en oscuridad, pero cuando el cultivo es irradiado en presencia del PS se produce la muerte celular. De forma consistente respecto a los estudios de generación de $^1O_2$, el impacto es mayor en el cado de ABAB y A_3B, respecto a A_4. Por otra parte, dos ABAB-Zn(II)Pcs catiónicas se han provado en estudios de fotoinactivación *in vitro* sobre *E. coli* y *S. Aureus*. Los resultados indican que ambas son fotoquímicamente activas, induciendo la inactivación bacteriana tras irradiar con luz roja, siendo mínimo el efecto del tipo de sustituyente catiónico utilizado. Una conclusión importante es que estos PS catiónicos han demostrado una actividad mayor que otras Pcs catiónicas relacionadas como resultado del diseño racional responsable de la capacidad mejorada de fotosensibilización de oxígeno, el adecuado balance de lipofilia/hidrofilia y la ausencia de agregación.

En resumen, estos hayazgos hacen a las Zn(II)Pcs con sustituyentes voluminosos trifluorometilfenilo excelentes candidatos como PS para PDT, especialmente aquellos con patrón se sustitución ABAB.

En la Parte 2 de esta tesis doctoral:

En cuanto a AABB Zn(II)Pcs quirales intraconectadas por la unidad binaftol, aunque ya habían sido previamente descritas, hemos mejorado la metodología previamente publicada, reduciendo el número de etapas sintéticas y obteniendo una batería de compuestos con buenos rendimentos. La primera familia contiene sustituyentes de tipo halógeno o etininilo, los cuales pueden ser posteriormente transformados para obtener una variedad de compuestos customizados con propiedades anfífilas. Algunas de estas Zn(II)Pcs muestran propiedades de autoensamblaje en disolventes no polares, formando nanoestructuras robustas y quirales en disolución. Esta propiedad convierte estos derivados en buenos candidatos para la preparación de anfífilos que autoensamblen en medio acuoso. La formación de nanoestructuras puede facilitar la circulación a través del torrente sanguíneo, y promover la captación celular a trvés del efecto EPR.

Con el objetivo de probar este diseño, hemos preparado dos tipos de AABB Zn(II)Pcs anfífilas con puente binaftilo. El primer enfoque incluye dos ABAB Pcs tetracatiónicas, funcionalizadas con piridinio y puentes de binaftilo no sustituidos o funcionalizados con cadenas de alquilo. Estos compuestos han demostrado capacidades de autoensamblaje en medios acuosos, formando vesículas esféricas con diferentes diámetros de media según el tipo de sustitución. Ambos compuestos han sido probados en ensayos fotodinámicos in vitro sobre E. coli y S. aureus. Hemos encontrado una relación directa entre el tamaño de la nanopartícula formada en medios de agua (más grande para el compuesto que carece de las cadenas de alquilo), la absorción de PS por las bacterias y la fototoxicidad, que es notablemente más alta para E. coli (Gram-negativa) normalmente más resistente a este tipo de tratamiento. Estos hallazgos prueban que estos compuestos son excelentes PS para aplicaciones PDI.

El segundo enfoque, que es decorar el resto de binaftol con cadenas de polietilenglicol, produce un anfífilo altamente orientado, capaz de autoensamblarse en agua en micelas supramoleculares, y se ha realizado un análisis cuidadoso del proceso de polimerización mediante técnicas espectroscópicas.